eman ta zabal zazu

Universidad
del País Vasco

Euskal Herriko
Unibertsitatea

NAZIOARTEKO
BIKAINTASUN
CAMPUSA

CAMPUS DE
EXCELENCIA
INTERNACIONAL

Computational study of statically confined electron systems by means of quantum chemical and machine learning techniques/ Estakikoki Konfinatutako Elektroi Sistemen Azterketa Konputazionala Machine Learning eta Kimika Kuantikoko Metodoak Erabiliz

XABIER TELLERIA ALLIKA

Supervised by
Dr. Jon Mattin Matxain Beraza and Dr. Jose Maria Mercero Larraza

OCTOBER 2022

Computational study of statically confined electron systems by means of quantum chemical and machine learning techniques/ Estakikoki Konfinatutako Elektroi Sistemen Azterketa Konputazionala Machine Learning eta Kimika Kuantikoko Metodoak Erabiliz

Dissertation presented in

Universidad del País Vasco Euskal Herriko Unibertsitatea

NAZIOARTEKO BIKAINTASUN CAMPUSA
CAMPUS DE EXCELENCIA INTERNACIONAL

DIPC

Submitted in fulfillment of the requirements of the

DOCTORAL PROGRAM IN THEORETICAL CHEMISTRY AND COMPUTATIONAL MODELLING

Presented by

XABIER TELLERIA ALLIKA

Supervised by

DR. JON MATTIN MATXAIN BERAZA

and

DR. JOSE MARIA MERCERO LARRAZA

Euskal Herriko Unibertsitatea/Universidad del País Vasco & Donostia International Physics Center

In DONOSTIA, OCTOBER 2022

CONTENTS

LIST OF FIGURES

LIST OF TABLES

Chapter 1

INTRODUCTION

In this chapter a general scope of this thesis will be provided. Throughout this thesis several theoretical tools have been developed in different fields such as quantum chemistry and supervised and semi-supervised machine learning. These tools have been employed in order to model the wavefunction and energy of systems composed by few electron systems with several spin states.

With the aim of contextualising this work, a brief overview of the electron correlation phenomenon and its description using quantum chemical methods based on many particle wavefunctions will be provided. So as to introduce the electron structure problem, the explanation was constrained to briefly describe the Hartree-Fock and Multi-Configurational methods employed in this work as well as pointing out the importance of including electron correlation effects for describing Wigner molecules and Hooke atoms. In addition, some machine learning methods (neural networks and semi-supervised learning) employed for either optimizing some basis functions or building phase diagrams efficiently will be briefly introduced.

1.1 THE ELECTRONIC STRUCTURE PROBLEM

The underlying basic question in all quantum chemistry may be stated as it follows: given an external potential $\mathcal{V}(\mathbf{r})$ which confines a given number of n interacting electrons with a given total spin S, what are the eigenfunctions of such system?

Despite the relative simpleness of this question, obtaining an accurate description of the electronic structure has been and still is a complex and fascinating field of study. In a naive attempt to give a brief historical perspective, a few milestones in the development of foundational ideas on how to tackle this problem will be listed. By the time basic principles governing the quantum realm (wave behaviour of matter, antisymmetric waves for describing electron systems etc.) were known [1, 2], we may consider first attempts to describe systems composed by Pauli [3], Sommerfeld [4], Fermi [5] and Thomas [6] among others. One of the most important

contributions of these works is the electron gas model which attempted to describe the filling and thermal properties of conducting electron systems in solids. Even though such models were able to answer certain questions concerning macroscopic properties, they still were not accurate enough to describe smaller scale condensed matter systems such as atoms and molecules.

Using the many electron Hamiltonian as a starting point, the Coulomb-like interaction among the electrons makes the systems be both: non-linear and non separable. In addition, if we were to solve the equation for a given electron, we would realise that the solution depends on all the electrons; thus, the solution of the problem depends on itself! By the year 1930, the combined works of Slater, Hartree and Fock resulted in the mono-determinantal Self Consistent Field (SCF) method which is in the heart of modern wave-function based techniques in Quantum Chemistry [7–10]. The key of this method is the following: if we introduce a one-body object called an orbital, we shall solve the corresponding system by focusing on the i-th electron moving on an averaged field created by the other $n-1$ electrons and the solutions should be self consistent. Later, in an independent way, Roothan and Hall incorporated the usage of basis functions to represent the Fock equations as a generalised eigenvalue matrix equation which could be solved computationally [11, 12] as is given by equation (1.1). This equation is a discretized matrix representation of the Fock eigenvalue problem given in equation (1.2).

$$\mathbf{F(C)C = ESC} \tag{1.1}$$

$$\left[h(i) + \sum_{b \neq a} J_b(i) - K_b(i) \right] \chi_a(i) = \epsilon_a \chi_a(i) \tag{1.2}$$

Even though Hartree-Fock methods constitute the first real step in electronic structure theory, it comes with its limitations, the most notorious of which is the fact that a single Slater determinant is employed to describe the many-particle system. The main drawback of such monodeterminantal character is the fact that the spatial distribution of opposite spin particles is just a direct product of the distributions of both particles (see equation (1.3)). Thus, the probability distributions $\psi_1(\mathbf{r}_1)^2$ and $\psi_2(\mathbf{r}_2)^2$ are independent i.e. they are not correlated; in the electronic structure community it is said that the Hartree-Fock wave functions lack of (opposite spin) electron correlation effects and therefore, the obtained energy is an upper bound of the real one [13].

$$P(\mathbf{r}_1, \mathbf{r}_2)d\mathbf{r}_1 d\mathbf{r}_2 = \int \Psi^2 d\mathbf{r}_1 d\mathbf{r}_2 d\omega_1 d\omega_2 = \psi_1(\mathbf{r}_1)^2 \psi_2(\mathbf{r}_2)^2 \tag{1.3}$$

Therefore, in order to account for electron correlation effects, it is mandatory to go beyond the single many-particle function (i.e. single Slater determinant). It can be shown than an arbitrary antisymmetric function of n variables can be exactly expanded in terms of all unique determinants formed from a complete set of one-particle functions $\{\chi_1\}$. Based on this fact and the requirement of expanding the wave-function as a combination of Slater determinants, the Configuration Interaction (CI) methods were developed. These take the HF wave-function and performs promotions of electrons to higher energy orbitals one by one (single excitations), by pairs (double excitations) and so on for all possible combinations obtaining the Full Configuration Interaction wave-function [13]. In practice, even if only same symmetry and spin excitations take part, FCI is hugely time consuming due to the large parameter space and CI expansions are normally truncated at doubles. However, when this expansion is truncated, the method becomes size inconsistent.

One solution to the size-consistency problem is the following: perform a FCI only in some selected orbitals and electrons that will mainly take part in the correlation effects; this is the so called Complete Active Space (CAS). When the Self Consistent Field (SCF) approach is applied on this spanned space, one gets the CASSCF method. Depending on the occupation number, two different kinds of orbital-spaces emerge: primary space (where active occupation number between 0 and 2 and inactive orbitals occupation number is always 2 live) and secondary space (orbitals that remain unoccupied). This approach can describe the static electron correlation as the many-body wave-function is described as a linear combination of Slater determinants [14–17] and, in addition, further dynamic correlation effects can be taking into account by means of perturbation schemes [18, 19].

1.2 IMPORTANCE OF ELECTRON CORRELATION

1.2.1 Wigner crystals and molecules

By means of rather basic concepts concerning quantum mechanics governing interactions of systems composed by electrons, in 1934 Wigner predicted that a low-density electron gas crystallizes [20] such that electrons get localized. In fact, since the Coulomb interaction by particle goes as $U_C \propto 1/r_s$ (where r_s is the average distance between particles) and the average kinetic energy goes as $K \sim 1/r_s^2$, it can be seen than for low densities (large values of average distance between particles r_s), Coulomb interactions govern over kinetic energy. Therefore, at sufficient low densities, there is a tendency for electrons to minimize the total energy of the system by getting localized; this is called a Wigner crystal. Transitions happening between these quantum states of matter called Fermi-liquids and Wigner crystals have experimentally been observed in plenty recent works [21–27] and, interestingly,

a substrate for Wigner crystals seem to be bilayer materials in which low densities are obtained by means of emerging moiré patterns [28–31].

In the context of non-periodic finite systems, localized electronic states are also called Wigner molecules and they emerge when the confinement of the electrons is rather weak [32–34]. Thus, in order to describe Wigner molecules or, in general, low density electron systems, electron correlation effects on both, energy and wavefunction, must be treated by means of high enough computational methods. Highly accurate densities for systems in low-correlation regimes as well as in high-correlation regimes have been obtained in the literature [35–38]. If similar systems containing larger number of electrons ($n > 2$) are to be considered, a richer variety of electronic states consisting on several ground state spin multiplicities and multi-determinantal features arise [39–41]. Although such systems can be employed to understand many-body interactions, the computational cost increases with the size of the system. In spite of these difficulties, these model systems have been repeatedly used in the calibration of electronic structure methods, for they provide very variable dynamic and nondynamic electron correlation regimes [42–44] that pose a great challenge for current computational methods. [37, 45–57] Such calibration has been possible because of the recent availability of highly accurate analytical and benchmark data.[39, 40, 58–64]

1.2.2   Quantum Dots and Hooke atoms

Quantum Dots (QDs) are regions of space where, due to a given external potential, particles such as electrons are confined. As these regions shrink, a critical size is reached at which properties of the microscopic world - as energy quantisation, electronic and magnetic structure - emerge. From a physical chemical point of view, a molecule or a nanoparticle that confines its valence electrons can also be taken as QDs. Nowadays, in the dawn of quantum technologies, QDs form a vast and interesting field of study. These systems constitute one of the most elemental components for nanoscale devices which have a wide range of applications such as: solar energy harvesting, optoelectronics and quantum computing devices among many others [65]. Very recent works show further fields of applications for QDs as thermoelectricity [66], catalysis [67–70] and, most remarkably, quantum computation [71–75].

One of the simplest and most adequate models used in theoretical studies concerning QDs are the so called Harmonium or Hooke's atoms in which electrons are confined in a spherical harmonic potential [76] for which the Hamiltonian is given as in equation (1.4). Such models contain parameters that may be tuned in order to represent features corresponding to real QDs [77, 78]. For instance, work carried out in our group using a Hookean exact three-body model to examine electron correlation in a two-electron spherical quantum dot confirmed that triplet-singlet transitions take place as the externally applied magnetic field increases[79]. However,

the limitation of using an exact model restricted our study to two-electron systems. That is, the analytical solutions[80] for specific curvature parameter of the two-electron Hooke atoms ($\omega^2 = \frac{1}{4}, \frac{1}{100} \ldots$) are well known, which can lead in principle to highly accurate densities for systems in low-correlation regimes ($\omega^2 \to \infty$) as well as in high-correlation regimes ($\omega^2 \to 0$) [35–38]. If similar systems containing larger number of electrons ($n > 2$) are to be considered, a richer variety of electronic states consisting on several ground state spin multiplicities and non-dynamical electron correlation (multi-determinantal features) arise [39–41]. Although such systems can be employed to understand many-body interactions, the computational cost increases with the size of the system.

$$H = -\frac{1}{2} \sum_{i=1}^{n} \nabla_i^2 + \frac{\omega^2}{2} \sum_{i=1}^{n} r_i^2 + \sum_{j>i=1}^{n} \frac{1}{r_{ij}} \tag{1.4}$$

As in Hooke model atoms, the incorporation of electron correlation effects has been shown to be essential for an adequate interpretation of the experimental spectra and transport properties in Quantum Dots [81–86]. In quantum dots, as opposed to real atoms, the effect of electron correlation may be varied at will through manipulation of the dimension and shape of the nanocrystal as well as of the strength, boundaries and symmetries of the confining fields[87, 88]. Besides, the electron-electron interaction can be screened due to lattice, the doping or the charges induced on the metal gates[89]. This fact makes the quantum dot many-body problem more complex than the more familiar atomic case.

Finally, Hooke model systems have been repeatedly used in the calibration of electronic structure methods, for they provide very variable dynamic and non-dynamic electron correlation regimes [42–44] that pose a great challenge for current computational methods. [37, 45–57]. Such calibration has been possible because of the recent availability of highly accurate analytical and benchmark data [39, 40, 58–63].

1.3 MACHINE LEARNING ASSISTANCE

IBM defines Machine Learning (ML) in the following way "Machine learning is a branch of Artificial Intelligence (AI) and computer science which focuses on the use of data and algorithms to imitate the way that humans learn, gradually improving its accuracy". According to this definition, any ML solution is based on two pillars: the data (which are empirically obtained abstract numbers) and an algorithm which operates upon these data in order to gain some kind of knowledge. In addition (as it is implicitly stated), employing a given algorithm, the quality of such knowledge improves as the number of data increases.

Machine learning methods are recently being employed in various fields of chemistry [90–93] such as: electronic structure theory development [94–98], efficient new phase discovery and phase diagram building [99–102], patterns in chemical properties [91, 103–106], obtaining Potential Energy Surfaces [107–111] and reaction paths and outcomes [112–114] among others. Taking this brief compilation of examples into account, ML methods are and will be important tools in chemical sciences.

From a wide perspective, there are two 'traditional' machine learning disciplines, the so called *unsupervised* and *supervised* learning paradigms. Given a set of data $X = \{x_1 \ldots x_n\}$ the former aims to find interesting structure in the data such as clustering and dimension reduction by techniques such as k-means Clustering, and Principal Component analysis. Meanwhile, the latter also considers one more set $Y = \{y_1 \ldots y_n\}$ and its goal is to learn a mapping which connects both sets X and Y by techniques such as Linear and Logistic Regression, Random Forests and Vector Supported Machines. Then, semi-supervised learning is halfway between these two; while still considering both X and Y sets, the number of elements in X is far larger than the number of elements in Y and thus any obtained mapping function turns out to be inaccurate [115–117].

In this work two supervised learning algorithms have been employed, i.e. Random Forests and Neural Networks as well as one semisupervised algorithms: Uncertainty Sampling.

1.3.1   Supervised learning: neural networks for prediction

As it has been stated in the previous section, supervised learning techniques aim to build a machine $f : X \to Y$ which is able to map a feature set X into a label set Y such that (bearing in mind the general ML definition) it gets better at doing so by increasing the size of both sets. Given a labelled data set $\mathcal{D}$, a proper ML algorithm is able to infer the required function f form training data contained in the set $\mathcal{T} \subset \mathcal{D}$ and an error for such inferred function can be obtained by using the complementary set $\mathcal{E} \subset \mathcal{D}, \mathcal{T} \cap \mathcal{E} = \emptyset$. Among the thousands of techniques designed for such purpose, in this work deep Neural Networks (NN) have been employed to infer optimal basis set parameters as it is shown in chapter 2.

In the mid of the XX century, with the aim of modelling how human brains process information, the works of W. S. McCulloch, W. Pitts and F. Rosenblatt gave rise to the first implementations of the perceptron [118, 119] which by means of non linear functions (as the sigmoid [120]) operating upon weighted sums of input gave certain logical or continuous outputs. As it has been proved, by arranging a given number of these neurons in layers and coupling these several layers such that the output of the i-th layer becomes the input of the $(i + 1)$-th one, these machines are (in principle) universal approximates [121–125]. That is, given enough data and large enough number of layers and neurons in each layer, these networks can be trained to approximate any arbitrary function.

1.3.2   Semisupervised learning

Most supervised machine learning prediction and classification models work provided the extension of the learning data set is large enough. Nevertheless, in many real-world situations, as in our case, obtaining independent variable values (labels) may be time-demanding or computationally/economically expensive. Thus, it is wise to gain further expertise based on already established available knowledge and invest our resources (will, time and money) in enlightening the darkest corners of our ignorance. Semi-supervised and active learning techniques can be applied upon data for which we have two different sets: a labelled set $\mathcal{L}$ and an unlabelled set $\mathcal{U}$. Namely, the labeled set $\mathcal{L}$ is composed by points formed as an ordered Cartesian product $(x_1, y_1) \ldots (x_l, y_l)$ where $Y_L = \{y_1 \ldots y_l\} \in \{1 \ldots C\}$ is the set of possible labels (categories). Then, we also have the unlabelled set $\mathcal{U}$ composed by $(x_{l+1}, y_{l+1}) \ldots (x_{l+u}, y_{l+u})$ points where the labels $Y_U = \{y_{l+1} \ldots y_{l+u}\} \in \{1 \ldots C\}$ are unknown and the cardinality of this set is much larger than the former one, $l << u$.

By doing so, we shall know where to map the next experiment to obtain phase diagrams as it has been done in very recent works [126, 127]. We have been using two complementary techniques: label propagation and uncertainty sampling.

Under the initial assumptions, we have built a grid in parameter space with $X = \{\mathbf{x}_1 \ldots \mathbf{x}_{l+u}\}$ coordinates from which a number l will be labelled with just one label form categories $Y = \{1 \ldots C\}$ and the remaining u coordinates are not labelled (of course, all categories are represented in the l labelled data, so $\text{card}(l) \geq \text{card}(C)$). We also assume that the number of unlabelled coordinates is far larger than the labelled ones $l << u$. The point here is to use the information (labels and coordinates) of the l labelled data and infer the probabilities for unlabeled data to belong to each of the C possible categories and compute the uncertainty based on these probabilities.

1.3.2.1   *Label Propagation Algorithm*

X. Zhu and Z. Ghahramani developed an algorithm named 'label propagation algorithm'[128] in which information from labelled data is propagated to unlabelled data in a stochastic process by means of Markov chains. Here, one defines a graph containing all -labelled and unlabelled- data and defines the connection strength (weight) by pairs. Using properties related to homogeneous Markov chains and stochastic matrices, it can be shown that the algorithm converges to a unique stationary solution (1.5) for any which initial guess for the matrix $\mathbf{Y}^{(0)}$ we may make.

$$\mathbf{Y}_u = (\mathbf{I} - \tilde{\mathbf{T}}_{uu})^{-1} \tilde{\mathbf{T}}_{ul} \mathbf{Y}_l \qquad (1.5)$$

The main drawback of this method is the fact that for dense or large enough grids, the computation of the matrix $(\mathbf{I} - \tilde{\mathbf{T}}_{uu})^{-1}$ is expensive or, in the worst case, the matrix is singular. This problem may be sidestepped by, instead of using the closed formula (8.5) taking an initial label vector and iterating it. Nevertheless, since convergence is reached after several iterations and large matrices are still involved, this algorithm is still costly for dense enough grids and this deficiency is more remarkable as the number of dimensions of the feature space increases. As an alternative, other, rather cheap, classifiers such as Random Forests (RF) can be used to solve the problem. Since RF do not have over fitting problems, using a large enough number of trees, the method is universal for all systems studied in this work. Therefore, the initialisation set is employed to train a RF model which will label the unlabelled points assigning them to each category with a given probability, that is, an equivalent approach as using label propagation.

1.3.2.2 *Uncertainty sampling*

Learning is widening our knowledge by gaining more information where our ignorance or uncertainty is deepest. In order to learn in an efficient way, one should focus on one's lack of expertise rather than what she/he already knows. Uncertainty sampling is a way of sampling just the points in which the uncertainty is the largest, but how can we measure uncertainty? Provided we have a probability distribution function $P_C(y|\mathbf{x})$ such that given a parameter vector $\mathbf{x}$ gives the probabilities of that point to belong to each of the categories y in the set $\{1 \ldots C\}$, we may define some uncertainty measures as: Least Confident (1.6), Margin (1.7) and Shannon Entropy (1.8). The first one maximizes the least likely (therefore the most uncertain) of the unlabelled data, the second one is more flexible than the former in the sense that it takes into account the two most likeliest prediction points. Finally, the Shannon entropy is a measure of information content; the less information a variable contains, the more we know about its nature [129].

$$u_{LC}(\mathbf{x}) = 1 - \max_{C} P(C|\mathbf{x}) \tag{1.6}$$

$$u_{MS}(\mathbf{x}) = 1 - [P(C_1|\mathbf{x}) - P(C_2|\mathbf{x})] \tag{1.7}$$

$$u_{SE}(\mathbf{x}) = -\sum_{C} P(C|\mathbf{x}) \log P(C|\mathbf{x}) \tag{1.8}$$

1.4   SCOPE OF THIS WORK

Once the state of the art concerning Wigner molecules, Hooke atoms and some machine learning techniques has been described, in this section the main goals of the present work will be provided. We shall now list the mains goals of this work:

1. Optimize distributed gaussian basis functions for correctly describing the one- and two-dimensionally confined electronic systems by means of machine learning approaches (Neural Networks) for variable confinement parameter $k = \omega^2$. Besides, set an optimal wavefunction based electronic structure method for obtaining accurate wavefunctions. Employ the settled protocole in order to study the Wigner location for small number of electrons $n = \{2, 3, 4\}$ in the high spin state.

2. Optimize one-centre even tempered basis functions using classical optimization techniques (simplex and Newton-Raphson) for properly describing three dimensional spherical Hooke atoms composed by few number of electrons $n = \{2, 4, 6, 8, 10\}$ and confinement parameter $k = \omega^2 = 1/4$. Settle an optimal wavefunction based method for obtaining accurate energies for the lowest laying singlet and triplet states.

3. Implement and improve machine learning methods based on semi-supervised learning and uncertainty sampling for obtaining phase diagrams efficiently and provide some chemically relevant systems.

4. Calculate analytical one-body integrals corresponding to gaussian confinement potentials in terms of gaussian basis functions and implement them in GAMESS US. Provide some examples related to the previous sections.

Chapter 2

QUASI-ONE DIMENSIONAL SYSTEMS

In this chapter, localization properties of systems composed by few electrons confined in a quasi-one-dimensional harmonic potential have been studied by semi-analytical procedures for two electron systems, and by more robust quantum chemical approaches concerning two, three and four electron systems in high spin state. By using electronic-structure properties obtained by multi-reference methods such as the one-body density and the particle-hole entropy, we have been able to define a path that connects the corresponding Wigner molecules with the Fermi liquids by varying the harmonic-potential confinement parameter k. We conclude that the particle-hole entropy is a smooth function of the confinement parameter and connects the two limit cases, and shows a maximum value which position depends on the number of electrons.

2.1   INTRODUCTION

In the previous chapter, some characteristics about the nature of the Wigner crystals and molecules have been introduced. Due to the intrinsic nature of such systems, in order to build models which represent those phases electron correlation effects must be properly described. Some previous studies tackled the issue of one-dimensional systems composed by few electrons ($n = 2, 3$ and 4) and the correlation effects varying the length of the confinement box and the computation method comparing ROHF with FCI [130]. Far from being only theoretical models, systems containing these number of electrons have been observed experimentally [131, 132].

In this chapter, we have studied one-dimensional systems with ($n = 2, 3$ and 4) electrons confined in harmonic potentials with several orders of magnitude for the confinement parameter k. In a first step, we have seen that singlet and triplet states for two electron systems have similar density profiles in the weak confinement regime ($k \rightarrow 0$) while for large confinement regime ($k \rightarrow \infty$) the density of each spin state converges to the free particle density. Then, for high spin states, for all number of electrons, we have computed the electron-hole entropy which is linked to correlation effects [133–135] and we have been able to connect two lowest entropy phases: the Wigner molecule and the Fermi liquid. These entropy curves depend on the number of electrons and the potential parameter k and, therefore, on the density of the system. In all cases we have observed there is a certain value of k for which the electron-hole entropy is maximal, hence static correlation effects play a big role.

2.2   COMPUTATIONAL PROTOCOL

2.2.1   Quantum mechanical model

In this chapter, we have studied systems composed by $n = \{2, 3, 4\}$ electrons which interact via Coulomb potentials among them and are confined in a one-dimensional harmonic well, hence the Hamiltonian of the system can be expressed as in equation (2.1).

$$H = -\frac{1}{2} \sum_{i=1}^{n} \nabla_i^2 + \frac{k}{2} \sum_{i=1}^{n} r_i^2 + \sum_{j>i=1}^{n} \frac{1}{r_{ij}} \tag{2.1}$$

As it is well known [136, 137], in the pure one-dimensional case the Coulomb operator is singular; in order to sidestep this problem, we shall solve the Schrödinger equation by using three dimensional basis functions distributed along one unique direction. The final energy is then obtained by subtracting the transverse components of the kinetic energy for each electron [138]. In this chapter, we will study the behavior of such quasi-one-dimensional systems.

2.2.2   Distributed Gaussian orbitals

In order to properly describe our systems, we use a one dimensional grid of gaussian functions given by equation (2.2) where the position of each basis function is distributed along the x axis $\mathbf{R}_i = (x_i, 0, 0)$.

$$\phi_i(\mathbf{r}; \alpha, \mathbf{R}_i) = \left(\frac{2\alpha}{\pi}\right)^{3/4} \exp(-\alpha(\mathbf{r} - \mathbf{R}_i)^2) \tag{2.2}$$

These gaussians have been set as follows: given a number of electrons n and a harmonic potential with curvature parameter k, the semiclassical turning points of the highest energy level are given as $x_0(n,k) = \pm\left(\frac{(2n+1)^2}{k}\right)^{1/4}$. Using these points as well as the position of the minimum of the potential well ($x = 0$) we place a basis function in each of them and we add m equidistant gaussians between the semi-classical turning points and $2m$ more to each side of these points. In this setting, there is a total number of $M = 3 + 4m$ basis functions and the distance between consecutive basis is given by $\delta = \frac{2|x_0|}{m+1}$. Since all basis functions had the same exponent α, the overlap between neighbouring functions is given as $S(\alpha, \delta) = \exp(-\alpha\delta^2/2)$. One may also rewrite the last overlap function in terms of a dimensionless parameter $\xi = \alpha\delta^2$ as $S(\xi) = \exp(-\xi/2)$. This dimensionless parameter characterizes the resolution of the basis set which in our case has been chosen to be $\xi = 1.0$ [130, 138–141] . By doing so, the exponents are dependent on the confinement, the number of electrons and the number of basis functions as $\alpha = \frac{\xi(m+1)^2}{4x_0^2(n,k)}$.

2.3   RESULTS AND DISCUSSION

2.3.1   Two electron system

As it has been introduced in the previous section, for each confinement strength parameter k, we have fixed the position of three gaussians: one where the confinement potential has its minimum ($x = 0$) and one on each classical turning points ($x = \pm x_0(k,n)$). Once these points are settled, we have added 100 equidistant gaussians ($\delta = \frac{x_0}{13}$) with the same exponent ($\alpha = \delta^{-2}$), 50 of them in between the two turning points and 25 at each side of them, giving rise to a total number of 103 basis functions.

Using these basis, we have computed the singlet and triplet spin states at CASSCF level of theory using several numbers of active orbitals for several values of the confinement parameter k. After having run some initial tests, we have concluded that the optimal active space is the one obtained from CASSCF(2,5). By using this

active window, we have been able to skip convergence problems arising from small occupation numbers while still capturing the main electron correlation features.

Once we have set the optimal level of theory, we have computed singlet and triplet states for several harmonic confinements with parameter k extending to several orders of magnitude. For each value of k and each spin state, we have analysed the resulting density of electrons using equation (2.3) where the functions $\varphi_i(\mathbf{r})$ are the natural orbitals and the coefficients γ_i are the occupation numbers. Some illustrative density profile plots are shown in figure 2.1.

$$\rho(\mathbf{r}) = \sum_{i=1}^{5} \gamma_i \varphi_i^*(\mathbf{r}) \varphi_i(\mathbf{r}) \tag{2.3}$$
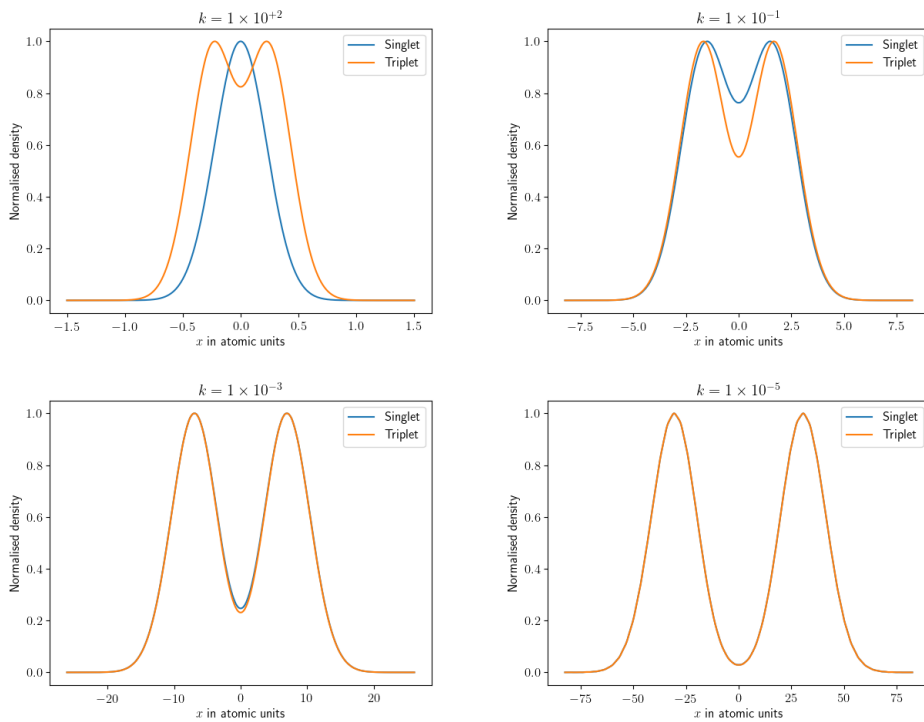
Figure 2.1: Normalised density profiles for singlet (blue) and triplet (orange) spin states for several confinement strengths k. Notice in the weak confinement limit, both profiles are alike and they differ in the strong confinement limit.

As it can be seen in figure 2.1, the density profile depends on the confinement parameter k and the spin state of the system. Computing the density evaluated at the maxima $\rho(x_{max})$ and the density evaluated at the minimum of the potential

well $\rho(0)$ for both spin states, we may define a measure of localization as the relative height of the density difference with respect to the density evaluated at the maximum, i.e. $\frac{\rho(x_{max})-\rho(0)}{\rho(x_{max})}$. The obtained values of this parameter for several k values are given in figure 2.2. As it can be seen, for small values of k (smaller than 1×10^{-6}) both spin states have similar location indices which are close to 1; that is, location is really happening and we shall say there is a Wigner molecule. As k increases, the location index of both spin states drops at the same rate until at a certain point around $k = 1 \times 10^{-4}$ they split. From this point on, the location index decreases faster for the singlet state than for the triplet one and at a certain point in between $k \in (1, 10)$ it drops to zero while the index for the triplet state converges asymptotically to a finite value given as $1 - \frac{e^{1/2}}{2} \approx 0.1756$. This last value corresponds to the one obtained for two independent harmonic oscillators one in the state $n = 0$ and the other one in $n = 1$ for which the density is given as $\rho(x) = \phi_0^2(x) + \phi_1^2(x)$. Therefore, we shall observe that for large values of k since the one-body energy is larger than the two-body one the correlation effects on the system are less relevant.
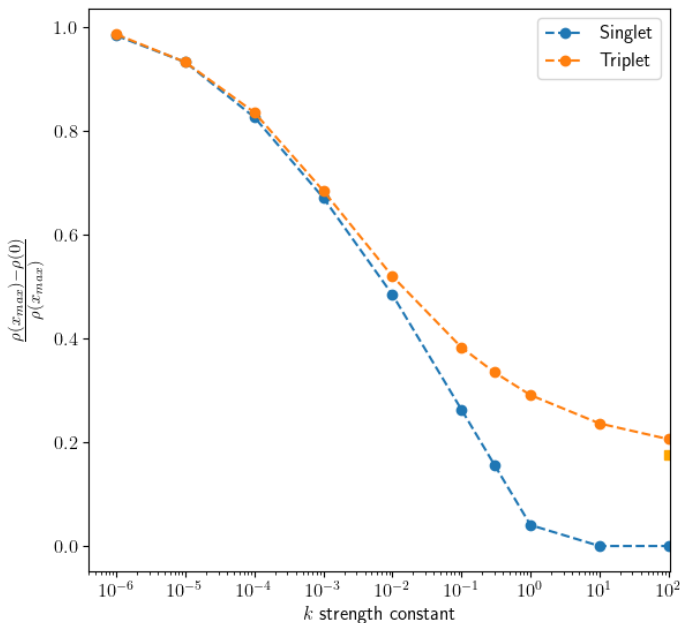
Figure 2.2: Variation of the location parameter with respect to the confinement parameter k for singlet and triplet states, the orange square represents the asymptotic limit for location index of the triplet state.

With the aim of gaining a deeper understanding of the monodeterminantal character of our system, we have studied how this character changes with respect to the confinement parameter k. After having performed further calculations at the same level of theory for several values of k for the high spin state, we have computed the particle-hole entropy given by equation (2.4) where the sum is done upon the natural orbitals. The obtained results are plotted in figure 2.3 where the trend for larger values of k has also been reported via exact computations [40, 41]. As it can be seen, we have obtained points in k for which the multideterminantal nature starts to arise, i.e. around $k = 1 \times 10^{-5}$, reaches a maximum around $k = 1 \times 10^{-3}$ and then goes to zero for large values of k.

$$S(k) = -\sum_{i=1}^{5} \gamma_i \log \gamma_i + (1 - \gamma_i) \log(1 - \gamma_i) \tag{2.4}$$
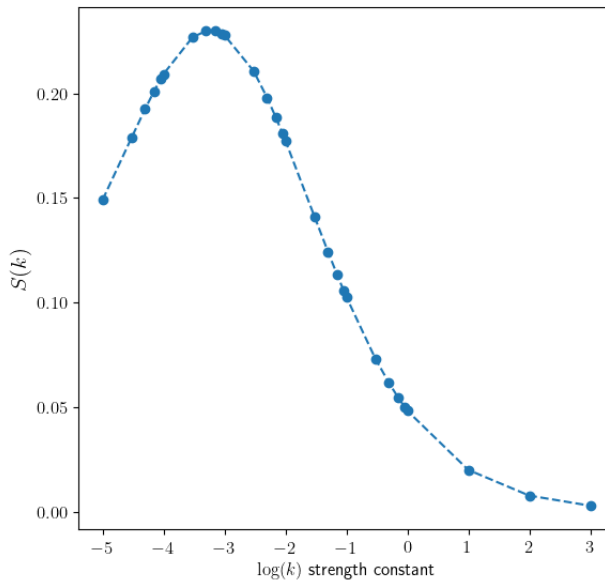
Figure 2.3: Particle-hole entropy for two electron system in high spin state for several values of confinement parameter k. Maximal entropy value is found for a value around $k = 1 \times 10^{-3.3}$

As we have stated, for large k values the independent particle model is a rather good description of our system and, based on the particle-hole entropy, the system can also be represented by a single determinant. Therefore, in the large confinement limit the resulting Fermi liquid is a quasi-monodeterminantal system and the particle-hole entropy will be zero. On the other hand, in the limit $k \to 0$ the system crystallizes

such that the two electrons localize (see figure (2.2)) and they can be said to form a Wigner molecule. Since this system is localized, and it is in the high spin configuration, it can also be described using a single determinant. Thus, in this limit, the particle-hole entropy of the Wigner molecule is also zero. Hence, we may infer the following behaviour: the two limit cases i.e. the Wigner molecule ($k \to 0$) and the Fermi liquid ($k \to \infty$) are monodeterminantal systems and their particle-hole entropy is zero. Nevertheless, as it can be seen in figure (2.3), this entropy varies as the confinement parameter increases such as it obtains a maximum value. Therefore, by increasing the confinement parameter k we connect the two monodeterminantal states by a path in which the multiconfigurational character of the system has a maximum. Boldly speaking, this can be seen as a transition state that connects the Wigner molecule with the Fermi liquid.

2.3.1.1 *Understanding the results using a minimal basis model*

With the aim of understanding how the two electron system behaves as the harmonic confinement parameter k changes, we have set up two analytical models with minimal gaussian functions. On the one hand, we have used a single gaussian basis with exponent α centered at the minimum of the harmonic potential given by equation (2.5) which will represent the required doubly occupied orbital for the singlet state $^1\Sigma_g = \sigma_0^{\uparrow\downarrow}$.

$$\sigma_0(\mathbf{r};\alpha_0) = \left(\frac{2\alpha_0}{\pi}\right)^{3/4} \exp(-\alpha_0\mathbf{r}^2) \tag{2.5}$$

On the other hand, we may place two gaussian functions, one on each classical equilibrium position given by $x_0 = \pm 1/(4k)^{1/3}$. Since these basis functions are not orthogonal, we may adapt them by symmetry and normalize them. As a result, we obtain an even function σ_g and an odd one σ_u given by equations (2.6) and (2.7) respectively. By using this functions, we can occupy each orbital by one electron with parallel spins obtaining a triplet state $^3\Pi_u = \sigma_g^{\uparrow}\sigma_u^{\uparrow}$.

$$\sigma_g(\mathbf{r};\mathbf{r}_0,\alpha_1) = \frac{1}{(2\pi)^{1/4}\sqrt{\frac{e^{2\alpha_1 x_0^2}+1}{\alpha_1^{1/2}}}}\left(e^{-\alpha_1(\mathbf{r}-\mathbf{r}_0)^2} + e^{-\alpha_1(\mathbf{r}+\mathbf{r}_0)^2}\right) \tag{2.6}$$

$$\sigma_u(\mathbf{r};\mathbf{r}_0,\alpha_1) = \frac{1}{(2\pi)^{1/4}\sqrt{\frac{e^{2\alpha_1 x_0^2}-1}{\alpha_1^{1/2}}}}\left(e^{-\alpha_1(\mathbf{r}-\mathbf{r}_0)^2} - e^{-\alpha_1(\mathbf{r}+\mathbf{r}_0)^2}\right) \tag{2.7}$$

In analogy to the H_2 molecule, this method is not able to describe dissociate singlet states [13]; nevertheless, the singlet and triplet states are quasi degenerate in the infinite dissociation limit. Bearing this in mind, we shall model the corresponding Fermi liquid as two electrons occupying a single gaussian orbital with singlet spin state and the Wigner molecule as two electrons occupying two different symmetry-adapted orbitals with triplet spin state.

For the singlet state in the minimal basis σ_0, the quasi-1D Hamiltonian contains three terms: the 3D kinetic energy, the 1D harmonic external potential and the 3D electron-electron interaction. Once the transverse components of the kinetic energy are removed, we obtain $T(\alpha_0) = \alpha_0$, the external potential energy $V(\alpha_0, k) = \frac{k}{4\alpha_0}$ and the two-electron energy $V_{ee}(\alpha_0) = 2\sqrt{\frac{\alpha_0}{\pi}}$; thus, the energy of the singlet with minimal basis can be written as in equation (2.8).

$$E(\alpha_0, k) = \alpha_0 + \frac{k}{4\alpha_0} + 2\sqrt{\frac{\alpha_0}{\pi}} \tag{2.8}$$

As a first approach, if we neglect the third term, given by the Coulomb repulsion, the non-interacting Singlet solution is given by $\alpha_{0,opt} = \sqrt{k}/2$, with a total energy of $E_{0S}(k) = k^{1/2} + k^{1/4}(2/\pi)^{1/2}$, this approximation is valid for *large* values of k. Therefore, although the Coulomb term of the energy is divergent for large values of k, the corresponding wavefunction will asymptotically converge to the non-interacting harmonic oscillator one. Notice that $E_{0S}(k)$ is an upper bound to the exact singlet energy $E_S(k)$. The complete minimization gives a four-degree polynomial equation in terms of $\alpha_0^{-1/2}$, i.e. $-\frac{k}{4}(\alpha_0^{-1/2})^4 + \frac{2}{\sqrt{\pi}}(\alpha_0^{-1/2}) + 1 = 0$. Considering Descartes's rule of signs, one shall realize that this equation has a single real positive root, thus the optimal value of the exponent $\alpha_{0,opt}$ is unique and can be obtained by using the quartic formula. Hence, if the exponent α_0 is optimized for all confinement strengths k, the singlet energy is only a function of k.

We continue our analysis with the triplet state. We consider first the non-interacting triplet, whose energy is obtained if we do not take into account the inter-electronic repulsion. The triplet energy is given by the sum of the two lowest levels of the harmonic oscillator, $\frac{1}{2}\sqrt{k}$ and $\frac{3}{2}\sqrt{k}$, thus $E_{0T}(k) = 2\sqrt{k}$. As it has been claimed in previous sections, since minimal number of orbitals for describing the triplet spin state is two, we may use the symmetry adapted orthonormal minimal basis $\{\sigma_g, \sigma_u\}$. The main advantage of using these basis functions is that they have even and odd parity with respect to the origin. Hence, since both, kinetic and potential energy operators are even, all off-diagonal elements are zero and, therefore, the one-body Hamiltonian is diagonal. These matrix elements are gives by:

$$T_{g,g}(\alpha_1; x_0(k)) = \frac{\alpha_1}{2}\frac{(1 - 4\alpha_1 x_0^2 + e^{2\alpha_1 x_0^2})}{1 + e^{2\alpha_1 x_0^2}} \tag{2.9}$$

$$T_{u,u}(\alpha_1; x_0(k)) \;=\; \frac{\alpha_1}{2} \frac{\left(-1 + 4\alpha_1 x_0^2 + e^{2\alpha_1 x_0^2}\right)}{1 + e^{2\alpha_1 x_0^2}} \tag{2.10}$$

$$V_{g,g}(\alpha_1, k; x_0(k)) \;=\; \frac{k}{8\alpha_1}\left(\frac{1 + e^{2\alpha_1 x_0^2}(1 + 4\alpha_1 x_0^2)}{1 + e^{2\alpha_1 x_0^2}}\right) \tag{2.11}$$

$$V_{u,u}(\alpha_1, k; x_0(k)) \;=\; \frac{k}{8\alpha_1}\left(\frac{-1 + e^{2\alpha_1 x_0^2}(1 + 4\alpha_1 x_0^2)}{-1 + e^{2\alpha_1 x_0^2}}\right) \tag{2.12}$$

For the one body energies, one shall remark the following aspects: given a non zero value for x_0, in the limit for large values of α_1, the kinetic energy converges to $\frac{1}{2}\alpha_1$, which is the kinetic energy of an electron trapped in a one-dimesional gaussian box. Besides, also for large values of α_1, the potential energy converges to $\frac{1}{2}kx_0^2$ which is the classical potential energy for a particle at positions $x = \pm x_0$.

Finally, the last interaction to take into account is the electron-electron repulsion. For the triplet spin state, there are two contributions: the Coulomb repulsion $(gg|uu)$ and the exchange interaction $(gu|gu)$. Evaluating the corresponding integrals, the interelectronic interaction is given by:

$$V_{ee}(\alpha_1; x_0(k)) = (gg|uu) - (gu|gu) = \frac{e^{4\alpha_1 x_0^2}}{e^{4\alpha_1 x_0^2} - 1}\left(\frac{\mathrm{erf}(2x_0\alpha_1^{1/2})}{2x_0} - 2\sqrt{\frac{\alpha_1}{\pi}}e^{-4\alpha_1 x_0^2}\right) \tag{2.13}$$

The first term in equation (2.13) corresponds to Coulombic repulsion while the second one (which is rapidly decreasing with the distance between the centres) is the exchange interaction. Also for V_{ee}, one shall observe that for a given non-zero value of x_0, in the large α_1 limit, the corresponding electron-electron interaction energy is given as $V_{ee} = \frac{1}{2x_0}$ which is the classical energy of two point particles at positions $x = \pm x_0$.

Employing all these integrals, we can express the energy of the triplet state as in equation (2.14). Once again, since α is variational and x_0 is given by k, we shall optimize the former parameter for each confinement strength k. As the function in terms of α is rather complex, we have adopted a numerical procedure to minimize the triplet energy for all k by varying α.

$$E_T = T_{gg} + V_{gg} + T_{uu} + V_{uu} + V_{ee} \tag{2.14}$$

Bearing all this in mind, we have obtained the corresponding energy curves for the singlet and the triplet spin states as a function of the confinement strength

k as can be seen in figure 2.4. For small values of k, both states are very close in energy while the triplet state is a bit bellow the singlet state, but for some value around $k = 5 \times 10^{-4}$ both lines cross and then the triplet state is higher in energy for all k. It is convenient to recall that for large k, the energy of the triplet state goes as $E_{0T} = 2k^{1/2}$ while the energy of the singlet state goes as $E_{0S} = k^{1/2} + (2/\pi)^{1/2}k^{1/4}$.
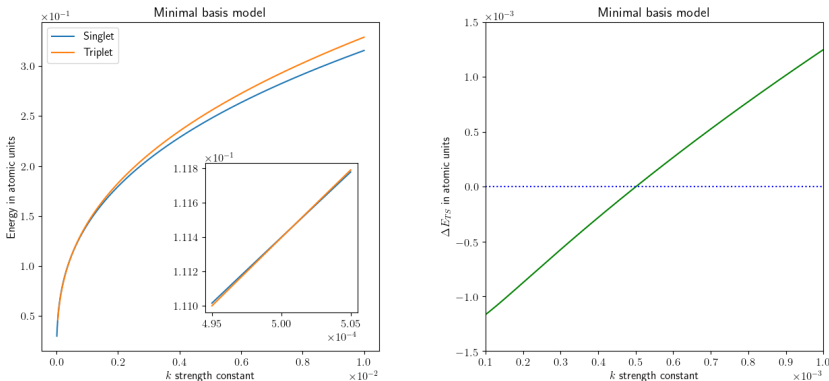
Figure 2.4: Energies for singlet and triplet spin states using minimal gaussian basis (left) and energy difference between the singlet and the triplet states for the two electron system using minimal basis (right). The zero energy gap happens around a value close to $k = 5 \times 10^{-4}$.

Considering the minimal basis model, we have shown that below a particular small value of k, the triplet state (which represent the more localized system) is lower in energy than the singlet state (which represents the less localized system) and beyond $k \approx 5 \times 10^{-4}$ we find the opposite situation. Thanks to this simple model, we have been able to determine the order of magnitude of k for which localization may happen.

2.3.2   Systems of three and four electrons

Based on the results of the previous section concerning two electron systems, we may briefly study systems composed by three and four electrons and see if we obtain similar behaviours. Bearing in mind the observed properties of the two electron system, we have constrained ourselves to the high spin state upon which CASSCF$(n, 2n)$ calculations (being n is the number of electrons) with the grid of gaussian basis functions stated in the previous sections have been performed. The obtained densities are shown in figure 2.5. Once again, we have computed the particle-hole entropies using the occupation numbers for each systems and the obtained results are graphically represented in figure 2.6.

As it can be seen, even though both curves have similar shape, the value of k for which the entropy is maximum depends on the number of electrons (the larger the number of electrons, the smaller the value of k at which the entropy reaches its maximum). We shall infer that the behaviour is similar to the two electron system and thus the conclusions are equivalent. In the light of these results, we shall define a kind of transition state taking place at the maximal entropy point $S(k_{max}, n)$ such that connects the Wigner molecule and Fermi liquid states. The size and position of such transition state depends, of course, on the number of electrons.
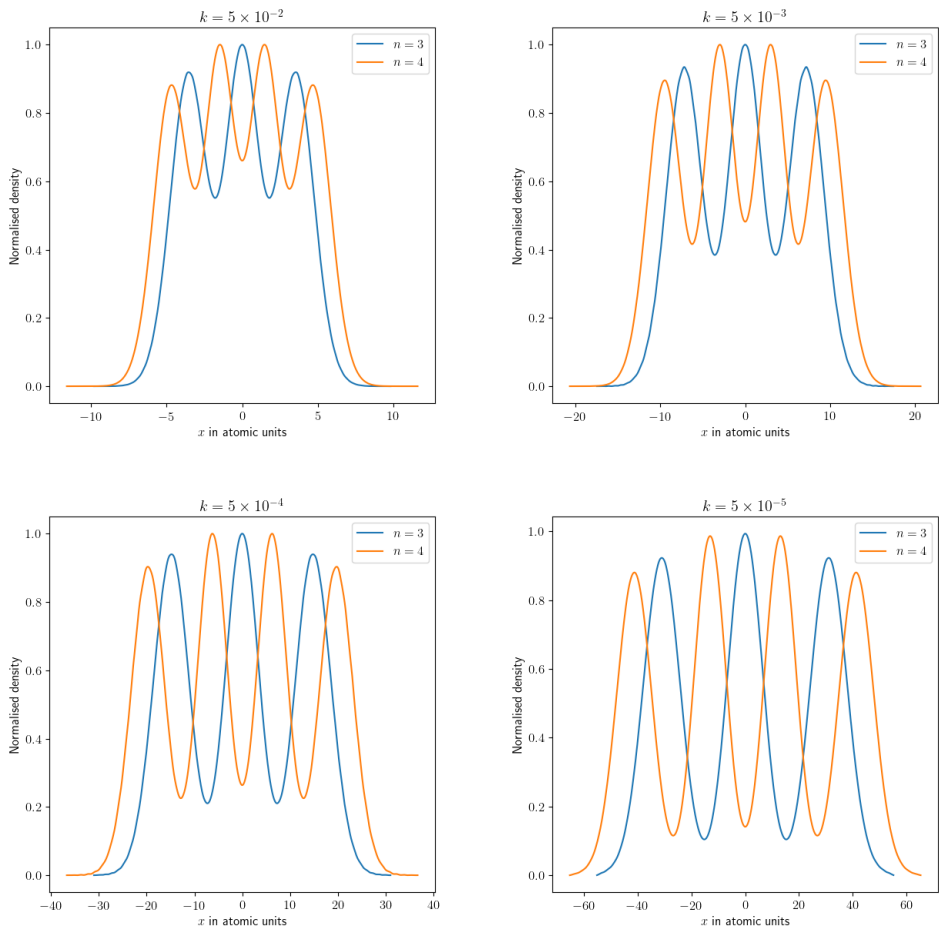
Figure 2.5: Normalised density profiles for three (blue) and four (orange) electron systems in high spin configuration for several confinement strengths k.
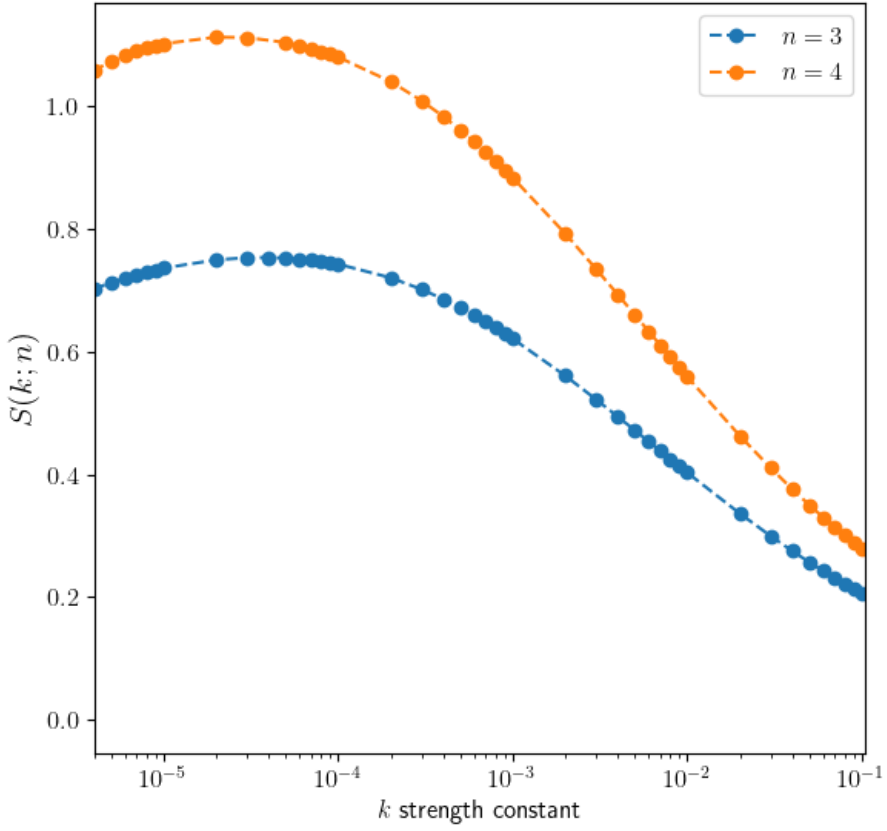
Figure 2.6: Computed electron-hole entropies for $n = 3, 4$ number of electrons with high spin state for several values of the confinement parameter k.

2.4   CONCLUDING REMARKS

In this chapter, we have studied systems composed by two, three and four electrons confined in a quasi-one-dimensional harmonic potential characterised by the confinement parameter k.

For the two electron system, we have obtained analytical formulations using a minimal basis set and a one-determinant wavefunction. In this way, we have been able to model the Wigner-molecule regime as a triplet with two identical gaussians basis functions and the Fermi liquid regime as a singlet with a single gaussian basis function. Using this scheme, we have minimized the energy of each system for several values of the confinement parameter k and have seen that a crossing between the two types of wavefunctions happens around $k = 5 \times 10^{-4}$. This indicates that, at this level of theory, some change in the nature of the wavefunction must take place around this value.

Basis sets composed of a large number of overlapping gaussian functions were also used in order to approach the limit of a complete basis set. We performed a scan of electronic structure derived properties such as one-particle density and particle-hole entropy and both indices coincide that for k values around 1×10^{-4} and 1×10^{-3} a transition is taking place either because the location index for the singlet and the triplet state start to diverge or because the particle-hole entropy reaches a maximum. Anyhow, the order of magnitude of k at which the transition starts is the same as the one obtained by the simplified model.

Extending the study to high-spin states concerning three and four electrons systems, we have observed the same behaviour. In the two limit cases, the density and the particle-hole entropies correspond to the ones expected for the Wigner molecule $(k \to 0)$ and the Fermi liquid $(k \to \infty)$. By varying the confinement parameter k, we have computed a smooth path connecting these extreme states such that the particle-hole entropy reaches a maximum. For very small values of the confinement parameter, we have obtained some numerical instabilities and have not obtained reliable information on how the hole-particle entropy behaves in this regime. Further work concerning the study of this regime can be done in a close future.

Chapter 3

QUASI-TWO DIMENSIONAL SYSTEMS

In this chapter, the process for obtaining optimal gaussian basis sets distributed in a hexagonal grid for modelling harmonically confined two dimensional systems is described. As a first step, these basis functions are optimized by means of the variational principle for one-body systems and the obtained results are compared to analytical energies. As a result, the obtained numerical values for the energies are not only accurate with respect to the analytical ones, but also degeneracy is preserved. Using properly optimized neural networks, we have been able to obtain general optimal basis functions for arbitrary values of the confinement parameter k in the range $(1 \times 10^{-9}, 1 \times 10^{1})$. The quality of the obtained basis functions increases with the number of functions and perform better for larger values of the confinement parameter k.

In progress

3.1 INTRODUCTION

A vastly employed practice in electronic structure simulations is to expand the corresponding many-body wave function in terms of one-electron basis functions. In the particular case of quantum chemistry, the most popular basis functions are gaussian functions sitting on each of the nuclei which compose the studied chemical system [142–144]. Besides, the use of floating gaussians includes some flexibility to better describe spread electronic density without the need of including an explicit nucleus [138, 145–149].

As it has been shown in previous works, distributed s-type gaussian orbitals are rather good basis functions for describing many-body fermionic systems [130, 138–140]. This approach may be employed to study two dimensional quantum systems which have wide experimental and theoretical interest [150–153]. However, the scale of some systems is of the order of the nanometer, for which if a single centre is considered, linear dependency problems will happen. In order to set an example, experimentally, Quantum Dots based on Graphene (GQD) and Transition Metal Dichalcogenides (TMDs) have been synthesised in a range of sizes in the interval 1-7 nm [154–163]. Among them, GQD with visible light photo-luminescence have diameters around 1.0-2.5 nm [164, 165]. With respect to moiré cells (as generalising Mott physics), the densities of such states are of the magnitude of $1 \times 10^{16} e^-/m^2$ [166–171] and for smaller densities, some author indicate the presence of Wigner crystallisation [172–175]. Since for such low densities (as it was firstly predicted by Wigner himself [20] and experimentally confirmed for 2D systems [176, 177]) the inter-electronic interaction energy is larger than the kinetic one, it is vital to describe the electron-electron interaction using accurate techniques [37, 39, 40, 42–64]. Bearing this in mind, setting a quantum chemical approach to model such large systems is crucial. We shall test the validity of our approach to describe Wigner location in many electron systems.

The final aim of this work is to obtain an optimal two-dimensional hexagonal mesh composed by s-type orbitals being α the exponent of such orbitals and δ the distance between closest neighbours. These two parameters are selected such that given a harmonic confinement strength k, the size of the mesh and a parameter ξ that indicates the overlap between neighbouring orbitals, one gets the minimal one-particle energy. With the aim of getting general tunable basis sets, an Artificial Neural Network has been trained to produce the optimal mesh. Once the basis set is optimised for given input parameters, we have used quantum chemical methods for computing properties concerning the electronic structure of harmonically confined systems of electrons. By doing so, all technologies employed in this field concerning high level methods such as the multi-reference ones can be applied in larger number of electrons.

3.2 COMPUTATIONAL PROTOCOL

3.2.1 Distributed Gaussian orbitals

Hexagonal grids composed by 3D s-type Gaussian orbitals given as in equation (3.1) have been employed. The number of gaussian functions is given by $M = 3g^2 - 5g + 1$ where $g \geq 3$ is related to the number of shells in the hexagonal pattern. In figure 3.1 a schematic representation of the geometry of the basis set is given for several values of g number.

$$\phi_i(\mathbf{r}; \alpha, \mathbf{R}_i) = \left(\frac{2\alpha}{\pi}\right)^{3/4} \exp(-\alpha(\mathbf{r} - \mathbf{R}_i)^2) \tag{3.1}$$
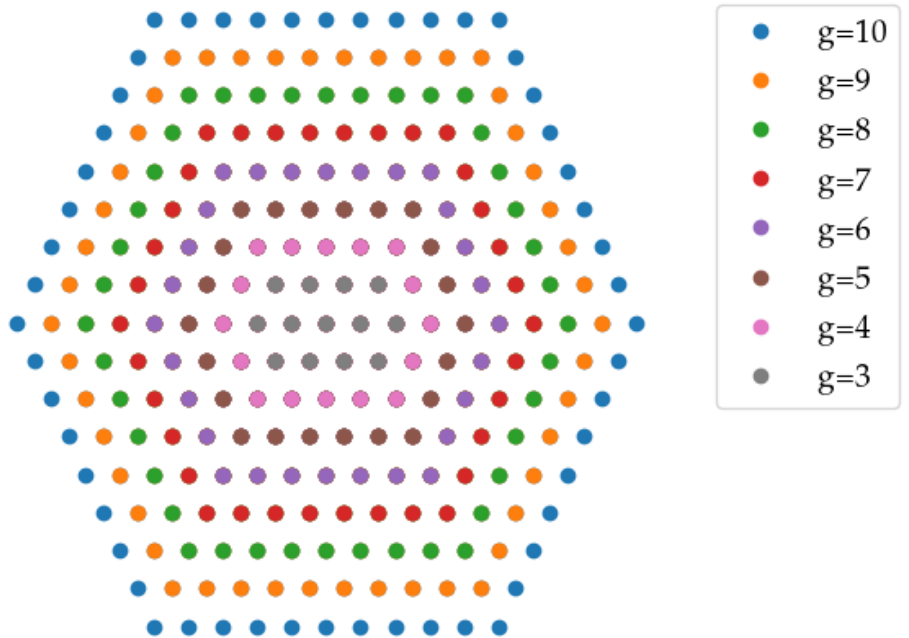
Figure 3.1: Geometry of the distributed gaussian functions according to g number. All distances between closest neighbours is given by the parameter δ.

Using this setting, all basis functions had the same exponent α and since the set $\{\mathbf{R}_i\}_M$ gives rise to a hexagonal pattern the distance between closest neighbours is the same for any two of them. The overlap between close-neighbouring functions is given as $S(\alpha, \delta) = \exp(-\alpha\delta^2/2)$ where δ is the distance between the stated neighbours. One may also rewrite the last overlap function in terms of a dimensionless parameter given as $\xi = \alpha\delta^2$ as $S(\xi) = \exp(-\xi/2)$; such dimensionless parameter characterizes the resolution of the basis set and controls the value of the entries of the overlap matrix. Due to the fact that too small values for ξ give rise to linear dependency problems (the overlap matrix becomes singular) while too large values imply that the overlap is not good enough to describe a continuous space, the optimal value of ξ has an upper and lower bound. Previous works have shown that this parameter must belong in a narrow interval around $\xi = 1.00$; in this work, we have taken several values in the interval $\xi \in [0.85, 1.15]$ [130, 138–140].

3.2.2 Quantum mechanical computations

In a first step, we have studied one-body problems using isotropic harmonic confinement potentials. For such systems, the general Hamiltonian is given by equation (3.2) which is separable (one term for each coordinate). Therefore, the ground state energy for the isotropic 2D harmonic oscillator is given as $E_0 = k^{1/2}$.

$$H(x,y) = \frac{1}{2}\left(-\partial_x^2 + kx^2 - \partial_y^2 + ky^2\right) = H(x) + H(y) \tag{3.2}$$

Using the basis described in the previous section, we can rewrite the corresponding one-body Schrödinger equation as a generalised eigenvalue problem (3.3) where $\mathbf{S}$ is the overlap matrix, $\mathbf{T}$ is the kinetic energy matrix, $\mathbf{V}$ is the potential energy matrix and $\mathbf{E}$ is the diagonal matrix containing the eigenvalues of the Hamiltonian while $\mathbf{C}$ contains the eigenvectors in its columns.

$$(\mathbf{T} + \mathbf{V})\mathbf{C} = \mathbf{ESC} \tag{3.3}$$

The corresponding matrix elements are given by equations (3.4), (3.5) and (3.6) respectively; notice that the elements of the kinetic and potential energy depend on the elements of the overlap, thus they can be defined in the same loop. Since the basis function are three dimensional in nature, by solving the general eigenvalue problem, we obtain quasi-2D solutions. In order to correct the obtained energies, since all gaussian have the same exponent, we may factorize out the transverse component of the wavefunction and subtract the corresponding contribution to the kinetic energy, which in this case equals $\alpha/2$ per electron [138]. By doing so, we obtain the corresponding corrected energies which correspond to the equivalent 2D system.

$$S_{ij} = \exp\left(-\frac{\alpha}{2}d_{ij}^2\right) \tag{3.4}$$

$$T_{ij} = \frac{\alpha}{2}(3 - \alpha d_{ij}^2)S_{ij} \tag{3.5}$$

$$V_{ij} = \frac{k}{8\alpha}(2 + \alpha[(x_i^2 + x_j^2) + (y_i^2 + y_j^2)])S_{ij} \tag{3.6}$$

As it has been stated in the previous section, if we set the value of the exponent $\alpha = \xi/\delta^2$ for various values of ξ, by means of the variational principle, (given (ξ, g, k)) we may optimize the ground state energy with respect to the distance between the basis functions δ.

3.3 RESULTS AND DISCUSSION

3.3.1 One particle systems

In a first step, we aim to gain some knowledge of how to build an appropriate basis grid exposed in previous section for a given system. That is, for a given potential characterized by the confinement parameter k, a given real number ξ which controls the size of the entries in the overlap matrix and a given number of basis functions represented by g, what is the optimal distance between neighboring basis δ_{opt} for describing our system?

In order to answer this question, we have taken the following steps: we optimize the one particle ground state energy with respect to distance between neighbouring basis by solving the matrix Schrödinger equation for several values of (k, ξ, g). We aimed to gain experience on several orders of magnitude for $k \in [1 \times 10^{-10}, 9]$ and have employed $\xi \in [0.85, 1.15]$ with $g \in [4, 10]$ numbers. A total number of 1190 optimized basis sets were obtained using the Brent optimization scheme for convex functions.

As a result of those optimizations, we extracted the first ten eigenvalues of the Hamiltonian and have compared them to the analytical values such that we obtain the relative error given as $\epsilon = \frac{E_i - E_{0,i}}{E_{0,i}}$ where E_i is the energy of the i-th state and $E_{0,i}$ is the corresponding analytical value. Results for such errors for optimized basis sets are given in figure 3.2. As it can be seen, even if this error gets larger for higher energy states, the maximal error in all the samples is of the order of 5 %. Another feature to be considered is the fact that not only the relative error must be taken into account, but also the fact that analytically degenerate states should remain degenerate in the numerical approach. In order to measure the difference of energy in each energy level for several states given (k, ξ, g) we have computed the relative standard deviation of each set and then performed statistics among all standard deviations. As it is shown in figure 3.2, the maximal relative standard deviation

is also of the order of $10^{-4}\%$, that is, in the worst case scenario levels that should be degenerate are not by an estimate of relative energy difference of 10^{-4}. Largest errors have been obtained by using small number of basis functions ($g = 4$) and large values for the overlap index $\xi = 1.15$; in the light of such evidence, we conclude that the optimized basis are rather good and they get better for larger values of ξ (in the studied domain) and g for all values of k. Hereafter, we will refer to the obtained data set as $\mathcal{D}$.
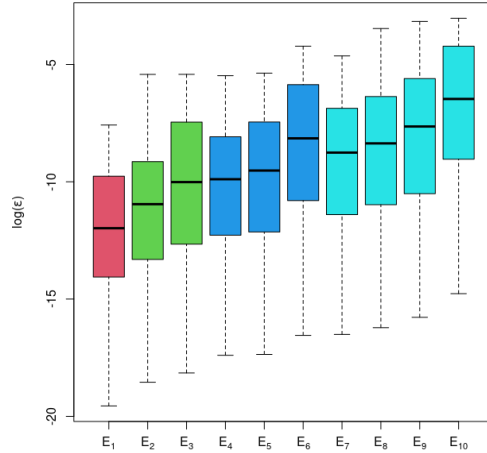
(a)
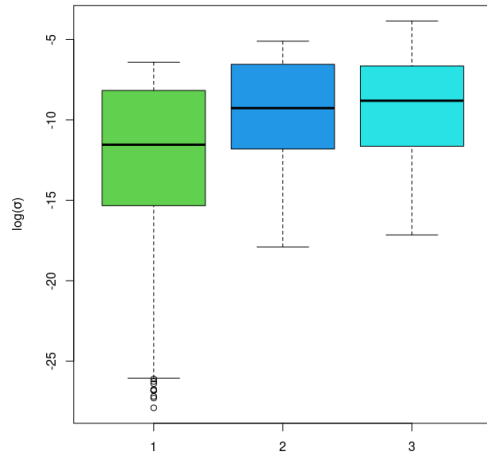
(b)

Figure 3.2: Logarithm of absolute errors (a) and standard deviations (b) for the ten first states and the first three degenerate groups with $(n_x + n_y) = \{1, 2, 3\}$. Same color state represent analytically degenerate states.

So far, we have discussed how given a confinement strength parameter k, an overlap controlling parameter ξ and a total number of basis functions given in terms of g, optimal values for the exponent and closest neighbour distances in an hexagonal grid can be obtained by minimizing the system's energy with respect to the latter parameters. The obtained optimal solutions do not only give accurate energies of the first ten states, but also preserve the degeneracies of each level. Hence, so far we have been able to obtain a data set which includes optimal grid and exponent parameters for several simulation conditions; now we shall pose the following question: we have stated that the obtained basis set are adequate for describing one-particle systems confined in two-dimensional harmonic potentials in the given data set $\mathcal{D}$ where δ_{opt} depends on the triad (k, ξ, g). However, there is an infinite amount of triads which are out of the data set and for which explicitly computed δ_{opt} values are not included. It is therefore necessary to infer a function $F : \mathbb{R}^2 \times \mathbb{N} \to \mathbb{R}$ such that $F(k, \xi, g) = \delta_{opt}$ for any arbitrary input. How can it be done?

In this chapter, we have tackled the problem by using neural networks as estimates for such F function. Since k and δ_{opt} expand over several orders of magnitude these variables are skewed; hence, the tail regions may act as outliers which adversely affect the performance of any regression-based model. In order to sidestep this problem, log transformations were performed upon the stated variables such that we obtain models of the form $f(\log k, \xi, g) = \log \delta_{opt}$.

Concerning the structure of the neural networks, we have used sigmoids as activation functions and the network was optimized by back propagation with quadratic loss function. We have trained and tested several models using 80% of entries chosen at random in $\mathcal{D}$ for building the training set $\mathcal{L}$ and the remaining 20% for building the testing set $\mathcal{T}$ for obtaining an estimate of the error for the predicted variable $\log \delta_{opt}$. Notice that in this case, the error of the predicted variable $\Delta(\log \delta_{opt})$ is an estimate of the relative error for δ_{opt}.

In order to obtain an optimal model, we have built several networks using two hidden layers with (i, j) neurons in each layer with $\{i, j\} = \{3, 4, 5, 6, 7\}$ and have computed the estimated 10-fold cross validated quadratic error $\Delta(\log \delta_{opt})$ for each of them. The errors of these models are represented in figure 3.3 using brighter colors for representing smaller relative errors. As it can be seen, for all models the relative error of the predicted δ_{opt} is in the range (2.75%,3.3%). The model for which the minimal error was detected was the one with (6,4) neurons in the hidden layer and it yielded a relative error of 2.75% in the estimation of δ_{opt}.

Since the optimal value of exponent of the gaussians is determined by (δ_{opt}, ξ), we may obtain an estimate for the error of the optimal exponent as $\Delta \alpha_{opt} = \frac{2\xi}{\delta_{opt}^2} \Delta \log \delta_{opt}$ which gets smaller for larger values of δ_{opt} which are obtained for small values of k. Therefore, the error of the estimated exponent gets smaller for smaller values of k. So far, we conclude the obtained basis sets many not be so performing for describing systems in loosely confined systems, i.e. for k values bellow 1×10^{-10}.
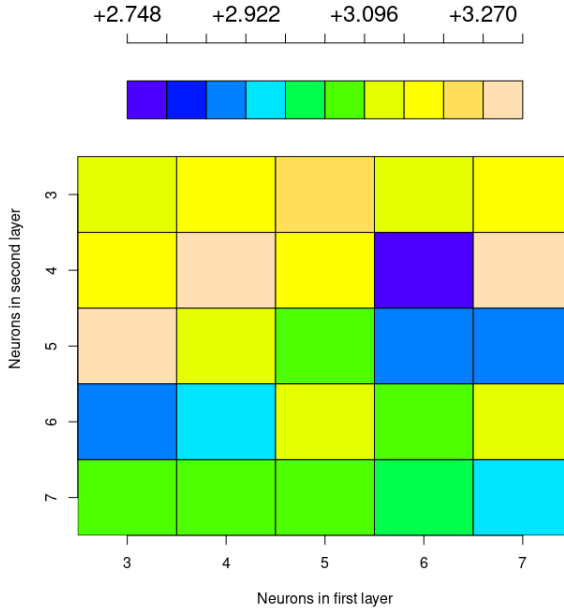
Figure 3.3: Obtained estimated relative errors for estimated δ_{opt} using various NN models consisting of two hidden layers with several number of neurons per layer.

In a nutshell, in this section we have developed a method for obtaining an estimate of optimal parameters of the basis function described in the corresponding section given a triad of numbers (k, ξ, g) which represent the strength of the confinement potential, the measure of the overlap matrix and the number of basis functions. By doing so, we are able to give an estimate for the distance between neighbouring basis with an estimated relative error of around 2.75% and the error of the estimated optimal exponent α_{opt} gets smaller for larger values of k.

3.3.2   Few particle systems

In order to test the validity of the obtained optimised basis sets for describing correlation effects, we have employed such basis for studying some systems concerning few electrons confined in two-dimensional isotropic harmonic potentials. The Hamiltonian employed for describing such systems is given by equation (3.7).

$$H = \frac{1}{2} \sum_{i=1}^{n} (k(x_i^2 + y_i^2) - \nabla_i^2) + \sum_{j>i=1}^{n} \frac{1}{r_{ij}} \tag{3.7}$$

One of the most characteristic observables derived from electron correlation effects are the Coulomb holes $h(u)$ which are defined as the difference in the intracule density $I(u)$ between correlated and uncorrelated wavefunctions. The explicit representation of the Coulomb hole function is given in equation (3.8) where $n_2(\mathbf{r}_1, \mathbf{r}_2)$ is the pair density and r_{12} is the module of the intracule coordinate, i.e. the interelectronic distance. This function gives a direct observable of the electron correlation effects and, in principle and by formulation, can be applied on any system with any symmetry. Nevertheless, since the quasi-two-dimensional systems studied in this work have cyllindric symmetry, an alternative function can be defined in order to describe the effects of electron correlation on the electronic density. In our approach, such function is given as in equation (3.9) which (instead of using the internal intracule coordinates) employs correlated and uncorrelated density functions along the radial coordinate r. That is, both densities are averaged over the angular and cylinder height coordinates.

$$h(u) = I^{corr}(u) - I^{uncorr}(u), \quad I(u) = \int n_2(\mathbf{r}_1, \mathbf{r}_2)\delta(u - r_{12})d\mathbf{r}_1\mathbf{r}_2 \qquad (3.8)$$

$$\tilde{h}(r) = \rho_{corr}(r) - \rho_{uncorr}(r), \quad \rho(r) = \int |\Psi(r, \theta, z)|^2 r d\theta dz \qquad (3.9)$$

In order to illustrate the effects of electron correlation on the density, we have computed the function given by equation (3.9) for two and three electrons ($n = \{2, 3\}$) in low and high spin states respectively. In these configurations, the Hartree-Fock orbitals are either doubly or singly occupied and all degenerate orbitals have the same occupation number. The required correlated and uncorrelated densities were computed at CASSCF($n, 8$) and unrestricted Hartree-Fock (UHF) levels of theory respectively using several confinement parameters k. For each confinement parameter, optimal gaussian exponents were obtained by means of the trained neural network model using a total number of 153 basis functions ($g = 8$) and closest neighbour overlap values $S = e^{-1/2}$ (that is $\xi = 1.00$); the obtained $\tilde{h}(r)$ functions are plotted in figures 3.4 and 3.5. For both systems, we shall observe some common features: firstly, for a given k, the correlated density is smaller than the uncorrelated one for regions closer to the origin (small values of r) and gets larger than the uncorrelated system for larger distances. Based on mass conservation, this observation suggests that correlated electrons expand in space in order to minimize Coulombic interactions. Second, as the value of the confinement parameter increases, the $\tilde{h}(r)$ function is contracted in space and the mass flow is sharper; that is, observed density decrease and increase happen more abruptly.
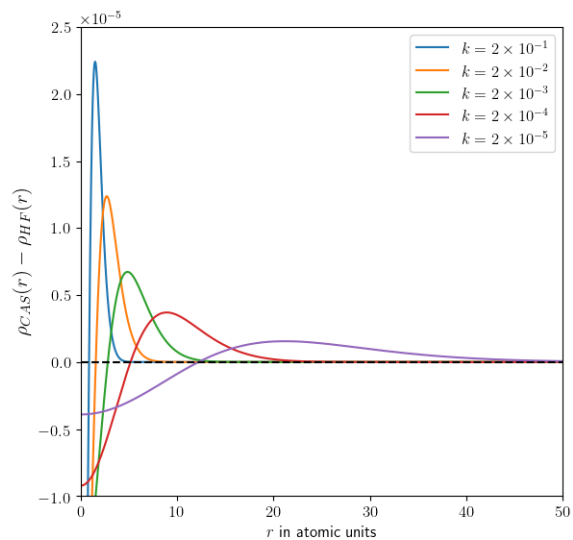
Figure 3.4: Density difference between the CASSCF(2,8) and HF singlet spin wave-functions as a function of the distance with respect to the potential minimum for several values of k.
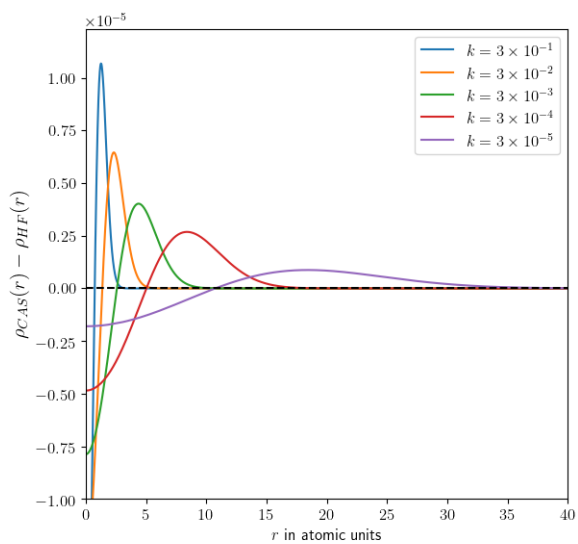
Figure 3.5: Density difference between the CASSCF(3,8) and HF quartet spin wave-functions as a function of the distance with respect to the potential minimum for several values of k.

3.4   CONCLUDING REMARKS

In this chapter, we have been able to obtain optimal gaussian basis sets distributed in a hexagonal grid for modelling harmonically confined two dimensional systems. As a first step, a data set (namely $\mathcal{D}$) containing entries relative to one-particle systems was obtained. These entries consisted of an optimal neighboring distance δ_{opt} for each triad of harmonic potential parameter, neighbouring-functions-overlap controlling parameter and number of total basis functions (k, ξ, g). The values of δ_{opt} have been obtained by diagonalizing the one-body Hamiltonian and optimizing the first root which, by means of the variational principle, is minimal. As it has been proofed, the obtained eigenvalues are not only accurate with respect to the analytical values, but also remain degenerate in the numerical frame. The maximal relative error for the eigenvalues was of the order of 5% while the maximal relative standard deviation in degenerate sets was of the order of 10^{-4}%.

Using this data set $\mathcal{D}$, two complementary sets were obtained, namely the training set $\mathcal{L}$ and the testing set $\mathcal{T}$ ($\mathcal{D} = \mathcal{L} \cup \mathcal{T}, \mathcal{L} \cap \mathcal{T} = \varnothing$). Using these sets, several neural networks consisting of two hidden layers were optimized such that given a triad $(\log k, \xi, g)$ an estimated value for $\log \delta_{opt}$ was obtained. The optimal network was obtained using six neurons in the first hidden layer and four neurons in the second one using sigmoids as activation functions. The network was optimized in order to minimize the quadratic loss function using a ten-fold cross validation scheme. As a result, the estimated relative error for the output values was of the order of 2.5% while the estimated error for exponents of the basis functions can be expressed as $\Delta \alpha_{opt} = \frac{2\xi}{\delta_{opt}^2} \Delta \log \delta_{opt}$ which gets smaller for larger values of k.

As an application of the obtained optimal basis sets for the study of correlation effects on many-particle systems, systems composed by two and three electrons in low and high spin states respectively were studied. In order to measure the impact of electron correlation, the difference in the density along the radial coordinate between CASSCF$(n, 8)$ and UHF wavefunctions were computed for k values in the range $(1 \times 10^{-5}, 1 \times 10^{-10})$ which lead to wavefunctions expanding in space the range of (20,100) atomic units. A decrease in density for small values of the radial coordinate and an increase in density for larger values of the radial coordinate for the correlated wavefunctions have been observed for both systems; this effect is more abrupt as the value of the confinement parameter k increases.

In conclusion, optimal distributed gaussian basis functions which extend in the real space range of (20,100) atomic units have been obtained by means of optimal neural networks. As future applications, such basis functions may be employed for describing systems of the size of two dimensional graphene quantum dots.

Chapter 4

SPHERICAL HOOKE ATOMS

Singlet and triplet spin state energies for three-dimensional Hooke atoms, i.e. electrons in a quadratic confinement, with even number of electrons (2, 4, 6, 8, 10) is discussed using Full-CI and CASSCF type wavefunctions with a variety of basis sets and considering perturbative corrections up to second order. The effect of the screening of the electron-electron interaction is also discussed by using a Yukawa-type potential with different values of the Yukawa screening parameter (λ_{ee}=0.2, 0.4, 0.6, 0.8, 1.0). Our results show that the singlet state is the ground state for 2 and 8 electron Hooke atoms, whereas the triplet is the ground spin state for 4, 6 and 10 electron systems. This suggests the following Aufbau structure $1s < 1p < 1d$ with singlet ground spin states for systems in which the generation of the triplet implies an inter-shell one electron promotion, and triplet ground states in cases when there is a partial filling of electrons of a given shell. It is also observed that the screening of electron-electron interactions has a sizable quantitative effect on the relative energies of both spin states, specially in the case of 2 and 8 electron systems, favouring the singlet state over the triplet. However, the screening of the electron-electron interaction does not provoke a change in the nature of the ground spin state of these systems. By analyzing the different components of the energy, we have gained a deeper understanding of the effects of the kinetic, confinement and electron-electron interaction components of the energy.

4.1   INTRODUCTION

Quantum dots have attracted considerable attention in the last years. The possibility of creating artificial atoms in which the electrons are confined to a center through a quadratic type potential opens the possibility of designing new nanoelectronic devices with properties at will, by precisely controlling the degree of confinement. For instance, transitions never observed in natural atoms can be obtained in the artificial ones, which could be of paramount importance in designing new lasers. [178] Another property that has attracted considerable attention is the determination of the triplet-singlet gap in confined systems, for their use as states of a qubit, or to implement logical gates in quantum computing. The excitation spectrum of two-electron two-dimensional (2D) quantum dots has been investigated by tunneling spectroscopy, [179] and the theoretical prediction of triplet-singlet transitions with increasing magnetic field has been experimentally corroborated. Although less studied, 3D quantum dots are also a subject of interest[86]. Examples of this are magnetically trapped fermion vapors confined by parabolic potentials[180, 181] or quantum defects in diamond crystals used as basic gadgets in quantum computing[182, 183].

One of the simplest and most adequate models used in theoretical studies concerning QDs are the so called Harmonium or Hooke's atom in which electrons are confined in a spherical harmonic potential [76]. Such models contain parameters that may be tuned in order to represent features corresponding to real QDs [77, 78]. For instance, work carried out in our group using a Hookean exact three-body model to examine electron correlation in a two-electron spherical quantum dot confirmed that triplet-singlet transitions take place as the externally applied magnetic field increases.[79] However, the limitation of using an exact model restricted our study to two-electron systems. That is, the analytical solutions[80] for specific curvature parameter of the two-electron Hooke atoms ($\omega^2 = \frac{1}{4}, \frac{1}{100} \ldots$) are well known, which can lead in principle to highly accurate densities for systems in low-correlation regimes ($\omega^2 \to \infty$) as well as in high-correlation regimes ($\omega^2 \to 0$) [35–38]. If similar systems containing larger number of electrons ($N_e > 2$) are to be considered, a richer variety of electronic states consisting on several ground state spin multiplicities and non-dynamical electron correlation (multi-determinantal features) arise [39–41]. Although such systems can be employed to understand many-body interactions, the computational cost increases with the size of the system.

As in Hooke model atoms, the incorporation of electron correlation effects has been shown to be essential for an adequate interpretation of the experimental spectra and transport properties in Quantum Dots. [81, 82, 84–86] In quantum dots, as opposed to real atoms, the effect of electron correlation may be varied at will through manipulation of the dimension and shape of the nanocrystal as well as of the strength, boundaries and symmetries of the confining fields[87]. Besides, the electron-electron interaction can be screened due to lattice, the doping or the charges induced on the metal gates[89]. This fact makes the quantum dot many-body problem more complex than the more familiar atomic case.

Finally, Hooke model systems have been repeatedly used in the calibration of electronic structure methods, for they provide very variable dynamic and non-dynamic electron correlation regimes [42–44] that pose a great challenge for current computational methods. [37, 45–57] Such calibration has been possible because of the recent availability of highly accurate analytical and benchmark data.[39, 40, 58–64]

Several well established methods for the elucidation of atomic/molecular electronic structure have been applied to quantum dots. Salient among these are diagonalizations of large configuration interaction representations of the Hamiltonian matrix (usually referred as "exact"diagonalizations)[184–189], Hartree-Fock (HF)[187, 190–192], coupled-cluster[193], density functional theory[194–197], and quantum Monte Carlo calculations[198]. Let us emphasize, however, that even for two-electron quantum dots,[199] it has been observed that in order to account properly for the electron correlation effects, one must go beyond perturbative schemes based on the independent-particle model or local spin-density functional theory.[179] Last but not least, some of us have found that the use of flexible basis set is crucial for a correct description of strong correlation effects in harmonium.[40, 54, 199] Work carried out in our group using a Hookean exact three-body model to examine electron correlation in a two-electron spherical quantum dot confirmed that triplet-singlet transitions take place as the externally applied magnetic field increases [79].

In the present paper, we address the orbital occupation pattern to establish the Aufbau principle for three-dimensional quantum dots with an even number of electrons (N_e=2, 4, 6, 8, 10). Full configuration interaction (Full-CI) for N_e=2, and complete active space self consistent field (CASSCF) type wavefunctions, for $N_e > 2$, are employed to account for electron correlation effects. On top of this, second-order perturbation corrections to these energies are also considered. Both the singlet and the triplet states will be evaluated in order to ascertain whether the ground state wavefunction is either spin unpolarized or spin polarized. This will provide, by the same token, the estimate of the triplet-singlet energy gap as the number of electrons of the quantum dots increases.

First, we have employed the Dunning's family of correlation consistent (CC) basis sets up to sextuple zeta. One should notice that these basis sets are optimized for Coulombic systems, and, therefore, for the sake of consistency, we have compared their accuracy with the available benchmark data. [39, 41, 62, 199] We report the full data as supplementary material. In summary, although these absolute energies do not reach full accuracy, the singlet-triplet gaps were in full agreement with the benchmark data, except for the ten-electron system for which qualitative differences were observed depending on which CC basis set was used. In order to further improve the performance of the basis set, we have optimized a set of even-tempered basis sets (ETBS hereafter) for the Hooke potential considering different number of electrons. After careful inspection, the best balance between accuracy and performance was obtained for the basis set optimized with six electrons in the singlet state, we call this basis set ETBS-6S, and it is the one mainly used throughout the paper.

Finally, we also introduce a model to take into account the screening of electron-electron interactions through an electron-electron Yukawa type potential (also known as Debye-Yukawa potential as reference to the Debye-Hückel theory so employed in the study of electrolytes and plasmas), as in prrevious works [200]. The screening in electron-electron interaction is often included by introducing an effective dielectric media [201–203]. In the present work, we analyze the use of a Yukawa potential, which at short range is similar to the Coulomb potential, to analyze the effect of the electron-electron screening in correlation effects. We observe that even for an extreme screening, correlation effects are still important, according to the corresponding Coulomb holes, highlighting the importance to adequately treat electron correlation in these systems.

4.2   COMPUTATIONAL METHODS

Let us consider the following generalized Hamiltonian operator (in atomic units) for our N_e-electron system:

$$\widehat{H} = -\sum_{i}^{N_e} \frac{1}{2}\nabla_{\mathbf{r}_i}^2 + \sum_{i}^{N_e} \frac{1}{2}\omega^2 \mathbf{r}_i^2 + \sum_{j>i}^{N_e} \frac{e^{-\lambda_{ee}r_{ij}}}{r_{ij}} \tag{4.1}$$

where $\mathbf{r}_i$ is the distance vector between the ith electron and the center of the harmonic potential, which for all the calculations of this paper is centered at the origin. This Hamiltonian represents a harmonically confined N_e-electron system, with a confinement strength ω^2, whose inter-electronic interaction has been screened statically by a Yukawa-like attenuated interaction potential, having a screening length λ_{ee}^{-1}.

Recall that for N_e=2 and λ_{ee}=0, the Hamiltonian operator of Eq. 4.1 corresponds to the two-electron Hooke atom, which can be separated into its intracular coordinates, namely, the electron-electron relative distance vector $\mathbf{r}=\mathbf{r}_1 - \mathbf{r}_2$ and the center of mass coordinate vector $\mathbf{R}=\frac{1}{2}(\mathbf{r}_1 + \mathbf{r}_2)$ as[80, 204]

$$\widehat{H} = -\frac{\nabla_{\mathbf{R}}^2}{4} + \omega^2 R^2 - \nabla_{\mathbf{r}}^2 + \frac{1}{4}\omega^2 r^2 + \frac{1}{r} \tag{4.2}$$

being $r = |\mathbf{r}|$ and $R = |\mathbf{R}|$, respectively. Eq. (2) unveils that the center of mass of the electrons will behave as a harmonic oscillator with a spring constant of $2\omega^2$ and a ground state energy of $E_{\mathbf{R}} = 3\sqrt{\omega^2}$. Likewise, Eq. (2) indicates as well, that the electrons will remain in the proximity of each other for they are retained within finite inter-electronic distances by the potential

$$V(r) = \frac{1}{4}\omega^2 r^2 + \frac{1}{r}, \tag{4.3}$$

which is best seen as an effective confinement potential. This model system is commonly known as Hooke atom, Hookean or harmonium.[205]

In summary, two types of systems have been considered in this paper:

- *Coulombic Hooke Atom:* The Hamiltonian includes an harmonic confinement term ($\omega^2 = 0.25$) with Coulombic like electron-electron repulsion ($\lambda_{ee} = 0.0$).

- *Yukawa Hooke Atom:* The Hamiltonian includes an harmonic confinement term ($\omega^2 = \frac{1}{4}$) and a Yukawa-type screened electron repulsion ($\lambda_{ee} = 0.2, 0.4, 0.6, 0.8, 1.0$).

The corresponding one-electron confinement integrals and the two-electron Yukawa-type integrals have been implemented by our group in an in-house code and the corresponding integral package interfaced with the `GAMESS-US` program [206, 207] to perform the calculations described in this work. HF, Full-CI, CASSCF and multireference second-order Möller-Plesset (MRMP2) methods were used along with various basis sets of aug-cc type, and optimized even-tempered basis set (ETBS) for 2, 4, 6 and 8 electrons systems. For each of the systems, the HF energy of the singlet state was calculated. The corresponding orbitals were used to perform Full-CI (in the case of 2-electron systems) and CASSCF and MRMP2 calculations in the case of 2, 4, 6, 8 and 10 electrons) for the singlet and triplet spin states.

As said in the introduction, we have employed two types of basis sets: i) standard Dunning's family of correlation consistent (cc) basis sets up to sextuple zeta and ii) even-tempered basis sets (ETBS) optimized for the Hooke atom. The drawback of aug-cc-pVNZ basis sets is that they are optimized for Coulombic systems. Therefore, we have compared their accuracy with the available benchmark data [39, 41, 62, 199] for Hookean systems. We report the full data as supplementary material, but in summary, the conclusion is that, although absolute energies with aug-cc-pVNZ basis sets do not reach full accuracy, the singlet-triplet gaps are in full agreement with the benchmark data. The only exception to this rule is the ten-electron system, which shows a more erratic behaviour with important qualitative differences concernig the ground state spin multiplicity among the various aug-cc-pVNZ basis sets.

In order to improve the absolute energies, we have optimized an even-tempered basis set in the presence of a harmonic potential ($\omega^2 = 0.25$) considering different number of electrons. We have employed uncontracted ETBS with angular momentum $L = 0$ to $L = 3$ and the same number N of primitives per shell. The L and N dependent exponents of the primitives are even-tempered following the scheme:

$$\zeta_{LN}^k(\omega^2) = \frac{\omega^2}{2}\alpha_{L,N}(\omega^2)\left[\beta_{L,N}(\omega^2)\right]^{k-1}, 1 \leq k \leq N, \qquad (4.4)$$

where the parameters α and β are optimized by minimizing the CASSCF (full electron and 13 active orbitals) energies. Similar strategies have been followed in previous publications. [56, 199, 208]

After careful inspection, the best balance between accuracy and performance was obtained for the basis set optimized with six electrons in the singlet state, we call to this basis set the ETBS-6S. This basis set can be characterized as an uncontracted 4(SPDF) basis set with the following exponent values: 0.2404032, 0.3130329, 0.4076051, 0.5307491. The total number of basis sets is 80, out of which 68 are linearly independent and these are the only one used in the calculations. The results for this basis set showed a better agreement in both absolute energies and singlet-triplet gaps with respect to the available benchmark data than the standard aug-cc-pVNZ series, and therefore, we focus our discussion on the results obtained with this basis set.

4.3   RESULTS AND DISCUSSION

This section is organized in accordance to the number of electrons of the system. Thus, we start our discussion with two electron systems, and then 4, 6, 8, and 10 electron systems follow. In the case of the two-electron Coulombic Hooke atom, the exact energy is known, [80, 204] and therefore, there is a benchmark value to calibrate the basis sets employed throughout this work. In the other cases, we will use the benchmark data available in the literature.[39, 41, 62, 199] Thus, the first section is dedicated to this calibration. Then, the discussion is centered on the triplet-singlet gap for each of the systems, focusing our discussion on the factors that affect this gap, such as the electron repulsion screening and the number of electrons in the system. To understand these trends, we analyze the corresponding natural orbitals, so that we can relate the solution to a specific electronic configuration. Based on this information, we come up with an *Aufbau* structure to describe the electron filling pattern in these confined systems.

4.3.1   Two-electron systems

The results for the two-electron Hooke-type atom with Coulombic electron repulsion are shown in table 4.1. We emphasize that for this system the exact energy for the singlet state is known, [80, 204] namely 2.0 a.u., and, therefore, we use this reference value to calibrate the accuracy of the various basis sets used throughout this work (table 4.1). There is a substantial difference between aug-cc-pVDZ and the rest of the basis sets. Full-CI energy for the singlet state is 2.055213 a.u. with this basis set. The use of aug-cc-pVTZ (25 basis functions including d orbitals) leads to a reduction of the energy error of one order of magnitude, leading to a Full-CI energy of 2.004107 a.u. To further reduce the energy error by one order of magnitude, one has to go up to the aug-cc-pV5Z basis set (2.000476 a.u.) with 105 basis functions. At this point, it is worth noticing that our results are of comparable accuracy to the best unextrapolated result reported by Matito et al. [199] for ω^2=0.25 , namely, 2.0002965 a.u., obtained using systematic sequences of Gaussian primitives with even-tempered

exponents. Finally, the use of the aug-cc-pV6Z basis set, which contains 182 basis functions, leads only to a minor improvement in the energy, 2.000196 a.u. Moreover, this basis set shows large linear dependencies, and in fact, the total number of molecular orbitals in the variational space is reduced to 139 upon elimination of linear dependencies. This fact has led us not to consider this basis set any further in this current work. Besides, two more basis sets have been tested, which will be referred as aug-cc-pV5Z* and aug-cc-pV6Z*. This basis set are created by removing the basis functions with angular momentum greater or equal to four. The reduction in size of the basis set is substantial, from 105 to 75 for aug-cc-pV5Z, and from 182 to 95 for aug-cc-pV6Z. Moreover, the latter basis set upon removal of g and h basis functions does not show linear dependencies. The reduction of basis set size has only minor effects in the energy. In the case of aug-cc-pV5Z basis set, the energy increases only from 2.000476 a.u. to 2.000685 a.u., whereas for aug-cc-pV6Z, from 2.000196 to 2.000426 a.u. Considering the performance of our optimized ETBS-6S basis set, it gives a value for the singlet of 2.000396 a.u., that is, the second lowest energy value and only improved by the considerably higher aug-cc-pV6Z basis set.

The triplet-singlet gap (Δ_{T-S}), in eV, for two-electron systems can be found in Table 4.1. Irrespective of the basis set employed in the calculation, the lowest energy orbital is of s-type, followed by a shell of p orbitals .[80] We will call to these orbitals the $1s$ and $1p$ orbitals. Hence, the singlet state is formed by the double occupation of the $1s$ orbital and the triplet state corresponds to the promotion of one of the $1s$ electrons to one $1p$ orbital plus a one-spin flip. The triplet-singlet gap is large. At the Full-CI/aug-cc-pV6Z level of theory, the gap is 9.86 eV and 9.78 eV for Full-CI/ETBS-6S, a very similar value to our reference value of 9.79 eV, which fully justifies the use of our ETBS-6S basis set as a good compromise between accuracy and computational cost. On the other hand, the better performance of the ETBS-6S basis set over the Dunning ones is more evident when more electrons are considered (see below), and therefore, we will discuss in the manuscript the results for the ETBS-6S basis set, in comparison with some values for the aug-cc-pV6Z* basis set. The results for the rest of the Dunning's basis sets can be found in Table 4.1 and 4.9.

Since the use of Full-CI is prohibitive as the number of electrons increases,we have analyzed the performance of CASSCF and MRMP2 methods, using the ETBS-6S basis sets. In Table 4.2, we report the energies obtained at the CASSCF and MRMP2 levels of theory using different active spaces. The results can also be visualized in Fig. 4.1, where we have analyzed the convergence of CASSCF (dashed line) and MRMP2 (continuum line) as we consider more orbitals (N_{orb} in the active window). We consider from a minimal window of 2 orbitals up to 13 orbitals, which correspond to the $1s$, $1p$, $1d$, $2s$ and $2p$ shells. The convergence in Δ_{T-S} is obtained quite fast, specially for MRMP2 method, with an excellent agreement with Full-CI results.

4.3.2 Four-electron systems

The results for the four-electron systems can be found in Tables 4.3 and 4.9, and in Fig. 4.1. In this case, the use of Full-CI was computationally prohibitive. On the other hand, multideterminantal wave functions are mandatory due to substantial near-degeneracy effects. Consequently, we have decided to use multiconfigurational wave functions of the CASSCF type. We have investigated active spaces that span from 4 to 13 orbitals, corresponding to the 1s, 1p, 1d, 2s and 2p shells. We have included the four electrons in this active orbital space and consider all possible excitations within the window that are compatible with the desired spin state (singlet or triplet). The starting orbitals for the CASSCF calculations correspond to the HF orbitals of the singlet state. The biggest calculation using 4 electrons and 13 orbitals for the CAS window leads to 2366 CSFs (Configuration State Functions) for the singlet state, and 3003 CSFs for the triplet state. We have also considered second-order perturbation corrections based on these CASSCF wavefunctions (MRMP2, hereafter).

The electronic structure of the singlet state presents double occupation of the 1s orbital and one of the 1p orbitals. The triplet state corresponds mainly to a configuration in which the 1s orbital is doubly occupied and two 1p orbitals have one electron each. Due to the degeneracy of the 1p shell, the resultant singlet and triplet CASSCF wavefunctions show large nondynamical correlation or near-degeneracy effects, and, therefore, the need to use multiple configurations in the wavefunction.

As one can see in Tables 4.3 and 4.9, the values of Δ_{T-S} are negative for all basis sets and methods considered, indicating that in the case of 4 electrons the confinement has led to a triplet-spin ground state. Notice from Fig. 4.1 that the convergence of the results with the window size is quite fast. The values of the triplet-singlet gap at the CAS(4,13) and MRMP2(4,13) levels of theory with the aug-cc-pV6Z* basis set are -1.11 eV and -1.08 eV, respectively, in nice agreement with the reference value by Cioslowski et al. [41] of -1.00 eV. The use of the ETBS-6S basis sets slightly improves these results, giving values of -1.06 and -1.04 eV at the CAS(4,13) and MRMP2(4,13) levels of theory. However, we can see that the CAS(4,13)/ETBS-6S energies are significantly closer to the reference values than the CAS(4,13)/aug-cc-pV6Z* ones. For instance, the energy value for the singlet and triplet states are 6.398720 and 6.359758 , respectively, in good agreement with the values of Cioslowski et al.[41] 6.385543 and 6.348830 a.u., respectively. The introduction of second-order perturbation corrections, albeit non-variational, further improves this agreement, giving energies, 6.390085 and 6.352024, that are even closer to the ones by Cioslowski et al.[41] An advantage of the MRMP2 energies (see Figure 4.1) is that they are less dependent on the active space of the CASSCF wavefunction and, thus, we can use a smaller active space without sacrificing the accuracy. The singlet-triplet gap obtained with MRMP2(4,13) is -1.04 eV, in very good agreement with the one by Cioslowski et al., [41] namely, -1.00 eV.

4.3.3   Six-electron systems

The results for the six electron systems can be found in Tables 4.4 and 4.9, and in Fig. 4.1. As in the previous case, we use CASSCF type wavefunctions, with different active spaces that go from a minimal 6 orbital window up to 13 orbitals ($1s$, $1p$, $1d$, $2s$, and $2p$), and include all six electrons. Our largest CAS window involves 26026 CSFs for the singlet state, and 39039 for the triplet.

The inclusion of two further electrons in the $1p$-shell yields a very similar triplet-singlet gap and trends close to the ones observed for 4-electron systems. Again, we obtain negative values for Δ_{T-S}, indicating that the ground state is a triplet. For instance, the value of Δ_{T-S} is -1.03 and -1.0 eV at the CAS(6,13)/ETBS-6S and MRMP2(6,13)/ETBS-6S levels of theory. A glance at Fig. 4.1 clearly demonstrates that the results are very well converged with respect to the window size, specially for the MRMP2 level of theory. The values for the aug-cc-pV6Z* basis set are very similar, namely, -1.06 and -1.05 eV. Our results for the singlet-triplet gap agree satisfactorily with the reference calculations for the 6-electron Hookean atom, [62] which yield a value of -0.95 eV with an energy of 12.066294 a.u. for the singlet and 12.031275 a.u. for the triplet. In the case of the six-electron system, ETBS-6S absolute energies again give a significant improvement over the aug-cc-pV6Z* ones. However, now the difference between our CASSCF/ETBS-6S and the reference energies of Strasburger[62] increases with respect to the 4-electron case. For instance, CAS(6,13)/ETBS-6S energies are 12.115772 and 12.077925 a.u. for singlet and triplet states, respectively, whereas the reference energies are 12.066294 and 12.031275 a.u.. However, the introduction of perturbation corrections lowers the energies to 12.082805 and 12.046142 a.u at the MRMP2(6,13)/ETBS-6S level of theory, yielding a triplet-singlet gap only differing by 0.05 eV with respect to the -0.95 eV gap obtained from the data of Strasburger. [62] In summary, although the quality of our absolute energies of each of the states decreases with the increasing number of electrons, the estimation of the triplet-singlet gap remains correct.

4.3.4   Eight-electron systems

Tables 4.5 and 4.9, and Fig. 4.1 summarize the results for 8-electron systems, using CASSCF wavefunctions with an active space composed of 8 to 13 orbitals ($1s$, $1p$, $1d$, $2s$, and $2p$ orbitals) and 8 electrons. In the case of our largest window, the CASSCF(8,13) wavefunction yields 143143 CSFs for the singlet state, and 234234 CSFs for the triplet. The corresponding second-order perturbative corrections can also be found in Table 4.5.

In the case of the singlet state, the 8-electron system corresponds to an electronic configuration in which the 1s and 1p shells are fulfilled. In the case of the triplet state, based on the analysis of the occupancies of natural orbitals, an electronic configuration of $1s^2 1p^5 1d^1$-type is observed with ETBS-6S and aug-cc-pV6Z* basis

sets, however, lower quality basis sets can yield an electronic configuration of $1s^2 1p^5 2s^1$-type (see Table 4.9). In other words, the gap between the $2s$ and $1d$ orbitals is sufficiently small so as to be sensible to the type of basis set. However, our best basis sets, according to the criteria of the lowest triplet energy, favours the $1s^2 1p^5 1d^1$ configuration and, therefore, we conclude that our orbital ordering is $1s < 1p < 1d < 2s < 2p$. This behavior reminds the situation that one encounters in transition metal atoms regarding the 3d/4s orbital ordering.

Irrespective of the type of configuration adopted, it is clear that the ground state of the 8-electron system is a singlet state, and presents a substantial gap with the triplet state, 7.66 eV at the CAS(8,13)/ETBS-6S level of theory and 7.37 eV at the MRMP2(8,13)/ETBS-6S level of theory. The latter results are reasonable well converged with respect to the CAS window size (see Fig. 4.1). The triplet-singlet gap is significantly smaller than the one found for the two-electron case, namely, 9.78 eV. This result suggests a decrease of the inter-shell gap as we move along this series: $1s < 1p < 1d$. However, our results differ significantly from the results of Varga et al [39] which reported a gap of 10.6 eV. A closer inspection to the absolute energies can clarify this difference. Our singlet and triplet CAS(8,13)/ETBS-6S energies are 19.05314 and 19.334793 a.u, respectively. When perturbation corrections are included the values are 18.997973 and 19.268892 a.u. The most accurate eight-electron Hooke atom results found in the literature up to date correspond to the ones of Varga et al [39] which are 19.038 and 19.430 a.u., leading to a gap of 10.6 eV, much higher than our triplet-singlet gap. However, notice that our variational value for the triplet state is lower than the results obtained by Varga et al [39] for their lowest triplet state, which suggests that we have been able to obtain a more accurate result for this state. In addition, since our results for 4- and 6-electron systems show a better agreement with the reference data, we believe that they are of higher accuracy than the ones of Varga et al [39] for the eight-electron system. It is worth mentioning that some discrepancy with the three-electron case published by Varga [39] has been reported in the literature [40]

4.3.5   Ten-electron systems

To the best of our knowledge, for the 10-electron system, there are not previous calculations in the literature. Tables 4.6 and 4.9, and Fig. 4.1, summarize the results for the 10-electron systems. We used CASSCF wavefunctions with an active space composed of 10 to 13 orbitals ($1s$, $1p$, $1d$, $2s$ and $2p$ orbitals) and 10 electrons. For the CASSCF(10,13) wavefunction, this yields 429429 CSFs for the singlet state, and 736164 CSFs for the triplet. Regarding the dominant electronic configuration, this is of $1s^2 1p^6 1d^2$ type for both singlet and triplet state. It is worth noticing that there is an important discrepancy among the various aug-cc type basis sets on the nature of the Aufbau principle for the 10-electron system, with the aug-cc-pV6Z* basis set favouring the filling of $1d$ orbitals (as for ETBS-6S), while the rest of the

basis-sets favour the filling of a 2s orbital (see Table 4.9). This has importance consequences in the relative energies of the singlet and triplet states, giving a singlet ground electronic state in the case that the filling of a 2s orbital is favoured, whereas a triplet ground state is obtained in the case that the filling of the 1d shell is prioritized. This highlights the importance of optimizing an appropriate basis set, which is adapted to the external potential of the system, like the ETBS-6S one. A remarkable aspect is that the Aufbau structure $1s > 1p > 1d$ remains throughout the whole 2-,4-,6-,8- and 10-electron series with the ETBS-6S basis set, since in all cases we obtain higher fractional occupation numbers for 1d orbitals than for the 2s one.

Using the ETBS-6S basis set, and irrespective of the method used, the triplet state is lower in energy than the singlet state, with a gap smaller than the one found for the 4- and 6-electron cases. Hence, When passing from 8- to 10-electron, the system changes the spin state of the ground state of the system. Our best estimate is -0.55 eV at CAS(10,13)/ETBS-6S level of theory and -0.74 eV at MRMP2(10,13)/ETBS-6S.

The convergence of the triplet-singlet gap with respect to N_{orb} is less satisfactory than for the cases of a lower number of electrons (see Fig. 4.1). We also noticed that the natural orbital occupation associated to the 1s orbital in the 10-electron case is always higher than 1.98. Therefore, we decided to remove this orbital and the two associated electrons form the CAS window, which allowed us to expand further the window size to include more virtual orbitals at a reasonable computational cost. When the occupation of the 1s orbital is set to 2.0 (magenta curve in Fig. 4.1), we obtain almost identical values of the triplet-singlet gap to the case in which the 1s orbital and its electrons participate in the definition of the CAS window (orange curve in Fig. 4.1). One can see in the figure that now we get quite well converged results finding a triplet-singlet gap of -0.64 eV at CASSCF(8,15)/ETBS-6S level of theory and -0.53 eV at MRMP2(8,15)/ETBS-6S level of theory, further conforming the triplet nature of the ground state of the 10-electron Hooke atom, and the smaller triplet-singlet gap with respect to the cases of 4 and 6 electrons.

4.3.6   Screened Hooke Atom

Due to the fact that the results for N_e=2,4,6, and 8 electron systems were quite converged for a window of 10 orbitals, we have considered the CASSCF(N_e, 10)/ETBS-6S and MRMP2(N_e,10)/ETBS-6S methods to analyze the effect that the screening of the electron-electron interaction has on the triplet-singlet gap. In the case of the 10-electron system, we also used the CAS(10, 10)/ETBS-6S and MRMP2(10,10)/ETBS-6S methods, but we also performed CAS(8, 14)/ETBS-6S and MRMP2(8,14)/ETBS-6S calculations, which are more converged results with respect to the window size, as demonstrated in the previous section. We have increased progressively the amount of screened electron-electron interactions by considering values of λ_{ee} of 0.2, 0.4, 0.6, 0.8, and 1.0; the results are summarized in Table 4.7 and Fig. 4.2.

   The nature of the spin of the ground state is not altered upon inclusion of screening effects (see Fig. 4.2A, top figure), namely 2- and 8-electron cases show singlet ground states, whereas 4-, 6- and 10-electron cases have triplet ground states. Nevertheless, the triplet-singlet gap is sensitive to the degree of electron-electron screening, specially in the case of 2 and 8 electrons. This is due to the fact that, based on the *Aufbau* structure, these systems form closed-shell structures for singlet spin states; hence, every two electrons share the same spatial orbital and interact strongly through two-body interacting. In these two cases, the introduction of screening effects produces a very substantial and gradual stabilization of the singlet state over the triple one (see Fig. 4.2B). Therefore, the reduction of the electronic repulsion leads to a more favourable spin pairing in these two systems. Thus, in the case of the two-electron Hooke atom, there is an increase in Δ_{T-S} from 9.78 to 11.51 eV when passing from full Coulombic to Yukawa λ=1.0 screened electron-electron potential at MRMP2(2,10)/ETBS-6S level of theory. This increase in Δ_{T-S} is even higher for the 8-electron case, from 7.28 to 10.48 eV. Notice that in these two cases the triplet is formed by promoting one electron to the next shell with higher angular momentum, and thus, our results suggest that the introduction of screening effects among the electrons results in an stabilization of the lower angular momentum shells, leading to larger gaps between the shells, and therefore, more pronounced triplet-singlet gaps.
   On the other hand, the 4-, 6-, and 10-electron cases are less affected by the screening of the electron-electron interactions (Figure 4.2A). These three cases show triplet ground states and the introduction of screening has again a stabilizing effect of the singlet state over the triplet one (see Figure 4.2B) but to a much lesser extent than in the case of 2- and 8-electron systems. Thus, in the case of 4 electrons, Δ_{T-S} changes from -1.04 to -0.78 eV, in the case of 6 electrons goes from -0.99 to -0.77 eV, and in the case of 10 electrons from -0.56 to -0.34 eV. Notice however, that even though in terms of absolute numbers this is a small effect, the screening of electron-electron interactions has been able to reduce almost to half the S/T gap in the case of 10 electron system. In general, we may conclude that there is a clear stabilization of the singlet over the triplet state upon screening effects, but this stabilization is not as large as to revert the nature of the spin of the ground state.

4.3.7   Decomposing the energy into different contributions

To get further insights of the different contributions into the above mentioned trends, in Table 4.8, we can find the decomposition of the total energy into kinetic, confinement and electron-electron repulsion terms for the 2-, 4-, 6-, 8-, and 10-electron Hooke atoms and the corresponding screened (λ_{ee}=1.0) Hooke atoms, using the CASSCF(N_e,10)/ETBS-6S energies.
   First, we analyze the different contributions to the triplet-singlet gap for the unscreened Hooke atom. We find two clear different patterns for the singlet (2- and 8-electron systems) and triplet ground states (4-, 6-, and 10-electron cases).
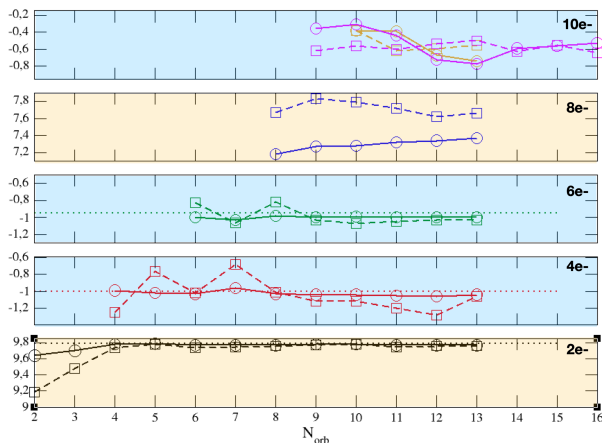
Figure 4.1: Triplet-singlet energy gap, in eV, calculated at the CAS(N_e,N_{orb}) (dashed line) and MRMP2(N_e,N_{orb}) (continuous line) levels of theory with the ETBS-6S basis set, as a function of the number of orbitals N_{orb} included in the active space. All cases correspond to a CASSCF wavefunction in which all electrons are included in the active space, except for the curves in magenta for the 10 electron system, that correspond to wavefunctions in which the 1s orbital occupation is set to 2, and therefore, the active space is composed of 8 electrons and N_{orb}-2 orbitals.
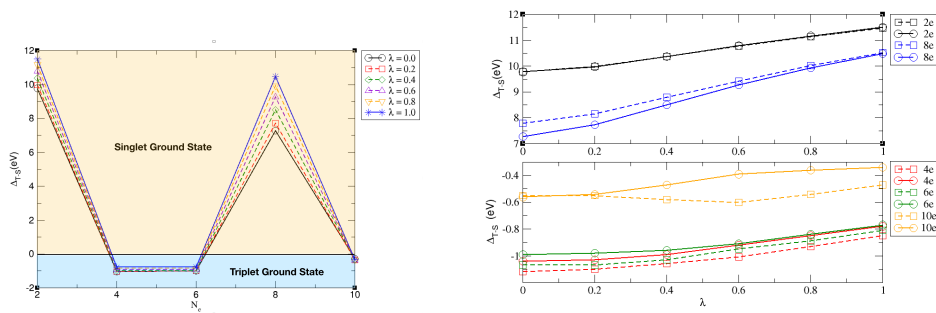
Figure 4.2: A) Left Figure: Triplet-singlet energy gap, in eV, calculated at the MRMP2(N_e,10) level of theory (2-, 4-, 6-, and 8-electron systems) and MRMP2(8,14) (10-electron system), as a function of the number of electrons and for different values of λ. B) Right Figure: Triplet-singlet energy gap, in eV, calculated at CAS(N_e,10) (dashed line) and MRMP2(N_e,10) (continous line) levels of theory for 2,4,6 and 8 electrons, and CAS(8,14) (dashed line) and MRMP2(8,14) (continuous line) levels of theory for the 10-electron system, as a function of the degree of screening (λ). All calculations were done with the ETBS-6S basis set.

In all cases, the electron-electron repulsion term is always negative, favouring the triplet state over the singlet one. However, while for 4, 6, and 10 electron systems, the $\Delta_{T-S}^{V_{ee}}$ is the leading term that governs the overall triplet-singlet gap, for 2 and 8 elecrons, this term is of lower magnitude than the kinetic Δ_{T-S}^{K} and the confinement terms $\Delta_{T-S}^{V_{conf}}$. Thus, the promotion of one electron to the next shell, as it happens in the triplet state of 2 and 8 electron systems, results in a very high increase of the kinetic and confinement energies, that can not be overcome by the lower electron-electron repulsion of the triplet state. However, the formation of the triplet states in 4-, 6-, and 10-electron systems corresponds to intra-shell promotions, with very small differences in the kinetic energy between singlet and triplet states and with a confinement contribution that favours the triplet over the singlet, although its magnitude is smaller than the energy gain obtained by decreasing the electron-electron repulsion.

We analyze now the influence of screening on the different components of the energy. We have selected a $\lambda_{ee}=1.0$ to perform this analysis. As one can see in Table 4.8, this value of λ_{ee} implies a very effective screening of the electron-electron interactions with a reduction between 78.1-89.6% of the electron-electron repulsion energy. As expected, this is the main energy component affected by the introduction of the screening. Nevertheless, the confinement and kinetic contributions are also substantially affected, with an increase in the kinetic energy and a lowering of the confinement energy, as the number of electrons increases. Thus, the increase in kinetic energy goes from a 5.8% in two-electron systems to 34% in 10-electron systems, whereas the reduction in confinement energy goes from 6-8 % in singlet and triplet two-electron cases to 28% when 10 electrons are considered. These trends can be explained in terms of a more compact electronic density upon reduction of the electron-electron repulsion, which augments the kinetic energy and reduces the confinement energy.

The influence of screening in the different contributions to Δ_{T-S} can also be found in Table 4.8. Again, we see different trends for 2- and 8-electron cases, and for 4-, 6-, and 10-electron cases. For 2- and 8-electron Hooke atoms, there is an important reduction in the electron-electron repulsion contribution to the triplet-singlet gap, which favours the singlet state by roughly 1 eV. In addition, due to the fact that there is an increase in the energy gap between shells upon screening, the confinement and kinetic energy contributions also augment and favour the singlet state. Therefore, in the 2- and 8-electron systems, the three contributions to Δ_{T-S} increase, and substantially favours the singlet state over the triplet one. In the case of 4- and 6-electron systems, the reduction in the electron-electron repulsion is very similar in both the triplet and singlets states and, therefore, its contribution to the changes in Δ_{T-S} is minimal. In these two cases, the kinetic Δ_{T-S}^{K} term is the main contributor to the slight changes in triplet-singlet gap upon screening. Finally, in 10 electron systems, both kinetic and electron-electron repulsion contribute equally. Nevertheless, the differences in these terms when introducing electron-electron screening are very

small compared to the 2- and 8-electron systems, and highlights the difference between inter- and intra-shell promotion when building the triplet state.

4.3.8   Coulomb Holes

Finally, in order to gain a deeper insight of the electron correlation effects, we have also calculated the Coulomb holes for the Coulombic and Yukawa confined ($\lambda_{ee} = 1.0$) systems. The Coulomb holes, $h(u)$, are defined as the difference in the intracule density, $I(u)$, of a correlated wavefunction, CASSCF(N_e,13) in our case, and an uncorrelated one, RHF or ROHF for singlet and triplet states, respectively.

$$h(u) = I^{\mathrm{CASSCF}}(u) - I^{\mathrm{RHF/ROHF}}(u) \, , \tag{4.5}$$

with $u = |r_{12}|$. The radial intracule density provides a distribution of the electron-electron distances and it is defined as,

$$I(u) \quad = \quad \int \int n_2(\mathbf{r}_1, \mathbf{r}_2) \delta(u - r_{12}) d\mathbf{r}_1 d\mathbf{r}_2, \tag{4.6}$$

where $n_2(\mathbf{r}_1, \mathbf{r}_2)$ is the pair density and r_{12} is the module of the intracular coordinate, namely, the interelectronic distance. Thus, the intracule density gives the probability of finding any two electrons at a certain distance u. The Coulomb hole is a measure of how electron correlation affects the probability of finding two electrons at a given distance. As this function only depends on the interelectronic distance, it provides a simple visualization of the distribution of electron-electron separations; by monitoring the changes in this distribution. We may gain further knowledge of the behaviour of electron correlation in these systems and how this is affected by the number of electrons, spin state and screening of electron-electron interaction.

Results are displayed in Figure 4.3. A common pattern is observed irrespective of the number of electrons: i) the Coulomb hole is more pronounced for singlet than for triplet states in both full Coulombic and screened systems and ii) the introduction of screening effects results in a significant reduction of the corresponding Coulomb holes. As expected, in general, the main effect of introducing electron correlation effects is an increase in the interelectronic distance, namely, the Coulomb holes show a depletion at short distances and a concomitant rise at larger distances. However, an interesting feature arises for screened systems in the case of singlet states with 4, 6 and 10 electrons: there is a depletion of the Coulomb hole at large distances. This feature is also observed to a lower extent for the 8-electron screened system with a triplet spin multiplicity. Therefore, in these cases, electrons are correlated in such way that they come closer compared to the Coulomb potential due to the attractive interaction at large distances. This can be explained by the tendency mentioned in the previous section of a more compact electronic cloud in screened

systems, which leads to a reduction of the confinement energy. Our results points to a relationship of the intrashell electron-electron correlation (as it occurs for singlet 4-, 6- and 10-electron and triplet 8-electron systems), with the promotion of a more compact electronic cloud.
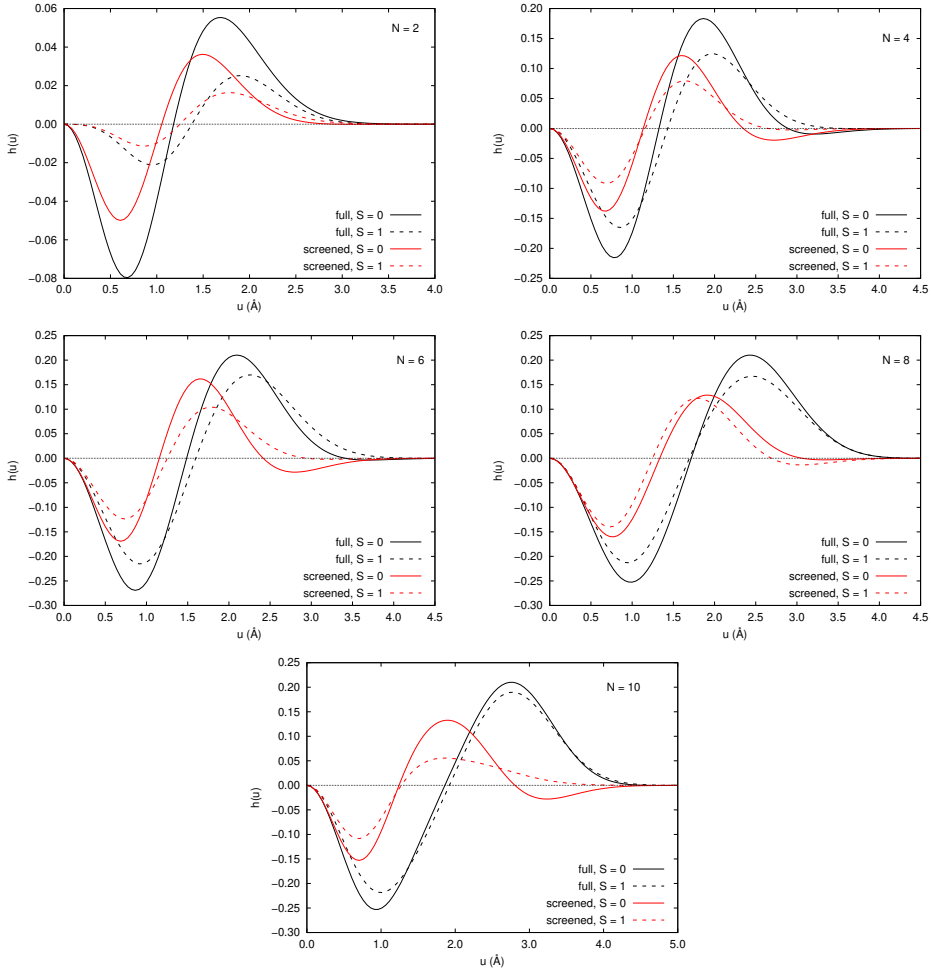
Figure 4.3: Coulomb holes calculated at the CASSCF(N_e,13)/ETBS-6S level of theory for both full (solid lines) and $\lambda_{ee} = 1.0$ screened-coulombic (dasshed lines) Hooke systems with different number of electrons (N_e=2,4,6,8 and 10) and for singlet(black lines) and triplet states (red lines).

4.4 CONCLUDING REMARKS

In the present chapter, we have presented a thorough study of 2-,4-,6-,8- and 10-electron systems confined in a spherical quantum dot in their singlet and triplet spin states, with the aim of determining the triplet-singlet gap for Hooke-type systems. The effect of screening the electron-electron interaction has also been taken into account effectively by the introduction of a Yukawa type potential.

Our results show an interesting pattern in the triplet-singlet gap as the number of electrons increases. Thus, singlet state is the ground state for 2 and 8, whereas the triplet state is the ground spin state in 4 and 6 electron systems. The situation for 10-electron system is again a triplet ground state, but with a gap smaller than the one found for 4 and 6 electrons. Our results can be readily rationalized in terms of the following orbital ordering $1s < 1p < 1d$, with a decrease in the successive energy gaps.

We have also observed that the screening of electron-electron interaction has a sizable effect, not only on the absolute energies for each state, but also on the triplet-singlet gap. The triplet-singlet gap for the 2 electron and 8 electron cases is specially sensible to the screening effect, favouring the singlet state over the triplet. This can be related to an increase of the corresponding gap between shells upon screening. However, the influence of screening in the triplet-singlet gap for 4-, 6- and 10-electron cases was much more reduced, favouring again the singlet state but, in no case, this screening produced a switch between spin states.

Table 4.1: HF and Full-CI energies (a.u.) of the singlet and triplet spin states for the two-electron Hooke atom ($\omega^2 = 0.25$; $\lambda_{ee} = 0.0$)

Basis	Size	Contraction	Singlet HF	Singlet FCI	Triplet FCI	Δ_{T-S} (eV)
aug-cc-pVDZ	9	(5s2p/3s2p)	2.087904	2.055213	2.386080	9.00
aug-cc-pVTZ	25	(7s3p2d/4s3p2d)	2.038634	2.004107	2.373537	10.05
aug-cc-pVQZ	55	(8s4p3d2f/5s4p3d2f)	2.038443	2.001484	2.383204	10.39
aug-cc-pV5Z*	75	(9s5p4d3f/6s5p4d3f)	2.038408	2.000685	2.373767	10.15
aug-cc-pV6Z*	95	(11s6p5d4f/7s6p5d4f)	2.038423	2.000426	2.362738	9.86
aug-cc-pV5Z	105	(9s5p4d3f2g/6s5p4d3f2g)	2.038400	2.000476	2.373701	10.16
aug-cc-pV6Z	182	(11s6p5d4f3g2h/7s6p5d4f3g2h)	2.038404	2.000196	2.362579	9.86
ETBS-6S	80	(4s4p4d4f/4s4p4d4f)	2.038400	2.000396	2.359673	9.78

Table 4.2: HF, CAS(2,N_{orb}) and MRMP2(2,N_{orb}) energies with the ETBS-6S basis set, in atomic units, for the singlet and triplet spin states o the two-electron Hooke atom. The RHF energy for the singlet state is 2.038400 and 2.038423 a.u. for the ETBS-6S and aug-cc-pV6Z* basis sets, respectively.

Basis	N_{orb}	CAS(N_e, N_{orb})		Δ_{T-S}	MRMP2(N_e,N_{orb})		Δ_{T-S}
		Singlet	Triplet	(eV)	Singlet	Triplet	(eV)
	2	2.026787	2.364478	9.19	2.006140	2.360420	9.64
	3	2.016225	2.364478	9.48	2.003759	2.360428	9.70
	4	2.006551	2.364478	9.74	2.001197	2.360601	9.78
	5	2.003410	2.362773	9.78	2.000701	2.360358	9.79
	6	2.003056	2.361106	9.74	2.000670	2.359828	9.77
	7	2.002705	2.361106	9.75	2.000637	2.359819	9.77
	8	2.002358	2.361106	9.76	2.000601	2.359820	9.77
	9	2.002019	2.361106	9.77	2.000559	2.359821	9.78
	10	2.001681	2.361106	9.78	2.000516	2.359828	9.78
	11	2.001630	2.359907	9.75	2.000513	2.359694	9.77
	12	2.001280	2.359859	9.76	2.000481	2.359687	9.77
	13	2.001082	2.359821	9.76	2.000461	2.359688	9.77
	FCI	2.000396	2.359673	9.78			
aug-cc-pV6Z*	13	2.001203	2.362886	9.84	2.000483	2.362749	9.86
aug-cc-pV6Z*	FCI	2.000426	2.362738	9.86			
Reference [80]		2.000000	2.359657	9.79			

Table 4.3: HF, CAS(4,N_{orb}) and MRMP2(4,N_{orb}) energies with ETBS-6S basis set, in atomic units, for the singlet and triplet spin states of the four-electron Hooke atom. The RHF energy or the singlet state is 6.505162 and 6.517905 for the EBTS-6S and aug-cc-pV6Z* basis sets, respectively.

Basis	N_{orb}	CAS(4, N_{orb})		Δ_{T-S}	MRMP2(4,N_{orb})		Δ_{T-S}
		Singlet	Triplet	(eV)	Singlet	Triplet	(eV)
	4	6.466497	6.420487	-1.25	6.393971	6.357443	-0.99
	5	6.436891	6.409056	-0.76	6.395878	6.358352	-1.02
	6	6.432908	6.395502	-1.02	6.395253	6.357424	-1.03
	7	6.412845	6.387924	-0.68	6.391439	6.356035	-0.96
	8	6.416955	6.379714	-1.01	6.392298	6.354322	-1.03
	9	6.412845	6.371627	-1.12	6.391439	6.353215	-1.04
	10	6.410052	6.368950	-1.12	6.391231	6.352928	-1.04
	11	6.409228	6.365185	-1.20	6.391078	6.352579	-1.05
	12	6.408315	6.361114	-1.28	6.390980	6.352180	-1.06
	13	6.398720	6.359758	-1.06	6.390085	6.352024	-1.04
aug-cc-pV6Z*	13	6.412708	6.371770	-1.11	6.403958	6.364288	-1.08
Reference[41]		6.385543	6.348830	-1.00			

Table 4.4: HF, CAS(6,N_{orb}) and MRMP2(6,N_{orb}) energies with ETBS-6S basis set, in atomic units, for the singlet and triplet spin states of the four-electron Hooke atom. The RHF energy or the singlet state is 12.253446 and 12.287010 for the EBTS-6S and aug-cc-pV6Z* basis sets, respectively.

Basis	N_{orb}	CAS(6, N_{orb})		Δ_{T-S}	MRMP2(6,N_{orb})		Δ_{T-S}
		Singlet	Triplet	(eV)	Singlet	Triplet	(eV)
	6	12.177056	12.154962	-0.60	12.091183	12.055694	-0.97
	7	12.171843	12.132887	-1.06	12.089361	12.051390	-1.03
	8	12.147118	12.117039	-0.82	12.086838	12.050945	-0.98
	9	12.137934	12.099985	-1.03	12.085660	12.048808	-1.00
	10	12.132401	12.094292	-1.04	12.084591	12.047936	-1.00
	11	12.126035	12.087898	-1.04	12.083819	12.047183	-1.00
	12	12.120721	12.082893	-1.03	12.083437	12.046636	-1.00
	13	12.114932	12.077925	-1.01	12.082804	12.046141	-1.00
aug-cc-pV6Z*	13	12.149632	12.110496	-1.06	12.120797	12.082391	-1.05
Reference[62]		12.066294	12.031275	-0.95			

Table 4.5: HF, CAS(8,N_{orb}) and MRMP2(8,N_{orb}) energies with ETBS-6S basis set, in atomic units, for the singlet and triplet spin states of the four-electron Hooke atom. The RHF energy or the singlet state is 19.190980 and 19.247016 for the EBTS-6S and aug-cc-pV6Z* basis sets, respectively.

Basis	N_{orb}	CAS(8, N_{orb})		Δ_{T-S}	MRMP2(8,N_{orb})		Δ_{T-S}
		Singlet	Triplet	(eV)	Singlet	Triplet	(eV)
	8	19.113340	19.395160	7.67	19.008248	19.272166	7.18
	9	19.083985	19.371303	7.82	19.003255	19.270391	7.27
	10	19.075987	19.362461	7.79	19.000736	19.268463	7.28
	11	19.069697	19.353362	7.72	19.000079	19.269118	7.32
	12	19.063989	19.343947	7.62	18.999332	19.269118	7.34
	13	19.053174	19.334793	7.66	18.997973	19.268892	7.37
aug-cc-pV6Z*	13	19.110238	19.437774	8.91	19.065563	19.386165	8.72
Reference[39]		19.038	19.430	10.6			

Table 4.6: HF, CAS(10,N_{orb}) and MRMP2(10,N_{orb}) energies with ETBS-6S basis set, in atomic units, for the singlet and triplet spin states of the four-electron Hooke atom. The RHF energy or the singlet state is 27.932821 and 28.174226 for the EBTS-6S and aug-cc-pV6Z* basis sets, respectively.

Basis	N_{orb}	CAS(10, N_{orb})		Δ_{T-S}	MRMP2(10,N_{orb})		Δ_{T-S}
		Singlet	Triplet	(eV)	Singlet	Triplet	(eV)
	10	27.828015	27.807466	-0.56	27.675164	27.665330	-0.27
	11	27.813009	27.790373	-0.62	27.678880	27.664692	-0.39
	12	27.795515	27.773761	-0.59	27.688082	27.663346	-0.67
	13	27.777241	27.757081	-0.55	27.689185	27.661990	-0.74
aug-cc-pV6Z*	13	28.020989	28.007019	-0.38	27.951539	27.937691	-0.38

Table 4.7: HF, CAS(N_e,10) and MRMP2(N_e,10) energies, in atomic units, for the singlet and triplet spin states of the s-Hooke model at different values of the λ screening parameter.

λ	HF	CAS(N_e, 10)		Δ_{T-S}	MRMP2(N_e,10)		Δ_{T-S}
	Singlet	Singlet	Triplet	(eV)	Singlet	Triplet	(eV)
				2-electron			
0.0	2.038400	2.001681	2.361106	9.78	2.000516	2.359828	9.78
0.2	1.879433	1.845903	2.212892	9.99	1.844644	2.211584	9.98
0.4	1.777898	1.750206	2.131426	10.37	1.748859	2.130299	10.38
0.6	1.710108	1.688101	2.084166	10.78	1.686715	2.083500	10.80
0.8	1.663091	1.645841	2.055639	11.15	1.644470	2.055161	11.17
1.0	1.629427	1.615941	2.037805	11.48	1.614631	2.037480	11.51
				4-electron			
0.0	6.505162	6.410052	6.368950	-1.12	6.391231	6.352928	-1.04
0.2	4.447821	5.522013	5.481478	-1.10	5.502540	5.464743	-1.03
0.4	5.098802	5.027175	4.988257	-1.06	5.008695	4.972340	-0.99
0.6	4.786937	4.729994	4.692890	-1.01	4.712556	4.678623	-0.92
0.8	4.584830	4.539335	4.505120	-0.93	4.524068	4.492776	-0.85
1.0	4.447821	4.411219	4.380074	-0.85	4.398160	4.369611	-0.78
				6-electron			
0.0	12.253446	12.133679	12.094292	-1.07	12.084454	12.047936	-0.99
0.2	10.066994	9.960398	9.921242	-1.07	9.909188	9.873006	-0.98
0.4	8.877716	8.792459	8.754633	-1.03	8.745296	8.710196	-0.96
0.6	8.171402	8.104086	8.069290	-0.95	8.064118	8.030753	-0.91
0.8	7.723094	7.671069	7.638238	-0.89	7.636670	7.605815	-0.84
1.0	7.424057	7.382940	7.353003	-0.81	7.354441	7.326141	-0.77
				8-electron			
0.0	19.190980	19.075987	19.362461	7.79	19.000736	19.268463	7.28
0.2	15.182763	15.084400	15.384014	8.15	15.005631	15.289623	7.73
0.4	13.068595	12.994991	13.317898	8.79	12.922972	13.235696	8.51
0.6	11.834935	11.781507	12.128228	9.43	11.719577	12.060148	9.27
0.8	11.060156	11.021423	11.389781	10.02	10.969653	11.334431	9.93
1.0	10.547028	10.518701	10.905855	10.53	10.475994	10.861138	10.48
				10-electron			
0.0	27.932821	27.828015	27.807466	-0.56	27.675164	27.665330	-0.27
0.2	21.621750	21.528857	21.511339	-0.48	21.375745	21.363283	-0.34
0.4	18.408818	18.334295	18.317410	-0.46	18.203431	18.190047	-0.36
0.6	16.573893	16.515099	16.499172	-0.43	16.408780	16.395457	-0.36
0.8	15.437499	15.390866	15.376062	-0.40	15.305881	15.293178	-0.35
1.0	14.692340	14.654914	14.641306	-0.37	14.587232	14.575380	-0.32

Table 4.8: Decomposition of the total energy (a.u.) of the singlet and triplet states into different contributions, kinetic energy, confinement energy (that is the one corresponding to the monoelectronic harmonium confinement operator), and electron-electron repulsion energy. Decomposition of the triplet-singlet gap Δ_{T-S} into kinetic (Δ^K_{T-S}), confinement ($\Delta^{V_w}_{T-S}$) and electron-electron repulsion terms ($\Delta^{V_{ee}}_{T-S}$). Two cases are considered: i) Hooke atom with standard Coulombic interactions between electrons and ii) s-Hooke in which the electron-electron interactions are screened by the Yukawa potential with λ_{ee}=1.0. Δ_{s-u} corresponds to the differences between the screened and unscreened calculation.

N_e	Model	Singlet Energy Components (a.u.)				Triplet Energy Components (a.u.)				Triplet-Singlet Gap (eV)			
		Kin. E.	V_{conf}	V_{ee}	Total E.	Kin. E.	V_{conf}	V_{ee}	Total E.	Δ^K_{T-S}	$\Delta^{V_w}_{T-S}$	$\Delta^{V_{ee}}_{T-S}$	Δ_{T-S}
2	Hooke	0.664231	0.888647	0.448803	2.001681	0.920322	1.093808	0.346977	2.361106	6.97	5.58	-2.77	9.78
	s-Hooke	0.702495	0.815055	0.098391	1.615941	0.974102	1.027525	0.036178	2.037805	7.39	5.78	-1.69	11.48
	Δ_{s-u}	0.038264	-0.073592	-0.350412	-0.385740	0.053780	-0.066283	-0.310799	-0.323301	0.42	0.20	1.08	1.70
	$\%\Delta_{s-u}$	5.8	-8.3	-78.1	-19.3	5.8	-6.06	-89.6	-13.7				
4	Hooke	1.575643	2.661960	2.172449	6.410052	1.575087	2.648067	2.145797	6.368950	-0.02	-0.38	-0.73	-1.12
	s-Hooke	1.802488	2.247689	0.361041	4.411219	1.810012	2.234690	0.335372	4.380074	0.20	-0.35	-0.70	-0.85
	Δ_{s-u}	0.226845	-0.414271	-1.811408	-1.998833	0.234925	-0.413377	-1.810425	-1.988876	0.22	0.03	0.03	0.27
	$\%\Delta_{s-u}$	14.4	-15.6	-83.4	-31.2	14.9	-15.61	-84.4	-31.2				
6	Hooke	2.298682	4.810967	5.024030	12.133679	2.296848	4.797225	5.000219	12.094292	-0.05	-0.37	-0.65	-1.07
	s-Hooke	2.815149	3.794034	0.773756	7.382940	2.821571	3.781367	0.750065	7.353003	0.17	-0.30	-0.64	-0.81
	Δ_{s-u}	0.516467	-1.016933	-4.250274	-4.750739	0.524723	-1.015858	-4.250154	-4.741289	0.22	0.03	0.01	0.26
	$\%\Delta_{s-u}$	22.5	-21.1	-84.6	-39.2	22.8	-21.18	-85.0	-39.2				
8	Hooke	2.889288	7.320715	8.865985	19.075987	3.129535	7.489993	8.742933	19.362461	6.54	4.61	-3.35	7.79
	s-Hooke	3.755694	5.445591	1.317417	10.518701	4.034318	5.638694	1.232843	10.905855	7.58	5.25	-2.30	10.53
	Δ_{s-u}	0.866406	-1.875124	-7.548568	-8.557286	0.904783	-1.851299	-7.510090	-8.456606	1.04	0.64	1.05	2.74
	$\%\Delta_{s-u}$	30.0	-25.6	-85.1	-44.9	28.9	-24.72	-85.9	-43.7				
10	Hooke	3.857152	10.517423	13.453440	27.828015	3.857015	10.511402	13.439049	27.807466	0.00	-0.16	-0.39	-0.56
	s-Hooke	5.168257	7.609567	1.877090	14.654914	5.171068	7.603958	1.866280	14.641306	0.08	-0.15	-0.29	-0.37
	Δ_{s-u}	1.311105	-2.907856	-11.576350	-13.173101	1.314053	-2.907444	-11.572769	-13.166160	0.08	0.01	0.10	0.19
	$\%\Delta_{s-u}$	34.0	-27.6	-86.0	-47.3	34.1	-27.66	-86.1	-47.3				

Table 4.9: Hartree-Fock and CASSCF energies, in atomic units, for the singlet and triplet spin states of the 4, 6 , 8 and 10-electron systems. Calculations done at the CAS-SCF(N_e,13) level of theory.

Basis	Hartree-Fock	CASSCF(N_e,13)		Δ_{T-S}
	Singlet	Singlet	Triplet	(eV)
		4 electrons		
aug-cc-pVTZ	6.508926	6.431129 [$1s^21p^2$]	6.378120 [$1s^21p^2$]	-1.44
aug-cc-pVQZ	6.534156	6.439280 [$1s^21p^2$]	6.396548 [$1s^21p^2$]	-1.16
aug-cc-pV5Z	6.539774	6.436668 [$1s^21p^2$]	6.394851 [$1s^21p^2$]	-1.14
aug-cc-pV5Z*	6.539818	6.436879 [$1s^21p^2$]	6.394866 [$1s^21p^2$]	-1.14
aug-cc-pV6Z*	6.517905	6.412708 [$1s^21p^2$]	6.371770 [$1s^21p^2$]	-1.11
		6 electrons		
aug-cc-pVTZ	12.285452	12.195292 [$1s^21p^4$]	12.147453 [$1s^21p^4$]	-1.30
aug-cc-pVQZ	12.282169	12.167338 [$1s^21p^4$]	12.125916 [$1s^21p^4$]	-1.13
aug-cc-pV5Z	12.315804	12.183503 [$1s^21p^4$]	12.144069 [$1s^21p^4$]	-1.07
aug-cc-pV5Z*	12.315906	12.185233 [$1s^21p^4$]	12.145583 [$1s^21p^4$]	-1.08
aug-cc-pV6Z*	12.287010	12.149632 [$1s^21p^4$]	12.110496 [$1s^21p^4$]	-1.06
		8 electrons		
aug-cc-pVTZ	19.337940	19.271538 [$1s^21p^6$]	19.714647 [$1s^21p^52s^1$]	12.06
aug-cc-pVQZ	19.204578	19.104295 [$1s^21p^6$]	19.505586 [$1s^21p^52s^1$]	10.92
aug-cc-pV5Z	19.261715	19.131805 [$1s^21p^6$]	19.493381 [$1s^21p^51d^1$]	9.84
aug-cc-pV5Z*	19.261851	19.137723 [$1s^21p^6$]	19.528024 [$1s^21p^52s^1$]	10.62
aug-cc-pV6Z*	19.247016	19.110238 [$1s^21p^6$]	19.437774 [$1s^21p^51d^1$]	8.91
		10 electrons		
aug-cc-pVTZ	28.699209	28.615431 [$1s^21p^62s^2$]	29.258914 [$1s^21p^62s^11d^1$]	17.51
aug-cc-pVQZ	28.186450	28.066966 [$1s^21p^62s^2$]	28.369080 [$1s^21p^62s^11d^1$]	8.22
aug-cc-pV5Z	28.197306	28.039504 [$1s^21p^62s^2$]	28.063383 [$1s^21p^62s^11d^1$]	0.65
aug-cc-pV5Z*	28.197450	28.050011 [$1s^21p^62s^2$]	28.157144 [$1s^21p^62s^11d^1$]	2.92
aug-cc-pV6Z*	28.174226	28.020989 [$1s^21p^61d^2$]	28.007019 [$1s^21p^61d^2$]	-0.38

* Modified basis set removing basis functions with $l \geq 4$

Chapter 5

ML ASSISTED PHASE DIAGRAMS

In this chapter we present a systematic procedure to build phase diagrams for chemically relevant properties by the use of a semi-supervised machine learning technique called uncertainty sampling. Concretely, we focus on ground state spin multiplicity and chemical bonding properties. As a first step, we have obtained single-eutectic-point-containing solid-liquid systems which have been suitable for contrasting the validity of this approach. Once this was settled, on the one hand, we have built magnetic phase diagrams for several Hooke atoms containing few electrons (4 and 6) trapped in spheroidal harmonic potentials. Changing the parameters of the confinement potential such as curvature and anisotropy and interelectronic interaction strength, we have been able to obtain and rationalise magnetic phase transitions flipping the ground state spin multiplicity from singlet (non magnetic) to triplet (magnetic) states. On the other hand, Bader's analysis is performed upon helium dimers confined by spherical harmonic potentials. Covalency is studied using descriptors as sign for $\Delta\rho(r_C)$ and $H(r_C)$ and the dependency on the degrees of freedom of the system is studied i.e. potential curvature ω^2 and inter atomic distance R. As a result, we have observed that there may exist a covalent bond between He atoms for short enough distances and strong enough confinement. This machine learning procedure could, in principle, be applied to the study of other chemically relevant properties involving phase diagrams, saving a lot of computational resources.

5.1 INTRODUCTION

Phase diagrams are graphical representations of functions f such that given a state vector $\mathbf{x} \in \mathbb{R}^n$ they tell us the phase C of such state being the latter a categorical variable ($f : \mathbf{x} \in \mathbb{R}^n \to C$). These diagrams are extensively used in physical, chemical and material sciences to understand how the properties of macroscopic systems change with external parameters such as pressure, temperature, composition etc. Hence, it is interesting to have a procedure to obtain the graphical representations of such f functions.

The brute force approach to obtain the phase diagrams goes as follows: the parameter space is uniformly discretised such that a grid composed by state points is obtained. Upon these state points, experiments or simulations can be carried out to determine the phase (label) of each point hence obtaining a phase diagram of the desired region. Even though this approach is conceptually simple and straightforward to automatise, it also carries two main drawbacks. On the one hand, since all points in the grid must be labelled, the process is expensive in terms of time and resources. On the other hand, it lacks of efficiency since there is no feedback coming from already obtained results.

As it has also be done in many fields of chemical sciences [103–114, 209], in order to improve the efficiency of sampling the discretised parameter space, Machine Learning techniques have been employed such that phase boundaries have been accurately described while evaluating less points than in the straightforward approach [126, 127].

In this chapter, we have focused our attention on some specific machine learning techniques, i.e. Semi-supervised Learning and Uncertainty sampling and have used first principle calculations in order to label each sampled point. Contrary to previous works, instead of applying Label Propagation algorithm (LP) [128], we employ Random Forests (RF) to compute the required uncertainties. The main advantage of this approach is that, contrary to LP, neither a large inverse matrix nor an iterated Markov chain process should be computed. Hence, information can be propagated to denser grids in a faster way. As a benchmark, we have tested the efficiency of this method on ideal solid-liquid systems which contain a single eutectic point. In order to extend this procedure to other chemical properties involving phase diagrams, we have used two simple systems: few electron Hooke atoms for studying ground state magnetic properties and He dimers for studying covalency.

For the former, we build ground state spin multiplicity phase diagrams for 4 and 6 electrons in a ellipsoidal Hooke atom taking as parameters the confinement potential curvatures and the electron-electron interaction screening parameter ($\omega_x^2, \omega_y^2, \omega_z^2, \lambda$) in $\mathbb{R}_+^4$ expressed as in Hamiltonian (5.1). As far as noble gas molecules are concerned, previous computational works in the field of such dimers confined in nanoclusters and nanotubes have reported inter nuclear distances in the range of $[1.265, 2.447]\mathring{A}$ for He$_2$ dimers [210–218]. All these works report shorter interatomic distances between the noble gas atoms. For some of these systems, bond descriptors as in Bader's

theory such as Laplacian of the density at the Bond Critical Point (BCP) $\Delta\rho(r_C)$ and total energy density at the BCP $H(r_C)$ are negative; this insinuates there may be covalent bonds between noble gas atoms under these conditions[214–216, 218]. In the present chapter, we study how covalency descriptors evaluated at the BCP evolve by varying the spherical confinement strength ω^2 as well as the internuclear distance R, both parameters contained in Hamiltonian (5.2).

$$H = \sum_{i=1}^{N} \left(-\frac{1}{2}\nabla^2_{\mathbf{r}_i} + \frac{1}{2}\mathbf{r}_i^\top \mathbf{W}\mathbf{r}_i \right) + \sum_{j>i=1}^{N} \frac{e^{-\lambda r_{ij}}}{r_{ij}}, \quad \mathbf{W} = \begin{pmatrix} \omega_x^2 & 0 & 0 \\ 0 & \omega_y^2 & 0 \\ 0 & 0 & \omega_z^2 \end{pmatrix} \tag{5.1}$$

$$H = -\frac{1}{2}\sum_{i=1}^{4}\nabla^2_{\mathbf{r}_i} - 2\sum_{J=1}^{2}\sum_{i=1}^{4}\frac{1}{r_{iJ}} + \sum_{j>i=1}^{4}\frac{1}{r_{ij}} + \frac{1}{2}\sum_{i=1}^{4}\mathbf{r}_i^T \mathbf{W}\mathbf{r}_i + \frac{1}{R} \tag{5.2}$$

The aim of this project has therefore been to set up a procedure in which chemically relevant properties such as ground state spin multiplicity and covalency in chemical bonding change character induced by external confinement potentials. This procedure could be systematically generalized to the study of other chemically relevant properties involving any type of phase diagrams. The obtained results indicate that this process enables to obtain sharper boundaries between the phases without the need of using any hyperparameter. All of this without losing the efficiency of uncertainty sampling, which, in our case, has enabled us to build proper phase diagrams using less than 2% of the points with respect to naive grid computations.

5.2 COMPUTATIONAL METHODS

5.2.1 Thermodynamic model for eutectic composition

As it is known, when two substances are mixed together their thermodynamical properties such as: vapor pressure, melting and boiling temperatures, specific volume etc. change depending on the activities of both substances. A mixture is considered to be ideal if the interactions between the molecules of both substances interact among them with similar interactions (in nature and strength) such that the difference in potential energies effects can be neglected. As a matter of fact, for ideal mixtures, the activities of each component correspond directly to their molar fraction.

We shall now consider a two component liquid-solid system at constant pressure which has the following properties and approximations:

- Both components are ideally miscible in the liquid phase.

- Both components are ideally unmissable in the solid phase (they form a heterogeneous solid).

- Fusion enthalpies do not depend strongly on temperature.
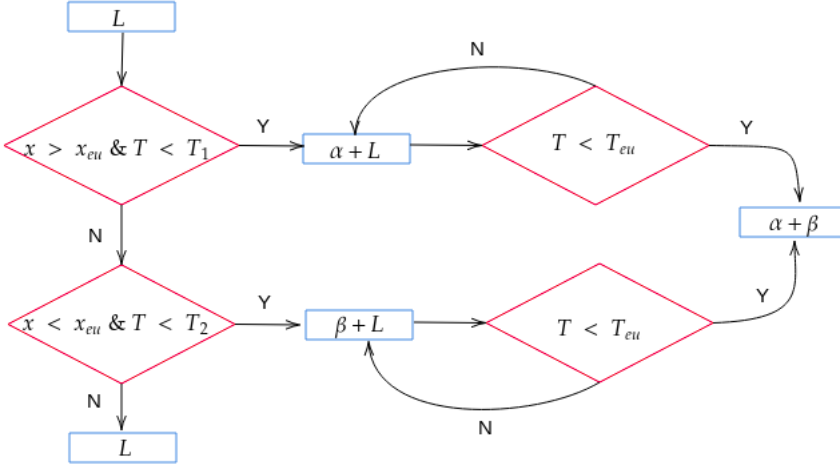
Figure 5.1: Decision tree used for labelling each point in the (x_1, T) plane using eutectic point coordinates and melting curves.

Bearing these properties in mind, one shall derive a relation that determines the molar fraction of each component x_i as a function of their respective fusion temperatures T_{f_i}, fusion enthalpy $\Delta H_{f,i}$ and system temperature T for each component as in equation (5.3).

$$\ln x_i = \frac{\Delta H_{f,i}}{R}\left(\frac{1}{T_{f,i}} - \frac{1}{T}\right) \quad , \sum_{i=1}^{2} x_i = 1 \tag{5.3}$$

The non linear system 5.3 can be solved using previously studied methods [219] such that the eutectic composition vector $\mathbf{x}_{eu}$ and the eutectic temperature T_{eu} are obtained. Now, for two component systems, once we obtain (x_{eu}, T_{eu}) we shall label any point in the (x_1, T) plane using the eutectic point coordinates as well as the melting curves given by equation (5.3) as it is shown in figure 5.1.

Thus, by using this rather simple scheme, we have been able to test the uncertainty sampling method on these systems which are of similar nature as the ones reported in previous works [126, 127] and found out at it is suitable.

5.2.2   Quantum chemical methods

5.2.2.1   *Hooke atoms*

Hooke atoms can be described by a general one body Hamiltonian that reads as in (5.1). Even if there are many works in the bibliography which study electronic structure problems based on Hamiltonians as (5.1) [80], nowadays it is still an interesting topic which can be related to: confined quantum systems [220, 221], electron correlation [222, 223] and many body theory [224, 225]. As far as the symmetry of the Hamiltonian (5.1) is concerned,

the diagonalizable matrix $\mathbf{W}$ contains information of the external (confinement) potential; depending on the degeneracy of this matrix g the system may be: spherical ($g=3$), spheroidal ($g=2$) or tri-axial ellipsoidal ($g=1$).

Here we have studied the case where the matrix $\mathbf{W}$ is diagonal with eigenvalues ω_q^2 which may have three- or two-fold degeneracy and the two body interaction is driven by a screened Coulomb potential where $\lambda \geq 0$. The necessary two body integrals where calculated and coded in `GAMESS US` in previous works realised in our team [226]. From a previous work on spherical Hookean atoms (chapter 4) we have been able to obtain some optimised even tempered basis sets for describing systems containing even number electrons ($n = 2, 4, 6, 8, 10$) with curvature $\omega^2 = 0.25$ at MRPT2(n,13) level; after careful inspection, we reached the conclusion that the best compromise between size and accuracy was given by the basis set obtained for 6 electron system in the singlet spin state, namely ETBS-6S. Based on this results, now we have used these basis functions; nevertheless, we have decided to reduce the active space down to 10 active orbitals. By doing so, electronic structure computations are faster and the error for $\omega^2 = 0.25$ with respect to the large active space is in the order of 1×10^{-3} Hartrees for absolute energies while as for the singlet-triplet gap is of the order of 8×10^{-2}eV. Either way, for larger or smaller active spaces, the absolute error with respect to reference values is of the order of 1×10^{-2} Hartrees while the singlet-triplet energy gap is of the order of 5×10^{-2} eV. Energies for both active spaces and reference values are summarized in Table 5.1.

Table 5.1: Energies in atomic units and energy gaps Δ_{T-S}in eV for singlet and triplet states for spherical Hooke atoms composed by 4 and 6 electrons with λ=0.0 and ω^2=0.25.

	MRPT2(n,10)/ETBS-6S			MRPT2(n,13)/ETBS-6S			Reference [**cioslowski:14jcp**, 39, 62, 80]		
n	Singlet	Triplet	Δ_{T-S}	Singlet	Triplet	Δ_{T-S}	Singlet	Triplet	Δ_{T-S}
4	6.3912	6.3529	-1.04	6.39010	6.3520	-1.04	6.3855	6.3488	-1.00
6	12.0846	12.0479	-1.00	12.0828	12.0461	-1.00	12.0663	12.0313	-0.95

5.2.2.2 *He dimers*

Several authors have studied confined chemically interesting systems as atoms and molecules by means of harmonic potentials [227]. In this study we have considered systems composed by two He atoms ($Z = 2$) with net null charge and singlet spin state. In each case, the nuclei are treated as in the Born-Oppenheimer approximation and they are centred in positions $\mathbf{R}_1$ and $\mathbf{R}_2$ with respect to the origin. Besides, we include a quadratic potential to model the confinement effects; this potential is represented by a diagonal quadratic form $\mathbf{W}$ with elements ω^2. The electronic Hamiltonian for such system can be written in atomic units as in equation (5.2) where lower case letters refer to electrons and capital case letters refer to nuclei. As a shortcut, we may name $R = |\mathbf{R}_1 - \mathbf{R}_2|$ as the internuclear distance since this is the most chemically relevant coordinate. In a first approximation, we have computed ground state singlet ($S = 0$) Hartree-Fock wave functions augmented correlation consistent triple zeta basis functions aug-cc-pVTZ for spherical harmonic potentials ($\omega_x^2 = \omega_y^2 = \omega_z^2$)

in a given point in the feature space (ω^2, R). Zooming into areas of interest, we have also performed CASSCF(4,10)/6-31++G** calculations in order to gain a deeper understanding of these systems. Electronic structure calculations have been carried out using `GAMESS US` sofware. Once we have obtained the wavefunction, we perform Bader's analysis upon the electronic density using `AIMPAC` software. The main features we extract form this analysis are: the laplacian of the electron density at the bond critical point $\Delta\rho(r_C)$, kinetic energy density at the bond critical point $G(r_C)$, potential energy density at the bond critical point $V(r_C)$ and total energy density at the bond critical point $H(r_C)$.

5.2.3   Semi-supervised learning techniques

Semi-supervised learning techniques are halfway between supervised and unsupervised techniques and are employed to obtain information connecting the feature set $X = \{x_1 \ldots x_n\}$ with the label set $Y = \{y_1 \ldots y_n\}$ despite the small number of available data [115–117]. In the context of phase diagram creation, once the parameter space has been discretised as a grid X, we may split these grid points in two set: a labelled set $\mathcal{L}$ (for which the phase is known) and an unlabelled set $\mathcal{U}$ (for which the phase is not known). Namely, the labeled set $\mathcal{L}$ is composed by points formed as an ordered Cartesian products $(x_1, y_1) \ldots (x_l, y_l)$ where $Y_L = \{y_1 \ldots y_l\} \in \{1 \ldots C\}$ is the set of possible labels (categories). Then, we also have the unlabelled set $\mathcal{U}$ composed by $(x_{l+1}, y_{l+1}) \ldots (x_{l+u}, y_{l+u})$ points where the labels $Y_U = \{y_{l+1} \ldots y_{l+u}\} \in \{1 \ldots C\}$ are unknown and the cardinality of this set is much larger than the former one, $l << u$. By doing so, we shall know where to map the next experiment to obtain phase diagrams as it has been done in very recent works [126, 127].

X. Zhu and Z. Ghahramani developed an algorithm named 'Label Propagation Algorithm'[128] in which information from labelled data is propagated to unlabelled data in a stochastic process by means of Markov chains. Here, one defines a graph containing all data -labelled and unlabelled- and defines the connection strength (weight) by pairs as in (5.4). We may observe the closer two points are, the stronger they interact and the interaction also depends on a hyper-parameter σ which can be tuned. As it was proved in [128], the Markov process (5.5) has a unique solution regardless the initial condition for $\mathbf{Y}$ and is given by (5.6).

$$w_{ij} = \exp\left(-\frac{\sum_{d=1}^{D}(x_i^{(d)} - x_j^{(d)})^2}{\sigma^2}\right) \tag{5.4}$$

$$\begin{bmatrix} \mathbf{Y}_l \\ \mathbf{Y}_u \end{bmatrix}^{(n+1)} = \begin{bmatrix} \tilde{\mathbf{T}}_{ll} & \tilde{\mathbf{T}}_{lu} \\ \tilde{\mathbf{T}}_{ul} & \tilde{\mathbf{T}}_{uu} \end{bmatrix} \begin{bmatrix} \mathbf{Y}_l \\ \mathbf{Y}_u \end{bmatrix}^{(n)} \tag{5.5}$$

$$\mathbf{Y}_u = (\mathbf{I} - \tilde{\mathbf{T}}_{uu})^{-1}\tilde{\mathbf{T}}_{ul}\mathbf{Y}_l \tag{5.6}$$

The main drawback of this method is the fact that for dense or large enough grids, the computation of the matrix $(\mathbf{I} - \tilde{\mathbf{T}_{uu}})^{-1}$ is computationally expensive or, in the worst case,

the matrix is singular. This problem may be sidestepped by, instead of using the closed formula (5.6) taking an initial label vector and iterating it as in equation (5.5). Nevertheless, since convergence is reached after several iterations and large matrices are still involved, this algorithm is still costly for dense enough grids and this deficiency is more remarkable as the number of dimensions of the feature space increases. As an alternative, other, rather cheap, classifiers such as Random Forests (RF) can be used to solve the problem. Since RF do not have over fitting problems, using a large enough number of trees, the method is universal for all systems studied in this chapter. Therefore, the initialisation set is employed to train a RF model which will label the unlabelled points assigning them to each category with a given probability, that is, an equivalent approach as using label propagation.

Once information is propagated to all unlabelled points, we must compute the labelling uncertainty in order to select the next point to be computed. Since using RF we obtain the probability for each point $\mathbf{x} \in \mathcal{U}$ to belong to each phase $P(C|\mathbf{x})$, we compute the uncertainty of such point $u(\mathbf{x})$ using Shannon entropy [129] as in equation (5.7) where the sum is performed upon all categories (phases).

$$u(\mathbf{x}) = -\sum_C P(C|\mathbf{x}) \log P(C|\mathbf{x}) \tag{5.7}$$

5.2.4   Work procedure and calculation setup

We have been following some steps repeatedly to obtain our solid-liquid, magnetic and covalency phase diagrams; let us first enumerate them and give a further explanation about them (see also Figure 5.2):

1. Create a suitable grid in the parameter space so that all categories will, in principle, be represented.

2. Select some initialisation points in the grid.

3. Carry out sorting tree or required electronic structure calculations upon the initialisation points and assign them a label corresponding to the output of the calculations.

4. Propagate the information from already computed grid points using trained RF model to the rest to obtain the guessed labels.

5. Compute Shannon's entropy and select the maximum entropy point to carry the computations in step 3 and repeat till maximum number of calculations is reached.

Step 1: We need all classes phases (in our case all four phases concerning the solid-liquid system, at least a ground state singlet and a ground state triplet or a covalent and non-covalent bond) in order to start the sampling procedure, thus we must build a grid in the parameter space of each system suitable for this. For the solid-liquid diagram, the composition x is in the range [0,1] and the temperature T is in the range [$0.25 \times \min(T_1, T_2), 1.25 \times \max(T_1, T_2)$] with a total number of 50000 grid points. In the case of Hooke atoms, the confinement strength parameters $\omega_{x,y}^2, \omega_z^2$ have been taken in the range [$0.20, 0.30$] since optimized basis set for spherical systems with $\omega^2 = 0.25$ were available (chapter 4) and the screening parameter λ was taken in the range [0.05,2.55] with the aim of representing slightly and strongly screened systems accounting for a total number of
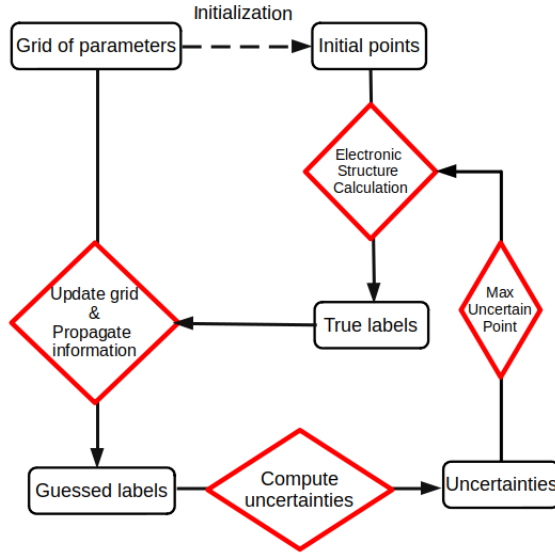
Figure 5.2: Flowchart for the general procedure for phase diagram construction.

3375 grid points. Finally, in relation to He dimers, broad ranges in interatomic distance $R \in [1.0, 4.0]$ Å and confinement strength $\omega^2 \in [0.0, 4.0]$ where employed giving rise to a total number of 250000 grid points.

Step 2: We select the initialisation points in the grid built in step 1. For the solid-liquid system, a total number of 50 uniform distributed points where selected taking the Cartesian product of 5 equidistant points for x and 10 equidistant points for T. With respect to Hooke atoms, by hypothesis, the edges of the parameter grid would contain all different phases; therefore, since three parameters were employed, the initialisation set was obtained using the extreme 8 points. Meanwhile, for the He dimers, the extrema of the grid were considered along with 100 points selected at random.

Step 3: Once a given point in the parameter grid is selected (either the initialisation ones or a new one coming from step 5), we carry out sorting tree or required electronic structure calculations in `GAMESS US` and we assign a label to this point depending on the result obtained either by the sorting tree, the sign of the energy gap Δ_{T-S} or density laplacian or total energy density.

Step 4: We propagate the label information from the data points to the unlabelled ones using 200 trees to form the RF.

Step 5: With the information from the previous step, we compute Shannon's entropy to all guessed points in the grid and select the one with the highest score. We take this point out of the unlabelled points pool $\mathcal{U}$, perform electronic structure calculations as in step 3 and update the labelled database $\mathcal{L}$.

5.3   RESULTS AND DISCUSSION

5.3.1   Solid-liquid phase diagrams with a single eutectic point

In a first step, in order to test the validity and usefulness of this approach, we have studied several solid-liquid phase diagrams for systems which include a single eutectic point considering the required idealisations and approximations. Thus, we have employed the methodology presented in work [219] and have chosen some examples involving binary mixtures: Ag/Si, $KNO_3/LiNO_3$ and K_2SO_4/Li_2SO_4. The required data were obtained from the same source [219].

For all cases, as a naive approach, we have computed grids in the (x_1, T) plane taking 100 points for x_1 in the [0,1] range and 500 points for T in the $[0.25 \times \min(T_{f,1}, T_{f,2}), 1.25 \times \max(T_{f,1}, T_{f,2})]$ range such that the total number of grid points was 50000. For the initialisation set, we have taken another grid with 5 points for x_1 and 10 points for T in the same ranges as the former one; then, we have sampled other 100 points using uncertainty sampling which gives a total number of 150 sampled points. In other words, in order to build a rather accurate phase diagram we have used a **0.3% of points** compared to the naive all grid approach. The obtained phase diagrams are represented in figures 5.3, 5.4 and 5.5.
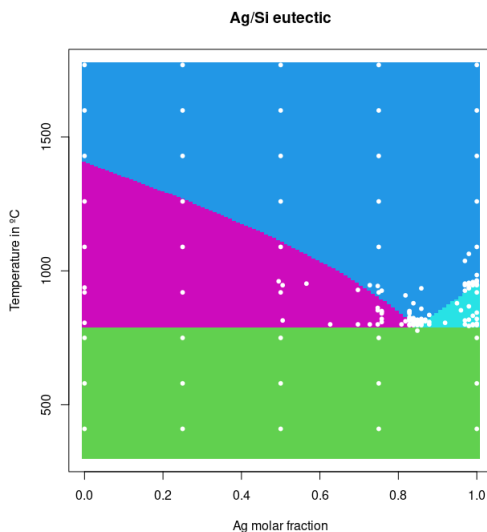
Figure 5.3: Ag/Si solid-liquid phase diagram. Green is the heterogeneous solid phase $\alpha + \beta$, dark blue is the homogeneous ideal liquid mixture L, light blue is $\beta + L$ and purple is $\alpha + L$; the white dots represent the sampled points.

As it has been observed in all three studied cases, the uncertainty sampling method samples more thoroughly the region where the larger number of phases coexist, i.e. near the eutectic point. Finding eutectic compositions is crucial for some pharmacological [228–230]
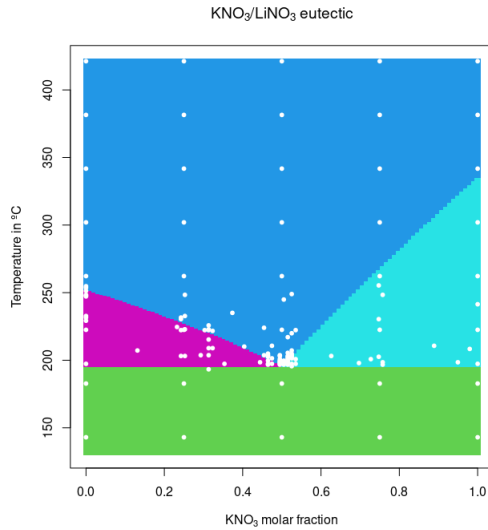
Figure 5.4: KNO$_3$/LiNO$_3$ solid-liquid phase diagram. Green is the heterogeneous solid phase $\alpha + \beta$, dark blue is the homogeneous ideal liquid mixture L, light blue is $\beta + L$ and purple is $\alpha + L$; the white dots represent the sampled points.
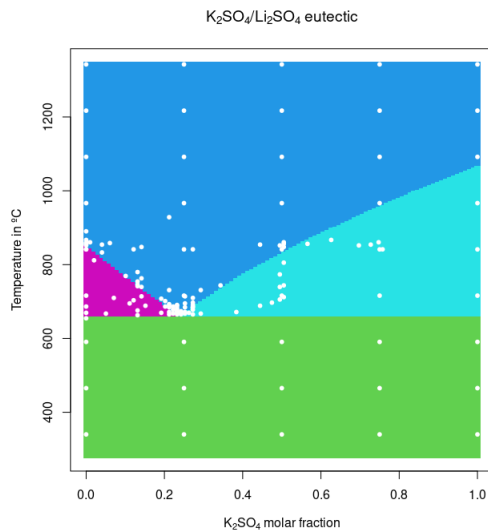
Figure 5.5: K$_2$SO$_4$/Li$_2$SO$_4$ solid-liquid phase diagram. Green is the heterogeneous solid phase $\alpha + \beta$, dark blue is the homogeneous ideal liquid mixture L, light blue is $\beta + L$ and purple is $\alpha + L$; the white dots represent the sampled points.

and green chemistry [231, 232] applications. Therefore, this method shall be interesting for discovering novel eutectic formulations.

5.3.2   Ground state spin multiplicity for Hooke atoms

For these systems, we have employed a grid in the $(\lambda, \omega_{xy}^2, \omega_z^2)$ space with 15 points for each dimension in the domain $[0.05, 2.55] \times [0.20, 0.30] \times [0.20, 0.30]$, therefore a total number of 3375 grid points. In this case, we have taken just 58 points in the grid to be computed, which is the 1.72 % of all points.

We shall start our discussion by describing the obtained ground state spin multiplicity phase diagrams. In figure 5.6 we find magnetic phase diagrams for 4 (left hand side) and 6 (right hand side) electron systems. The vertical axis represents the electron-electron interaction screening parameter λ while the horizontal one represents the ratio between the confinement along the x/y axis and the z axis $\varepsilon = \frac{\omega_{x,y}^2}{\omega_z^2}$. We shall proceed to analyse the obtained diagrams.

On the one hand, for 4 electron systems, one shall observe that singlets (non magnetic states labelled in red) appear in regions for which $\omega_{x,y}^2$ is large, ω_z^2 is small and, for some $(\omega_{xy}^2, \omega_z^2)$ points close to the boundary, they are more abundant as λ increases. Under the anisotropic potential induced by the fact that $\omega_{x,y} > \omega_z$ the one body energies along the z axis are smaller than in the x, y plane and in virtue of the *Aufbau* principle, the former will be occupied firstly giving rise to singlet states. Given an anisotropic enough potential for which the ground state is still a triplet (as in the spherical case), we may still obtain a transition to the singlet state by increasing the screening potential λ as by doing so we are turning off the exchange interaction which does not compensate the high spin state and one body interactions will impose singlet spin states.

On the other hand, for 6 electron systems it is obvious that some features of the phase diagram differ from the one obtained for the 4 electron system. First, the ground state spin multiplicity behaves in the opposite way as compared to the case for 4 electrons; in this case, singlet states appear for small values for $\omega_{x,y}^2$ curvatures and at the same time large values for ω_z^2. Besides, the behaviour with respect to the electron interaction screening parameter λ is the same as in the previous case, the higher it is (for a couple of suitable curvatures $(\omega_{x,y}^2 < \omega_z^2)$ the most likely it is for that potential to give rise to a singlet spin multiplicity for the electronic ground state.

In both cases, for large values of the Yukawa-like screening parameter in the electron-electron interaction λ, quantum exchange interaction becomes weaker and both systems show ground state spin multiplicity transition in the close neighbourhood of the vertical line $\varepsilon = 1$. Besides, in the low λ values regime where exchange interaction are not negligible, in both cases we may observe that spin transition does not happen as soon as we distort the spherical symmetry of the potential; we observe there is an inertia to hold the high spin state (triplet S=1 against singlet S=0). This is a natural consequence of exchange interaction as it lowers the total energy of the system via same spin particles; thus the more particles with same spin there are, the more stable the system becomes.

Taking it up to the non-interacting electron system $(\lambda \to \infty)$, the Hamiltonian is only composed by one-particle operators for which the orbital energy eigenvalues in atomic units are given by 5.8. In this case, depending on the asymmetry parameter ε which is defined
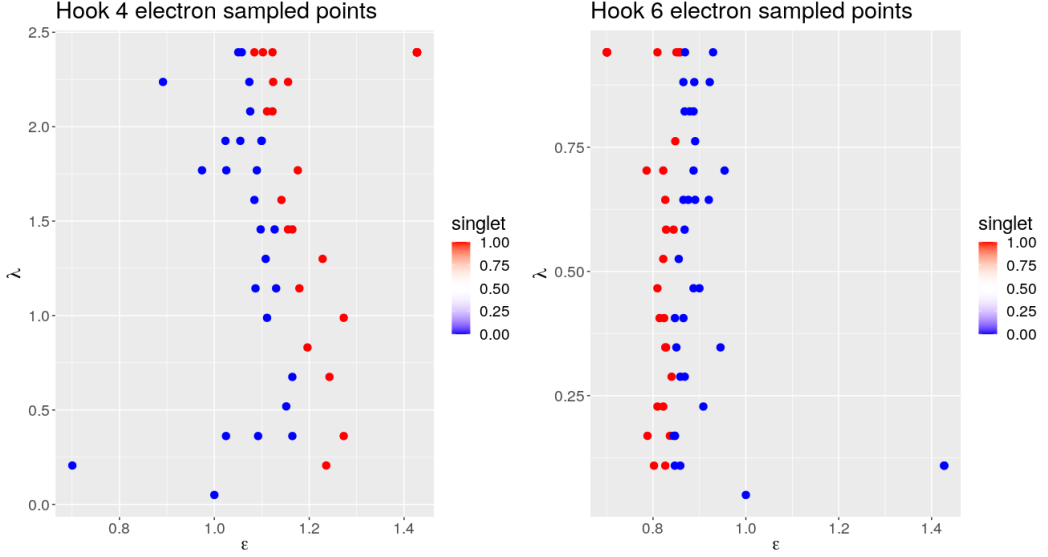
Figure 5.6: Sampled points in the (ϵ, λ) plane. Red indicates singlet ground spin state while blue indicates triplet ground spin state

as the ratio between the axial confinement parameters $\omega_{x,y}^2$ and ω_z^2, the energy of the p orbitals will split as it is shown in Figure 5.7. Taking into account the Pauli's exclusion principle, we may fit up to a couple of electrons in each orbital and, according to Hund's rule, in case of degeneracy they will occupy degenerate orbitals such that total spin is maximised. Keeping these two many-body quantum rules in mind, it is easy to see that the ground state spin multiplicity does not only depend on the confinement potential but also in the number of electrons.

$$\epsilon_{n_x, n_y, n_z} = \omega_{x,y}(n_x + n_y + 1) + \omega_z \left(n_z + \frac{1}{2}\right) \tag{5.8}$$

When the confinement is sharper along the z direction than in the x and y directions $(\omega_z^2 > \omega_{x,y}^2)$ (this is sphericity parameter $\varepsilon < 1$), the degeneracy of the p orbital splits into two main groups, the p_z orbital (higher in energy) and the plane composed by the still degenerate p_x and p_y (lower in energy). Therefore, when we distort the spherical symmetry in this way nothing essential happens to 4 electron systems as far as ground state spin multiplicity is concerned. However, for six electron systems, as ε gets smaller, the energy of the p_z orbital goes higher and we obtain a point in which all p_x and p_y orbitals are doubly occupied while p_z orbital is empty. If we are to fit all 6 electrons in this potential, we shall see that the ground state spin multiplicity is the singlet; thus, magnetic properties are altered in the process of comprising the sphere.

On the contrary, instead of compressing the sphere, if we stretch it along the z axis we obtain a smaller curvature along this direction $(\omega_z^2 < \omega_{x,y}^2)$ and the sphericity parameter becomes $\varepsilon > 1$. Once again, according to the one-body energy formula (5.8) this implies the
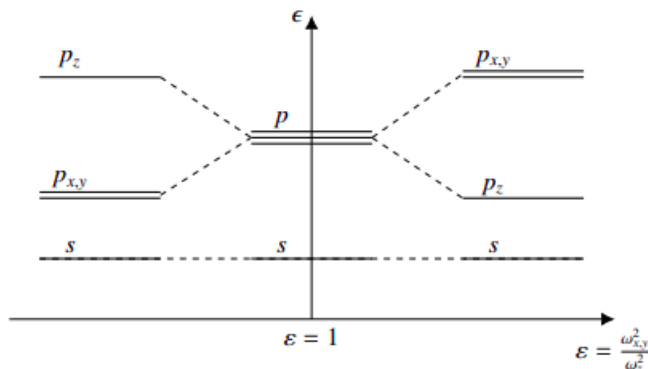
Figure 5.7: Schematic atomic orbital energy splitting along asymmetry parameter ϵ

orbital energies, degenerate in the spherical case, split into two branches: the p_z orbital (this time lower in energy) and the plane composed by the still degenerate p_x and p_y (higher in energy). Applying the occupancy rules, one shall see that for 4 electron systems the ground state multiplicity is the singlet (all paired electrons) while for 6 electron systems there is no change as long as ground state multiplicity is concerned. As opposed to the previous case, the magnetic properties for the 4 electron system alter along this transformation while the 6 electron system is able to keep its magnetic properties.

5.3.3 Detecting covalent bonding in spherically confined He$_2$ systems

In a first step, we have built the covalency phase diagrams shown in Figure 5.8 at HF/aug-cc-pVTZ level using as label the sign (red for negative and blue for positive) of the laplacian of the density at the bond critical point $\Delta\rho(r_C)$ and the total energy density at the bond critical point $H(r_C)$. In total, we have computed 500×500 grid points in the $[0.10, 4.00] \times [1.00, 4.00]$ interval in the (ω^2, R) plane taking 104 points for initialisation and 200 more for building the diagram therefore **using 0.1216% of all grid points**.

In these diagrams we represent the confinement curvature ω^2 in the vertical axis and the interatomic distance R in the horizontal one. As it can be seen for $\Delta\rho(r_C)$, negative values are obtained in regions where the interatomic distance lays around 1.00 and 1.52 Å and confinement curvatures larger than 2.00. On the other hand, as far as $H(r_C)$ is concerned, we have found negative values for all interatomic distances shorter than 1.50 Å. Beyond this threshold, we may observe that for large enough harmonic confinement curvature, the sign of the total energy density at the BCP switches from positive to negative; the curvature required to make this switch happen is larger as we increase the inter atomic distance between the He atoms.

At this level of theory, for the range in which there are covalency indicators, our model comes in terms with previous works based on all-atom calculations on similar systems. For example for He$_2$@C$_{20}$H$_{20}$ where the He-He distance is reported to be 1.265Å and positive
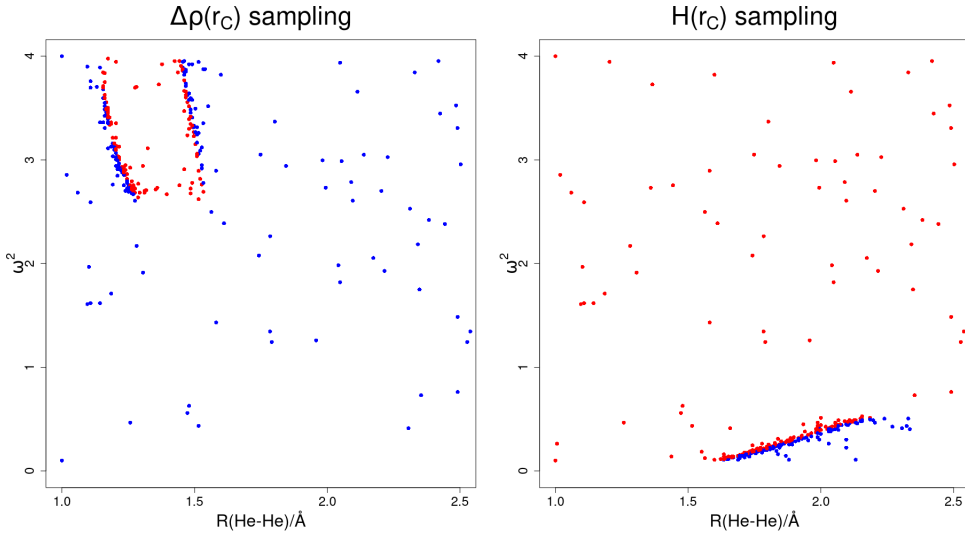
Figure 5.8: Sign of total energy density for He_2 system computed at HF/aug-cc-pVTZ level, red is for negative and blue is for positive.

value for $\Delta\rho(r_C)$ [210] which is compatible with our calculations for $\omega^2 < 2.00$. Also for interatomic distances smaller than $1.60 \mathring{A}$, for $He_2@B_{12}N_{12}$ and $He_2@B_{16}N_{16}$ systems 1.306 $\mathring{A}$ and 1.456 $\mathring{A}$ distances are reported [216]. For these two systems, positive $\Delta\rho(r_C)$ are reported while total energy density is negative in the former (around 1×10^{-2} a.u.) and zero in the latter which comes along with our results. For larger distances, in a recent work 1.520 $\mathring{A}$ and 1.546 $\mathring{A}$ distances are reported for $He_2@C_{36}$ and $He_2@C_{40}$ respectively [212]; the reported sign of $\Delta\rho(r_C)$ and $H(r_C)$ are positive (of the order of 5×10^{-3} atomic units). Finally, He atom couples confined in B_{40} cages have been reported to be $1.672 - 1.640$ $\mathring{A}$ apart [217] and $\Delta\rho(r_C)$ and $H(r_C)$ both turned out to be positive which is compatible with our results for small ω^2 values.

So far, results concerning the nature of bonding in helium dimer obtained by our harmonic confinement model seem to agree with all atom models for several cages. Bearing in mind that real cages may induce a rather small potential curvature ω^2 and the fact that switch in the sign of $H(r_C)$ happens somewhere in the interval $[1.40, 2.60]$ $\mathring{A}$ for internuclear distance, we shall focus our attention on studying this region and include electron-correlation effects in our calculations. Hence, we have performed CASSCF(4,8)/aug-cc-pVTZ calculations in this region. To do so, we have taken a 20×20 grid points in the (ω^2, R) plane with evenly separated points in the $(0.00, 1.00) \times (1.40, 2.6)$ domain. Using these points, we have computed level maps as in Figure 5.9. In the three maps, we indicate the interatomic distance in the horizontal axis, the confinement curvature in the vertical axis and we have computed level maps for three Bader descriptors (from left to right): $\Delta\rho(r_C)$, $H(r_C)$ and $-G(r_C)/V(r_C)$ which take values in different ranges according to each descriptor labelled in red for low values and in blue for higher ones. As we can see for $\Delta\rho(r_C)$, we have found positive values in this domain and it increases as the interatomic

distance is shorter an it is not highly dependent on ω^2 specially for rather short interatomic distances. For $H(r_C)$ we have found negative values which get smaller (more negative) as we shorten the internuclear distance and increase the confinement curvature which is compatible with prior HF calculations as well as with all-atom calculations in which more negative values for this parameter appear when the size of the confining cage is smaller.
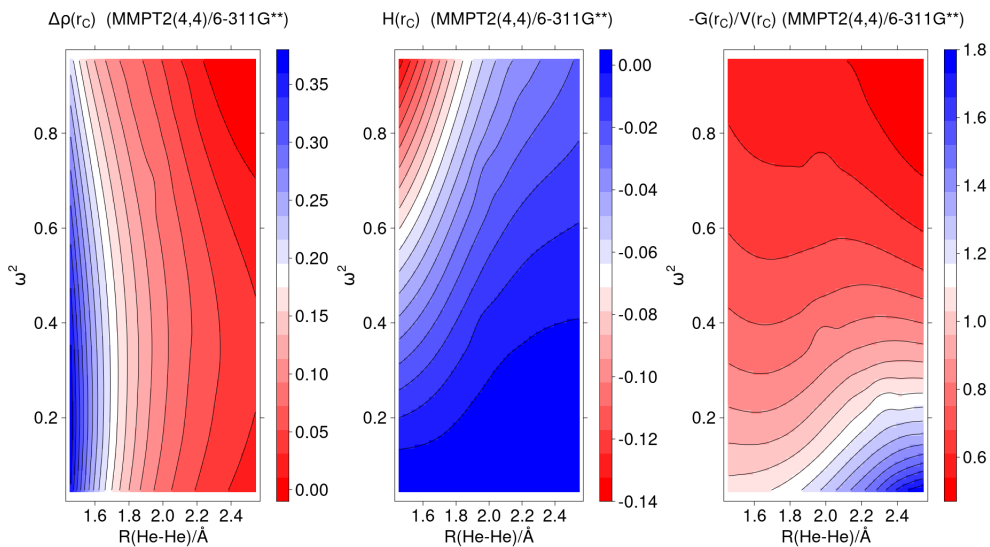
Figure 5.9: Covalency indicators for MMPT2(4,8)/aug-cc-pVTZ calculated densities for spherical confinement, from left to right: $\Delta\rho(r_C)$, $H(r_C)$ and $-G(r_C)/V(r_C)$. Red shades indicate low values, white indicates medium and blue shades indicate high values.

5.4 CONCLUDING REMARKS

In this chapter we have been able to produce computationally affordable magnetic and covalency phase diagrams for some few electron Hooke atoms and helium dimers confined in harmonic potentials respectively by sampling the potential feature space by means of semi-supervised learning technologies. Contrary to the conventional way of explicitly calculating every point in a grid, we have taken several initialisation points and have propagated their information using classifiers based on Random Forest, which, compared to label propagation algorithm, has enabled us to study dense grids. By just calculating the points where information is maximal, we have been able to reduce the number of required computations (in our case the required points for computation were below 2% of all grid points).

The validation of the method employing RFs was performed by computing analytical ideal solid-liquid phase diagrams involving a single eutectic point. As it has been shown, this method samples all interphases, specially the neighbourhood of the eutectic point in which all four phases coexist.

From previous works on 4 and 6 electron systems confined in spherical harmonic potentials with curvature $\omega^2 = 0.25$, it is known that the ground state spin multiplicity of these systems is a triplet ($S=1$) and the first singlet ($S=0$) lays around 1 eV above in energy. If we consider the electrons do not interact among them, the whole system behaves as a system composed by n bodies which still must fulfill basic many-body systems features as: Pauli's exclusion principle, *Aufbau* filling principle and Hund's rule. Under these assumptions, we state that ground state spin multiplicity will be imposed by the symmetry of the confining potential and, by altering the symmetry of it, we may obtain ground state multiplicities either singlets or triplets depending on the potential parameters, the strength of interelectronic interactions and the number of electrons.

On the other hand, Bader analysis performed upon confined helium dimers by means of harmonic potential seems to be a rather good model which captures the main features of all atom approaches. As far as sign of density laplacian and total energy density is concerned, all trends have been correctly described by this simple model which shows that effective confinement potentials can be employed to capture the essence of complex confined systems and rather simple models can be employed to describe them. This fact enabled the usage of high theoretical level computations upon these systems.

As a first step for many other applications of chemical interest, we conclude these machine learning techniques may be useful for classification and exploration.

Chapter 6

GAUSSIAN CONFINEMENT AND CONNECTION TO HOOKE ATOMS

In this chapter, we have computed and implemented one-body integrals concerning gaussian confinement potentials over gaussian basis functions. Then, we have set an equivalence between gaussian and Hooke atoms and we have observed that, according to singlet and triplet state energies, both systems are equivalent for large confinement depth for a series of even number of electrons $n = 2, 4, 6, 8$ and 10. Unlike with harmonic potentials, gaussian confinement potentials are dissociative for small enough depth parameter; this feature is crucial in order to model phenomena such as ionization. In this case, in addition to corresponding Taylor-series expansions, the first diagonal and sub-diagonal Padé approximant were also obtained, useful to compute the upper and lower limits for the dissociation depth. Hence, this method introduces new advantages compared to others.

Submitted to IJQC

6.1 INTRODUCTION

Gaussian potential wells have attracted attention in the scientific community in a wide range of fields. On the one hand, in theoretical condensed matter field for modelling and gaining further knowledge on Quantum Dots (QDs) in semiconductors (such as GaAs) and confined systems [233–236]. Recent works concerning two and three dimensional quantum dots study properties of these impurities such as Aharonov-Bohm oscillations [237], decoherence effects [238], thermo-magnetic properties [239–242], interactions with electric and laser fields [243–248], topological dependence on the stated properties [249, 250], quantum entanglement[251], mathematical modelling [252–254] and even few-electron systems confined in such potentials [255, 256]. On the other hand, Ali-Bodmer potentials for describing α particles interactions in nuclear physics[257] are still employed in nuclear structure calculations with α clustering [258–260].

In the latter field (in which only one-body equations are considered) the gaussian shaped interactions are treated as such. However, in the condensed matter and electronic structure community (where many-body problems arise) these functions are approximated by using harmonic potentials also known as Hooke atoms. Some of such systems composed by 2 electrons have closed form solutions [80] which are employed as benchmarks when testing novel electronic structure methods [36, 37, 261–265]. Besides, there are plenty of works in the literature where high theoretical level computations have been performed for larger systems [41, 266].

Although harmonic potentials found in Hookean systems are a sensible approximation, when describing bound states in QDs and artificial atoms, there are two main inconveniences. First, by using such potentials, one loses molecular structure since any linear combination of many centre harmonic potentials will give rise to a new harmonic potential. Second, harmonic potentials have an infinite number of bound states, therefore, processes such as ionization and dissociation cannot be properly modelled.

Minding the gap between one-particle confined in a gaussian-like potential problems and many-body systems confined in harmonic potentials, in this work we have computed the required one-body integrals for gaussian potentials using, also, gaussian basis functions so employed in quantum chemistry. By doing so, we have set sail in three paths concerning these systems: we have studied deeply confined (high values depth parameter V_0) atomic systems with even number of electrons ($n = 2, 4, 6, 8$ and 10) by computing their singlet-triplet gap and relating them to equivalent Hooke atoms studied in previous works. Besides, we have studied dissociation limits for 2 electron systems in singlet spin state with Yukawa-like screening interaction.

6.2 COMPUTATIONAL METHODS

In this work we have studied systems of even number of electrons ($n = 2, 4, 6, 8$ and 10) confined within a three dimensional gaussian potential and screened electron-electron interactions writing the one-centre Hamiltonian as in (6.1). The two-body (four-centre) integrals concerning the screened Yukawa-like inter-electronic interactions were already computed and implemented for gaussian basis functions by our group [226] in GAMESS US.

$$H = -\frac{1}{2}\sum_{i=1}^{n}\nabla_{\mathbf{r_i}}^2 - \sum_{i=1}^{n}V_0 e^{-\frac{\omega^2}{2V_0}\mathbf{r}_i^2} + \sum_{j>i=1}^{n}\frac{e^{-\lambda|\mathbf{r_j}-\mathbf{r_i}|}}{|\mathbf{r_j}-\mathbf{r_i}|} \tag{6.1}$$

The election of the exponent in the gaussian confinement function in Hamiltonian (6.1) is not a fact of chance. It has been selected so that for any value of the depth parameter V_0, the curvature of the confinement function is kept constant to $\frac{1}{2}\omega^2$; by doing so, we have been able to relate these new calculations to former ones from the literature.

In preceding works, we have optimised some even-tempered gaussian basis functions for spherical harmonic potentials with curvature $\omega^2 = \frac{1}{2}$ and even number of electrons ($n = 2, 4, 6, 8$ and 10) at Complete Active Space Self Consistent Field (CASSCF) and Second Order Multi Reference Many-body Perturbation (MRMP2) levels of theory using n electrons and 13 orbitals in the active space. We have observed that the most balanced (concerning accuracy and size) basis set was the one obtained for six electron systems with singlet spin state, namely ETBS-6S basis. We have used the same basis and method throughout this chapter conditioning the exponent of the gaussian confinement function so that the curvature is kept as in the optimised Hooke system for each individual atom.

6.2.1 One-body integrals concerning Gaussian confinements

We need to obtain the one-body integrals for N centre external potentials defined as in (6.2); as it is commonly done in quantum chemistry, if we expand atomic orbitals as contracted gaussian primitive functions, the inner integrals to be computed have the form (6.3).

$$V_{ext}(\mathbf{r}) = -\sum_{i=1}^{N} V_{0,i} e^{-\beta_i(\mathbf{r}-\mathbf{R}_{0,i})^2} \tag{6.2}$$

$$\int G_1(\alpha_1, \mathbf{R}_A, l_1, m_1, n_1) G_2(\alpha_2, \mathbf{R}_B, l_2, m_2, n_2) e^{-\beta_i(\mathbf{r}_1-\mathbf{R}_{0,i})^2} d\mathbf{r}_1 \tag{6.3}$$

We take the next step by applying the Gaussian Product Theorem [267–269] upon the two basis functions G_1 and G_2 so we obtain another gaussian namely G_P:

$$G_P = K\sum_{l=0}^{l_1+l_2}\sum_{m=0}^{m_1+m_2}\sum_{n=0}^{n_1+n_2} f_l f_m f_n (\mathbf{x}_1 - \mathbf{X}_P)^l (\mathbf{y}_1 - \mathbf{Y}_P)^m (\mathbf{z}_1 - \mathbf{Z}_P)^n e^{-\gamma_P(\mathbf{r}_1-\mathbf{R}_P)^2}$$

For which the characteristic constants and coefficients are defined as:

$$K = \exp\left(-\frac{\alpha_1\alpha_2}{\gamma_P}(\mathbf{R}_A - \mathbf{R}_B)^2\right)$$

$$\mathbf{R}_P = \frac{\alpha_1\mathbf{R}_A + \alpha_2\mathbf{R}_B}{\gamma_P} \quad , \quad \gamma_P = \alpha_1 + \alpha_2$$

$$f_l = \sum_{i=0}^{l_1} \sum_{j=0}^{l_2} (X_P - X_A)^{l_1-i} \binom{l_1}{i} (X_P - X_B)^{l_2-j} \binom{l_2}{j}$$

$$f_m = \sum_{i=0}^{m_1} \sum_{j=0}^{m_2} (Y_P - Y_A)^{m_1-i} \binom{m_1}{i} (Y_P - Y_B)^{m_2-j} \binom{m_2}{j}$$

$$f_n = \sum_{i=0}^{n_1} \sum_{j=0}^{n_2} (Z_P - Z_A)^{n_1-i} \binom{n_1}{i} (Z_P - Z_B)^{n_2-j} \binom{n_2}{j}$$

As the potential energy function is yet a gaussian function itself with zero angular momentum, we apply the Gaussian Product Theorem again upon the potential function and the Gaussian obtained in the previous step G_P. Then we obtain a new Gaussian, namely, G_Q given as:

$$G_Q = K' \sum_{l'=0}^{l} \sum_{m'=0}^{m} \sum_{n'=0}^{n} f_{l'} f_{m'} f_{n'} (\mathbf{x}_1 - \mathbf{X}_Q)^{l'} (\mathbf{y}_1 - \mathbf{Y}_Q)^{m'} (\mathbf{z}_1 - \mathbf{Z}_Q)^{n'} e^{-\gamma_Q (\mathbf{r}_1 - \mathbf{R}_{Q,i})^2}$$

Where the constants and coefficients are:

$$K' = \exp\left(-\frac{\beta_i \gamma_P}{\gamma_Q} (\mathbf{R}_P - \mathbf{R}_{0,i})^2\right) \quad , \quad \mathbf{R}_Q = \frac{\beta_i \mathbf{R}_{0,i} + \gamma_P \mathbf{R}_P}{\gamma_Q} \quad , \quad \gamma_Q = \beta_i + \gamma_P$$

$$f_l = \sum_{i=0}^{l'} (X_Q - X_{0,i})^{l'-i} \binom{l'}{i}$$

$$f_m = \sum_{i=0}^{m'} (Y_Q - Y_{0,i})^{m'-i} \binom{m'}{i}$$

$$f_n = \sum_{i=0}^{n'} (Z_Q - Z_{0,i})^{n'-i} \binom{n'}{i}$$

Now -using the properties of the exponential function and considering the distance squared dependency of the exponent- we can acknowledge the integral (6.3) is in fact composed by the product of three integrals; one for each spacial variable. It can therefore be written as in (6.7)

$$I(x, y, z) = KK' \left[I(x) I(y) I(z) \right] \tag{6.7}$$

And each integral is given as:

$$I_i(x) = \sum_{l=0}^{l_1+l_2} f_l \sum_{l'=0}^{l} f_{l'} \int_{-\infty}^{\infty} (x_i - X_Q)^{l'} e^{-\gamma_Q (x_i - X_Q)^2} dx_i$$

$$I_i(y) = \sum_{m=0}^{m_1+m_2} f_m \sum_{m'=0}^{m} f_{m'} \int_{-\infty}^{\infty} (y_i - Y_Q)^{m'} e^{-\gamma_Q (y_i - Y_Q)^2} dy_i$$

$$I_i(z) = \sum_{n=0}^{n_1+n_2} f_n \sum_{n'=0}^{n} f_{n'} \int_{-\infty}^{\infty} (z_i - Z_Q)^{n'} e^{-\gamma_Q (z_i - Z_Q)^2} dz_i$$

Notice we have exchanged the order of integration and summation and we are allowed to do so as both, the integral and summation, are totally convergent, the former because we are dealing with functions which live in the Schwartz space and the latter because the summation is finite. We may also notice that all three integrals are the momenta of a Gaussian distribution for which the general formula is given by equation (6.9). Since the Gaussian distribution is even with respect to reflection plane where the point $t_1 = T_Q$ in contained, only even order momenta will be different from zero.

$$\int_{-\infty}^{\infty} (t_i - T_Q)^k e^{-\gamma_Q (t_i - T_Q)^2} dt_i = \frac{\Gamma\left(\frac{k+1}{2}\right)}{\gamma_Q^{(k+1)/2}} \quad , k = 0, 2, 4 \ldots \tag{6.9}$$

One last remark concerns the evaluation of the gamma function obtained in equation (6.9). As we have mentioned, the moment parameter k must be even for the integral not to vanish, using a property of the gamma function, we may evaluate it using a product as:

$$\Gamma\left(n + \frac{1}{2}\right) = \sqrt{\pi} \frac{1 \cdot 3 \cdot 5 \ldots (2n-1)}{2^n} \quad , \quad n \in \mathbb{N}$$

$$\Gamma\left(\frac{k}{2} + \frac{1}{2}\right) = \begin{cases} \sqrt{\pi}, & \text{if } k = 0 \\ \sqrt{\pi} \prod_{r=1}^{k-1,2} \frac{r}{2}, & \text{otherwise} \end{cases}$$

Thus, each of the three spatial components of the matrix element containing the i-th centre are given as simple nested sums and products as in (6.11).

$$I_i(x) = \sum_{l=0}^{l_1+l_2} f_l \sum_{l'=0}^{l,2} f_{l'} \frac{\sqrt{\pi}}{\gamma_Q^{(k+1)/2}} \prod_{l''=1}^{l'-1,2} \frac{l''}{2} \tag{6.11}$$

We have coded these integrals as a subroutine in FORTRAN70 in order to add them to the *source* file for the one body integral packages in the open code package GAMESS-US.

6.3   RESULTS AND DISCUSSION

6.3.1   Deeply confined one centre systems with even number of electrons

We have performed Complete Active Space Self Consistent Filed (CASSCF) and Second Order Multi Reference Many-body Perturbation (MRMP2) calculations using $m = 10, 11, 12$ and 13 orbitals in the active space upon systems composed by small even number of electrons $n = 2, 4, 6, 8$ and 10 confined in a single three-dimensional gaussian potential well as in Hamiltonian (6.1). In order to make sure that our new results are sensible and make a connection with former works on Hook atoms with these numbers of electrons, we have taken 30 values for the gaussian depth parameter V_0 evenly spaced in the range $[-300.0, -10.0]$ (in au), set the screening parameter $\lambda = 0.0$ and the curvature parameter $\omega^2 = \frac{1}{4}$. With the aim of gaining a deeper insight of the connection between Gaussian and Hookean systems, we have expanded the Gaussian potential energy function in a power series as in equation (6.12). If we keep the first three terms in this Taylor expansion, we may notice that we assume an error in potential energy which is proportional to the inverse of the gaussian potential depth as in equation (6.13). If we further assume that kinetic energy and electron interaction energy do not depend strongly on potential depth (which is a sensible assumption for deep potentials), the Gaussian system energy E_G and the equivalent (in the sense of curvature) Hookean system energy E_H are related as in equation (6.14) where $g(n, \omega^2)$ is the average value of the first anharmonic term and depends on the number of electrons n and the curvature of the equivalent Hookean ω^2. In other words, the first anharmonic term is treated as a first-order perturbation for the Hooke atom. Even if the number of electrons, the depth and the curvature are kept constant, we may infer that spin state of the wave-function also plays a role since rather different one-body functions may take part in building the whole many-body wave functions; therefore, altering the third term average value in equation (6.13).

$$V_G = -\sum_{i=1}^{n}\sum_{k=0}^{\infty} \frac{\left(-\frac{\omega^2}{2}\right)^k V_0^{1-k} r_i^{2k}}{k!} \tag{6.12}$$

$$V_G = -nV_0 + \frac{\omega^2}{2}\sum_{i=1}^{n} r_i^2 - \frac{\omega^4}{8V_0}\sum_{i=1}^{n} r_i^4 + \mathcal{O}\left(\frac{\omega^6 n}{V_0^2}\right) \tag{6.13}$$

$$E_G = -nV_0 + E_H - \frac{g(n, \omega^4)}{V_0} + \mathcal{O}\left(\frac{\omega^6 n}{V_0^2}\right) \tag{6.14}$$

If we study the Gaussian system's energy variation with respect to the potential depth, we shall observe that to a great extent, the main contribution to this variation is the number of electrons as in equation (6.15). This last expression may also be obtained by applying the Hellmann–Feynman theorem differentiating the Hamiltonian (6.1) with respect to V_0 and taking into account that in deeply confined systems $\frac{\omega^2}{2V_0}$ goes to zero (6.16).

$$\frac{dE_G}{dV_0} = -n + \mathcal{O}\left(\frac{\omega^4}{V_0^2}\right) \tag{6.15}$$

$$\frac{dE_G}{dV_0} = -\left\langle \sum_{i=1}^{n} e^{-\frac{\omega^2 r_i^2}{2V_0}}\left(1 + \frac{\omega^2 r_i^2}{2V_0}\right)\right\rangle \sim -n, V_0 \to \infty \tag{6.16}$$

Hereby, based on the power series representation for the potential energy function in equation (6.12) and considering T and V_{ee} do not heavily depend on a specific V_0 but rather on the curvature of the potential ω^2, we may state that -just considering the first anharmonic term- the shifted energy of the gaussian system $E_G + nV_0$ depends linearly on the inverse of the gaussian potential depth $1/V_0$ and the ordinate is just the Hookean system energy with curvature ω^2. We have performed several calculations as stated in the previous paragraph and we have obtained the Hookean energy E_H and the first anharmonic term (written for simplicity as g) by linear regression; all regression estimates are contained in table 6.1.

Table 6.1: Hookean energy E_H (au) and g (au^2) terms obtained by linear regression using data obtained by CASSCF(n,m)/ETBS-6Sand MRMP2(n,m)/ETBS-6S calculations.

		E_{CAS}^S		E_{MRMP2}^S		E_{CAS}^T		E_{MRMP2}^T	
n	m	E_H	g	E_H	g	E_H	g	E_H	g
2	10	2.001718	0.3214578	2.000553	0.3214138	2.36111	0.4615673	2.359877	0.4623589
	11	2.001569	0.3220647	2.000541	0.3214695	2.359966	0.4629399	2.359749	0.4629238
	12	2.001353	0.3219344	2.000521	0.3214604	2.359883	0.4629516	2.359746	0.4629451
	13	2.001233	0.3221784	2.000509	0.3214931	2.35988	0.4629387	2.359746	0.4629558
4	10	6.41014	1.330105	6.391462	1.331209	6.369164	1.314156	6.353142	1.31538
	11	6.405534	1.329927	6.391097	1.331188	6.365399	1.315223	6.352794	1.315585
	12	6.401805	1.332317	6.390674	1.331675	6.361329	1.316371	6.352395	1.315823
	13	6.398952	1.331355	6.390306	1.331604	6.360014	1.305258	6.352244	1.314446
6	10	12.13421	2.784703	12.08499	2.786157	12.09482	2.767391	12.04846	2.768882
	11	12.12679	2.788366	12.0844	2.786919	12.08947	2.763241	12.04783	2.768251
	12	12.12125	2.788358	12.08397	2.786566	12.08349	2.770115	12.04719	2.768935
	13	12.11545	2.783258	12.08333	2.786984	12.07844	2.771766	12.04666	2.769276
8	10	19.07563	3.931056	19.00154	4.625022	19.36024	4.555748	19.27003	4.672289
	11	19.07066	4.728791	19.00104	4.728537	19.35476	4.703725	19.2721	4.905097
	12	19.06393	4.689791	19.00023	4.703367	19.34488	4.823247	19.27197	5.007794
	13	19.05414	4.735014	18.99894	4.729663	19.33712	4.901288	19.27023	4.921244
10	10	27.83390	7.339055	27.69036	7.533762	27.80165	7.224892	27.66912	7.522172
	11	27.81091	7.453328	27.68948	7.638288	27.78357	7.424963	27.66788	7.547430
	12	27.789871	7.5806211	27.693892	7.5958861	27.768859	7.5651956	27.666607	7.5712475

We may observe that Hooke atom energies for singlet and triplet states agree with those obtained in former works (chapter 4) at the same level of theory and in the worst case scenario, the Hookean energy has $1 \times 10^{-5} au$ error obtained by error estimation in routine linear regression; thus, the calculation protocol error is larger than the one from

the regression. As far as first anharmonic terms g are considered, they are obtained by taking the slope of the linear regression which -in the worst case scenario- has an error of $4 \times 10^{-4} au$. If we take a deeper insight of the g values, we may immediately notice that, for a given spin state either singlet or triplet, does not dramatically change with the size of the active space while it is highly dependent on the number of electrons n. Besides the number of electrons, this anharmonic term also depends on the spin state taking the two electron system as the most notorious one. From the previously exposed theory this behaviour was expected since g represents a sum over electrons of an averaged value of a quartic potential with respect to a many-body normalised wave-function; therefore, g condenses a lot of information about the system: the curvature,the number of electrons and the spin state.

In the worst case scenario -the one for CASSCF(8,10)(S)/ETBS-6S calculations- the regression correlation parameter was $R^2 = 0.9623$. However, this is a pretty odd case and the average value for this statistic is $R^2 = 0.9991$. It can also be seen that even the Hooke atom energy is comparable to the ones obtained by other methods, the anharmonic contribution g is quite different even if we compare it to the one obtained by including dynamical correlation effects via perturbation methods at the same theory level. We have also observed that as soon as the active space size is augmented, the correlation parameter gets rapidly closer to 1 approaching perfect linear dependency.

6.3.2   Loosely confined two electron systems with screened Coulomb interaction

Based on the fact that two electron systems with singlet spin state have at least one occupied bound state, we have been wondering at which point of gaussian potential depth the whole systems dissociates $(E_G(V_0^d) = 0)$. On top of this, we have also considered electron-electron interaction to be screened and in what measure it affects the loosely bound system's stability. Hence, we have modelled these systems using Hamiltonians as in equation (6.17) where the confinement Gaussian potential has been defined as in the previous section and the electronic Coulomb interaction is replaced by a Yukawa-like potential with exponent $\lambda > 0$. We have taken 10 values for λ parameter in the evenly separated range $[0.10, 1.00]$ and 20 values for V_0 also in a evenly separated range $[-1.50, -0.50]$ at MRMP2(2,13)/ETBS-6S level of theory for singlet states; the results for these calculations can be found in figure 6.1.

Points with positive energies in this plot are somehow meaningless since positive energies belong to dissociated systems (scattering states); nevertheless, energies are positive and real since the basis function themselves create the Dirichlet boundaries. At a first glimpse, one shall observe that the dissociation limit depth is smaller as λ is larger (therefore electron-electron interaction is weaker).

Let us try to make sense of the obtained results. As in the previous section, we have expanded our Gaussian systems energy now taking an additional term as in equation (6.18) where the anharmonic contributions g_1 and g_2 are generally taken as positive despite the fact the sign is alternating in the original Taylor-like series. Now, we shall obtain E_H, g_1 and g_2 from data using linear regression (omitting all $E_G > 0$ data) via small
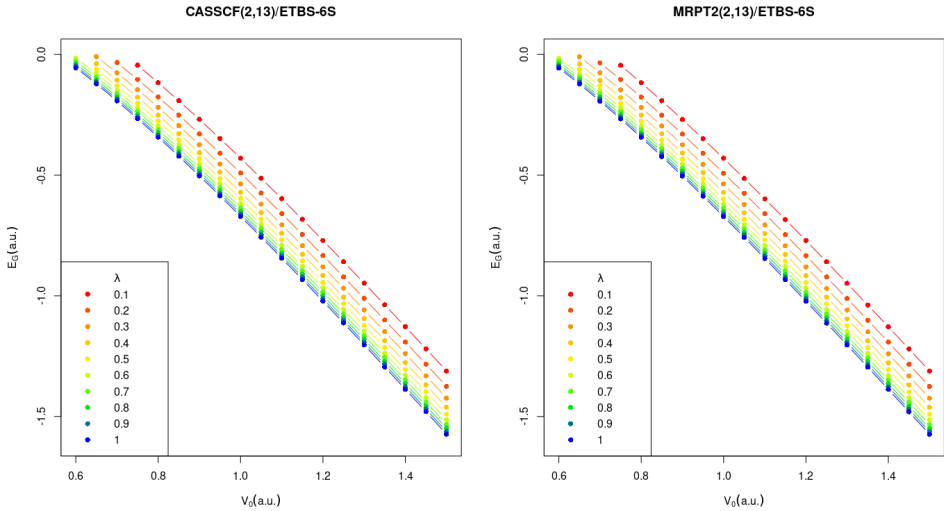
Figure 6.1: Energies for gaussian confinement with two electrons in singlet spin state for several screening parameter λ values.

squares minimisation; from the residues, we may notice that they follow an expected cubic polynomial trend due to the fact that we have trimmed the Taylor-like series at that order.

$$H = -\frac{1}{2}\sum_{i=1}^{2}\nabla_i^2 - \sum_{i=1}^{2}V_0 e^{-\frac{\omega^2}{2V_0}r_i^2} + \frac{e^{-\lambda r_{12}}}{r_{12}} \tag{6.17}$$

$$E_G + 2V_0 = E_H + \frac{g_1}{V_0} + \frac{g_2}{V_0^2} + \mathcal{O}\left(\frac{\omega^8}{V_0^2}\right) \tag{6.18}$$

Once we have obtained the coefficients we can solve the equation (6.18) for E_G as in equation (6.19) where we still have a Taylor-like series. Now, we can exploit an interesting property of the energy function: in the Taylor-like series signs are alternating, therefore it is a Stiljies function. That means if we obtain the main Padé sequence (i.e. the sequence containing the diagonal and lower diagonal Padé approximants $\mathcal{P}_N^N\left(\frac{1}{V_0}\right)$ and $\mathcal{P}_{N+1}^N\left(\frac{1}{V_0}\right)$ respectively), we shall obtain physically relevant values such as the dissociation limit of the system. Since we only have obtained the first three coefficients of the Taylor-like series, the highest order main Padé sequence we shall obtain is the one composed by the diagonal approximant $\mathcal{P}_1^1(V_0^{-1})$ and the subdiagonal approximant $\mathcal{P}_2^1(V_0^{-1})$ given in equations (6.20) and (6.21) respectively. It is known that the sequence $\mathcal{P}_2^1(V_0^{-1})$ will converge to the right energy from bellow while $\mathcal{P}_1^1(V_0^{-1})$ will converge from above. For obtaining the dissociation limit, we take these Padé approximants solve them for V_0 obtaining the lower and upper limit of the dissociation depths V_0^{d-} and V_0^{d+} respectively in terms of the physical quantities E_H, g_1 and g_2 for a given screening parameter λ. All obtained results are condensed in table 6.2.

$$\frac{E_G}{V_0} = -2 + \frac{E_H}{V_0} + \frac{g_1}{V_0^2} + \frac{g_2}{V_0^3} + \mathcal{O}\left(\frac{\omega^8}{V_0^4}\right) \tag{6.19}$$

$$\mathcal{P}_1^1\left(\frac{1}{V_0}\right) = -\frac{2g_1 + E_H - 2E_H V_0}{g_1 - E_H V_0} \tag{6.20}$$

$$\mathcal{P}_2^1\left(\frac{1}{V_0}\right) = \frac{(4g_1 + 2E_H)V_0^2 - (4g_2 + 4g_1 E_H)V_0}{-(E_H^2 + 2g_1)V_0^2 + (g_1 + 2g_2 + E_H)V_0 + (g_2 E_H - g_1^2)} \tag{6.21}$$

Table 6.2: Hooke atom energy (E_H), first anharmonic terms (g_1, g_2) and bound dissociation limits obtained for several screening parameter values for 2 electron systems with singlet spin state at CASSCF(2,13)/ETBS-6S and MRMP2(2,13)/ETBS-6S levels. All values are given in atomic units.

	E_H		g_1		g_2		V_0^{d-}		V_0^{d+}	
λ	CASSCF	MRMP2	CASSCF	MRMP2	CASSCF	MRMP2	CASSCF	MRMP2	CASSCF	MRMP2
0.1	1.9379	1.9372	-0.3839	-0.3839	0.0163	0.0164	0.731	0.730	0.771	0.770
0.2	1.8719	1.8712	-0.3829	-0.3830	0.0200	0.0201	0.689	0.688	0.731	0.731
0.3	1.8204	1.8197	-0.3802	-0.3803	0.0232	0.0233	0.657	0.657	0.701	0.701
0.4	1.7770	1.7753	-0.3712	-0.3691	0.0232	0.0220	0.635	0.634	0.680	0.680
0.5	1.7397	1.7394	-0.3578	-0.3587	0.0203	0.0208	0.618	0.617	0.664	0.663
0.6	1.7143	1.7135	-0.3568	-0.3569	0.0233	0.0234	0.603	0.603	0.649	0.648
0.7	1.6902	1.6890	-0.3487	-0.3482	0.0223	0.0222	0.593	0.592	0.639	0.638
0.8	1.6702	1.6686	-0.3418	-0.3406	0.0215	0.0211	0.584	0.584	0.630	0.630
0.9	1.6532	1.6514	-0.3354	-0.3339	0.0206	0.0201	0.578	0.577	0.624	0.624
1.0	1.6376	1.6369	-0.3280	-0.3281	0.0192	0.0192	0.573	0.572	0.619	0.618

If we focus our attention upon a given λ value and study a given estimated physical property, we shall notice that including dynamic correlation effects via perturbation methods does not quite make a big difference with respect to the same quantity obtained by regular CASSCF method.

Now, as far as E_H is concerned, this energy is smaller as λ increases which is to be expected for Hooke atoms. In contrast to the stated former results, in this very work, we obtained a Hooke two electron singlet atom energy for $\lambda = 0.2, 0.4, 0.8$ and 1.0 to be $E_H = 1.8459, 1.7502, 1.6881, 1.6458$ and 1.6159 a.u. respectively at CASSCF/ETBS-6S while in table 6.2 the obtained energies are in average 0.025 a.u. higher. As we have discussed in the previous section, accurate Hooke energies are obtained for deep potentials, nevertheless, in this section we have been dealing with loosely confined systems. Therefore, on the basis of this approximation, we may state that our estimations are rather reasonable and both regimes have pretty unique features.

As for the anharmonic terms, g_1 we may obverse it also gets smaller as λ increases. We may hypothesise that as electron-electron interaction gets weaker, correlation effects are also turned off and electrons are more likely found in the centre of the potential well, thus this first anharmonic term becomes smaller. On the other hand, the second anharmonic term g_2 gets a maximum for $\lambda = 0.6$ and then decreases.
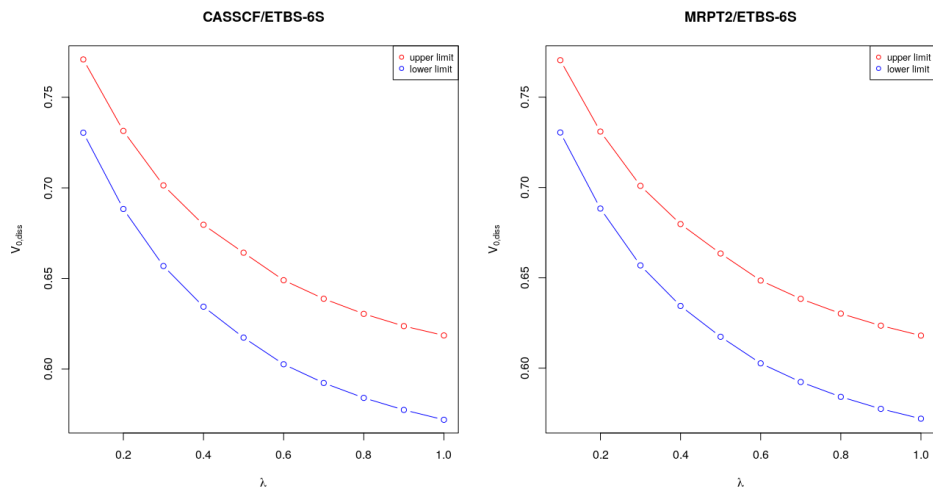
Figure 6.2: Limit dissociation potentials for several λ values.

Finally, the lower and upper bounds for the limit ionization potentials have in the worst case scenario a 0.046 a.u. amplitude as we may observe that we have predicted their behaviour in terms of physical constants by setting the corresponding Padé approximants (6.20) and (6.21) to zero and solving for V_0. We shall see that these limit potentials are shallower and asymptotic to a limit value at which only one-body interactions are relevant. Thus, we get an obvious conclusion, as electron-electron interaction is turned off the potentials does not need to do so much "work" to confine the interacting particles and shallower potentials are still able to confine them. We may find a visual summary in figure 6.2.

6.4   CONCLUDING REMARKS

In this work we have computed and implemented the required one-body integrals for quantum particles confined in gaussian potential wells for which the centre of the basis function and the centre of the potentials do not need to coincide. Such implementation has been interfaced to electronic structure software `GAMESS-US` so that we can make use of its quantum chemical computation machinery to study systems of electrons confined in dissociative potentials.

Firstly, we have performed computations on deeply confined systems (large V_0 parameter) with controlled width parameter such that the curvature of the potential at the minimum point was $\omega^2 = 0.25$. Since previous results on harmonic potentials have been well established for $n = 2, 4, 6, 8$ and 10 electrons, by means of Taylor series we have shown our calculations are compatible with the former ones.

Finally, we have studied dissociative systems composed by two electrons in which the conventional Coulomb operator was substituted by Yukawa potentials. In this case, we have not only obtained the corresponding Taylor-series expansion but also the first diagonal and sub-diagonal Padé approximant which were useful to compute the upper and lower limits for the dissociation depth for several screening parameters λ.

Chapter 7

SUMMARY, MAIN CONCLUSIONS AND FUTURE WORKS

In this last chapter, we have not only summarized the main results and conclusions obtained in the present research work, but also have sketched new research lines based on the gained knowledge.

In particular, we have focused our attention on the possibility of applying gaussian confinement potentials so as to model endohedrally doped cage clusters. In this case, the doping atom is explicitly represented in the model Hamiltonian while the confinement potential can be adapted so as to mimic properties of the all atom system. Hence, the potential parameters, namely (V_0, β) can be chosen such that relevant properties like ionization energies, electron affinities and singlet-triplet gaps obtained from employing full Hamiltonian approaches can be recovered from the simplified models.

With the aim of obtaining accurate results without compromising the computational capacities, the developed machine learning methods can be adapted and extended for building reliable simplified models. On the one hand, optimization schemes similar to the ones described in chapters 3 and 4 can be employed to obtained optimal basis functions given some input potential parameters and doping agent's atomic number. On the other hand, if some properties such as lowest laying spin state multiplicity, the sign of singlet-triplet gap or the sign of magnetic coupling constants change by varying the external potential parameters, methods presented in chapter 5 can be employed for building phase diagrams for such properties efficiently.

7.1   MAIN CONCLUSIONS

In this thesis work some advances concerning systems of electrons confined by static potentials have been provided. First, computational protocols for studying systems of few electrons with several total spin numbers confined in one, two and three dimensional harmonic potentials have been developed. In particular, on the one hand, adequate either distributed or one-centre even-tempered gaussian basis functions have been obtained by means of classical convex optimization techniques. On the other hand, these basis functions along with the employed multi referential CASSCF and MRPT2 methods have been proven to accurately describe Wigner location phenomenon for weak confinement potentials, ground state spin multiplicities, Aufbau structure and singlet-triplet energy gaps.

For spherical Hooke atoms, based on the Aufbau structure of the system, the spin multiplicity of the lowest energy configuration purely depends on the number of electrons. However, if spherical symmetry is broken such that the harmonic confinement along a given axis differs from the confinement along the perperndicular plane (i.e. $\omega_z^2 \neq \omega_{x,y}^2$), the ground state spin multiplicity does not only depend on the number of electrons, but also on how spherical symmetry has been broken. Given a number of electrons, a machine learning method based on semi-supervised learning and uncertainty sampling has been develop in order to obtain ground state spin multiplicity phase diagrams efficiently in the space composed by the stated confinement parameters and the electron-electron screening parameter. In addition, this method has also be proven to be performing when applied on further chemically relevant systems such as solid-liquid binary systems and chemical bonding analysis.

As an extension to harmonic confinement potentials, gaussian confinement potentials have been introduced so as to properly describe many-centre molecular features, dissociation processes and anharmonic contributions. The required one-body integrals have been implemented in GAMESS US; the validity of such implementation has been proven by comparing the equivalent Hooke atom energies with the ones obtained in previous works in the literature and our own results.

The results and methodologies developed in the present work can be extended to further systems such as ones consisting on different confinement regimes, larger number of electrons with richer number of ground state spin multiplicities and employed the obtained models to more realistic systems by appropriately fitting the potential parameters to all-atom systems.

7.2 FURTHER WORKS

In a nutshell, in this thesis we have developed computational protocols which lead to: obtaining optimal basis sets for harmonically confined one-, two-, and three-dimensional systems; implementing machine learning algorithms for optimizing some of the stated basis functions obtaining phase diagrams efficiently and implementing and proofing the validity of gaussian confinement potentials. With the aim of extending the gained knowledge to other systems and based on the expertise of our group, we have considered to apply the developed models on the study of endohedrally doped cage clusters. We shall now introduce the two main topics concerning this work: endohedrally doped cage clusters (so related to artificial atoms or superatoms) and quantum systems confined by static potentials. After discussing some works and results obtained in both fields, we will establish a bridge between both disciplines and present our approach to do so.

On the one hand, clusters are somewhere between bulk materials and molecules, which makes them have interesting electronic properties. Among these systems, we may find the spherical hollow nanoclusters which may be doped as it was firstly done for lanthanum in fullerene-60 La@C_{60} [270] followed by other similar systems [271, 272] and the so interesting N@C_{60} which potentially can be used as an atomic clock [273]. Besides fullerene-based-species, we may also find systems called "superatoms" [274–277] as Al_{12} cages which depending on the dopant can give rise to superhalogens (using B as dopant), super alkali metals (using P as dopant), superchalcogen (using Ca as dopant) or stable 40 electron species using Si as dopant [278]. Other interesting systems are the ones based on semiconductor clusters for which confinement-induced properties such as tunable absorption, emission and photoluminescence have been observed [279–285]. In line with superatom systems, "atomic" properties arise from collective behaviour of the whole electronic structure; nevertheless, some species such as atoms confined in semi-conducting clusters [286–290] for which the cluster acts only as a confinement, atomic properties are very similar to the ones observed by isolated dopant elements.

On the other hand, gaussian potential wells have been employed in rather theoretical electronic structure studies [252–256] as well as in more "applied" condensed matter studies concerning: quantum dots [233–237], thermo-magnetic properties [239–242] and interactions with electric and laser fields [243–248]. These potentials are pretty similar to harmonic potentials so employed in benchmark for electronic structure methods [36, 37, 41, 80, 261–266] with the subtle difference that they have a finite number of bound states and can give rise to molecular structure (chapter 6).

Bearing these two concepts in mind, as a first step, we would like to model confined alkali metal and halogen atoms in gaussian potentials and study their behaviour concerning ionization energy and electronic affinity in material clusters. We have obtained approximated estimates for such energies based on free atoms' ionization energy, their highest occupied atomic orbital and the gaussian confinement parameters by using the Helmann-Feyman theorem as well as first order perturbation methods and checked the validity of such approximations by means of explicit calculations.

7.2.1   Some preliminary results concerning endohedral systems

The general Hamiltonian for an atom with nuclear charge Z and n electrons confined in a gaussian potential with depth and width parameters V_0 and β respectively can be written as in equation (7.1).

$$H = -\frac{1}{2}\sum_{i=1}^{n}\nabla_i^2 - Z\sum_{i=1}^{n}\frac{1}{r_i} + \sum_{j>i}^{n}\frac{1}{r_{ij}} - V_0\sum_{i=1}^{n}e^{-\beta r_i^2} \tag{7.1}$$

If we consider monodeterminantal wave functions, apply the adiabatic approximation (Koopmans' theorem) and use the Helmann-Feynman theorem, we obtain an approximate variation of the ionization potential with respect to confinement depth in terms of the confinement potential paramenters and the nth atomic orbital:

$$\begin{aligned}
\frac{\partial I}{\partial V_0} &= -\left\langle \Psi_{ion} \left| \sum_{i=1}^{n-1} e^{-\beta r_i^2} \right| \Psi_{ion} \right\rangle + \left\langle \Psi_{atom} \left| \sum_{i=1}^{n} e^{-\beta r_i^2} \right| \Psi_{atom} \right\rangle \\
&\approx \left\langle \phi(\mathbf{r}_n) \left| e^{-\beta r_n^2} \right| \phi(\mathbf{r}_n) \right\rangle
\end{aligned}$$

Thus, if we consider V_0 as a small parameter, we may integrate the result obtained by Helmann-Feynman theorem in the range $V_0' \in [0, V_0]$ such that we obtain an approximate value for the ionization potential I in terms of the unconfined ionization potential I_0, the confinement potential and the nth atomic orbital as in (7.2). Of course, in this approximation we are taking for granted that the shape of the atomic orbital and, in general, the wave function is uncoupled to the potential parameters V_0 and β which is not true according to electronic structure computations concerning Hooke atoms (chapters 4 and 5). Thus, the curvature of the potential defined as $\omega^2 = 2\beta V_0$ may be an interesting parameter for future discussions.

As an alternative formulation, one shall apply perturbation methods upto first order correction for energy and keep the unperturbed wave function using V_0 as the required small parameter. Still in a monodeterminantal formulation and using the adiabatic approximation, it can be shown that one reaches the same result for approximated ionization energies.

$$I \approx I_0 + V_0 \left\langle \phi(\mathbf{r}_n) \left| e^{-\beta r_n^2} \right| \phi(\mathbf{r}_n) \right\rangle \tag{7.2}$$

Using a similar strategy, if we consider the neutral atom is composed by n electrons and, therefore, the anion by $n+1$ electrons, electron affinity A can be defined as the negative sign of ionization energy of the anionic species and therefore it is straightforward to see that it can approximately be expressed as in equation (7.3).

$$A \approx A_0 - \frac{V_0}{n} \left\langle \phi(\mathbf{r}_{n+1}) \left| e^{-\beta r_{n+1}^2} \right| \phi(\mathbf{r}_{n+1}) \right\rangle \tag{7.3}$$

As it can be seen from both equations (7.2) and (7.3), considering V_0 is small enough, if β is very small i.e. a low curvature confinement, the effect of the potential on the system is such that it shifts the ionization energies by a factor of V_0. On the contrary, if β is large enough, the potential will have no effect on the system since, in the limit, it approaches a null measure index function.

Now, the key point is to compute the integral in equations (7.2) and (7.3) in which information about electronic structure and confinement potential is encoded. As it is commonly done in quantum chemistry, we expand basis functions in terms of contracted gaussian primitive functions and by electronic structure computations we obtain the coefficients of such basis orbitals to obtain atomic (molecular) orbitals. Hence, we shall rewrite the required integral as a bilinear form as in (7.4) where the matrix $\mathbf{V}$ contains information about the interaction between the pth and q^{th} primitive gaussian functions with the confinement potential (these integrals are given in chapter 6), the matrix $\mathbf{C}$ contains the qth primitive expansion coefficients for the ith basis function and the vector $\mathbf{\Phi}$ contains the expansion coefficients of the basis functions for the nth electron obtained by electronic structure calculations.

$$\left\langle \phi(\mathbf{r}_n) \left| e^{-\beta r_n^2} \right| \phi(\mathbf{r}_n) \right\rangle = \sum_{jipq} c_j^\dagger c_i c_p^{(j)\dagger} c_q^{(i)} \int g_p^\dagger g_q e^{-\beta r_n^2} d^3 r = (\mathbf{C\Phi})^\dagger \mathbf{VC\Phi} \qquad (7.4)$$

With the aim of exploring if these approximations are valid at HF/6-311++G level for alkali metals M=Li,Na,K and MP2/6-311++G level for halogens X=F,Cl in order to describe ionization potentials and electron affinities in confined systems. We have also carried out calculations concerning H atom at HF/6-311++G level so that we could gain a better picture concerning ionization potential. In order to obtain a general picture, we have built a 20×20 grid in the $(V_0, \beta) \in [-0.500, -0.001] \times [0.10, 2.00]$ domain and have computed the error ε in each point by comparing the explicitly obtained ionization energy I with the one obtained by means of formulas (7.2) and (7.3), namely I_{theo} as $\varepsilon = \frac{|I - I_{theo}|}{|I|} \times 100$. As it can be seen in figure 7.1, the obtained error does not only depend on the confinement potential parameters but also on the atomic number of the atom we are studying. For all cases the obtained error is smaller for small values of the potential depth parameter V_0, which is expected from the perturbation-method scheme. Another shared feature is the fact that, in general, the error gets smaller for larger values of the width parameter β; we may also highlight the cases concerning Na and K for which the error seems to have a minimum for some values of the width parameter.

So far, we have taken the first steps to study this kind of systems. There are many ways in which our predictions can be improved: extend the theory to multi reference wavefunctions, obtain optimized basis sets for each element given the confinement parameters (V_0, β) in a similar way as in chapter 3, compute further terms in the perturbation series and so on.
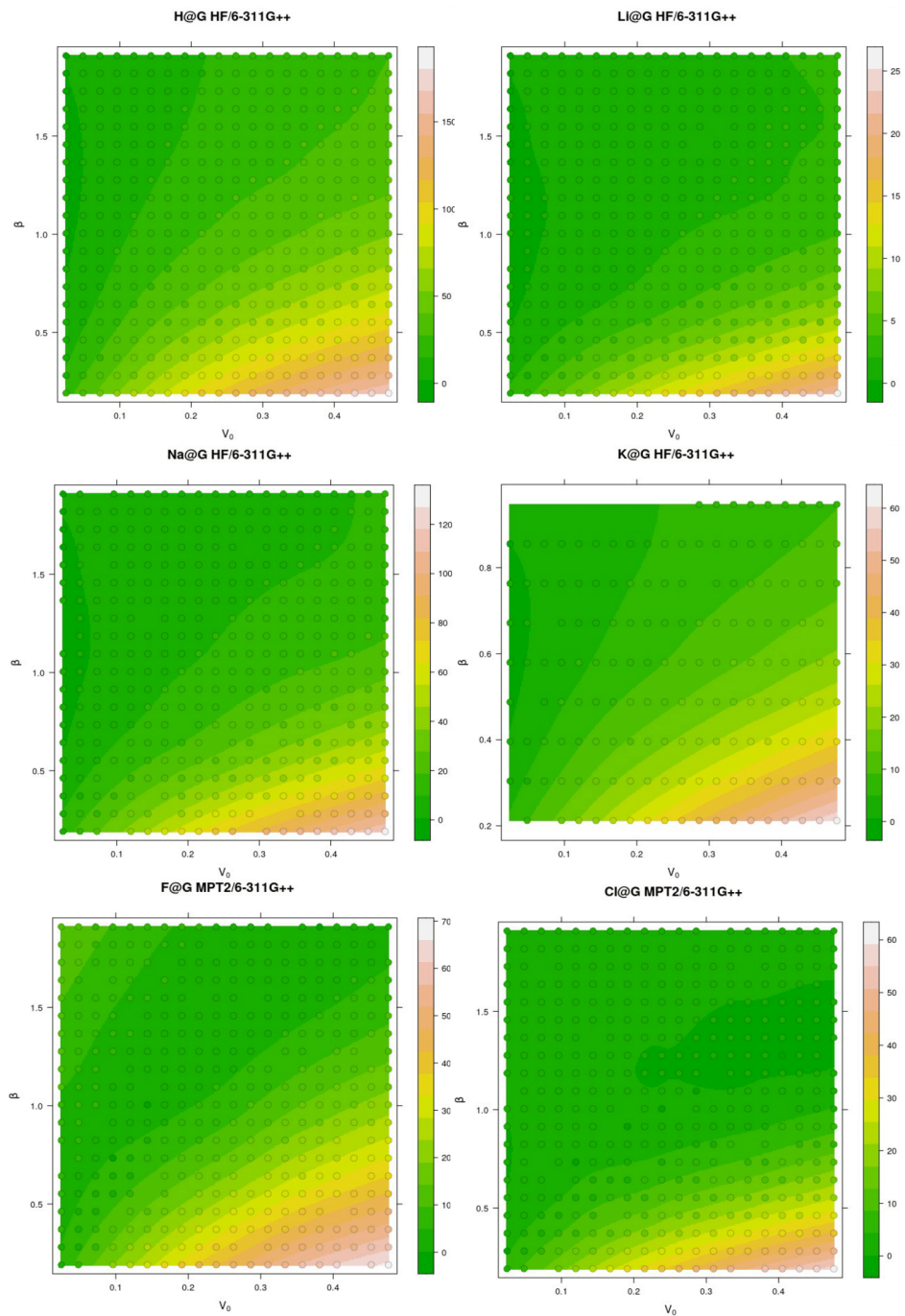
Figure 7.1: Error percentage using explicit and approximated energies.

Chapter 8

EUSKARAZKO LABURPENA

Atal honetan, tesi honen irismen orokorra jaso dugu. Tesi honetan zehar, hainbat alor ezberdinetan (hala nola: kimika kuantikoa, gainbegiratutako eta erdi-gainbegiratutako makina-ikaskuntza) garaturiko tresnak erabili izan dira potentzial estatikoen bidez konfinaturiko elektroi gutxiz osatutako sistemen uhin-funtzioak eta berezko energiak modelizatzeko.

Lan honen testuingurua deskribatzeko asmoarekin, korrelazio elektronikoa zer den eta kimika kuantikoak hori deskribatzeko dituen partikula anizdun uhin funtzioetan oinarrituruko metodoak era laburrean deskribatuko ditugu. Egitura elektronikoaren problemari dagokionez, testu honetan Hartree-Fock eta metodo multi konfigurazionalak deskribatzera mugatu gara; era berean, Wigner-en molekulen eta Hooke-n atomoen eredu kuantitatiboak egiterako orduan korrelazio elektronikoa era egokian deskribatzeak duen garrantzia ere aipatuko dugu. Gainera, oinarri funtzioen optimizaziorako eta fase-diagramak modu eraginkorrean eraikitzeko ahalbideratzen dituzten makinen-ikaskuntza metodo batzuk (sare neuronalak eta erdi-gainbegiratuak) era laburrean deskribatuko ditugu.

8.1 SARRERA

8.1.1 Egitura elektronikoaren problema

Kimika kuantikoaren oinarrizko galdera honela formula dezakegu: demagun $\mathcal{V}(\mathbf{r})$ kanpopotentzial baten bidez haien artean elkarrekintza elektrostatikoak pairatzen dituzten eta osozko S spin zenbakia daukaten n elektroiz koposaturiko sistema bat dugula; orduan, zeintzuk dira sistema horren funtzio propioak?

Itaun hori era nahiko sinplean adierazita egon arren, hainbat elektroiz osaturiko sistemen uhin-funtzioak era egokian deskribatzea gaur egun ere gai konplexu eta erakargarria da. Ikuspegi historiko laburra emateko xedez, problema hori ebazteko eman diren oinarrizko ideiei eta garapenei buruzko zerrenda laburra emango dugu. Behin mundu kuantikoan gertatzen diren fenomenoak (materiaren uhin portaera, elektroi sistemei dagozkien uhin antisimetrikoen natura eta abar) ezagunak zirela [1, 2], elektroi sistemak deskribatzeko lehen urratsak Pauli-k [3], Sommerfeld-ek [4], Fermi-k [5] eta Thomas-ek [6] (beste batzuen artean) eman zituztela esan genezake.

Euren lanen ekarpenik garrantzitsuenetariko bat elektroi gasen eredua da; helburu nagusia elektroien betetze-egitura eta material solido eroaleetan duten ekarpena deskribatzea

da. Nahiz eta eredu hori propietate makroskopikoei buruzko zenbait galderari erantzuteko gai izan, oraindik ez zen behar bezain zehatza eskala txikiagoko sistemak deskribatzeko, besteak beste, atomoak eta molekulak.

Elektroi anizdun Hamiltondarrak hartuta, elektroien arteko elkarrekintza Coulomb-iarraren eraginez ebatzi behar diren ekuazioak ez dira ez linealak, ez banakorrak. Halaber, elektroi bakar bati dagozkion ekuazioak ebatzi nahi izango bagenitu, partikula horri dagokion soluzioa gainontzeko elektroien menpekoa dela ohartuko ginateke. Beste era batean esanda, problemaren soluzioa bere buruarekiko menpekoa da. 1930 urte inguruan Slater-ek, Hartree-k eta Fock-en gaur egun kimika kuantikoan oinarrizkoa den determinante bakardun eremu auto konsistentearen metodoa garatu zuten [7–10]. Metodo horren gakoak hurrengo hauek dira: orbital izendun gorputz bateko objektu bat definituta, intereseko sistema ebazteko bera konposatzen duten i elektori bakoitza gainontzeko $n-1$ elektroiek eraturiko batezbesteko eremu batean mugitzen da; era berean, sistema osatzen duten partikula guztiei dagozkien soluzioak haien artean konsistenteak izan behar dira. Gero, Roothan-ek eta Hall-ek (bakoitzak bere aldetik) oinarri funtzioak erabiliz, Fock-en ekuazioak balore propio orokortuen ekuazio matrizial moduan idaztea lortu zuten [11, 12]. Horrela, Fock-en balio propioen problema abstraktua ((8.1) ekuzioa) era matrizial diskretizatuan adierazi dezakegu (8.2), eta metodo konputazionalen bidez ebazteko gai gara.

$$\left[h(i) + \sum_{b \neq a} J_b(i) - K_b(i) \right] \chi_a(i) = \epsilon_a \chi_a(i) \tag{8.1}$$

$$\mathbf{F(C)C} = \mathbf{ESC} \tag{8.2}$$

Hartree-Fock metodoak egitura elektronikoaren teoriaren garapenerako lehen urrats garrantzitsuak badira ere, beraien mugapenak badituzte. Nagusiena gorputz anitzeko sistemaren uhin-funtzioa Slater-en determinante bakar baten bitartez deskribatzean datza. Metodo monodeterminantalen desabantaila nagusia zera da: aurkako spina duten partikula biren banaketa espaziala ez-menpekoak diren partikulen banaketen biderkadura zuzena da (ikusi (8.3) ekuazioa). Horrela, $\psi_1(\mathbf{r}_1)^2$ eta $\psi_2(\mathbf{r}_2)^2$ elkarrekiko askeak dira; hau da, probabilitate banaketak ez daude korrelazionatuta. Egitura elektronikoaren hizkuntzan, Hartree-Fock uhin funtzioek (aurkako spinari dagokion) elektroi-korrelazio eza dutela esaten da, eta metodo horien bitartez lortzen den energia osoa benetako sistemarena baino handiagoa da [13].

$$P(\mathbf{r}_1, \mathbf{r}_2) d\mathbf{r}_1 d\mathbf{r}_2 = \int \Psi^2 d\mathbf{r}_1 d\mathbf{r}_2 d\omega_1 d\omega_2 = \psi_1(\mathbf{r}_1)^2 \psi_2(\mathbf{r}_2)^2 \tag{8.3}$$

Aipatutakoaren ondorioz, elektroi korrelazioak eragiten dituen fenomenoak era egokian deskribatu ahal izateko determinante bakarreko uhin funtzioaren erabilera baino haratago joan behar dugu. Edozein n aldagaidun funtzio asimetriko gorputz $\{\chi_1\}$ bateko funtzioez konposaturiko determinante paregabeen serie moduan era zehatzean gara dezakegula ezaguna da. Horretan oinarritutuz eta uhin funtzioa Slater-en determinanteen konbinazio lineal moduan garatuz, konfigurazio elkarrekintza metodoak (CI methods ingelesez) garatu

zituzten. Hurbilketa horiek HF uhin funtzio bat hartuz elektroien promozio bakarrak, bikoitzak eta ordena handiagokoak burutuz lor daitezkeen determinante posible guztiak eskuratzen baditugu, konfigurazio elkarrekintza osoko (FCI ingelesez) uhin funtzioa lortzen dugu [13].

Praktika, simetria eta spin bereko kitxikapenak bakarrik hartzen badira ere, parametro espazioaren neurria dela eta, FCI metodoak konputazionalki garestiak dira eta normalean CI garapenak kitxikapen bakar edo bikoitzetan mozten dira. Serie garapen horiek moztuz gero, metodo horiek tamaina sendotasuna galtzen dute; arazo horri aurre egiteko proposaturiko soluzioa zera da: aurretiaz aukeraturiko orbital eta elektroi jakin batzuen gaineko FCI metodoa aplikatzea. Metodo hauek espazio aktibo osoko (CAS ingelesez) metodoak dira; gainera, eremu autokonsistenetaren metodoa ere gehitzen badiegu, CASSCF metodoak lortzen ditugu. Hurbilketa hau erabiliz, elektroi korrelazio estatikoa Slater-en determinan-teen konbinazio lineal moduan eraturiko uhin funtzioen bidez deskriba dezakegu [14–17] eta, horren gainean, perturbazio metodoak aplikatuz, korrelazio dinamikoaren eragina ere eskuratu dezakegu [18, 19].

8.1.2 Korrelazio elektronikoaren garrantzia

8.1.2.1 *Wigner-en kristalak eta molekulak*

1934an Wigner-ek, elektroien elkarrekintzak erregulatzen dituzten mekanika kuantikoari buruzko kontzeptu nahiko oinarrizkoak erabiliz, dentsitate baxuko gas elektroi batek lokalizatzeko joera izango duela iragarri zuen [20]. Izan ere, partikula bakoitzaren Coulomb-en elkarrekintzari egiten dion ekarpena $U_C \propto 1/r_s$ erakoa bada (hemen r_s partikulen arteko batezbesteko distantzia da) eta batezbesteko energia zinetikoa $K \sim 1/r_s^2$ erakoa izanda, dentsitate baxuetan (r_s parametroaren balore handientzat), Coulomb-en elkarrekintzen ekarpena energia zinetikoaren baino handiagoa dela argi ikus dezakegu. Beraz, dentsitate baxuetan, elektroiek sistemaren energia osoa minimizatzeko joera dutenez, lokalizatu egingo dira; horri Wigner kristalizazioa deritzogu. Fermi-ren likidoen eta Wigner-en kristalen arteko trantsizioak hainbat lan garaikidetan esperimentalki behatu dituzte [21–27].

Periodikoak ez diren sistema finitoen kasuan, egoera elektroniko lokalizatuei Wigner molekulak ere deitzen zaie, eta elektroiak potentzial ahulen bidez konfinaturik daudenean agertzen dira [32–34]. Horrela, Wigner molekulak edo, oro har, dentsitate baxuko elektroi sistemak deskribatzeko, elektroi korrelazio efektuak biengan (energia eta uhin-funtzioa) metodo konputazional egokiak erabiliz tratatu behar dira. Korrelazio baxuko eta altuko erregimenei dakozkien sistemen dentsitateak era oso zehatzean lortu izan dira literaturan agertzen diren hainbat lanetan[35–38]. Antzeko egoeratan, baina, elektroi kopuru handiagoa duten sistemak ($n > 2$) ikertuko bagenitu, oinarrizko egoerazko hainbat spin egoera eta karaktere multideterminantal konplexua duten hainbat sistema aurkituko genituzke [39–41]. Sistema horiek hainbat gorputzeko elkarrekintzak ulertzeko erabil genitzakeen arren, kostu konputazionala handiagoa da sistemaren tamainaren arabera. Zailtasun tekniko hauek berezkoak badira ere, eredu hauek behin eta berriz erabili izan dituzte egitura elektronikoko metodoen kalibraketetan [37, 42–57]. Horiek posible izan dira datu analitiko eta erreferentziazko kalkulu oso zehatzak lortu dituztelako [39, 40, 58–64].

8.1.2.2   *Puntu kuantikoak eta Hooke-n atomoak*

Puntu kuantikoak (QDs ingelesez) espazioko eskualdeak dira, non kanpoko potentzial bati esker, elektroiak bezalako partikulak konfinatuta dauden. Eskualde horiek uzkurtzen diren heinean, tamaina kritikoa lortzen da, eta mundu mikroskopikoaren propietateak agertzen dira, hala nola, energia kuantizazioa. Ikuspuntu fisiko-kimiko batetik, molekula bat edota nanopartikula bat ere balentzia elektroiak mugatzen dituen puntu kuantikotzat har genitzake. Gaur egun, teknologia kuantikoen egunsentian, QDS ikasketa eremu zabal eta interesgarria da. Sistema horiek osagai oinarrizkoenetako bat osatzen dute nanosfera-aparailuetarako; aplikazio batzuen artean: eguzki-energia bilketa, optoelektronika eta konputazio kuantikorako gailuen garapena [65]. Hainbat ikerketa garaikidetan ere, puntu kuantikoen aplikazioak termoelektrizitate [66], katalisi [67–70] eta, bereziki berriz, konputazio kuantikora [71–75] hedatu dituzte.

Puntu kuantikoei buruzko ikerketa teorikoetan erabiltzen diren eredu sinple eta egokienetariko bat Harmonium edo Hooke-n atomoak dira. Eredu horietan, elektroiak potentzial harmoniko esferiko baten bidez konfinaturik daude [76] eta sistemaren Hamiltondarra (8.4) ekuazioan agertzen da. Eredu horiek benetako QD-ei dagozkien ezaugarriak irudikatzeko aproposak diren parametroak ere badituzte [77, 78]. Esate baterako, gure taldean burututako lan batean Hooke-n hiru gorputzeko eredu zehatz bat erabiliz, QD esferiko batean triplete-single spin egoeren arteko trantsizioak kanpoko eremu magnetikoa handitzen den heinean gertatzen direla baieztatu dugu [79]. Hala ere, eredu zehatzak erabiltzeak gure ikerketa bi elektroiz osoturiko sistemetara mugatu zuen. Izan ere, kurbatura balio jakin batzuentzat ($\omega^2 = \frac{1}{4}, \frac{1}{100} \ldots$) elektroi biz konposaturiko Hooke-n atomoaren soluzio analitikoak ezagunak dira eta, printzipioz, korrelazio txiki ($\omega^2 \to \infty$) eta handidun ($\omega^2 \to 0$) sistemak ikertzeko lehen hurbilketa gisa har ditzakegu.

$$H = -\frac{1}{2} \sum_{i=1}^{n} \nabla_i^2 + \frac{\omega^2}{2} \sum_{i=1}^{n} r_i^2 + \sum_{j>i=1}^{n} \frac{1}{r_{ij}} \tag{8.4}$$

Hooke-en ereduzko atomoetan bezala, elektroi korrelazio efektuen inkorporazioa funtsezkoa dela ikusi da puntu kuantikoen espektro eta garraio propietateak behar bezala interpretatzeko [81–86]. Puntu kuantikoetan, atomo errealetan ez bezala, korrelazio elektronikoaren efektua nahierara alda daiteke nanokristalaren dimentsioa eta forma manipulatuz, baita kanpo eremuen indarra, muga baldintzak eta simetriak aldaraziz ere [87, 88]. Bestalde, sare kristalinoa, dopatzaileak edota metalezko atarietan agertzen diren induzitutako kargen eraginez, elektroi-elekroi elkarrekintzak pantailatu daitezke [89].

Azkenik, Hooke-n atomoetan oinaturrituriko ereduak behin eta berriro erabili izan dira egitura elektronikoko metodoen kalibrazioan korrelazio dinamiko eta ez dinamikoa aztertzeko erregimen anitzak baitituzte [42–44]. Kalibrazio horien bitartez, konputazionalki garestiak diren hainbeste metodoren garapena burutzen da [37, 45–57] eskura dauden erantzun analitikoak eta kalitate handidun datuak erabilita [39, 40, 58–63].

8.1.3   Ikasketa automatikoaren laguntza

IBM-ek honela definitzen du ikasketa automatikoa (ML edo Machine Learning ingelesez): makinen ikaskuntza adimen artifiziala (AI ingelesez) eta informatika zientzien adarra, gizakiek ikasteko duten modua imitatzeko datuen eta algoritmoen erabileran zentratzen dena". Definizio horren arabera, edozein ML soluzio bi zutabetan oinarritzen da: datuak (enpirikoki lortzen diren zenbaki abstraktuak) eta horiek nolabaiteko ezagutza lortzeko erabiltzen dituen algoritmo bat. Gainera (inplizituki esaten denez), algoritmo jakin bat erabiliz, ezagutza horren kalitatea hobetu egiten da, datuen kopurua handitu ahala.

Ikasketa automatikotik eratorritako hainbat metodo kimikaren hainbat alorretan erabiltzen hasi dira [90–93]; beste batzuen artean: teoria elektronikoaren garapena [94–98], fase berrien aurkikuntza eta fase diagramen eraiketa [99–102], propietate kimikoen patroiak aurkitzea [91, 103–106], energia potentzialaren gaizalak lortzea [107–111] eta erreakzio bideak eta produktuak aurresatea [112–114]. Adibide horiek kontuan hartuta, ML metodoak zientzia kimikoetan tresna garrantzitsuak direla eta izango direla ikusten dugu.

Ikuspegi zabal batetik, makina ikaskuntza tradizionalean bi diziplina nagusi daude: gainbegiratu gabeko eta gainbegiratutako ikasketa paradigmak deritzenak. $X = \{x_1 \dots x_n\}$ izeneko datu sorta bat izanik, lehenengoak datu sortan agertzen diren egiturazko patroi interesgarriak aurkitu nahi ditu, hala nola, multzokatze eta dimentsio murrizketan teknikak erabiliz (aldagai nagusien analisia, adibidez). Bigarrena, aldiz, bigarren datu sorta bat $Y = \{y_1 \dots y_n\}$ ere hartuz, bi sorten arteko loturak aztertzen ditu; teknika hauen artean: erregresio ereduak eta ausazko basoak ditugu. Erdi-gainbegiratutako ikasketa mutur bi hauen arteko paradigma da; oraindik bi sorta X eta Y baditugu ere, lehenengoan dauden elementu kopurua bigarrenean daudenarena baino askoz handiagoa da. Hori dela eta, mapeatze funtzioak lortzea ezinezkoa edo zehaztasun txikiduna izaten da [115–117].

Lan honetan bi algoritmo gainbegiratu erabili ditugu: ausazko basoak eta sare neuronalak, baita algoritmo erdi-gainbegiratu bat ere: ziurgabetasun laginketa.

8.1.3.1   *Gainbegiratutako ikaskuntza: sare neuronalen bidezko iragartzea*

Aurreko atalean aipatu dugun bezala, teknika gainbegiratuen helburua $f : X \to Y$ funtzio bat lortzea da, non X datu sortan agertzen diren ezaugarrizko balioak Y datu sortan agertzen diren menpeko aldagaiekin lotzen diren. Gainera (ML tekniken definizio orokorra izanik), zenbat eta datu kopuru handiagoa izan, lortutako funtzioaren kalitatea hainbat eta handiagoa izango da. Etiketatutako datu sorta $\mathcal{D}$ bat eta honetatik eratorritako $\mathcal{T} \subset \mathcal{D}$ ikasketa eta frogatze $\mathcal{E} \subset \mathcal{D}(\mathcal{T} \cap \mathcal{E} = \emptyset)$ sortak izanda, ML algoritmo egoki bat bilatzen ari garen f funtzioa inferitzeko gai da. Horretarako diseinatutako milaka tekniken artean, lan honetan sare neuronalak oinarri funtzioetan agertzen diren parametro optimoak inferitzeko erabili ditugu.

XX. mendearen hasieran, giza garunek informazioa nola prozesatzen duten modelatzeko helburuarekin, W. S. McCulloch, W. Pitts eta F. Rosenblatt-en lanen emaitza nagusienetarikoa pertzeptroiaren lehen inplementazioa izan zen [118–120]. Frogatu izan zuten bezala, neurona horien kopuru zehatz bat geruzetan ordenatuz eta horiek era jakin batean elkarren artean konektatuz lortzen ditugun makinak (printzipioz) hurbiltzaile unibertsalak dira [121–125]. Hau da, datu kopuru nahikoa eta geruza eta geruza bakoitzean neurona kopuru handia izanda, sare horiek edozein funtzio arbitrariotara hurbiltzeko gauza dira.

8.1.3.2   *Erdi-gainbegiratutako ikaskuntza*

Gainbegiraturiko ikaskuntza teknika gehienei esker lorturiko iragarpenen eta sailkapen eredu zehatzak izaten dira, baldin eta ikaskuntza-datuen kopurua nahiko handia bada. Hala eta guztiz ere, errealitatean agertzen diren egoera askotan, (gure kasuan bezala) ez-menpeko aldagaiaren etiketak lortzea denbora aldetik edo ekonomikoki garestia izan daiteke. Beraz, ezagutza eskuragarrian oinarrituriko esperientzia gehiago lortzea eta gure baliabideak (borondatea, denbora eta dirua) gure ezjakintasunaren zokorik ilunenak argitzen inbertitzea zuhurra da. Erdi-gainbegiraturiko eta ikasketa aktiboko teknikak datuen arabera aplika daitezke, eta horretarako bi multzo desberdin ditugu.

Erdi-gainberiraturiko ikaskuntza eta ikaskuntza aktiboko teknikak bi datu sorta desberdin ditugun kasuetan aplika ditzakegu: etiketaturiko sorta bat $\mathcal{L}$ eta etiketatu gabeko beste sorta bat $\mathcal{U}$. Izenak adierazi bezala, ekiketaturiko data sorta ezugarri eta etiketen biderkadura Cartesiar ordenatuz osaturiko $(x_1, y_1)\ldots(x_l, y_l)$ itxuradun puntuek osatzen dute, non $Y_L = \{y_1 \ldots y_l\} \in \{1 \ldots C\}$ kategoria posible guztien sorta den. Bestalde, etiketa gabeko eta $(x_{l+1}, y_{l+1})\ldots(x_{l+u}, y_{l+u})$ puntuez osaturiko sorta $\mathcal{U}$ ere badugu, non $Y_U = \{y_{l+1} \ldots y_{l+u}\} \in \{1 \ldots C\}$ etiketak ezezagunak diren eta sorta honen kardinalitatea aurrekoarena baino askoz handiagoa den $l << u$.

Horrela, lan oso berrietan egin den moduan [126, 127], fase diagramak erakitzeko asmoz, hurrengo esperimentua zein baldintzapetan egin jakiteko datu sorta hauetan dagoen informazioa erabil genezake.

Hasierako hipotesiak kontuan izanda, parametro espazioa diskretizatuz $X = \{\mathbf{x}_1 \ldots \mathbf{x}_{l+u}\}$ itxurako sare bat eraiki dugu, non lehenengo l puntuak hasierako konputazioen bidez $Y = \{1 \ldots C\}$ sortan agertzen diren kategoria guztiak agertzen direlarik etiketatuko ditugun eta gainontzeko u puntuak (hasiera batean) etiketatu gabe geratuko diren $l << u$. Jarraian, lehen l puntuetako etiketen informazioa gainontzeko puntuetara hedatuz, etiketatu gabeko puntuek C kategoria posible guztietan egoteko duten probabilitate banaketak lortuko ditugu, adibidez, etiketen hedapen algoritmoa erabiliz.

X. Zhu-k eta Z. Ghahramani-k "etiketen hedapena" garatu zuten algoritmoari esker [128] etiketatutako datuen informazioa etiketatu gabeko datuetara Markov-en prozesu baten bidez hedatzen da. Hor, etiketatutako eta etiketarik gabeko datu guztiak biltzen dituen grafo bat eta binakako elkarrekintzak modulatzen dituzten pisuak definitzen ditugu. Markov-en kate homogeneoen eta matrize estokastikoen propietateak erabiliz, edozein hasierako baldintza $\mathbf{Y}^{(0)}$ hartuta ere, algoritmoak soluzio geldikor bakar batera konbergitzen duela frogatu zuten (8.5).

$$\mathbf{Y}_u = (\mathbf{I} - \tilde{\mathbf{T}}_{uu})^{-1}\tilde{\mathbf{T}}_{ul}\mathbf{Y}_l \tag{8.5}$$

Metodo horren desabantaila nagusia $(\mathbf{I} - \tilde{\mathbf{T}_{uu}})^{-1}$ matrizearen konputazioan datza, erabilitako sareak nahiko handiak edo dentsoak badira, objektu horren konputazioa garestia edo ezinezkoa izan daiteke. Arazo hori saihesteko, (8.5) ekuazioan agertzen den formula itxia erabili beharrean, hasierako etiketa bektore bat hartu eta Markov-en ereduan irteratuz informazioa hedatzea lortzen dugu. Hala eta guztiz ere, matrize handiak erabiltzerakoan konbergentzia lortzeko hainbat iterazio egin behar direnez, algoritmo horrek astuna izaten jarraitzen du; batez ere, sareen dentsitatea edota dimentsio kopurua handitzen baditugu. Alternatiba gisa, konputazionalki merkeagoak diren klasifikatzaileak (esaterako, ausazko

basoak) problema hori ebazteko tresna aproposak dira. Gain-doitze arazorik izaten ez dutenez, zuhaitz kopuru nahiko handia erabiliz lan honetan ikertutako sistema guztiak ikasteko metodo unibertsalak dira. Gauzak horrela, hasierako datu sorta bat erabiliz ausazko basoetan oinarrituriko modelo bat entrenatzen dugu; hori erabiliz, etiketatu gabeko puntuek eta kategoria bakoitzean egoteko duten probabilitateak eskuratzen ditugu. Horrela eginik, etiketen hedapen algoritmoa erabiltzearen baliokidea den metodo bat ezarri dugu.

Ikastea honetan datza: gure ezjakintasuna sakonena den alorretan informazio gehiago lortzea alor horri buruz dugun ezagutza zabaltzeko. Modu eraginkorrean ikasi ahal izateko, norberak ezagutza eza duen puntuetan arreta jarri behar du. Ziurgabetasun laginketa ziurgabetasun handiena duten puntuen laginak hartzea ahalbideratzen digun metodoa da, baina, nola kuantifika genezake ziurgabetasuna? Demagun probabilitate banaketa funtzio bat dugula $P_C(y|\mathbf{x})$ zeinek, parametro bektore bat $\mathbf{x}$ emanik, $\{1 \dots C\}$ kategorietan egoteko y probabilitateak ematen dizkigun. Horrela, eskuratutako propabilitateak erabiliz, puntu jakin baten ziurgabetasuna hainbat eratan defini dezakegu: konfiantza txikiena (8.6), ziurgabetasun marginala (8.7) eta Shannon-en entropia (8.8). Lehenak etiketarik gabeko datuen aukerarik txikiena (horregatik zalantzagarriena) maximizatzen du; bigarrena aurrekoa baino malguagoa da, bi iragarpenik probableenak kontuan hartzen baititu. Azkenik, Shannon-en entropia informazio edukiaren neurria da; aldagai batek zenbat eta informazio gehiago izan, honen naturari buruz orduan eta gutxiago dakigu [129].

$$u_{LC}(\mathbf{x}) = 1 - \max_C P(C|\mathbf{x}) \tag{8.6}$$

$$u_{MS}(\mathbf{x}) = 1 - [P(C_1|\mathbf{x}) - P(C_2|\mathbf{x})] \tag{8.7}$$

$$u_{SE}(\mathbf{x}) = -\sum_C P(C|\mathbf{x}) \log P(C|\mathbf{x}) \tag{8.8}$$

8.2   LAN HONEN HELBURUA

Wigner-en molekulei, Hooke-n atomoei eta makinen ikaskuntzako teknika batzuei buruzko artearen egoera deskribatu ondoren, atal honetan oraingo lanaren helburu nagusiak jasoko ditugu:

1. Dimentsio batean eta bitan indar-parametro desberdinen ($k = \omega^2$) bidez potentzial harmonikoetan konfinaturik dauden sistemak deskribatzeko erabiltzen diren oinarri funtzio gausstar banatuak optimizatzea ML teknikak (sare neuronalak) erabiliz. Horretaz gain, egitura elektronikoa lortzeko ahalbideratzen duten metodo optimoak eskuratzea eta horiek $n = \{2, 3, 4\}$ elektroidun spin garaiko sistemak ikertzeko erabiltzea.

2. Zentru bateko oinarri funtzioak teknika klasikoen bidez (simplex eta Newton-Raphson) optimizatuz hiru dimentsiotako $n = \{2, 4, 6, 8, 10\}$ elektroidun eta $k = \omega^2 = 1/4$ potentzial parametrodun Hooke-n atomoen deskribapen egokia eskuratzea eta horri dagokion metodo optimoan oinarrituta, oinarrizko singlete eta tripletearen energia zehatzak erdiestea.

3. Makinen ikaskuntza-metodoak hobetzea eta inplementatzea. Erdi-gainbegiratutako ikaskuntzan eta ziurgabetasun laginketa tekn100ketan oinarrituta, fase diagramak eraginkortasunez lortzea eta kimikoki esanguratsuak diren sistema batzuk hornitzea.

4. Konfinamendu potentzial gausstarrei eta oinarri funtzio gausstarrei dagozkien gorputz bakarreko integral analitikoak kalkulatzea eta GAMESS US kodean inplementatzea. Aurreko ataletan lorturiko emaitzekin lotura duten kalkuluak burutzea.

8.3 EGINDAKO LANEN LABURPENAK

8.3.1 Sasi dimentsio bateko sistemak

Aurreko lan batzuetan, potentzial esplizitu gabeko eta elektroi gutxidun sistemak aztertu zituzten kutxa-luzera aldakorrak erabiliz, eta korrelazio elektuak ROHF (geruza irekiko Hatree-Fock uhin funtzio mugatua) eta FCI (konfigurazio-elkarrekintza osozko uhin funtzioa) uhin funtzio metodoen bitartzen ikertu zituzten [130]. Sistema horiek berezko interes teorikoa badute ere, lan honetan ikerturiko elektroi kopuru berberak dituzten sistemak esperimentalki behatu dituzte [131, 132].

Lan honen lehen kapituluan, sasi dimentsio batean potentzial harmonikoen bidez konfinaturik dauden elektroi gutxidun ($n = \{2, 3, 4\}$) sistemen lokalizazio propietateak aztertu ditugu. Horrela, bada, sistema horiek modelizatzeko, (8.9) ekuazioan agertzen den eragile Hamiltondarra erabili dugu.

$$H = -\frac{1}{2}\sum_{i=1}^{n}\nabla_i^2 + \frac{k}{2}\sum_{i=1}^{n}r_i^2 + \sum_{i=1, j>i}^{n}\frac{1}{r_{ij}} \tag{8.9}$$

Literaturan jakina denez, dimentsio batean Coulomb-en eragilea singularra da [136, 137]; arazo hori konpontzeko, hiru dimentsionalak diren eta lerro baten hedatzen diren s motako oinarri funtzioak erabili ditugu. Hori dela eta, dimentsio puru bat izan beharrean, sistema sasi-unidimentsionala dela diogu. Aurreko lanetan forgatu duten moduan, oinarri horiek erabiliz lorturiko energiari sobera dauden zeharkako osagai bien ekarpena kenduz, sistemaren energia zuzendua lortzen dugu [138]. Kasu honetan, lortutako uhin funtzioak era egokian errepresentatzeko asmoarekin, $x = 0$ puntuan zentraturiko eta x noranzkoan hedatzen den dimentsio bateko tarte erregulardun sare batean zehar s motako funtzio gausstar normalizatuak kokatu ditugu. Oinarri funtzio horiek (8.10) ekuazioaren bidez adierazita daude; hemen, $\mathbf{R}_\mu = (x_\mu, 0, 0)^T$ bektoreak μ funtzioaren zentru-koordenatuak ematen ditu.

$$\phi_\mu(\mathbf{r}; \alpha, \mathbf{R}_\mu) = \left(\frac{2\alpha}{\pi}\right)^{3/4}\exp(-\alpha(\mathbf{r} - \mathbf{R}_\mu)^2) \tag{8.10}$$

Era honetan definituriko segmentuaren luzera beteriko egoeraren energia garaieneko itzulera puntuak $x_0(n, k) = \pm\left(\frac{(2n+1)^2}{k}\right)^{1/4}$ erabiliz definitu dugu. Puntu horietariko bakoitzean eta $x = 0$ puntuan funtzio bana jarri ondoren, tarte erregularretan banaturiko beste $4m$ funtzio jarri ditugu eta itzulera puntu klasiko bien artean $2m$ daude. Hortaz, guztira $M = 3 + 4m$ s motako funtzio jarri ditugu eta alboz alboko funtzioen arteko distantzia $\delta = \frac{2x_0}{m+1}$ izan da. Funtzio guzti horiek α berretzaile bera dutenez, ondoz ondoko funtzioen arteko gainezarpen integrala $S(\alpha, \delta) = \exp(-\alpha\delta^2/2) = \exp(-\xi/2)$ da. Lan honetan, aurreko hainbatetan oinarrituz [130, 138–141] , gainezarpen parametroa $\xi = 1.0$ balioan finkatu dugu. Ondorioz, α berretzaiela potentzial harmonikoaren naturaren (k) eta guztira erabilitako oinarri funtzioen kopuruaren menpekoa da $\alpha = \frac{\xi(m+1)^2}{4x_0^2(n,k)}$. Lan honetan, $m = 25$ jarri dugu.

Wigner-en lokalizazioa karakterizatzekotan, sistemaren propietate bi erabili ditugu: gorputz bateko dentsitatea (8.11) eta partikula-hutsune entropia (8.12). Lehenengoan, $\varphi_i(\mathbf{r})$ orbital naturalak dira eta γ_i koefizienteak korrelazio elektronikoaren garrantziarekin lotzen ditugun okupazio zenbakiak dira [291, 292]. Bigarrenean, aurrekoan bezala, okupazio zenbakiak erabiliz partikula-hutsune entropia agertzen da. Definizioz, adierazpen hori erabiliz lorturiko balioak absolutuki zenbat eta handiagoak izan, sistema osoaren karaktere multideterminantala orduan eta handiagoa izango da.

$$\rho(\mathbf{r}) = \sum_i \gamma_i \varphi_i^*(\mathbf{r})\varphi_i(\mathbf{r}) \tag{8.11}$$

$$S = -\sum_i \gamma_i \log \gamma_i + (1 - \gamma_i)\log(1 - \gamma_i) \tag{8.12}$$

Elektroi biz osaturiko sistemak modelizatzeko, CASSCF(2,5) metodoen bidez hainbat k balioentzat spin singlete eta triplete egoeren egitura elektronikoen kalkuluak burutu ditugu. Spin egoera bakoitzarentzat gorputz bateko dentsitateak eskuratu ditugu (2.1 irudia). Ikus dezakeguenez, lorturiko dentsitate profila k konfinamendu parametro eta spin egoeraren menpekoa da. Espero bezala, k balio handientzat egoera singleteari dagokion dentsitateak maximo bakarra dauka, ordea, egoera tripleteak (Pauliren esklusio printzipioa dela eta) bi mutur ditu. k balio txikien kasuan, aldiz, spin egoera biek maximo bi dituzte eta antzeko dentsitate profila daukate. Sistema horien izaera multideterminantalaren natura aztertzekotan, hainbat k baliori dagokien egoera tripletearen partikula-hutsune entropiak kalkulatu ditugu. 2.3 irudian ikus dezakegun moduan, k balio handien kasuan partikula-hutsune entropia zerorantza doa. Horrek konfinamendu sendoaren mugan partikula independentearen eredua sistemaren deskribapen ona dela eta lortzen den Fermi-ren gasaren deskribatzeko Slater-en determinante bakar nahikoa dela esan nahi du. Lorturiko kurbaren itxura aurretiaz egindako lanetan lorturiko emaitzekin bateragarria dela [40, 41] adierazi behar dugu. Konfinamendu parametroaren balioa txikitzen joan ahala, karaktere multideterminantalari dagokion entropia handiko egoera lortzen dela ikusi dugu, eta entropiak bere balio maximoa $k = 5 \times 10^{-4}$ inguruan izan ondoren, berriz jaisten hasten da.

Sistema honi buruzko ezagutza handiagoa izatekotan, oinarri minimodun eredu analitiko bi erabili ditugu. Alde batetik, α berretzailedun eta potentzial harmonikoaren minimoan zentraturiko gausstar bat erabiliz, bi elektroiz okupaturiko orbitala lortzen dugu, horrela egoera singletearen (Fermi-ren likidoa) eredua lortzen dugularik $^1\Sigma_g = \sigma_0^{\uparrow\downarrow}$. Beste aldetik, $x_0 = \pm 1/(4k)^{1/3}$ oreka puntu klasiko bakoitzean α berretzailedun oinarri gausstar bat kokatu eta simetria adaptatuz sistemari dagozkion (2.6) (bikoitia, konbinazio simetrikoa) eta (2.7) (bakoitia, konbinzio antisimetrikoa) orbitalak lortu ditugu. Azken horiek erabiliz, egoera tripletearen (Wigner-en kristala) eredu sinplifikatua lortu dugu $^3\Pi_u = \sigma_g^{\uparrow}\sigma_u^{\uparrow}$. Spin egoera bakoitzarentzari dagokion oinarriei dagozkien gorputz bat eta biko integralak kalkulatuz, egoera bakoitzaren energia espresioak lortu ditugu. Kasu bietan energia k konfinamendu parametroa eta α oinarrien berretzailearen funtzioa dela frogatu ondoren, k bakoitzarentzat energia minimizatu dugu α hura parametro bariazional gisa hartuz. Horrela eginik, egoera bakoitzaren energia optimoaren kurbak lortu ditugu (ikusi 2.4. irudia). Lorturiko emaitzetan oinarrituz, k balio txikientzat, spin egoera bien energiak oso antzekoak izanda, triplearen energia singlearena baino zerbait txikiagoa da. Ostera,

$k = 5 \times 10^{-4}$ puntuaren inguruan singletea tripletea baino egonkorragoa bilakatzen dela ikusi dugu. Emaitz hauek metodo aurreratuak erabiliz erdietsitakoekin erkatuz, eredu sinple hau lokalizazioa zein k balio inguruan agertuko den aurresateko erabilgarria dela ondorioztatu dugu.

Emaitza hauek hartuta, hiru eta lau elektroiz osoturiko sistemtan antzeko joerak agertzen diren ikertu nahi izan dugu. Asmo horrekin, CASSCF$(n, 2n)$ (non, n elektroi kopurua den), bakoitzari dagokion gausstarrez eraturiko sarea erbiliz, spin altuko kalkuluak burutu ditugu. Horien irteera balioak erabiliz, hainbat k-ri dagozkien dentsitateak (2.5 irudia) eta partikula-hutsune entropiak (2.6 irudia) kalkulatu ditugu.

Horietan ikus dezakegunez, kurba bien itxura antzekoa badute ere, entropia maximoari dagokion k-ren balioa elektroi kopuruaren menpekoa da: zenbat eta elektroi kopurua handiagoa izan, orduan eta txikiagoa izango da k horren balioa. Azterturiko sistema guztiek antzeko joera kualitatiboa dutela nabaritu dugu; ondorioz, Fermi-ren likidoa eta Wigner-en kristalaren arteko trantsizio antzeko prozesu bat $S(k_{max}, n)$ puntuarekin defini daitekelakoan gaude. Puntu horren posizioa elektroi kopuruaren menpekoa izango da.

Batutako emaitzetan oinarrituta zera ondorioztatu dugu: konfinamendua ezartzen duen kanpo potentzial harmonikoaren k parametroaren balio bezain txikientzat sistema eratzen duten elektroiek lokalizatzeko joera dute; horrela, Wigner-en molekula bat eratzen da. Are gehiago, hainbat konfinamendu parametrori dagozkien elektroi-hutsune entropiak kalkulatuz, egoera lokalizatu eta ez-lokalizatuen arteko entropia maximodun trantsizio egoerak aurkitu ditugu.

8.3.2 Sasi bi dimentsio sistemak

Dimentsio bateko kasua bi dimentsiotara orokortuz, hainbat elektroiz osoturiko sistemak deskribatzeko, kimika kuantikoan ohikoak diren nukleoetan zentraturiko [142–144] zein espazioko edozein puntu arbitrariotan zentraturiko [138, 145–149] funtzio gausstarrak erabiltzen ditugu. Sistema horiek interes teoriko zein esperimentala dutenez [150–153], egitura elektronikoaren teorian oinarrituko metodoak erabili ahal izateko beharrezkoak diren protokolo konputazioanalak garatzea premiazkoa da. Hala ere, sistema batzuen eskala nanometroaren ordenakoa da, eta horretarako zentro bakar bat aztertzen bada, menpekotasun linealeko arazoak gertatuko dira. Adibide bat ematearren, esperimentalki lorturiko grafenoan oinarrituriko puntu kuantikoek (GQD) eta trantsizio metalen dikalkogenuroetan (TMD) oinarrituriko nanopartikula batzuek 1-7 nm-ko tamaina dute [154–163]. Lan honen bigarren kapituluan, bi dimentsioko potentzial harmoniko simetrikoen bidez konfinaturik dauden hainbat elektroiz osoturiko sistemak deskribatzeko behar diren oinarri gaussstar batzuk proposatu ditugu. Gainera, lorturiko oinarri funtzioak potentzial harmonikoaren konfinamendu parametroa k, oinarri funtzio kopuru totala eta gainezarpen parametroarekiko optimioak dira.

Horrela, (8.10) ekuazioan agertzen diren s motako orbital gausstarrak sare hexagonal bateko nodoetan kokatu ditugu. Kasuaren arabera, guztira $M = 3g^2 - 5g + 1$ oinarri funtzio erabili ditugu, non $g \geq 3$ zenbaki osoak 3.1 irudian agertzen den patroi hexagonalak dituen zerrenda kopurua adierazten duen. Konfigurazio honetan ondoz ondoko funtzioen arteko gainezarpen integrala $S(\alpha, \delta) = \exp(-\alpha\delta^2/2) = \exp(-\xi/2)$ da, non δ ondoz ondoko funtzioen arteko distantzia den. Definitu dugun $\xi = \alpha\delta^2$ gainezarpen parametroaren balioaren arabera, menpekotasun linealak (balore oso txikiak) edo gune ez-jarraituak (balore oso handiak) izan ditzakegu. Aurretiaz buruturiko lanetan oinarrituta [130, 138–140], lan honetan $\xi \in [0.85, 1.15]$ tarteko balioak aztertu ditugu.

Lehen urratsean, potentzial harmoniko isotropiko bidimentsional batean konfinaturik dagoen partikula bateko problemei erreparatu diegu. Horrela, sistema haorei dagokien Hamiltondarra (8.13) ekuazioan agertzen dela eta bere oinarrizko egoeraren energia zehatza $E_0 = k^{1/2}$ dela atzeman dugu.

$$H(x,y) = \frac{1}{2}\left(-\partial_x^2 + kx^2 - \partial_y^2 + ky^2\right) = H(x) + H(y) \tag{8.13}$$

Deskribaturiko oinarri funtzioak erabiliz, gorputz bateko Schrödinger-en ekuazioa (8.14) adierazpenean agertzen den balore propio orokortuen problema moduan adierazi dugu. Hor, T energia zinetikoa, V energia potentziala, S gainezarpen, E balio propio eta C bektore propio matrizeak dira. Forgatu dugun moduan, energia zinetiko eta potentzialaren matrize horiei dagozkien elementuak gainezarpen matrizearen elementuen menpekoak direnez, guztiak bukle berean definitu ditzakegu. Izatez, erabilitako oinarri funtzioak hiru dimentsionalak direnez, egitan Schrödinger-en ekuazioa ebatziz, sasi bi dimentsioko emaitzak erdiesten ditugu. Lorturiko energiak (balore propioak) zuzentzeko, gausstar guztiek berretzaile bera dutenez, zeharkako osagaiaren ekarpenaren ondorioz lortzen dugun gehiegizko energia zinetikoa kedu dugu. Kasu honetan elektroi bakoitzeko $\alpha/2$ energia ekarpena kendu dugu.

$$(\mathbf{T} + \mathbf{V})\mathbf{C} = \mathbf{ESC} \tag{8.14}$$

Printzipio bariazionalean oinarrituta, (ξ, g, k) balio jakin batzuentzat oinarrizko egoeraren energia ondoz ondoko funtzioen arteko distantziarekiko optimizatuz, hainbat sarreraz osaturiko $\mathcal{D}$ datu basea lortu dugu.

Enpirikoki frogatu dugun legez, era horretan lorturiko Hamiltondarraren balio propioak ez dira bakarrik zehatzak izan, hendekaturiko mailen natura erreproduzitzeko gai ere izan gara. Datu base honetan agertzen diren sarreren eta emaitza analitikoen arteko errore erlatibo maximoa %5ekoa izan da eta hendekaturiko sortentzat kalkulaturiko desbideratze estandar erlatiboa %10^{-4}koa izan da.

$\mathcal{D}$ datu basea erabilik, osagarriak diren sorta bi lortu ditugu: ikasketa sorta bat $\mathcal{L}$ eta aztertze $\mathcal{T}$ sorta bat ($\mathcal{D} = \mathcal{L} \cup \mathcal{T}, \mathcal{L} \cap \mathcal{T} = \varnothing$). Horiek erabiliz, bi geruza ezkutuz eta neurona kopuru aldakordunez eraturiko hainbat sare neuronal optimizatu ditugu eta horien funtsa $(\log k, \xi, g)$ sarrera moduan emanik $\log \delta_{opt}$ irteera balioa lortzea da. Lorturiko sare optimalak aktibazio funtzio sigmoideak, lehen geruzan sei neurona eta bigarrenean lau ditu. Optimizazioa 10 aldiz gurutzaturiko balioztatzearen bidez egindako errore kuadratikoen minimizazioa burutuz lortu dugu. Emaitza gisa, irteerako balioen estimaturiko errore erlatiboa %2.5ekoa dela ikusi dugu; horren ondorioz, oinarri funtzioen berretzaileen errorea $\Delta \alpha_{opt} = \frac{2\xi}{\delta_{opt}^2} \Delta \log \delta_{opt}$ moduan adierazi dugu. Ohartu azken errore hau txikiagoa bihurtzen dela k konfinamendu parametroaren balioa handitzen den heinean.

Lortutako oinarri funtzio optimoek hainbat elektroiz konposaturiko sistemetan agertzen diren korrelazio efektuak deskribatzeko duten gaitasuna frogatzeko asmoz, bi eta hiru elektroiz osoturiko eta spin baxu eta altuko sistemak aztertu ditugu. Horretarako,(8.15) ekuazioan agertzen den eragile Hamiltondarra erabili dugu.

$$H = \frac{1}{2} \sum_{i=1}^{n} (k(x_i^2 + y_i^2) - \nabla_i^2) + \sum_{j>i=1}^{n} \frac{1}{r_{ij}} \tag{8.15}$$

Efektu horien neurri kuantitatiboa izateko, koordenatu erradialean zehar CASSCF(n,8) mailan eta UHF mailan kalkulaturiko uhin funtzioen arteko dentsitate diferentzia kalkulatu dugu $k \in (1 \times 10^{-5}, 1 \times 10^{-10})$ balioak erabiliz. Koordenatu erradialaren balio txikientzat uhin korrelatuaren dentsitatea ez korrelatuarena baino txikiagoa dela ikusi dugu. Aldiz, koordenatu erradialaren balio handientzat uhin korrelatuaren dentsitatea ez korrelatuarena baino handiagoa dela ikusi dugu. Efektu hori nabariagoa da k parametroaren balioa handitzen den heinean.

Laburbilduz, (20,100) unitate atomikoko tamaina duten sistemak deskribatzeko sare neuronalen bidez lorturiko sare hexagonaletan banaturiko oinarri funtzio gausstarrak lortu ditugu. Etorkizuneko aplikazio gisa, bi dimentsioko grafenoan oinarrituriko puntu kuantikoen tamainako sistemak deskribatzeko erabili ahal izango ditugu.

8.3.3   Hiru dimentsioko Hooke-n atomoa

Puntu kuantikoei buruzko ikerketa teorikoetan erabiltzen diren eredu sinple eta egokienetako bat Harmonium edo Hooke-n atomoa deritzona da, non elektroiak potentzial esferiko harmoniko baten bidez konfinatuta dauden [76]. Eredu horiek sistema errealen propietateak simulatzeko doi ditzakegun hainbat parametro dituzte [77, 78]. Esate baterako, gure taldean egindako lan batean kanpo eremu magnetiko bat aplikatuz, bi elektroidun Hooke-n atomo batean gertatzen den singlete-triplete trantsizioa eta horretan korrelazio elektronikoak duen garrantzia aztertu genuen [79]. Hala ere, eredu zehatzak erabiltzeak gure ikerketa bi elektroi sistemetara mugatu zuen. Izan ere, bi elektroiz osoturiko Hooke-n atomoaren kasuan, konfinamendu parametro zehatz batzuentzat baino ($\omega^2 = \frac{1}{4}, \frac{1}{100} \dots$) ez dago soluzio analitikorik[80]. Balio horiek zehatzak badira ere, korrelazio baxu ($\omega^2 \to \infty$) eta altuko ($\omega^2 \to 0$) konfinamenduei buruzko informazioa lortzeko erabilgarriak dira [37, 39, 40, 42–64] [42–44].

Laugarren kapituluan azaldu dugunez, Hooke-n atomoak deskribatzeko bezain egokiak diren oinarriak lortzea premiazkoa da. Sistema Coulomb-arrentzat optmizaturiko aug-cc oinarri nahiko handiak erabiliz elektroi gutxiko sistemak era egokian deskribatzeko gai bagara ere, elektroi kopurua handitzen dugun heinean (hartu 10 elektroidun sistemen adibidea) menpekotasun linealen arazoez gain, ez gara gauza izan oinarrizko egoeraren spin anizkoiztasuna eta, ondorioz, sistemaren betetze egitura era egokian deskribatzeko. ETBS-6S oinarri funtzioak erabiliz (erreferentziazko balioekin alderatuta), behatu dugun errore handiena mHartree ordenekoa izan da.

Kapitulu honetan egoera singlete eta tripletean dauden $n = \{2, 4, 6, 8, 10\}$ elektroiz osoturiko $\omega^2 = 0.25$ konfinamendu parametroa duten Hooke-en atomoak deskribatzeko eta singlete-triplete energia tartea eskuratzeko prozedura bat aurkeztu dugu. Gainera, Yukawa-ren potentzialak erabiliz, elektroi-elektroi elkarrekintzetan pantailatze efektuak duen eragina aztertu dugu, eta, (8.16) ekuazioan agertzen den eragile Hamiltondarra erabiliz, sistema hauen gaineko egitura elektronikoaren kalkuluak burutu ditugu.

$$H = -\sum_i^n \frac{1}{2}\nabla_i^2 + \sum_i^n \frac{1}{2}\omega^2 r_i^2 + \sum_i^n \sum_{j>i}^n \frac{e^{-\lambda_{ee}r_{ij}}}{r_{ij}} \qquad (8.16)$$

Energia absolutuentzat balio zehatzak lortzekotan, $\omega^2 = 0.25$ konfinamendu parametroa erabiliz, hainbat elektroi kopuru desberdin ($n = \{2, 4, 6, 8, 10\}$) dituzten spin egoera singlete eta triplea duten sistementzat optimoak diren oinarri funtzioak lortu ditugu. Horrela, kontraturik gabeko $L = 0$ eta $L = 3$ momentu angeluarren arteko eta N geruzadun oinarriak erabili ditugu; horien berretzaileak L eta N zenbakiekiko duten menpekotasuna (8.17) ekuazioan adierazi dugu.

$$\zeta_{LN}^k(\omega^2) = \frac{\omega^2}{2}\alpha_{L,N}(\omega^2)\left[\beta_{L,N}(\omega^2)\right]^{k-1}, 1 \leq k \leq N \qquad (8.17)$$

Azken ekuazio honetan agertzen diren $\alpha_{L,N}(\omega^2)$ eta $\beta_{L,N}(\omega^2)$ parametroak CASSCF(n, 13) eta bi elektroien kasuan FCI mailan lorturiko energiak minimizatuz lortu ditugu; optimizazio prozesu gisa simplex eta Newton-Raphson metodoak erabili ditugu [56, 293, 294].

Arretaz ikuskatu ondoren, sei elektroi egoera singletean den sistemarentzako lorturiko oinarriek (izenez ETBS-6S) zehaztasunaren eta errendimenduaren arteko oreka onena dutenak direla ondorioztatu dugu. Funtzio horiek trinkotu gabeko 4(SPDF) oinarriak dira eta (8.17) ekuazioan agertzen diren parametro optimoak $\alpha_{L,N} = 0.240432$ eta $\beta_{L,N} = 1.3021162$ izan dira. Horrela, lortzen den berretzaileen segida: 0.2404032, 0.3130329, 0.4076051, 0.5307491 da. Guztira ETBS-6S sorta 80 oinarri funtzioek osatzen dute eta horietariko 68 linealki askeak dira.

Bi elektoriz osoturiko sistema Coulomb-iarren emaitzak 4.1 taulan agertzen dira; spin egoera singletearen energia zehatza 2.0 unitate atomikoa (a.u.) dela kontuan izanda, sistema honentzat lorturiko emaitzak gainontzekoenen emaitzen kalitatea kalibratzeko erabili ditugu. Oinarri funtzioen segidan ikusten dugun moduan, FCI mailan: 2.055213 (aug-cc-pVDZ), 2.004107 (aug-cc-pVTZ), 2.000476 (aug-cc-pV5Z) eta 2.000196 (aug-cc-pV6Z) unitate atomiko izan dira. Emaitza horiek literatuan agertzen direnekin bat badatoz ere, singlete-triplete energia tartean errorea 0.15 eV-koa da. Ostera, maila beran ETBS-6S oinarriak erabiliz, energia abosuluez gain, tarte horren errorea 0.01 eV-koa izan da; ondorioz, lan honetan garaturiko oinarriak erabiltzea justifikaturik dago. Elektroi kopurua handitu ahala FCI metodoak oso garestiak bilakatzen direnez, CASSCF eta MRMP2 metodoek ETBS-6S oinarriekin lortzen duten zehaztasuna analisatu dugu; 4.2 taulan hainbat espazio aktibo erabiliz lorturiko emaitzak bilduta daude. Ikusten den moduan, era honetan erdietsitako emaitzak FCI metodoaren emaitzen antzekoak dira.

Lau elektroiz osoturiko sistementzat, jada, FCI kalkuluak burutzea oso garestia da; bestalde tripletearen oinarrizko egoeran ekarpen handiena duen konfigurazioan $1p$ orbitaletan spin bereko bi elektroi daudenez, uhin funtzio multideterminantalak erabiltzea premiazkoa da. $1p$ geruzaren hendekapena dela eta, spin egoera bien uhin funtzioak deskribatzeko hainbat konfigurazio biltzen dituzten uhin funtzioak erabili behar ditugu. Gure kasuan, $CASSCF(4, m)$ eta $MRMP2(4, m)$ ($m = 4, 5 \ldots 13$) metodoei esker lorturiko emaitzak 4.3 taulan biltzen dira. $CAS(4,13)/aug$-cc-pV6Z* eta $MRMP2(4,13)/aug$-cc-pV6Z* metodoak erabiliz, singlete-triplete energia tartea 1.11 eV eta 1.08 eV dira hurrenez hurren; emaitza hauek berez literaturan agertzen direnen antzekoak(1.00 eV)[41] diren arren, $CAS(4,13)/ETBS$-6S eta $MRMPT2(4,13)/ETBS$-6S metodoekin lorturiko energia absolutuen balioen erroreak (erreferentziazko balioekin konparatuz) txikiagoak izanda, singlete-tripletearen emaitza ere hobea dela ikusi dugu. Alegia, singlete-triplete energia artearen balioak 1.06 eta 1.04 eV izan dira.

Sei elektroiz osoturiko sistementzat (aurreko kasuaren antzeko eran), tripletearen oinarrizko egoeran ekarpen handiena duen konfigurazioan $1p$ bi orbitaletan spin bereko bi elektroi eta beste orbitalean aurkako spina duten bi elektroi daudenez, uhin funtzio multideterminantalak erabiltzea ere beharrezkoa da. Beraz, $CASSCF(6, m)$ eta $MRMP2(6, m)$ ($m = 6, 7 \ldots 13$) metodoei esker eskuraturiko emaitzak 4.4 taulan biltzen dira. Ikusi dogunez, $1p$ geruzan beste bi elektroi gehitu arren, singlete-triplete energia tartea aurreko kasuaren antzekoa da; kapitulu honetan optimizaturiko oinarriak erabiliz, 1.03 eV eta 1.00 eV-ko balioak lortzen ditugu (hurrenez hurren) $CAS(6,13)/ETBS$-6S eta $MRMP2(6,13)/ETBS$-6S mailetan. Gainera, lortutako emaitzak literaturan agertzen den 0.95 eV-ko emaitzarekin [62] bat datoz. Energia absolutuen zehaztasuna elektroi kopuruarekin txikitzen den arren, estimaturiko singlete-triplete tarteen balioak zuzenak izaten jarraitzen dutela ikusi dugu.

Oinarrizko egoera elektronikoaren uhin funtzio monodeterminantala geruza itxikoa bada ere, zortzi elektroidun sistemak ere $CASSCF(8, m)$ eta $MRMP2(8, m)$ ($m = 8, 9 \ldots 13$)

metodoei esker aztertu ondoren, erdietsitako emaitzak 4.5 taulan bildu ditugu. Aurreko kasua erreferentzia gisa hartuz, beste bi elektroi gehitzen baditugu, $1p$ orbital guztiak beterik egongo dira; horren ondorioz, oinarrizko egoera elektronikoaren spin anizkoiztasuna singletea da, horrela, determinante bakarreko uhin funtzioaren konfigurazio elektronikoa $1s^2 1p^6$ motakoa da singletearentzat eta $1s^2 1p^5 2s^1$ tripletearentzat. Optimizaturiko oinarriak medio, -7.66 eV eta -7.37 eV-ko singlete-triplete energia tarteak lortu ditugu CAS(8,13)/ETBS-6S eta MRMP2(8,13)/ETBS-6S mailetan hurrenez hurren. Varga-k eta lankideek sistema horrentzat -10.6 eV-ko singlete-triplete energia tartea lortu zuten[39], emaitza hau guk lortutakoa baino nahiko handiagoa da. Hala ere, guk metodo bariazionalaren bitartez erdietsitako egoera tripletearen energia eurena baino baxuagoa denez, gure metodoa zehatzagoa dela ondorioztatu dugu. Gainera, lau eta sei elektroiz osoturiko sistemen kasuan, guk eskuratutako emaitzak ere literaturan agertzen direnen antzekoagoak izanda [39], zortzi elektroiz osoturiko sistemak deskribatzeko zehaztasun handiagoa ere lortu dugula ikusi dugu.

Kapitulu honetan agertzen den ekarpen nagusia hamar elektroiz osoturiko sistemen azterketa da; izan ere, daikigunik, literaturan ez dugu aurkitu sistema horiei buruzko ikerketarik. Emaitzak 4.6 taulan laburbildu ditugu. Jasotako kasuetan egindako anztera, sistema horien gaineko CASSCF$(10, m)$ eta MRMP2$(10, m)$ $(m = 10, 11 \ldots 13)$ metodoei esker ETBS-6S oinarriak erabiliz dagozkien egitura elektronikoak kalkulatu ditugu. Konfigurazio elektroniko nagusia aztertuz, bai singletea zein tripletearen betetze egitura $1s^2 1p^6 1d^2$ motakoa dela behatu dugu. Kasu honetan, oinarri funtzioen optimizazioaren beharrizana nabaria izan da; aug-cc oinarriei dagokienez, aug-cc-pV6Z* direnak erabiliz, ETBS-6S-ekin gertatzen den bezala, $1d$ orbitalen betetzea $2s$-ena baino lehenago gertatzen da. Aldiz, mota horretako gainonzteko oinarrien kasuan alderantzizkoa gertatzen da eta, ondorioz, *Aufabu* betetze egitura eta oinarrizko egoeraren spin multiplizitate okerrak lortzen dira. Horrek, kanpo potentzial funtzioei egokitzen zaizkien oinarri funtzio optmioak lortzeko premia azpimarratzen du.

Elektroien arteko elkarrekintzek singlete-triplete energia tartean eta betetze egituran duten eragina aztertzekotan, potentzial Coulomb-iarrak erabili beharrean, $\lambda_{ee} = \{0.2, 0.4, 0.6, 0.8, 1.0\}$ pantailatze parametrodun Yukawa-ren potentzialak aukeratu ditugu. Ikusi dugun moduan, pantailaturiko potentzialek ez dute oinarrizko egoeraren spin anizkoiztasuna aldatzen; hau da, bi eta zortzi elektroidun sistemen oinarrizko egoera singleta izaten jarraitzen du eta lau, sei eta hamar elektroidun kasuetan tripletea. Bestalde, singlete-triplete energia tartea pantailatze parametroarekiko menpekoa dela nabaritu dugu. Izan ere, *Aufbau* egitura hartuz, spin egoera singleteak geruza itxidun espezieek eratzen dute; orduan, elektroi bikote orok orbital espazial bera partekatzen dute eta haien mugimendua horretan mugaturik dagoenez, bi gorputzeko elkarrekintza sendoak sortzen dira. Horrenbestez, elektroien arteko elkarrekintzak apantailatzeak egoera singletearen egonkortze nabaria dakar eta spin-en parekatzea errazten da. Alde batetik, elektroi biz osoturiko sistemetan, potentzial Coulomb-arrentzat ($\lambda_{ee} = 0.0$) singlete-triplete tartea 9.78 eV da eta pantailatze nagusienaren kasuan ($\lambda_{ee} = 1.0$) 11.51 eV. Tarte horren igoera oraindik nabariagoa da zortzi elektroiz osoturiko sistemetan, non 7.28 eV ($\lambda_{ee} = 0.0$) izatetik 10.48 eV ($\lambda_{ee} = 1.0$) izatera igarotzen den. Beste aldetik, lau, sei eta hamar elektroiz osaturiko sistemen kasuan, pantailatzeak singlete-triplete energia tartean duen eragina ahulagoa da. Izan ere, lau eltroidun kasuan tarte hori -1.04 eV ($\lambda_{ee} = 0.0$) izatetik -0.78 eV ($\lambda_{ee} = 1.0$) izatera pasatzen da; sei eltroidun kasuan -0.99 eV ($\lambda_{ee} = 0.0$) izatetik -0.77 eV ($\lambda_{ee} = 1.0$)

eta hamar elektroidun kasuan -0.56 eV ($\lambda_{ee} = 0.0$) izatetik -0.34 eV ($\lambda_{ee} = 1.0$). Ohartu azken kasu hauentzat gertatzen den singlete-triplete energia tartearen aldaketa absolutuki txikia izan arren, erlatiboki aldekta nabariak direla. Orokorrean, elektroien arteko elkarrekintzak pantailatzeak egoera singletea tripletea baino gehiago egonkortzen duela ikusi dugu, horren ondorioz, singlete-triplete tarteen balioak aldatu egiten dira elektroi kopuruaren arabera.

Sistema guztientzat, horien energia osoa ekarpen hauetran deskonposatu dugu: zinetiko, konfinamendu eta elektroi-elektroi elkarrekintza. Horrela, CAS(N_e,10)/ETBS-6S mailan $N_e = \{2, 4, 6, 8, 10\}$ elektroiz osoturiko egoera singlete eta tripleteen eta energia deskonposaketak 4.8 taulan bildu ditugu. Singlete-triplete energia tarteari dagokionez, kasu guztietan elektroi-elektroi elkarrekintzen arteko diferentziak beti positiboak dira; horrek egoera tripletea egonkortzen du. Lau, sei eta hamar elektroiz osoturiko sistemetan $\Delta_{T-S}^{V_{ee}}$ energia tarte horren ekarpen nagusiena da; bestalde, bi eta zortzi elektroidun sistementzat, ekarpen hura Δ_{T-S}^{K} ekarpen zinetikoa eta $\Delta_{T-S}^{V_{conf}}$ konfinamendu ekarpena baino magnitude txikiagoduna da. Ondorioz, azken sistema horien egoera tripleteentzat gertatzen den elektroi baten promozioak energia zinetiko eta potentzialaren igoera elektroien arteko alderapenaren murriztea txikiagoa da. Gainontzeko sistemetan, beharrezkoak diren promozioak geruza berean gertatzen direnez, egoera tripletea da hain zuzen gehien egonkortzen dena.

Coulomb-en eragilearen ordez Yukawa-rena erabiltzerakoan (λ_{ee}=1.0) elektroien arteko elkarrekintzetatik eratorritako energia ekarpenek % 78.1-89.6eko jaitsiera izan dutela atzeman dugu. Hain zuzen ere, pantailatzeak osagai horrengan eragin handiena izan du; elektroi kopurua handitu ahala, energia zinetikoa ere handitu eta energia potentziala txikitu egin da. Singlete-triplete energia tarteei dagokienez, bi eta zortzi elektroidun sistemetan, pantailatzeak egoera singletea 1 eV inguru egonkortzen; horrela, sistema horientzat Δ_{S-T} tartearen magnitudea handitu egiten da. Lau eta sei elektroidun sistemetan, spin egoera bietan pantailatzearen eragina antzekoa denez, horrek ez du eragin handirik Δ_{S-T} tartean. Kasu bi horietan energia tarte horren ekarpen handiena energia zinetikoen diferentziak eragin du. Azkenik, hamar elektroiz osoturiko sistemetan, bai energia zinetikoa zein elektroi-elektroi elkarrekintzen ekarpenak antzekoak dira.

Azkenik, sistema hauetan elektroi korrelazioak eragiten dituen fenomenoak hobeto ulertzeko, sistema Coulomb-arrenzat eta apantailaturiko sistementzat ($\lambda_{ee} = 1.0$) Coulomb-en zuloak kalkulatu ditugu. Zulo horiek, $h(u)$, uhin funtzio korrelatuaren (gure kasuan CASSCF(n,13) mailan lorturikoa) eta ez korrelatuaren (RHF edo ROHF kasuz kasu oinarrizko egoera elektronikoaren spin anizkoiztasuna singletea edo tripletea den arabera) $I(u)$ dentsitate intrakularren arteko diferentzia da. Horrela izanik, Coulomb-en zuloak korrelazio elektronikoaren eraginez elektroi bikote baten posizio erlatiboan nola eragiten neurtzen du. Lortutako emaitzak 4.3 irudian agertzen dira. Elektroi kopuruaz aparte, kasu guztietan patroi bera atzeman dugu: i) Coulomb-en zuloa pronuntziatuagoa da singletearentzat tripletearentzat baino bai potentzial Coulomb-iarrentzat zein apantailatuentzat ere eta ii) potentzial apantailatuek Coulomb-en zuloen agerpena asko indargetzen dute. Espero bezala, orokorrean, elektroi korrelazioaren eraginez, elektroien arteko distantzia handitu egiten da; hau da, Coulomb-en zuloek distantzia laburretan dentsitate murrizketa eta distantzia luzeetan (masa kontserbazioaren ondorioz) dentsitate igoera eragiten dute. Alabaina, lau, sei eta hamar elektroiz osoturiko sistemek ezaugarri interesgarri bat dute: distantzia laburretan ohikoa den dentsitate murrizketaz gain, distantzia luzeenetan ere horrelako bat gauzatzen da. Neurri txikiagoan, zortzi elektroi tripleteren kasuan ere fenemeno hori agertzen da.

Horren agerpena, geruza egitura eta elkartruke elkarrekintzen naturan oinarrituz azaldu dezakegu.

Laburbilduz, lan honetan lortu ditugun emaitzak hartuta, singlete-triplete energia tartearen seinuak elektroi kopuruarekiko menpekotasuna dauka. Hain zuzen ere, 2 eta 8 elektroidun sistemen oinarrizko spin egoera singletea da eta 4, 6 eta 10 elektroidun sistementzat, aldiz, tripletea dela ikusi dugu. HF mailan kalkulaturiko geruza itxiko espezien orbitalen hendekapenetan eta elektroi kopuruaren araberako oinarrizko egoeraren spin multiplizitatean oinarrituta, $\omega^2 = 0.25$ kurbaturadun Hooke-n atomo esferikoen betetze egitura $1s < 1p < 1d$ dela ondorioztatu dugu.

Halaber, elektroien arteko elkarrekintzak apantailatzeak ez bakarrik egoera bakoitzeko energia absolutuetan, baita singlete-triplete energia tartean ere eragin nabarmena duela ohartu gara. Energia diferentzia hau bereziki agerikoa da 2 eta 8 elektroidun sistemetan.

8.3.4   Makina ikaskuntza bidez lorturiko fase diagramak

Fase diagramak $\mathbf{x} \in \mathbb{R}^n$ egoera bektore bat emanda horri dagokion aldagai kategoriko baten balioa ematen digun f funtzioen errepresentazio grafikoak dira ($f : \mathbf{x} \in \mathbb{R}^n \to C$). Hauek fisika, kimika eta materialen zientzietan ikertzen diren propietate makroskopikoek kanpo paremetroekiko (tenperatura, presioa, konposizioa eta abar) duten menpekotasuna aztertzeko erabili ohi diren tresnak dira. Ondorioz, aipaturiko f funtzio horiek lortzeko prozedurak garatzeak premiazko garrantzia dauka.

Diagrama horiek lortzeko erarik errezena: parametroen espazioa uniformeki diskretizatu ondoren, egoera puntuz osaturiko sare bat lortzen dugu. Puntu horien gainean, esperimentuak edo simulazioak burutuz eurei dagokien etiketa (fasea) eskuratzen dugu; horrela, aukeratu dugun domeinuaren fase diagrama erdiesten dugu. Prozedura hau kontzeptualki sinplea eta automatizatzeko erraza bada ere, bi desabantaila nagusi ditu. Alde batetik, sareko puntu guztien etiketak eskuratzea beharrezkoa denez, prozesu osoa garestia izan daiteke. Beste aldetik, metodo horren eraginkortasuna mugatua da, izan ere kalkulaturiko puntuen eskuraturiko informazioa erabiltzen ez dugunez, eskuraturiko jakintza estatikoa da.

Zientzia kimikoen hainbat alorretan egin den moduan [91, 103–114], parametro espazio diskretizatuan gauzatutako laginketa prozesuaren eraginkortasuna hobetzekotan, ikasketa automatikoko teknikak erabiltzen dira [126, 127].

5. kapituluan, ikasketa automatikoko bi teknika erabili ditugu: erdi-gainbegiraturiko ikasketa eta ziurgabetasun laginketa. Horiez gain, lagunduriko puntuen etiketak egitura elektronikoaren kalkuluen bidez lortu ditugu. Aurretiaz buruturiko lanetan ez bezala, etiketen hedapen algoritmoa [128] erabili beharrean, beharrezkoak diren ziurgabetasunak ausazko basoen bidez konputatu ditugu. Metodo honen abantaila nagusia zera da: ez da beharrezkoa ez matrize handien alderantzizkoa kalkulatzea ezta Markov-en kateak konputatzea. Horren ondorioz, informazioa sare dentsoagoetara era azkarragoan heda daiteke. Era laburrean adierazita, garaturiko metodoak hurrengo pausoak jarraitzen ditu (ikusi 5.2 irudia):

1. Printzipioz, parametro espazioan kategoria guztiak biltzen dituen sarea eraiki.

2. Sare horretako hainbat hasierako puntu aukeratu.

3. Hasierako puntu horien gaineko kalkuluak burutu eta horien emaitzetan oinarrituz dagozkien etiketak esleitu.

4. Ezagunak diren puntuen informazioa sare osora hedatu RF ereduak erabiliz.

5. Shannon-en entropia konputatuz, balio maximodun puntua aukeratu eta 3. urratsera bueltatu.

Garaturiko metodo horren eraginkortasuna frogatzeko asmoarekin, puntu eutektiko bakar bat duten solido-likido sistema bitarren fase diagramak eskuratu ditugu. Prozedura hura interes kimikoa duten beste sistema batzuetan aplikatzekotan, sistema sinple bi hartu ditugu: elektroi gutxiz osoturiko Hooke-n atomoen egoera magnetikoak eta He dimeroan agertzen den loturaren izaera kobalentea.

Lehenengo kasuan, jakina denez, substantzia puru bi nahasten direnean hainbat propietate termodinako (hala nola: lurrun presioa, urtze eta irekitze tenperatura, bolumen espezifikoa eta abar) nahaste horren osagaien aktibitateen arabera aldatzen dira. Espezie desberdinen molekulen arteko elkarrekintzak espezie berekoenen antzekoak direnean,

nahastea ideala dela esaten dugu. Horrela, egergia potentzialen desberdintasunak arbuila-
garriak dira eta, sistema idealetan, osagai bakoitzaren aktibitatea bere frakzio molarra da.
Orduan, azterturiko likido-solido sistema bitarretan hurbilketa hauek hartu ditugu:

- Osagai biak idealki nahaskorrak dira fase likidoan.
- Osagai biak idealki ez-nahaskorrak dira fase solidoan (solido heterogeneo bat eratzen
  dute).
- Fusio entalpiak tenperaturarekiko askeak dira.

Propietate horiek kontuan izanik, osagai bakoitzaren frakzio molarra x_i eta fusio en-
talpia $\Delta H_{f,i}$ medio, (8.18) ekuazioan agertzen den osagai bakoitzerako fusio tenperatura
T_{f_i} lortzen dugu. Era horretan lortzen den ekuazio ez linealen sistema ebazteko metodoak
ezagunak dira [219]; soluzio gisa konposizio eutektikoaren bektorea $\mathbf{x}_{eu}$ eta horren urtze ten-
peratura T_{eu} lortzen ditugu. Gure kasuan, behin (x_{eu}, T_{eu}) puntua lortuta, horren koorde-
natuak eta (8.18) urtze kurbak erabiliz, (x_1, T) planuko edozein punturen faseak 5.1 irudian
agertzen den eskema erabiliz jakin ditzakegu. Sistema horiek ilustratzeko xedearekin, Ag/Si,
KNO$_3$/LiNO$_3$ and K$_2$SO$_4$/Li$_2$SO$_4$ sistemak hartu ditugu [219]. Kasu guztietan, hurbilketa
sinple bat jarraituz, (x_1, T) planua $[0, 1] \times [0.25 \times \min(T_{f,1}, T_{f,2}), 1.25 \times \max(T_{f,1}, T_{f,2})]$
domeinuan 100×500 tamainako sare uniforme bat erabiliz diskretizatu dugu; horrela
sarean guztira 50000 puntu daude. Hasierako datu sorta gisa, adierazitako domeinuan
5×10 tamainako sare uniformeko puntuak hartu ondoren, beste 100 punturen datuak
ziurgabetasun laginketan oinarrituta jaso ditugu. Horrela, guztira 150 puntu lagindu di-
tugu kasu bakoitzean. Beste era batean esanda, 5.3, 5.4 and 5.5 irudietan agertzen diren
fase diagramak eratzeko, planu diskretizatuaren %0.3 puntu baino ez ditugu erabili. Hiru
adibideentzat ikus dezakegunez, ziurgabetasun laginketa metodoak erabiliz, zonalde baten
inguruan zenbat eta fase trantsizio gehiago egon, orduan eta puntu gehiago laginduko
ditugu; nabaria da puntu eutektikoaren inguruan jasotako lagin dentsitatea. Prozedura hau
interesgarria izan daiteke farmakologia [228–230] eta kimika orlegian [231, 232] erbilgarriak
diren konposizio eutektikoak bilatzeko.

$$\ln x_i = \frac{\Delta H_{f,i}}{R} \left(\frac{1}{T_{f,i}} - \frac{1}{T} \right) \quad , \sum_{i=1}^{2} x_i = 1 \tag{8.18}$$

Bigarren kasuan, Hooke-n atomoak deskribatzeko (8.19) Hamiltondarra erabili dugu.
Literaturan sistema horien egitura elektronikoari buruzko hainbat lan egon arren, gaur egun
ere hainbat alorretan aplikazio interesgarriak dituzten sistemak dira, esaterako: sistema
kuantiko konfinatuak [220, 221], korrelazio elektronikoaren ikerketa [222, 223] eta materia
kondentsatuaren teoria [224, 225]. (8.19) ekuazioan agertzen den eragilearen simetriari
dagokionez, $\mathbf{W}$ matrize diagonalgarri eta positiboki definituak kanpo pontentzialaren
informazio guztia biltzen du; horren balio propioen g hendekapenaren arabera simetria:
esferikoa $g = 3$, esferoidala $g = 1$ edo triaxial elipsoidala $g = 1$ izango da.

$$H = \sum_{i=1}^{n} \left(-\frac{1}{2} \nabla_{\mathbf{r}_i}^2 + \frac{1}{2} \mathbf{r}_i^\top \mathbf{W} \mathbf{r}_i \right) + \sum_{j>i=1}^{n} \frac{e^{-\lambda r_{ij}}}{r_{ij}}, \quad \mathbf{W} = \begin{pmatrix} \omega_x^2 & 0 & 0 \\ 0 & \omega_y^2 & 0 \\ 0 & 0 & \omega_z^2 \end{pmatrix} \tag{8.19}$$

Atal honetan, hiru edo bi aldiz hendekaturik eta ω_q^2 balio propioak dituen **W** matrizeak eta elektroien arteko potentzial apantailatuak $\lambda \geq 0$ ikertu ditugu. Eragile Hamiltondar horiek medio, 4 eta 6 elektroiz osoturiko Hooke-n atomo elipsoidalen oinarrizko egoerari dagokion spin multiplizitatearen fase diagramak eraiki ditugu. Horretarako, parametro gisa (8.19) Hamiltondarrean agertzen diren kanpo potentzialaren konfinamendu parametroak eta Yukawaren pantailatze parametroa $(\omega_x^2, \omega_y^2, \omega_z^2, \lambda) \in \mathbb{R}_+^4$ erabili ditugu.

4. kapituluan ikusi dugun moduan, $\omega^2 = 0.25$ konfinamendu parametroa duen konfinamendu harmonikoaren bidez 4 eta 6 elektroiz osoturiko Hooke-n atomo esferikoen oinarrizko spin egoera tripletea da ($S = 1$) eta horrengandik hurbilen dagoen egoera singletea ($S = 0$) 1 eV-tara dago. Sistema horientzat, $(\lambda, \omega_{xy}^2, \omega_z^2)$ espazioan koordenatu bakoitzarenztat 15 puntudun sare unifome bat eraiki dugu $[0.05, 2.55] \times [0.20, 0.30] \times [0.20, 0.30]$ domeinuan; horrela sareak guztira 3375 puntu ditu. Gure kasuan, sare osotik 58 puntu baino ez hartuz (puntu guztien % 1.72) oinarrizko spin egoeren fase diagramak eskuratzeko gai izan gara. 5.6 irudietan, ardatz bertikalak λ pantzailatze parametroaren balioa adierazten du eta horizontalak $\varepsilon = \frac{\omega_{x,y}^2}{\omega_z^2}$ anisotropia parametroaren balioa adierazten du. Alde batetik, lau elektroiz osoturiko sistementzat, singleteak (puntu gorriz adierazitako egoera ez magnetikoak) $\omega_{x,y}^2$ balio handi, ω_z^2 balio txiki eta λ handiagoentzat agertzen direla ikus dezakegu. $\omega_{x,y} > \omega_z$ izateak eragiten duen anisotropiaren eraginez, z ardatzean zehar gorputz bateko energiak x, y planoan barrena baino txikiagoak dira; $Aufbau$ betetze egitura medio, p_z orbitalak okupaturik egongo dira eta oinarrizko egoeraren spina singletea izango da. Bestalde, sei elektroiz osoturiko sistemei erreparatuz, erdietsitako fase diagraman hainbat desberdintasun atzeman ditugu. Kasu horretan, λ pantailatza parametroarekiko joera bera izan arren, singleteak $\omega_{x,y}^2$ balio txiki, ω_z^2 balio handi eta λ handiagoentzat agertzen direla ikus dezakegu. Sistema bientan, Yukawa-ren potentzialean agertzen den λ parametroak balio handiak hartzen dituenean, natura kuantikoa duen elkartruke elkarrekintza ahulagoa egiten da eta oinarrizko egoeraren spin anizkoitztasunaren trantsizioa $\varepsilon = 1$ bertikalaren inguruan gauzatzen da. Partikula askeen limitera eramanda ($\lambda \rightarrow \infty$), Hamiltondarra gorputz bateko eragilez konposaturik dago, hauen energia orbitala (8.20) ekuazioan agertzen da. Muturreko kasu horretan, $\varepsilon = \omega_{x,y}^2/\omega_z^2$ asimetria parametroaren balioaren arabera, p orbitalen hendekapena 5.7 irudian agertzen den moduan apurtzen da. Pauli-ren esklusio printzipioaren arabera, orbital bakoitzean aurkako spina duten elektroi bi egon daitezke; Hund-en araua erabiliz, orbitalak hendekaturik dauden kasuan, banan banan beteko dira spin totala maximizatzen delarik. Gorputz anizdun sistemei dagozkien kontzeptu horiek buruan izanda, oinarrizko egoera elektronikoaren spin anizkoitztasuna anisotropia parametroa eta elektroi kopuruaren menpekoa dela ondorioztatu dugu.

$$\epsilon_{n_x, n_y, n_z} = \omega_{x,y}(n_x + n_y + 1) + \omega_z \left(n_z + \frac{1}{2} \right) \tag{8.20}$$

Hirugarren kasuan, gas noble molekulei dagokionez, aurretiazko lan konputazionaletan ondorioztatu zuten moduan, dimero hauen atomoen arteko distantzia $[1.265, 2.447]\text{Å}$ ordenekoa da nanokluster eta nanotutuetan konfinaturik dauden He_2 molekulen kasuan [210–218]. Zitaturiko sistema batzuetan eskuraturiko lotura kobalentearen deskribatzaileei (Bader-en teorian aipatzen diren loturaren puntu kritikoan kalkulaturiko dentsiatearen Laplacetarra eta energia totalaren dentsitatearen seinua) erreparatuz, $\Delta\rho(r_C)$ eta $H(r_C)$-ren seinuak negatiboak izanik, balditza hauetan dauden helio atomoen arteko loturaren

natura kobalentea dela ondorioztatu dute [214–216, 218]. 4. kapituluan, lotura kobalentearen deskribatzaileek kanpo potentzial esferiko harmonikoaren indar parametroa ω^2 eta nukleoen arteko distantziarekiko R duten menpekotasuna aztertu ditugu. Parametro hauek (8.21) Hamiltondarrean agertzen dira.

$$H = -\frac{1}{2}\sum_{i=1}^{4}\nabla_{\mathbf{r}_i}^2 - 2\sum_{J=1}^{2}\sum_{i=1}^{4}\frac{1}{r_{iJ}} + \sum_{j>i=1}^{4}\frac{1}{r_{ij}} + \frac{1}{2}\sum_{i=1}^{4}\mathbf{r}_i^T\mathbf{W}\mathbf{r}_i + \frac{1}{R} \qquad (8.21)$$

Lehen pausuan, 5.8 irudian agertzen diren kobalentzia fase diagramak HF/aug-cc-pVTZ mailan eskuratu ditugu. Etiketa gisa, Laplace-tarrak $\Delta\rho(r_C)$ eta energia totalaren dentsitateak $H(r_C)$ lotura puntu kritikoan duten seinuak erabili ditugu. Era berean, parametro espazioa 500×500 sare bat erabiliz diskretizatu dugu $[0.10, 4.00] \times [1.00, 4.00] \subseteq (\omega^2, R)$ domeinuan eta guztira horren 200 puntu erabiliz (0.1216%) kobelentzia fase diagramak eskuratu ditugu. Maila honetan lortrako $\Delta\rho(r_C)$-ren kasuan ikus dezakegunez, balio negatiboak nukleoen arteko distantzia 1.00 eta 1.52 $\mathring{A}$ tartean dagoenean eta 2.00 kurbatura baino balio handiagoentzat agertzen da. Beste aldetik, $H(r_C)$-ri dagokionez, nukleoen arteko distantzia 1.50 $\mathring{A}$ baino txikiagoa denean balore negatiboak aurkitu ditugu edozein kurbatura balio erabiliz. Atari balore hori gaindituz, lotura puntu kritikoan ebaluaturiko energia totalaren dentsitatearen seinua aldatu egiten da potentzial kurbatura handitzen dugun heinean; seinu aldaketa hura gertatzeko behar den kurbatura potentzial minimoa nukleoen arteko distantziarekin gorakorra da. Teoria maila honetan, gure erdua erabiliz lorturiko emaitzak hain lan aurrekarietan lorturikoenen antzekoak dira; esate baterako, He$_2$@C$_{20}$H$_{20}$ sisteman He-He distantzia 1.265$\mathring{A}$ izanik $\Delta\rho(r_C)$-ren balio positiboa ematen dute [210], gure kasuarekin erkatuz $\omega^2 < 2.00$. Helio atomoen arteko distantzia 1.60$\mathring{A}$ baino txikiagoa den sistementzat (He$_2$@B$_{12}$N$_{12}$ eta He$_2$@B$_{16}$N$_{16}$)[216] $\Delta\rho(r_C)$ balio positiboak eta $H(r_C)$ balio negatiboak eman dituzte. Intereseko sistema horreri buruz gehiago ikastekotan, 20×20 sare uniforme bat eraiki dugu $(0.00, 1.00) \times (1.40, 2.6) \subseteq (\omega^2, R)$ domeinuan eta puntu bakoitzean CASSCF(4,8)/aug-cc-pVTZ kalkuluak burutu ondoren, $\Delta\rho(r_C)$ eta $H(r_C)$ eskuratu ditugu; horrela, 5.9 irudian agertzen diren sestra kurbak eraiki ditugu. $\Delta\rho(r_C)$-ri erreparatuz, domeinu osoan balio positiboak aurkitu ditugu eta bere magnitudea handitu egiten da nukleoen arteko distantzia txikitzen den heinean; era berean kurbatura parametroarekiko ia askea da. Azkenik, domeinu horretan $H(r_C)$-ren balio negatiboak eskuratu ditugu eta euren magnitudea handitu egiten da nukleoen arteko distantzia txikitzen den heinean; azken behaketa hori HF kalkuluetatik eta atomo guztiak erabiliz lorturiko emaitzekin bateragarria dela nabaritu dugu.

Laburbilduz, atal honetan ikuspuntu kimikotik interesgarriak diren hainbat aplikazio emanda, ML teknikak fase diagramak eraikitzeko eta fase berriak aurkitzeko tresna erabilgarriak direla ondorioztatu dugu.

8.3.5   Potentzial gausstarrak

Konfinamendu potentzial gausstarrek komunitate zientifikoaren arreta erakarri dute. Alde batetik, materia kondentsatuaren teorian matrize erdieroaleetan integraturiko puntu kuantikoen ereduak lortzeko erabiltzen dituzte [233–236]. Berriki bi eta hiru dimentsioko puntu kuantikoei buruzko lanetan hainbat propietateren ereduak lortzeko erabili dituzte, besteak beste: Aharonov-Bohm oszilazioak [237], koherentzia galera efektuak [238], propietate termomagnetikoak [239–242], kanpo eremuen elkarrekintzak [243–248], propietateen menpekotasun topologikoak [249, 250], elkartze kuantikoa [251], eredugintza matematikoa [252–254], elektroi gutxidun sistemak [255, 256] eta abar. Beste alde batetik, fisika nuklearrean α partikulen arteko elkarrekintzak deskribatzen dituzten Ali-Bodmer potentzialak [257] oraindik ere egitura nuklearreko ereduetan erabiltzen dituzte [258–260]. Azken horietan, potentzial gausstarrak diren moduan erabiltzen diren arren, materia kondentsatuari buruzko lanetan egitura elektronikoaren kalkuluak egiterakoan, potentzial gausstarren ordez horiei hurbiltzen diren potentzial harmonikoak erabiltzen dira. Horiei, Hooke-n atomoan deritze. Horiek kasu batzuetan hurbilketa aproposak izaten badira ere, puntu kuantikoen loturiko egoerak deskribatzerako orduan hainbat mugapen dituzte. Lehenik, potentzial horiek erabiltzeak egitura molekularraren galera dakar; izan ere, hainbat puntutan zentraturiko potentzial harmonien konbinazio lineal ororen emaitza beste zentru bakar bateko potentzial harmonikoa da. Bigarrenez, potentzial harmonikoei infinitu loturiko egoera eslei diezazkiekegu; hortaz, ionizazioa eta disoziazioa bezalako prozesuak deskribatzea ezinezkoa da.

Lan honen 6. kapituluan, hiru dimentsioko zentru bakarreko potentzial gausstarretan konfinaturik dauden $n = \{2, 4, 6, 8, 10\}$ elektroidun sistemak (8.22) ekuazioan agertzen den Hamiltondarra erabiliz aztertu ditugu. Dagozkion bi gorputzetako Yukawa elkarrekintzei dagozkien integralak gure taldean aurretiz egindako lanetatik berreskuratu ditugu [226].

$$H = -\frac{1}{2}\sum_{i=1}^{n}\nabla_i^2 - \sum_{i=1}^{n}V_0 e^{-\beta r_i^2} + \sum_{j>i=1}^{n}\frac{e^{-\lambda r_{ij}}}{r_{ij}} \qquad (8.22)$$

Potentzial gausstarren bidez konfinaturiko sistemak aztertzeko, beharrezkoak diren N zentru dituen eta (8.23) ekuazioan agertzen den kanpo potentzialari dagozkion matrize elementuak kalkulatu behar ditugu. Gure kasuan, kimika kuantikoan egin ohi denez, matrize elementuak oinarri funtzio gausstarrak erabiliz (8.24) ekuazioan agertzen diren moduan lortu ditugu. Integral hauen kalkulua egiteko, funtzio gausstarren biderkadura teorema (ingelesez Gaussian product theorem) bi aldiz aplikatuz, balio analitiko itxiak eskuratu ditugu.

$$V_{ext}(\mathbf{r}) = -\sum_{i=1}^{N}V_{0,i}e^{-\beta_i(\mathbf{r}-\mathbf{R}_{0,i})^2} \qquad (8.23)$$

$$\int G_1(\alpha_1, \mathbf{R}_A, l_1, m_1, n_1)G_2(\alpha_2, \mathbf{R}_B, l_2, m_2, n_2)e^{-\beta_i(\mathbf{r}_1-\mathbf{R}_{0,i})^2}d\mathbf{r}_1 \qquad (8.24)$$

Kalkulaturiko integralen emaitzak egokiak direla eta potentzial hauei buruz gehiago ikastearren, lehendabiziko kalkulu batzuk burutu ditugu. Horien emaitzetan oinarrituta, lorturiko integralen balioa eta horien inplementazio konputazionala zuzenak direla frogatu dugu.

Lehenik, $\{n = 2, 4, 6, 8, 10\}$ elektroiz osoturiko spin egoera singletea eta tripletean dauden sistemen gaineko CASSCF eta MRMP2 kalkuluak $m = \{10, 11, 12, 13\}$ orbital erabiliz burutu ditugu. Sistema hauek 4. kapituluan agertzen direnekin lotura eratzeko asmoz, V_0 parametroaren balio handiak eta zabalera parametro aproposdun potentzial gausstarretan konfinaturiko sistemak aztertu ditugu $\omega^2 = 2\beta V_0 = 1/4$. Hori dela eta, kapitulu hortan aurkezturiko EBTS-6S oinarriak erabiltzea egokia izan da. Ildo berean, V_0 parametroaren 30 balio aukeratu ditugu uniformeki banaturiko $[10.0, 300.0]$ tartean. Hain balio handiak hartuz, funtzio potentzial gausstarraren Taylor-en serie moduan adierazi dugu. Garapen horretan agertzen diren lehen hiru gaiak potentzial harmoniko baliokideei dagozkien elementuak dira; gainera, batezbesteko energia zinetikoak T eta elkarrekintza Coulomb-iarrek V_{ee} potentzial sakonera parametroarekiko menpekotasunik ez dutela hartzen badugu, sistema gausstarraren energia E_G eta sistema Hooke-ar baliokidearen energiak E_H (6.14) ekuazioaren bidez loturik daude. Adierazpen hori erabiliz eta egitura elektronikoaren kalkuluetatik eskuratutako datuak erabiliz, E_H eta lehen zuzenketa anharmonikoa g erregresio linealen bitartez determinatu ditugu (ikusi 6.1 taula). Ikusi dugunez, erregresioen bidez eskuratutako E_H balioak 4. kapituluan agertzen diren antzekoak dira; lorturiko errorerik handiena 1×10^{-5} Hartree-koa izan da. Lehenengo gai anharmonikoari dagokionez, errorerik handiena 4×10^{-4} unitate atomikoduna izan da. Atzeman dugunez, horren balioa ez da nabari aldatzen espazio aktiboan dauden orbital kopuruarekin, n elektroi kopurua eta spin egoerarekiko, ordea, menpekotasuna nabariagoa da (bi elektroiz koposaturiko sistemen kasua nabarmena da). Korrelazio koefizienteari erreparatuz, kasu guztiak hartuz, bere batezbesteko balioa $R^2 = 0.9991$ izan da eta kasurik okerrena CASSCF(8,10)(S)/ETBS-6S kalkuluetatik eratorritakoa $R^2 = 0.9623$.

Azkenik, potentzial gausstarren bidez konfinaturik eta egoera singlean dauden bi elektroiz osoturiko sistemek behintzat loturiko egoera bat dutela kontuan izanik, sistema horiek zein potentzial sakonera baliorentzako disoziatzen diren aztertu dugu $(E_G(V_0^d) = 0)$. Gainera, elektroien arteko elkarrekintzek disoziazio prozesuan duten eragina ikertzeko xedearekin, Yukawa-ren potentzialean agertzen diren λ parametroaren 10 balio hartu ditugu $[0.10, 1.00]$ tarte uniformean. Era berean, sakonera parametroaren 20 balio hartu ditugu $[0.50, 1.50]$ uniformeki banaturiko tartean eta egitura elektronikoaren kalkuluak CASSCF(2,13)/ETBS-6S eta MRMP2(2,13)/ETBS-6S mailetan burutu ditugu (ikusi 6.1 irudia). Aurreko kasuan egin dugun antzeko eran, potentzial gausstarra Taylor-en serie moduan garatu dugu, baina kasu honetan bigarren gai anharmonikoa ere hartu dugu; horrela, adierazpen funtzional egokia erabiliz, E_H, g_1 eta g_2 balioak erregresio linealen bidez estimatu ditugu. 6.2 taulan agertzen diren emaitzak kontuan izanik, erregresio tekniken bidez estimaturiko balioek perturbazio metodoek gehitzen duten korrelazio dinamikoarekiko askeak dira azterturiko λ balio guztientzat; horrela, CASSCF eta MRMP2 metodoen bidez lorturiko estimazioak antzekoak direla ohartu gara. Horrela, eskuraturiko sistema Hooke-ar baliokidearen energia E_H gero eta txikiagoa da λ handitzen den heinean; hala eta guztiz ere, 4. kapituluan agertzen diren CASSCF/ETBS-6S mailan eskuraturiko emaitzekin alderatuta, era honetan lorturiko energiak batezbeste 0.025 a.u. altuagoak dira. Antzeko neurriko erroreak espero ditugu, izan ere, Hooke-n atomo baliokideen energiak era zehatzean

lortzeko, disoziazio limitean baino, sakonki konfinaturiko sistemak ikertu behar ditugu. Gai ez harmonikoei dagokienez, g_1 txikitzen doa λ handitzen den heinean. Hipotesi nagusia: elektroi-elektroi elkarrekinztak ahultzen diren heinean, korrelazio efektuak ere itzaltzen joango dira eta elektroiak potentzial putzuaren minimotik hurbil aurkitzeko aukera handitu egiten da; hortaz sistema osoa "harmonikoagoa" da eta g_1-en magnitudea txikitu egiten da. Bestalde, g_2 bigarren gai anharmonikoa hazi egiten da $\lambda = 0.6$ punturaino eta gero txikitzen hasten da.

Disoziazio atarien balioa ahalik eta zehatzenak eskuratzekotan, Taylor-en garapenaren gaien seinuak alternatuak direla frogatu ondoren, funtzioa Stiljies motakoa dela ohartu gara. Hori horrela, Padé-ren sekuentzia nagusiak hartuta ($\mathcal{P}_1^1(V_0^{-1})$ eta $\mathcal{P}_2^1(V_0^{-1})$) disoziazio sakonera limitearen goi eta behe mugak determinatu ditugu. 6.2 irudian ikus dezakegunez, pantailatze parametroa zenbat eta handiagoa izan, elektroi-elektroi elkarrekintzak orduan eta ahulagoak izango dira eta potentzialak ez du zertan hain sakona izan behar partikulak konfinaturik (energia negatibodun egoera) mantentzeko.

8.4 EMAITZA NAGUSIAK

8.4.1 Konfinamendu harmonikoa ikertzeko protokolo konputazionalen garapena

Tesi honetako 3., 4. eta 5. kapituluetan, sasi bat, sasi bi eta hiru dimentsiodun potentzial Harmonikoetan konfinaturiko elektroi gutxidun sistemak aztertzeko konputazio protokoloen garapena aurkeztu dugu.

Alde batetik, sasi-bat eta sasi-bi dimentsiotako sistemak aztertzeko, hiru-dimentsioko s motako oinarri funtzio gausstar banatuak erabili ditugu. Lehenengoentzat behar adina funtzio banatu ziren uniformeki banatutako sare batean zehar. Funtzio horiei dagozkien berretzaileak α eta zentruak $\{r_i\}$, k konfinamendu parametroaren menpekoak izanik, potentzialaren informazioa integraturik dute; bestalde, ondoz-ondoko funtzioen arteko gainezarpen integralaren balioa $S(\alpha, \delta) = \exp(-\alpha\delta^2/2) = \exp(-1/2)$ ezarri dugu. Bigarrenarentzat, funtzio gausstarrak sare hexagonal batean banaturik daudela, ondoz ondoko oinarri funtzioen arteko distantzia δ, gainezarpen parametroa ξ, konfinamendu parametroa k eta oinarri-funtzio konpuru totala emanik dagozkien α berretzaileak bariazionalki optimizatu ditugu. Zenbait optimizazio egin ditugu konfinamendu parametroen hedadura handia azaltzeko. Partikula bakarraren eredutik lorturiko emaitza analitikoak erabiliz, sare neuronal ereduak optimizatu eta trebatu genituen emaitza horiek edozein baliotara hedatzeko helburuarekin. Konfigurazio horiek erabiliz eredu horientzat errore txikiak lortu ez ezik, metodo multi-erreferentzialei esker konfinamendu txikiko sistemetan agertzen den Wigner-en lokalizazioa modu egokian errepresentatu ere egin dugu.

Beste alde batetik, lau geruzaz osoturiko zentru bakarreko oinarri funtzioak (izenez 4SPDF) $k = \omega^2 = 1/4$ konfinamendu parametrodun Hooke-n hiru-dimentsioko atomoentzat optimizatu ditugu. Hainbat elektroi kopuru ($n = \{2, 4, 6, 8, 10\}$), spin egoera (singlete eta triplete) eta pantailatze parametroren ($\lambda = \{0.0, 0.2, 0.4, 0.6, 0.8, 1.0\}$) optimizazioak burutu ondoren, oinarri unibertsal optimoa sei elektroiz eta egoera singleteko sistemarako lortutakoa zela ondorioztatu dugu (izenez ETBS-6S). Oinarri horiek baliatuta, sistema guztien singlete eta triplete spin egoeren energia absolutuak lortuz, aurretiz argitaraturiko emaitzekin bat datozela ikusi dugu. Horrez gain, lortutako singelete-triplete diferentzia balioak zehatzak eta sistemaren Aufbau egitura zuzena ere badela egiaztatu dugu.

8.4.2 Ziurgabetasun laginketen metodoen inplementazioa fase diagramak lortzeko

Bosgarren kapituluan, ETBS-6S oinarriaren optimizazio-prozesua eta zehaztasuna deskribatu ditugu. Aipatu bezala, horiek medio direla, Hooke-n atomo esferikoen egitura elektronikoko kalkuluen bidez lortzen den Aufbau egitua $1s < 1p < 1d$ dela ikusi dugu. Betetze-egitura honetan oinarrituz, lau eta sei elektroiz osaturiko Hooke-n atomo esferikoen oinarrizko egoeraren spin multiplizitatea tripletea dela berehala ikusi dugu. Hala eta guztiz ere, simetria esferikoa apurtuz gero, p orbitalak ez dira gehiago hendekaturik egongo, eta talde bitan bereiziko dira: $\{p_x, p_y\}$ eta $\{p_z\}$; horrela, oinarrizko egoeraren spin multipliz-

itatea simetria esferikoa nola hausten den eta sistema konposatzen duen elektroi kopuruaren menpekoa izango da.

Hooke-n atomo ez-esferikoen oinarrizko egoeraren spin aniztasuna (singletea edo tripletea) zein baldintzatan ezartzen den ulertzeko, 6. kapituluan erdi-gainbegituriko ikaskuntzan eta ziurgabetasun laginketa metodoetan oinarritutako makina-ikaskuntza prozedura bat proposatu dugu.

Lehen pauso gisa, proposaturiko prozesua ilustratzeko, puntu eutektiko bakar bat duten ereduzko solido-likido sistema batzuen fase diagramak lortu ditugu. Ikus dezakegunez, ziurgabetasun laginketa teknikei esker, algoritmoa iterfase guztiak lagintzeko gai da, bereziki, puntu eutektikotik hurbil dauden puntuak.

Hooke-n atomo anisotropikoei dagokienez, x eta y norabideetan $\omega_{x,y}^2$ konfinamendu parametroa eta z norabidean ω_z^2 konfinamendu parametroa ezarri ditugu. Gainera, elektroi-elektroi elkarrekintza modulatzen duen λ Yukawa parametroarekin ere hainbat froga egin ditugu. Adierazitako laginketa prozesua gauzatu ondoren, kasu esferiko guztientzat $(\omega_{x,y}^2 = \omega_z^2, \forall \lambda)$ oinarrizko egoeraren spin multiplizitatea tripletea izan dela atzeman dugu. Bestalde, $\omega_z^2 > \omega_{x,y}^2$ den kasuetan, lau elektroidun sistementzat oinarrizko egoeraren spin multiplizitatea singletea den bitartean, sei elektroidun sistementzat tripletea izaten jarraitzen du. Kontrara, $\omega_z^2 < \omega_{x,y}^2$ den kasuetan, sei elektroidun sistementzat oinarrizko egoeraren spin multiplizitatea singletea den bitartean, lau elektroidun sistementzat tripletea izaten jarraitzen du. Sistema eredugarri horiek etorkizunean erabili ahal izango dira elektroi kopuru handiagoek osatutako sistemak aztertzeko.

Azkenik, metodoaren erabileraren garrantzia ilustratzen duen beste adibide bat emateagatik, potentzial esferiko harmonikoetan konfinaturiko helio-dimeroen izaera kobalentea Bader-en teorian agertu ohi diren lotura deskribatzaileak erabiliz aztertu dugu. Kasu honetan, helio atomoen arteko lotura kimikoaren izaera kobalentea neurtu dugu, lotura puntu kritikoan kalkulatutako dentsitatearen Laplacetarraren eta guztizko energia-dentsitatearen zeinuak erabiliz. Gainera, potentzialaren konfinamendu parametroa eta distantzia internuklearra, fase-diagrama eraikitzeko kanpoko parametro gisa erabili ditugu. Egoera kobalenteen eskualde ezberdinak iragarri arren, kualitatiboki deskribatzaile biek nukleoen arteko distantzia txiki eta konfinamendu balio handietan egoera kobalenteen existentzia aurresaten dute.

8.4.3 Konfinamendu gausstarrei dagozkien gorputz bateko integralak inplementatu eta aurretiaz lorturiko emaitzak hedatu

Orain arte ikertutako sistemetan, elektroiak potentzial harmonikoen bidez konfinaturik egon dira. Eredu horiek puntu kuantikoen eta atomo artifizialen loturiko egoerak deskribatzeko lehen hurbilketa gisa erabil ditzakegun arren, ez dira kapaz sistema errealetan garrantzitsuak diren hainbat ñabardura deskribatzeko. Lehenik, hainbat puntutan zentraturiko potentzial harmonikoen konbinazio lineal bat oraindik potentzial harmoniko bat denez, zentru anitzetatik eratorritako egitura molekularra behatzea ezinezkoa da. Bigarrenez, potentzial harmonikoek infinitu egoera lotu dituzte; hori dela eta, ionizazioa eta disoziazioa bezalako prozesuak deskribatzeko erabilezinak dira.

Lan honen zazpigarren kapituluan, konfinamendu gausstarren garrantzia eta propietate orokorrak aipatzen ditugu; besteak beste (potentzial harmonikoak ez bezala) egitura molekularra eta loturiko egoera kopuru finituak dituztela. Horretaz gain, beharrezkoak diren gorputz bateko integralen kalkuluaren formulazioa adierazi dugu.

Potentzial horiek erabiliz, lehendabiziko emaitza batzuk emateko asmoarekin, kasu ilustratzaile bi aurkeztu ditugu. Alde batetik, sakonki konfinaturiko (V_0 sakonera parametroaren balio handiak) elektroi kopuru bikoitiz ($n = \{2, 4, 6, 8, 10\}$) eraturiko sistemen singlete-triplete energia tartea CASSCF(n, m)/ETBS-6S eta MRPT2(n, m)/ETBS-6S mailetan $m = \{10, 11, 12, 13\}$ orbital aktibo erabiliz kalkulatu eta aurretiaz Hooke-n atomoentzat lorturiko emaitzekin alderatu ditugu. Taylor-en serieak eta erregresio linealak tarteko, Hooke-n atomo baliokidearen energia eta lehen gai anharmonikoa erregresiotik lorturiko parametroak erabiliz lortu ditugu. Era horretan lorturiko Hooke-n atomo baliokidearen energiak eta laugarren kapituluan agertzen direnak oso antzekoak direla ikusi dugu. Beste alde batetik, Yukawa potentzialen bidez elkarrekitzen eta spin egoera singletea duten elektroi biz osoturiko sistemaren disoziazio mugak ikertu ditugu. Kasu honetan, Taylor-en serieak erabili beharrean, konbergentzia azkarragoa duten Padé-ren sekuentzia nagusietara jo dugu; horrela, objektu horien propietateetan oinarrituta, hainbat pantailatze parametrori dagozkien goi eta behe disoziazio mugak lortu ditugu.

8.5   ONDORIO NAGUSIAK

Lan honetan potentzial estatikoen bidez konfinaturiko elektroi sistemei buruzko aurrerapen batzuk jaso dira. Lehenik, bat, bi eta hiru dimentsioko potentzial harmonikoei esker, hainbat spin zenbaki dituzten elektroi gutxiz konposaturiko sistemak aztertzeko konputazio-protokoloak garatu ditugu. Zehazki, batetik, optimizazio teknika klasikoen bidez, zentru bakarreko eta dimentsio baten eta bitan banaturiko oinarri funtzio gausstar egoki batzuk lortu ditugu. Beste alde batetik, oinarri funtzio horiek CASSCF eta MRPT2 metodo multi erreferentzialak erabiliz: konfinamendu ahulean gauzatzen den Wigner-en lokalizazioa eta singlete-triplete energia tarteak modu egokian deskribatzeko gai izan gara.

Hooke-n atomo esferikoen kasuan, sistemaren Aufbau egitura hartuta, oinarrizko ego-eraren spin anizkoitztasuna elektroi kopuruaren menpekoa da. Halere, simetria esferikoa apurtu egiten da ($\omega_z^2 \neq \omega_{x,y}^2$) oinarrizko egoeraren spin multiplizitatea elektroi kopuruaren menpe egoteaz gain, simetria hori hautsi izan dugun eraren menpekoa ere bada. Elektroi kopuru jakin bat hartuta, erdi gainbegiraturiko eta ziurgabetasun lagineketa teknikak erabiltzen dituen garaturiko makina ikasketa metodo baten bidez, konfinamendu eta pan-tailatze parametroen menpekoak diren oinarrizko egoeraren spin multiplizitatearen fase diagramak eraikitzea lortu dugu. Gainera, metodo hori kimikoki esanguratsuak diren beste sistema gehiago ikertzeko (solido-likido nahaste binarioak eta lotura kimikoaren naturaren analisia) erabilgarria dela frogatu dugu.

Potentzial harmonikoen luzapen gisa, zentru anitzetatik eratorritako propietate moleku-larrak, disoziazio prozesuak eta ekarpen anharmonikoak biltzen dituzten konfinamendu potentzial gausstarrei sarrera eman diegu. Beharrezkoak diren gorputz bateko integralak GAMESS-US softwear-ean inplementatzeaz gain, baliokideak diren sistema Hooke-ondarrekin alderatuz lorturiko emaitzei erreparatuz potentzial bi horien arteko lotura ere frogatu dugu.

Etorkizun hurbilean, lan honetan lortutako emaitzak eta garaturiko metodoak konfina-mendu erregimen gehiagotara eta sistema errealistagoetara hedatuko ditugu.

8.6 ETORKIZUNERAKO LANAK

Laburbilduz, lan honetan sasi-bat, sasi-bi eta hiru dimentsiotan potentzial harmonikoen bidez konfinaturiko elektroi sistemak deskribatzeko beharrezkoak diren protokolo konputazioanalak garatu ditugu. Horretarako, makina ikaskuntzan oinarrituriko hainbat teknika erabili ditugu beharrezkoak diren oinarri funtzioak optimizatzeko eta egitura elektronikotik eratorritako propietateei dagozkien fase diagramak irudikatzeko. Azkenik, konfinamendu potentzial gausstarrei dagozkien gorputz bakarreko integralak lortu eta inplementatu ondoren, potentzial harmonikoarekin lorturiko emaitzekin daukaten lotura ere ezarri dugu.

Lortutako ezagutza beste sistema batzuetara hedatzeko helburuz, eta gure taldearen esperientzian oinarrituta, lan honetan garaturiko ereduak dopaturiko kluster endoedrikoetan aplikatzea kontsideratu dugu. Orain, proiektu honi buruzko bi gai nagusiak aurkeztuko ditugu: atomo artifizial eta superatomoekin loturik dauden dopaturiko kluster endoedrikoak eta potentzial estatikoei esker konfinaturiko sistema kuantikoak. Bi alorretan eskuratutako lan eta emaitza batzuk eztabaidatu ondoren, bi diziplinen arteko zubi bat ezariko dugu eta gure ikuspegia aurkeztuko dugu.

Alde batetik, klusterrak materia kondentsatuaren eta molekulen artean daude, eta horrek propietate elektroniko interesgarriak izatea eragiten du. Sistema horien artean, hutsik dauden nanokluster esferikoak aurki daitezke, esate baterako aintzindaria izan zen fulereno 60 lantanorekin dopaturiko klusterra La@C_{60} [270], antzekoak diren beste hainbat [271, 272] eta potentzialki erloju atomiko gisa erabil daitezkeen fulereno nitrogeno klusterrak [273]. Fulerenoan oinarritutako espeziez aparte, "superatomo" izendun hainbat sistema ere badaude[274–277], besteak beste, Al_{12} kutxen kasuan, dopatzailearen naturaren arabera, sistema osoa superhalogeno (boroarekin dopatuz), superalkalino (fosforoarekn dopatuz), superkalkogeno (kaltzioarekin dopatuz) edo 40 elektroidun sistema egonkor gisa (siliziorekin dopatuz) har dezakegu [278]. Beste sistema interesgarri batzuk kluster erdieroaleetan oinarritutakoak dira, zeinetarako hainbat propietate doikor (xurgapena, emisioa eta fotoluminesezentzia) hauteman diren [279–285]. Sistema superatomikoetan, propietate "atomikoak" egitura elektroniko osoaren portaera kolektibotik sortzen dira; haatik, kluster erdieroaleetan konfinaturiko atomoen kasuan, sistema osoaren propietateak elementu dopante isolatuetan behatutakoen oso antzekoak dira [286–290].

Beste alde batetik, konfinamendu potentzial gausstarrak egitura elektronikoari buruzko bai lan teorikoetan [252–256], bai materia kondentsatuari buruzko lan aplikatuagoetan erabili izan dituzte; hala nola: puntu kuantikoak [233–237], propietate termo-magnetikoen ikerketa [239–242] eta LASER eta eremu elektrikoak eta materiaren arteko elkarrekintzak aztertzeko [243–248]. Potentzial horiek egitura elektronikoko metodoetan lorturiko emaitzak kalibratzeko eta horien kalitatea neurtzeko erabiltzen diren potentzial harmonikoen antzekoak diren arren [36, 37, 41, 80, 261–266], haien arteko desberdintasun nagusia lehenengoa egitura molekularrak eta loturiko egoera finituak deskribatzeko gai dela da (6. kapitulua).

Bi kontzeptu horiek (dopaturiko kluster erdieroaleak eta potentzial gausstarrak) kontuan inzanda, lehen urrats bezala, potentzial gausstarretan konfinatuta dauden metal alkalinoen eta halogenoen ionizazio energiak eta afinitate elektronikoak ikertzea gustatuko litzaiguke. Atomo askeen ionizazio energia, okupaturiko energia garaienaren orbitala eta lehen ordeneko perturbazio metodoa (eta Helmann-Feyman teorema aplikatuz) erabiliz,

energia horien hurbilezko balioak erdietsi ditugu eta euren balioak kalkulu esplizituetatik lorturiko emaitzekin erkatu ditugu.

Sistema endohedrikoentzako hasierako emaitza batzuk

V_0 sakonera eta β zabalera parametroak dituen potentzial gausstar baten bidez Z zenbaki atomikodun eta n elektroidun atomo baten Hamiltondarra (8.25) ekuazioaren bidez adieraziko dugu.

$$H = -\frac{1}{2}\sum_{i=1}^{n}\nabla_i^2 - Z\sum_{i=1}^{n}\frac{1}{r_i} + \sum_{j>i}^{n}\frac{1}{r_{ij}} - V_0\sum_{i=1}^{n}e^{-\beta r_i^2} \tag{8.25}$$

Uhin funtzio monodeterminantalak hartuta, hurbilketa adiabatikoa (Koopmans-en teorema) eta Helmann-Feyman teorema aplikatuz, ionizazio potentzialak sakonera parametroarekiko duen menpekotasunari dagokion eta n-garren orbital atomikoaren menpekoa den espresio hurbildu bat lortu dugu:

$$\begin{aligned}\frac{\partial I}{\partial V_0} &= -\left\langle \Psi_{ion}\left|\sum_{i=1}^{n-1}e^{-\beta r_i^2}\right|\Psi_{ion}\right\rangle + \left\langle \Psi_{atom}\left|\sum_{i=1}^{n}e^{-\beta r_i^2}\right|\Psi_{atom}\right\rangle \\ &\approx \left\langle \phi(\mathbf{r}_n)\left|e^{-\beta r_n^2}\right|\phi(\mathbf{r}_n)\right\rangle\end{aligned}$$

Horrela, V_0 parametroaren balioa txikia dela hartzen badugu, Helmann-Feynman teorema erabiliz eskuraturiko espresioa $V_0' \in [0, V_0]$ tarte txikian integratuz gero, ionizazio energiaren espresio hurbildua lortu dugu (ikusi (8.26)). Formulazio alternatiboa: V_0 parametroaren balio txikiak hartuz, lehen ordeneko perturbazio zuzenketa erabiliz emaitza bera eskuratu dugu. Jakina, hurbilketa horretan dagokion orbital atomikoaren (eta era orokorrean uhin funtzio osoaren) forma potentzial paratroekiko askea dela aintzat hartu dugu; kasu orokorrean hori ez da zuzena Hooke-n atomoen kasuan ikusi dugun moduan (4. eta 5. kapituluak). Ondorioz, $\omega^2 = 2\beta V_0$ moduan definituriko kurbatura parametroa etorkizuneko ikerketetan kontuan izateko ezaugarri adierazgarria izango dela uste dugu.

$$I \approx I_0 + V_0\left\langle \phi(\mathbf{r}_n)\left|e^{-\beta r_n^2}\right|\phi(\mathbf{r}_n)\right\rangle \tag{8.26}$$

Antzeko estrategia jarraituz, n elektroidun atomo neutro bat eta honi dagokion $n+1$ elektroidun anioia hartuz, A afinitate elektronikoa anioiaren ionizazio energia baina seinu negatiboa duen kantitate bezala definituz, (8.27) ekuazioan agertzen den hurbilketa lortu dugu.

$$A \approx A_0 - V_0\left\langle \phi(\mathbf{r}_{n+1})\left|e^{-\beta r_{n+1}^2}\right|\phi(\mathbf{r}_{n+1})\right\rangle \tag{8.27}$$

Adierazpen bietan ((8.26) eta (8.27)) ikus dezakegun moduan, V_0 parametroaren balio adin txikiak hartuta, β parametroaren balioa ere txikia bada, potentzial gausstarrak sistema

osoaren ioniazio potentzialarengan duen eragin bakarra V_0 baliodun lerrokatze batean datza. Aitzitik, β parametroaren balio handien limitean, potentzial gaustarra neurri bako funtzio indizialaren antzekoa izango da eta ez du energian ekarpenik izango.

Horrela, bada, (8.26) eta (8.27) adierazpenetan agertzen diren integralak kalkulatzea beharrezkoa da. Kimika kuantikoan egin ohi den moduan, oinarri funtzioak funtzio gausstar primitibo moduan garatzen ditugu eta egitura elektronikoko konputazioen bidez garapen horietan agertzen diren koefizienteak lortzen ditugu. Beraz, beharrezkoak diren integralak (8.28) ekuazioan agertzen den forma bilinear moduan idatz ditzakegu; hemen, $\mathbf{V}$ matrizeak p eta q-garren oinarri primitiboen eta potentzial gausstarraren arteko elkarrekintzak biltzen ditu (integral horien garapenak 6. kapituluan agertzen dira), $\mathbf{C}$ matrizeak q funtzio primitiboetan oinarrituriko i-garren oinarriaren garapen koefizienteak biltzen ditu eta $\mathbf{\Phi}$ bektoreak egitura elektronikoko kalkulua burutu ondoren lortzen dugun n-garren elektroiak okupatzen duen orbital molekularraren koefizienteak biltzen ditu.

$$\left\langle \phi(\mathbf{r}_n) \left| e^{-\beta r_n^2} \right| \phi(\mathbf{r}_n) \right\rangle = \sum_{jipq} c_j^\dagger c_i c_p^{(j)\dagger} c_q^{(i)} \int g_p^\dagger g_q e^{-\beta r_n^2} d^3r = (\mathbf{C\Phi})^\dagger \mathbf{VC\Phi} \qquad (8.28)$$

Proposaturiko hurbilketak egokiak diren ziurtatzeko asmotan, HF/6-311++G mailan M=Li,Na,K metal alkalinoen eta MP2/6-31++G mailan X=F,Cl halogenoen elgitura elektronikoen bidezko ionizazio potentzialak eta afinitate elektronikoak konputatu ditugu. Irudi orokor bat lortzeko xedearekin, $(V_0, \beta) \in [-0.500, -0.001] \times [0.10, 2.00]$ tartea 20×20 tamainako sare batean diskretizatutakoan, sareko puntu bakoitzeko kalkulu esplizituak egin eta bakoitzari dagokion $\varepsilon = \frac{|I - I_{theo}|}{|I|} \times 100$ errorea kalkulatu dugu. 7.1 irudian ikus dezakegunez, lorturiko errorea kontsideraturiko atomoa eta konfinamendu potentzialaren parametroen menpekoa da. Kasu guztietan, lortutako errorea txikiagoa da sakontasun parametroaren balio txikietarako, perturbazio metodoen formulazioan espero den moduan. Beste ezaugarri partekatu bat zabalera parametroaren balio handiagoetarako lorturiko errorea, oro har, txikiagoa dela ohartu gara.

Orain arte, mota horretako sistemak aztertzeko lehen urratsak eman ditugu. Gure iragarpenak hobetzeko modu asko daude: teoria uhin funtzio multideterminantalak biltzen dituen metodoetara hedatu, 2. kapituluan egin den antzerako (V_0, β) parametroei dagozkien oinarri funtzio optimoak lortu, perturbazio garapenean agertzen diren termino gehiago kalkulatu eta abar.

BIBLIOGRAPHY

[1] E. Schrödinger, "An ondulatory theory of the mechanics of atoms and molecules," *Phys. Rev.*, vol. 28, pp. 1049–1070, 6 1926.

[2] W. Heisenberg, "Über quantentheoretische umdeutung kinematischer und mechanischer beziehungen.," *Zeitschrift für Physik*, vol. 33, no. 1, pp. 879–893, 1925.

[3] W. Pauli, "Über den zusammenhang des abschlusses der elektronengruppen im atom mit der komplexstruktur der spektren," *Zeitschrift für Physik*, vol. 31, no. 1, pp. 765–783, 1925.

[4] A. Sommerfeld, "Zur elektronentheorie der metalle," *Die Naturwissenschaften*, vol. 15, no. 41, pp. 825–832, 1927.

[5] A. Zannoni, *On the quantization of the monoatomic ideal gas*, 1999. arXiv: `cond-mat/9912229 [cond-mat.stat-mech]`.

[6] L. H. Thomas, "The calculation of atomic fields," *Mathematical Proceedings of the Cambridge Philosophical Society*, vol. 23, no. 5, 542–548, 1927.

[7] D. R. Hartree, "The wave mechanics of an atom with a non-coulomb central field. part i. theory and methods," *Mathematical Proceedings of the Cambridge Philosophical Society*, vol. 24, no. 1, pp. 89–110, 1928.

[8] ——, "The wave mechanics of an atom with a non-coulomb central field. part ii. some results and discussion," *Mathematical Proceedings of the Cambridge Philosophical Society*, vol. 24, no. 1, pp. 111–132, 1928.

[9] V. Fock, "Näherungsmethode zur lösung des quantenmechanischen mehrkörperproblems," *Zeitschrift für Physik*, vol. 61, no. 1-2, pp. 126–148, 1930.

[10] J. C. Slater, "The theory of complex spectra," *Phys. Rev.*, vol. 34, pp. 1293–1322, 10 1929.

[11] C. C. J. Roothaan, "New developments in molecular orbital theory," *Reviews of Modern Physics*, vol. 23, no. 2, pp. 69–89, 1951.

[12] G. G. Hall and J. E. Lennard-Jones, "The molecular orbital theory of chemical valency viii. a method of calculating ionization potentials," *Proceedings of the Royal Society of London. Series A. Mathematical and Physical Sciences*, vol. 205, no. 1083, pp. 541–552, 1951.

[13] A. Szabo and N. S. Ostlund, *Modern Quantum Chemistry*. Dover Publications, 1996.

[14]   B. O. Roos, P. R. Taylor, and P. E. Sigbahn, "A complete active space scf method (casscf) using a density matrix formulated super-ci approach," *Chemical Physics*, vol. 48, no. 2, pp. 157–173, 1980.

[15]   J. Ivanic, "Direct configuration interaction and multiconfigurational self-consistent-field method for multiple active spaces with variable occupations. i. method," *The Journal of Chemical Physics*, vol. 119, no. 18, pp. 9364–9376, 2003.

[16]   H. Werner and P. J. Knowles, "A second order multiconfiguration scf procedure with optimum convergence," *The Journal of Chemical Physics*, vol. 82, no. 11, pp. 5053–5063, 1985.

[17]   ——, "An efficient internally contracted multiconfiguration–reference configuration interaction method," *The Journal of Chemical Physics*, vol. 89, no. 9, pp. 5803–5814, 1988.

[18]   K. Andersson, P. Malmqvist, and B. O. Roos, "Second-order perturbation theory with a complete active space self-consistent field reference function," *The Journal of Chemical Physics*, vol. 96, no. 2, pp. 1218–1226, 1992.

[19]   J. Finley, P. Åke Malmqvist, B. O. Roos, and L. Serrano-Andrés, "The multi-state caspt2 method," *Chemical Physics Letters*, vol. 288, no. 2, pp. 299–306, 1998.

[20]   E. Wigner, "On the interaction of electrons in metals," *Phys. Rev.*, vol. 46, pp. 1002–1011, 11 1934.

[21]   E. Rousseau, D. Ponarin, L. Hristakos, O. Avenel, E. Varoquaux, and Y. Mukharsky, "Addition spectra of wigner islands of electrons on superfluid helium," *Phys. Rev. B*, vol. 79, p. 045 406, 4 2009.

[22]   M. Saitoh, "Melting criterion of two-dimensional wigner crystals on thin films of liquid helium," *Surface Science*, vol. 229, no. 1, pp. 356–358, 1990.

[23]   V. T. Dolgopolov, "Quantum melting of a two-dimensional wigner crystal," *Physics-Uspekhi*, vol. 60, no. 7, pp. 731–742, 2017.

[24]   H. Deng, L. Pfeiffer, K. West, K. Baldwin, L. Engel, and M. Shayegan, "Probing the melting of a two-dimensional quantum wigner crystal via its screening efficiency," *Physical Review Letters*, vol. 122, no. 11, 2019.

[25]   H. Li *et al.*, "Imaging two-dimensional generalized wigner crystals," *Nature*, vol. 597, no. 7878, pp. 650–654, 2021.

[26]   H. Pan, F. Wu, and S. Das Sarma, "Quantum phase diagram of a moiré-hubbard model," *Phys. Rev. B*, vol. 102, p. 201 104, 20 2020.

[27]   G. Koolstra, G. Yang, and D. I. Schuster, "Coupling a single electron on superfluid helium to a superconducting resonator," *Nature Communications*, vol. 10, no. 1, 2019.

[28] S. Narasimhan and T.-L. Ho, "Wigner-crystal phases in bilayer quantum hall systems," *Phys. Rev. B*, vol. 52, pp. 12 291–12 306, 16 1995.

[29] B. Padhi, C. Setty, and P. W. Phillips, "Doped twisted bilayer graphene near magic angles: Proximity to wigner crystallization, not mott insulation," *Nano Letters*, vol. 18, no. 10, pp. 6175–6180, 2018.

[30] Y. Zhou *et al.*, "Bilayer wigner crystals in a transition metal dichalcogenide heterostructure," *Nature*, vol. 595, no. 7865, pp. 48–52, 2021.

[31] B. Padhi, R. Chitra, and P. W. Phillips, "Generalized wigner crystallization in moiré materials," *Phys. Rev. B*, vol. 103, p. 125 146, 12 2021.

[32] R. Egger, W. Häusler, C. H. Mak, and H. Grabert, "Crossover from fermi liquid to wigner molecule behavior in quantum dots," *Phys. Rev. Lett.*, vol. 82, pp. 3320–3323, 16 1999.

[33] A. Ghosal, A. D. Glucu, C. J. Umrigar, D. Ullmo, and H. U. Baranger, "Incipient wigner localization in circular quantum dots," *Phys. Rev. B*, vol. 76, p. 085 341, 8 2007.

[34] L. Zeng, W. Geist, W. Y. Ruan, C. J. Umrigar, and M. Y. Chou, "Path to wigner localization in circular quantum dots," *Phys. Rev. B*, vol. 79, p. 235 334, 23 2009.

[35] V. Sahni, *Quantal Density Functional Theory II*. Springer Berlin, 2014.

[36] P. Gori-Giorgi and A. Savin, "Study of the discontinuity of the exchange-correlation potential in an exactly soluble case," *International Journal of Quantum Chemistry*, vol. 109, no. 11, pp. 2410–2415, 2009.

[37] W. M. Zhu and S. B. Trickey, "Exact density functionals for two-electron systems in an external magnetic field," *JCP*, vol. 125, p. 094 317, 2006.

[38] M. Pedersen Lohne, G. Hagen, M. Hjorth-Jensen, S. Kvaal, and F. Pederiva, "Ab initio computation of the energies of circular quantum dots," *Phys. Rev. B*, vol. 84, p. 115 302, 11 2011.

[39] K Varga, P Navratil, J Usukura, and Y Suzuki, "Stochastic variational approach to few-electron artificial atoms," *PRB*, vol. 63, no. 20, p. 205 308, 2001.

[40] J. Cioslowski, K. Strasburger, and E. Matito, "The three-electron harmonium atom: The lowest-energy doublet and quadruplet states," *JCP*, vol. 136, no. 19, p. 194 112, 2012.

[41] J. Cioslowski and K. Strasburger, "Five- and six-electron harmonium atoms: Highly accurate electronic properties and their application to benchmarking of approximate 1-matrix functionals," *The Journal of Chemical Physics*, vol. 148, no. 14, p. 144 107, 2018.

[42] E. Ramos-Cordoba, P. Salvador, and E. Matito, "Separation of dynamic and nondynamic correlation," *PCCP*, vol. 18, pp. 24 015–24 023, 2016.

[43]   E. Ramos-Cordoba and E. Matito, "Local descriptors of dynamic and nondynamic correlation," *JCTC*, vol. 13, pp. 2705–2711, 2017.

[44]   M. Via-Nadal, M. Mayorga, E. Ramos-Cordoba, and E. Matito, "Singling out dynamic and nondynamic correlation," *The Journal of Physical Chemistry Letters*, vol. 10, Jun. 2019.

[45]   P. Hessler, J. Park, and K. Burke, "Several theorems in time-dependent density functional theory," *PRL*, vol. 82, p. 378, 1999.

[46]   P. M. Laufer and J. B. Krieger, "Test of density-functional approximations in an exactly soluble model," *PRA*, vol. 33, no. 3, pp. 1480–1491, 1986.

[47]   S. Kais, D. R. Hersbach, N. C. Handy, C. W. Murray, and G. J. Laming, "Density functionals and dimensional renormalization for an exactly solvable model," *JCP*, vol. 99, p. 417, 1993.

[48]   C. Filippi, C. J. Umrigar, and M. Taut, "Comparison of exact and approximate density functionals for an exactly soluble model," *JCP*, vol. 100, p. 1290, 1994.

[49]   C.-J. Huang and C. J. Umrigar, "Local correlation energies of two-electron atoms and model systems," *PRA*, vol. 56, p. 290, 1997.

[50]   M. Taut, A. Ernst, and H. Eschrig, "Two electrons in an external oscillator potential: Exact solution versus one-particle approximations," *J. Phys. B*, vol. 31, p. 2689, 1998.

[51]   Z. Qian and V. Sahni, "Physics of transformation from schrödinger theory to kohn-sham density-functional theory: Application to an exactly solvable model," *PRA*, vol. 57, p. 2527, 1998.

[52]   S. Ivanov, K. Burke, and M. Levy, "Exact high-density limit of correlation potential for two-electron density," *JCP*, vol. 110, p. 10 262, 1999.

[53]   E. V. Ludeña, V. Karasiev, A. Artemiev, and D. Gómez, "Functional n-representability in density matrix and density functional theory: An illustration for hooke's atom," in *Many-electron Densities and Reduced density matrices*, J. Cioslowski, Ed. New York: Kluwer Academic/Plenum Publishers, 2000, ch. 10.

[54]   J. Cioslowski and E. Matito, "Benchmark full configuration interaction calculations on the lowest-energy 2p and 4p states of the three-electron harmonium atom," *JCTC*, vol. 7, p. 915, 2011.

[55]   J. Cioslowski, M. Piris, and E. Matito, "Robust validation of approximate 1-matrix functionals with few-electron harmonium atoms," *JCP*, vol. 143, no. 21, p. 214 101, 2015.

[56]   M. Rodríguez-Mayorga, E. Ramos-Cordoba, F. Feixas, and E. Matito, "Electron correlation effects in third-order densities," *PCCP*, vol. 19, pp. 4522–4529, 2017.

[57] M. Rodríguez-Mayorga, E. Ramos-Cordoba, M. Via-Nadal, M. Piris, and E. Matito, "Comprehensive benchmarking of density matrix functional approximations," *PCCP*, vol. 19, pp. 24 029–24 041, 2017.

[58] J. Cioslowski and K. Pernal, "The ground state of harmonium," *JCP*, vol. 113, p. 8434, 2000.

[59] J. Cioslowski and E. Matito, "Note: The weak-correlation limit of the three-electron harmonium atom," *JCP*, vol. 134, no. 11, p. 116 101, 2011.

[60] C Amovilli and N. H. March, "Hookean atom with four electrons: On the formation of a tetrahedral wigner molecule in the weak trapping limit," *PRA*, vol. 83, no. 4, p. 044 502, 2011.

[61] J. Cioslowski, "The weak-correlation limits of few-electron harmonium atoms," *JCP*, vol. 139, no. 22, p. 224 108, 2013.

[62] K. Strasburger, "The order of three lowest-energy states of the six-electron harmonium at small force constant," *JCP*, vol. 144, no. 23, p. 234 304, 2016.

[63] J. Cioslowski and K. Strasburger, "Harmonium atoms at weak confinements: The formation of the wigner molecules," *JCP*, vol. 146, no. 4, p. 044 308, 2017.

[64] ——, "Five-and six-electron harmonium atoms: Highly accurate electronic properties and their application to benchmarking of approximate 1-matrix functionals," *JCP*, vol. 148, no. 14, p. 144 107, 2018.

[65] T. Chakraborty, *Quantum Dots*. Elsevier, 2008.

[66] A. H. et al, "Role of metallic leads and electronic degeneracies in thermoelectric power generation in quantum dots," *Physical Review Research*, vol. 2, no. 1, 2020.

[67] Y. G. et al, "Exceptional catalytic nature of quantum dots for photocatalytic hydrogen evolution without external cocatalysts," *Advanced Functional Materials*, vol. 28, no. 33, p. 1 801 769, 2018.

[68] M. L. et al, "Quantum-dot-derived catalysts for co2 reduction reaction," *Joule*, vol. 3, no. 7, pp. 1703–1718, 2019.

[69] J. T. et al, "1% defect enriches mos2 quantum dot: Catalysis and blue luminescence," *Nanoscale*, vol. 12, pp. 4352–4358, 7 2020.

[70] Y. Chen and X. Bai, "A review on quantum dots modified g-c3n4-based photocatalysts with improved photocatalytic activity," *Catalysts*, vol. 10, p. 142, 1 2020.

[71] E. Connors, J. Nelson, and J. Nichol, "Rapid high-fidelity spin-state readout in si/si-ge quantum dots via rf reflectometry," *Physical Review Applied*, vol. 13, no. 2, 2020.

[72] R. Leon *et al.*, "Coherent spin control of s-, p-, d- and f-electrons in a silicon quantum dot," *Nature Communications*, vol. 11, no. 1, 2020.

[73] L. Vandersypen and M. Eriksson, "Quantum computing with semiconductor spins," *Physics Today*, vol. 72, no. 8, pp. 38–45, 2019.

[74] J. Yoneda *et al.*, "A quantum-dot spin qubit with coherence limited by charge noise and fidelity higher than 99.9%," *Nature Nanotechnology*, no. 2, pp. 102–106, 2018.

[75] D. Walkup *et al.*, "Tuning single-electron charging and interactions between compressible landau level islands in graphene," *Physical Review B*, vol. 101, no. 3, 2020.

[76] S. M. Reimann and M. Manninen, "Electronic structure of quantum dots," *Rev. Mod. Phys.*, vol. 74, pp. 1283–1342, 4 2002.

[77] L.-W. Wang and A. Zunger, "Linear combination of bulk bands method for large-scale electronic structure calculations on strained nanostructures," *Phys. Rev. B*, vol. 59, pp. 15 806–15 818, 24 1999.

[78] G. Bester, "Electronic excitations in nanostructures: An empirical pseudopotential based approach," *Journal of Physics: Condensed Matter*, vol. 21, no. 2, p. 023 202, 2008.

[79] E. V. Ludeña, X. Lopez, and J. M. Ugalde, "Non-born-oppenheimer treatment of the h2 hookean molecule," *J. Chem. Phys.*, vol. 123, p. 024 102, 2005.

[80] M. Taut, "Two electrons in an external oscillator potential: Particular analytic solutions of a coulomb correlation problem," *Physical Review A*, vol. 48, no. 5, pp. 3561–3566, 1993.

[81] R. Ashoori, H. Stormer, J. Weiner, L. Pfeiffer, K. Baldwin, and K. West, *Phys. Rev. Lett.*, vol. 71, p. 613, 1993.

[82] D. Pfannkuche and S. Ulloa, *Phys. Rev. Lett.*, vol. 74, p. 1194, 1995.

[83] M. Tews, *Ann. Phys. (Leipzig)*, vol. 13, p. 249, 2004.

[84] P. Drouvelis, P. Schmelcher, and F. Diakonos, *Phys. Rev. B*, vol. 69, p. 035 333, 2004.

[85] P. A. Maksym, H Imamura, G. P. Mallon, and H Aoki, "Molecular aspects of electron correlation in quantum dots," *Journal of Physics: Condensed Matter*, vol. 12, no. 22, R299–R334, 2000.

[86] H. Yakobi, E. Eliav, and U. Kaidor, "Electronic structure of three-dimensional isotropic quantum dots by four-component relativistic coupled cluster methods," *The Journal of Chemical Physics*, vol. 134, p. 054 503, 2011.

[87] D. Heitmann, V. Gudmundsson, M. Hochgräfe, R. Krahne, and D. Pfannkuche, *Physica E*, vol. 14, p. 37, 2002.

[88] Y. Lozovik and S. Volkov, *Phys. Sol. State*, vol. 45, p. 364, 2003.

[89] J. Adamowski, A. Kwaśniowski, and B. Szafran, "Lo-phonon-induced screening of electron–electron interaction in d-centres and quantum dots," *J. Phys.: Condens. Matter*, vol. 17, p. 4489, 2005.

[90]   A. C. Mater and M. L. Coote, "Deep learning in chemistry," *Journal of Chemical Information and Modeling*, vol. 59, no. 6, pp. 2545–2559, 2019.

[91]   T. F. G. G. Cova and A. A. C. C. Pais, "Deep learning for deep chemistry: Optimizing the prediction of chemical patterns," *Frontiers in Chemistry*, vol. 7, 2019.

[92]   N. Artrith *et al.*, "Best practices in machine learning for chemistry," *Nature Chemistry*, vol. 13, no. 6, pp. 505–508, 2021.

[93]   C. Sutton, M. Boley, L. M. Ghiringhelli, M. Rupp, J. Vreeken, and M. Scheffler, "Identifying domains of applicability of machine learning models for materials science," *Nature Communications*, vol. 11, no. 1, 2020.

[94]   S. Dick and M. Fernandez-Serra, "Machine learning accurate exchange and correlation functionals of the electronic density," *Nature Communications*, vol. 11, no. 1, 2020.

[95]   K. Choo, A. Mezzacapo, and G. Carleo, "Fermionic neural-network states for ab-initio electronic structure," *Nature Communications*, vol. 11, no. 1, 2020.

[96]   J. T. Margraf and K. Reuter, "Pure non-local machine-learned density functional theory for electron correlation," *Nature Communications*, vol. 12, no. 1, 2021.

[97]   T. W. Ko, J. A. Finkler, S. Goedecker, and J. Behler, "A fourth-generation high-dimensional neural network potential with accurate electrostatics including non-local charge transfer," *Nature Communications*, vol. 12, no. 1, 2021.

[98]   H. Kulik *et al.*, "Roadmap on machine learning in electronic structure," *Electronic Structure*, 2022.

[99]   E. A. Engel, A. Anelli, M. Ceriotti, C. J. Pickard, and R. J. Needs, "Mapping uncharted territory in ice from zeolite networks to ice structures," *Nature Communications*, vol. 9, no. 1, 2018.

[100] C. Zeni *et al.*, "Data-driven simulation and characterisation of gold nanoparticle melting," *Nature Communications*, vol. 12, no. 1, 2021.

[101] H. Niu, L. Bonati, P. M. Piaggi, and M. Parrinello, "Ab initio phase diagram and nucleation of gallium," *Nature Communications*, vol. 11, no. 1, 2020.

[102] B. Cheng, G. Mazzola, C. J. Pickard, and M. Ceriotti, "Reply to: On the liquid–liquid phase transition of dense hydrogen," *Nature*, vol. 600, no. 7889, E15–E16, 2021.

[103] Y.-C. Lo, S. E. Rensi, W. Torng, and R. B. Altman, "Machine learning in chemoinformatics and drug discovery," *Drug Discovery Today*, vol. 23, no. 8, pp. 1538 –1546, 2018.

[104] S. Gugler, J. P. Janet, and H. J. Kulik, "Enumeration of de novo inorganic complexes for chemical discovery and machine learning," *Mol. Syst. Des. Eng.*, vol. 5, pp. 139–152, 1 2020.

[105] F. Piroozmand, F. Mohammadipanah, and H. Sajedi, "Spectrum of deep learning algorithms in drug discovery," *Chemical Biology & Drug Design*, vol. 96, no. 3, pp. 886–901, 2020.

[106] J. P. Janet, L. Chan, and H. J. Kulik, "Accelerating chemical discovery with machine learning: Simulated evolution of spin crossover complexes with an artificial neural network," *The Journal of Physical Chemistry Letters*, vol. 9, no. 5, pp. 1064–1071, 2018.

[107] O. T. Unke and M. Meuwly, *Machine learning potential energy surfaces*, 2019. arXiv: `1909.08027 [physics.chem-ph]`.

[108] G. Schmitz, I. H. Godtliebsen, and O. Christiansen, "Machine learning for potential energy surfaces: An extensive database and assessment of methods," *The Journal of Chemical Physics*, vol. 150, no. 24, p. 244 113, 2019.

[109] P. O. Dral, A. Owens, A. Dral, and G. Csányi, "Hierarchical machine learning of potential energy surfaces," *The Journal of Chemical Physics*, vol. 152, no. 20, p. 204 110, 2020.

[110] X. Xie, K. A. Persson, and D. W. Small, "Incorporating electronic information into machine learning potential energy surfaces via approaching the ground-state electronic energy as a function of atom-based electronic populations," *Journal of Chemical Theory and Computation*, vol. 16, no. 7, pp. 4256–4270, 2020.

[111] O. T. Unke, D. Koner, S. Patra, S. Käser, and M. Meuwly, "High-dimensional potential energy surfaces for molecular simulations: From empiricism to machine learning," *Machine Learning: Science and Technology*, vol. 1, no. 1, p. 013 001, 2020.

[112] C. W. Coley, R. Barzilay, T. S. Jaakkola, W. H. Green, and K. F. Jensen, "Prediction of organic reaction outcomes using machine learning," *ACS Central Science*, vol. 3, no. 5, pp. 434–443, 2017.

[113] H. Gao, T. J. Struble, C. W. Coley, Y. Wang, W. H. Green, and K. F. Jensen, "Using machine learning to predict suitable conditions for organic reactions," *ACS Central Science*, vol. 4, no. 11, pp. 1465–1476, 2018.

[114] T. D. Rhone *et al.*, *Predicting outcomes of catalytic reactions using machine learning*, 2019. arXiv: `1908.10953 [physics.chem-ph]`.

[115] B. Settles, *Active Learning*. Morgan Claypool, 2012.

[116] ——, "Active learning literature survey," University of Wisconsin–Madison, Computer Sciences Technical Report 1648, 2009.

[117] D. Lewis and W. Gale, "A sequential algorithm for training text classifiers," *Proceedings of the ACM SIGIR Conference on Research and Development in Information Retrieval*, vol. 49, pp. 3–12, 1994.

[118] W. S. McCulloch and W. Pitts, "A logical calculus of the ideas immanent in nervous activity," *The Bulletin of Mathematical Biophysics*, vol. 5, no. 4, pp. 115–133, 1943.

[119] F. Rosenblatt, "The perceptron: A probabilistic model for information storage and organization in the brain.," *Psychological Review*, vol. 65, no. 6, pp. 386–408, 1958.

[120] G. Cybenko, "Approximation by superpositions of a sigmoidal function," *Mathematics of Control, Signals, and Systems*, vol. 2, no. 4, pp. 303–314, 1989.

[121] K. Hornik, M. Stinchcombe, and H. White, "Multilayer feedforward networks are universal approximators," *Neural Networks*, vol. 2, no. 5, pp. 359–366, 1989.

[122] K. Hornik, "Approximation capabilities of multilayer feedforward networks," *Neural Networks*, vol. 4, no. 2, pp. 251–257, 1991.

[123] E. Gelenbe, Z.-H. Mao, and Y.-D. Li, "Function approximation with spiked random networks," *IEEE Transactions on Neural Networks*, vol. 10, no. 1, pp. 3–9, 1999.

[124] P. Tabuada and B. Gharesifard, "Universal approximation power of deep neural networks via nonlinear control theory," *CoRR*, vol. abs/2007.06007, 2020. arXiv: 2007.06007.

[125] P. Kidger and T. J. Lyons, "Universal approximation with deep narrow networks," *CoRR*, vol. abs/1905.08539, 2019. arXiv: 1905.08539.

[126] K. Terayama *et al.*, "Efficient construction method for phase diagrams using uncertainty sampling," *Physical Review Materials*, vol. 3, no. 3, pp. 033 802–1–033802–8, 2019.

[127] C. Dai and S. Glotzer, "Efficient phase diagram sampling by active learning," *The Journal of Physical Chemistry B*, vol. 124, no. 7, pp. 1275–1284, 2020.

[128] Z. G. X. Zu and J. Lafferty, "Learning from labeled and unlabeled data with label propagation," *Proceesings of the 20th International Conference on Machine Learning*, pp. 912–919, 2003.

[129] C. Shannon, "A mathematical theory of communication," *Bell system technical journal*, vol. 27, no. 4, pp. 623–656, 1948.

[130] A. Diaz-Marquez, S. Battaglia, G. L. Bendazzoli, S. Evangelisti, T. Leininger, and J. A. Berger, "Signatures of wigner localization in one-dimensional systems," *The Journal of Chemical Physics*, vol. 148, no. 12, p. 124 103, 2018.

[131]   S.-C. Ho *et al.*, "Imaging the zigzag wigner crystal in confinement-tunable quantum wires," *Phys. Rev. Lett.*, vol. 121, p. 106 801, 10 2018.

[132]   I. Shapir *et al.*, "Imaging the electronic wigner crystal in one dimension," *Science*, vol. 364, no. 6443, pp. 870–875, 2019.

[133]   K. J. H. Giesbertz and R. van Leeuwen, "Natural occupation numbers: When do they vanish?" *The Journal of Chemical Physics*, vol. 139, no. 10, p. 104 109, 2013.

[134]   S. Di Sabatino, J. A. Berger, L. Reining, and P. Romaniello, "Reduced density-matrix functional theory: Correlation and spectroscopy," *The Journal of Chemical Physics*, vol. 143, no. 2, p. 024 108, 2015.

[135]   A. D. Gottlieb and N. J. Mauser, "New measure of electron correlation," *Phys. Rev. Lett.*, vol. 95, p. 123 003, 12 2005.

[136]   E. T. Whittaker and G. N Watson, *A course of modern analysis. An introduction to the general theory of infinite series and of analytic functions, with an account of the principal transcendental functions.* 1927.

[137]   S. Flugge and H. Marshall, *Rechenmethoden der Quantentheorie.* Springer, 1952.

[138]   L. Brooke *et al.*, "Distributed gaussian orbitals for the description of electrons in an external potential," *Journal of Molecular Modeling*, vol. 24, no. 8, 2018.

[139]   M. Escobar Azor, E. Alves, S. Evangelisti, and J. A. Berger, "Wigner localization in two and three dimensions: An ab initio approach," *The Journal of Chemical Physics*, vol. 155, no. 12, p. 124 114, 2021.

[140]   M. E. Azor *et al.*, "A Wigner molecule at extremely low densities: a numerically exact study," *SciPost Phys. Core*, vol. 1, p. 1, 1 2019.

[141]   E. Alves, G. L. Bendazzoli, S. Evangelisti, and J. A. Berger, "Accurate ground-state energies of wigner crystals from a simple real-space approach," *Phys. Rev. B*, vol. 103, p. 245 125, 24 2021.

[142]   E. R. Davidson and D. Feller, "Basis set selection for molecular calculations," *Chemical Reviews*, vol. 86, no. 4, pp. 681–696, 1986.

[143]   P. M. Gill, "Molecular integrals over gaussian basis functions," in ser. Advances in Quantum Chemistry, J. R. Sabin and M. C. Zerner, Eds., vol. 25, Academic Press, 1994, pp. 141–205.

[144]   D. R. Yarkony, *Modern Electronic Structure Theory.* World Scientific Publishing Company, 1995.

[145]   G. Tasi and A. G. Császár, "Hartree–fock-limit energies and structures with a few dozen distributed gaussians," *Chemical Physics Letters*, vol. 438, no. 1-3, pp. 139–143, 2007.

[146]   E. Perlt, M. Brüssel, and B. Kirchner, "Floating orbital molecular dynamics simulations," *Physical chemistry chemical physics : PCCP*, vol. 16, Mar. 2014.

[147]   E. Perlt, C. Apostolidou, M. Eggers, and B. Kirchner, "Unrestricted floating orbitals for the investigation of open shell systems," *International Journal of Chemistry*, vol. 8, p. 194, Jan. 2016.

[148]   Z. Shen and J. Herzfeld, "Floating orbitals reconsidered: The difference an imaginary part can make," *ACS Omega*, vol. 3, no. 9, pp. 10 992–10 998, 2018.

[149]   S. Battaglia *et al.*, "Distributed gaussian orbitals for molecular calculations: Application to simple systems," *Molecular Physics*, vol. 118, no. 4, p. 1 615 646, 2019.

[150]   Z. Liu, L. Wang, and K. Shen, "Energy spectra of three electrons in si/sige single and vertically coupled double quantum dots," *Phys. Rev. B*, vol. 85, p. 045 311, 4 2012.

[151]   D. Miserev and O. P. Sushkov, "Prediction of the spin triplet two-electron quantum dots in si: Towards controlled quantum simulations of magnetic systems," *Phys. Rev. B*, vol. 100, p. 205 129, 20 2019.

[152]   J. C. Abadillo-Uriel, B. Martinez, M. Filippone, and Y.-M. Niquet, "Two-body wigner molecularization in asymmetric quantum dot spin qubits," *Phys. Rev. B*, vol. 104, p. 195 305, 19 2021.

[153]   H. E. Ercan, S. N. Coppersmith, and M. Friesen, "Strong electron-electron interactions in si/sige quantum dots," *Phys. Rev. B*, vol. 104, p. 235 302, 23 2021.

[154]   D. Pan *et al.*, "Cutting sp2 clusters in graphene sheets into colloidal graphene quantum dots with strong green fluorescence," *J. Mater. Chem.*, vol. 22, pp. 3314–3318, Jan. 2012.

[155]   J. Shen, Y. Zhu, X. Yang, J. Zong, J. Zhang, and C. Li, "One-pot hydrothermal synthesis of graphene quantum dots surface-passivated by polyethylene glycol and their photoelectric conversion under near-infrared light," *New J. Chem.*, vol. 36, pp. 97–101, 1 2012.

[156]   Q. Wang, H. Zheng, Y. Long, L. Zhang, M. Gao, and W. Bai, "Microwave–hydrothermal synthesis of fluorescent carbon dots from graphite oxide," *Carbon*, vol. 49, no. 9, pp. 3134–3140, 2011.

[157]   D. Pan, J. Zhang, Z. Li, and M. Wu, "Hydrothermal route for cutting graphene sheets into blue-luminescent graphene quantum dots," *Advanced Materials*, vol. 22, no. 6, pp. 734–738, 2010.

[158]   D. Gopalakrishnan, D. Damien, and M. M. Shaijumon, "Mos2 quantum dot-interspersed exfoliated mos2 nanosheets," *ACS Nano*, vol. 8, no. 5, pp. 5297–5303, 2014.

[159]   B. L. Li, L. X. Chen, H. L. Zou, J. L. Lei, H. Q. Luo, and N. B. Li, "Electrochemically induced fenton reaction of few-layer mos2 nanosheets: Preparation of luminescent quantum dots via a transition of nanoporous morphology," *Nanoscale*, vol. 6, pp. 9831–9838, 16 2014.

[160] Y. Wang and Y. Ni, "Molybdenum disulfide quantum dots as a photolu-
       minescence sensing platform for 2,4,6-trinitrophenol detection," *Analytical
       Chemistry*, vol. 86, no. 15, pp. 7463–7470, 2014.

[161] ——, "Molybdenum disulfide quantum dots as a photoluminescence sensing
       platform for 2,4,6-trinitrophenol detection," *Analytical Chemistry*, vol. 86,
       no. 15, pp. 7463–7470, 2014.

[162] X. Ren, L. Pang, Y. Zhang, X. Ren, H. Fan, and S. F. Liu, "One-step
       hydrothermal synthesis of monolayer mos2 quantum dots for highly efficient
       electrocatalytic hydrogen evolution," *J. Mater. Chem. A*, vol. 3, pp. 10 693–
       10 697, 20 2015.

[163] H. Lin, C. Wang, J. Wu, Z. Xu, Y. Huang, and C. Zhang, "Colloidal synthe-
       sis of mos2 quantum dots: Size-dependent tunable photoluminescence and
       bioimaging," *New J. Chem.*, vol. 39, pp. 8492–8497, 11 2015.

[164] M. A. Sk, A. Ananthanarayanan, L. Huang, K. H. Lim, and P. Chen, "Re-
       vealing the tunable photoluminescence properties of graphene quantum dots,"
       J. Mater. Chem. C, vol. 2, pp. 6954–6960, 34 2014.

[165] Z. Liu *et al.*, "Size effect of graphene quantum dots on photoluminescence,"
       Molecules, vol. 26, no. 13, 2021.

[166] Y. Cao *et al.*, "Correlated insulator behaviour at half-filling in magic-angle
       graphene superlattices," *Nature*, vol. 556, no. 7699, pp. 80–84, 2018.

[167] Y. Cao *et al.*, "Unconventional superconductivity in magic-angle graphene
       superlattices," *Nature*, vol. 556, no. 7699, pp. 43–50, 2018.

[168] N. F. Q. Yuan and L. Fu, "Model for the metal-insulator transition in graphene
       superlattices and beyond," *Phys. Rev. B*, vol. 98, p. 045 103, 4 2018.

[169] C. Xu and L. Balents, "Topological superconductivity in twisted multilayer
       graphene," *Phys. Rev. Lett.*, vol. 121, p. 087 001, 8 2018.

[170] M. Yankowitz *et al.*, "Tuning superconductivity in twisted bilayer graphene,"
       Science, vol. 363, no. 6431, pp. 1059–1064, 2019.

[171] Y. Choi *et al.*, "Electronic correlations in twisted bilayer graphene near the
       magic angle," *Nature Physics*, vol. 15, no. 11, pp. 1174–1180, 2019.

[172] L. Bonsall and A. A. Maradudin, "Some static and dynamical properties of
       a two-dimensional wigner crystal," *Phys. Rev. B*, vol. 15, pp. 1959–1973, 4
       1977.

[173] C. C. Grimes and G. Adams, "Evidence for a liquid-to-crystal phase transition
       in a classical, two-dimensional sheet of electrons," *Phys. Rev. Lett.*, vol. 42,
       pp. 795–798, 12 1979.

[174] B. Padhi, C. Setty, and P. W. Phillips, "Doped twisted bilayer graphene near
       magic angles: Proximity to wigner crystallization, not mott insulation," *Nano
       Letters*, vol. 18, no. 10, pp. 6175–6180, 2018.

[175]   E. Alves, G. L. Bendazzoli, S. Evangelisti, and J. A. Berger, "Accurate ground-state energies of wigner crystals from a simple real-space approach," *Phys. Rev. B*, vol. 103, p. 245 125, 24 2021.

[176]   C. C. Grimes and G. Adams, "Evidence for a liquid-to-crystal phase transition in a classical, two-dimensional sheet of electrons," *Phys. Rev. Lett.*, vol. 42, pp. 795–798, 12 1979.

[177]   Y. P. Monarkha and V. E. Syvokon, "A two-dimensional wigner crystal (review article)," *Low Temperature Physics*, vol. 38, no. 12, pp. 1067–1095, 2012.

[178]   D. Gammon, *Nature*, vol. 405, p. 899, 2000.

[179]   C. Ellenberger *et al.*, *Phys. Rev Lett.*, vol. 96, p. 126 806, 2006.

[180]   B DeMarco and D. Jin, "Onset of fermi degeneracy in a trapped atomic gas," *Science*, vol. 285, p. 1703, 1999.

[181]   A. Truscott, K. Strecker, W. McAlexander, G. Partridge, and R. Hulet, "Observation of fermi pressure in a gas of trapped atoms," *Science*, vol. 291, p. 2570, 2001.

[182]   B. Pingault *et al.*, "Coherent control of the silicon-vacancy spin in diamond," *Nature Communications*, vol. 8, no. 1, 2017.

[183]   Y.Zhou, A. Rasmita, K. Li, Q. Xiong, I. Aharonovich, and W. Gao, "Coherent control of a strongly driven silicon vacancy optical transition in diamond," *Nature Communications*, vol. 8, no. 1, 2017.

[184]   P. Maksym and T. Chakraborty, *Phys. Rev. B*, vol. 45, p. 1947, 1992.

[185]   J. Kinaret, Y. Meir, N. Wingreen, P. Lee, and X. Wen, *Phys. Rev. B*, vol. 46, p. 4681, 1992.

[186]   P. Hawrylak, *Phys. Rev. Lett.*, vol. 71, p. 3347, 1993.

[187]   D. Pfannkuche, V. Gudmundsson, and P. Maksym, *Phys. Rev. B*, vol. 47, p. 2244, 1993.

[188]   S. Yang, A. MacDonald, and D. Johnson, *Phys. Rev. Lett.*, vol. 71, p. 3194, 1993.

[189]   J. Palacios, L. Martin-Moreno, G. Chiappe, E. Louis, and C. Tejedor, *Phys. Rev. B*, vol. 50, p. 5760, 1994.

[190]   C. C. Chamon and X. Wen, *Phys. Rev. B*, vol. 49, p. 8227, 1994.

[191]   M. Fujito, A. Natori, and H. Yasunaga, *Phys. Rev. B*, vol. 53, p. 9952, 1996.

[192]   C. Yannouleas and U. Landmann, *Phys. Rev. Lett.*, vol. 82, p. 5325, 1999.

[193]   T. Henderson, K. Runge, and R. Bartlett, *Chem. Phys. Lett.*, vol. 337, p. 138, 2001.

[194]   M. Macucci, K. Hess, and G. Iafrate, *Phys. Rev. B*, vol. 48, p. 17 354, 1993.

[195]   M. Koskinen, M. Manninen, and S. Raimann, *Phys. Rev. Lett.*, vol. 79, p. 1389, 1997.

[196]   H. Hirose and N. Wingreen, *Phys. Rev. B*, vol. 59, p. 4604, 1999.

[197]   M. Gattobigio, P. Capuzzi, M. Polini, R. Asgari, and M. P. Tossi, *Phys. Rev. B*, vol. 72, p. 045 306, 2005.

[198]   A. Filinov, M. Bonitz, and Y. E. Lozovik, *Phys. Rev. Lett.*, vol. 86, p. 3851, 2001.

[199]   E. Matito, J. Cioslowski, and S. F. Vyboishchikov, "Properties of harmonium atoms from fci calculations: Calibration and benchmarks for the ground state of the two-electron species," vol. 12, p. 6712, 2010.

[200]   L. V. Dias da Silva, C. H. Lewenkopf, and N. Studart, "Orbital magnetic properties of quantum dots: The role of electron-electron interactions," *Phys. Rev. B*, vol. 69, p. 075 311, 2004.

[201]   E. Barnes, J. P. Kestner, N. T. T. Nguyen, and S. Das Sarma, "Screening of charged impurities with multielectron singlet-triplet spin qubits in quantum dots," *Phys. Rev. B*, vol. 84, p. 235 309, 23 2011.

[202]   H. Yakobi, E. Eliav, and U. Kaldor, "Electronic structure of three-dimensional isotropic quantum dots by four-component relativistic coupled cluster methods," *The Journal of Chemical Physics*, vol. 134, no. 5, p. 054 503, 2011. eprint: https://doi.org/10.1063/1.3533778.

[203]   R. N. Pereira *et al.*, "Dielectric screening versus quantum confinement of phosphorus donors in silicon nanocrystals investigated by magnetic resonance," *Phys. Rev. B*, vol. 79, p. 161 304, 16 2009.

[204]   E. Santos, "Cálculo aproximado de la energía de correlación entre dos electrons," *An. R. Soc. Esp. Fís. Quím.*, vol. 64, p. 117, 1968.

[205]   N. R. Kestner and O. Sinanoglu, "Study of electron correlation in helium-like systems using an exactly soluble model," vol. 128, p. 2687, 1962.

[206]   M.W.Schmidt *et al.*, "General atomic and molecular electronic structure system," *J. Comput. Chem.*, vol. 14, pp. 1347–1363, 1993.

[207]   M.S.Gordon and M.W.Schmidt, "Theory and applications of computational chemistry, the first forty years," in C.E.Dykstra, G.Frenking, K.S.Kim, and G.E.Scuseria, Eds. Amsterdam: Elsevier, 2005, ch. Advances in electronic structure theory: GAMESS a decade later.

[208]   M. Rodríguez-Mayorga, E. Ramos-Cordoba, X. Lopez, M. Solà, J. M. Ugalde, and E. Matito, "The coulomb hole of the ne atom," *ChemistryOpen*, vol. 8, no. 4, pp. 411–417, 2019.

[209]   T. F. G. G. Cova and A. A. C. C. Pais, "Deep learning for deep chemistry: Optimizing the prediction of chemical patterns," *Frontiers in Chemistry*, vol. 7, p. 809, 2019.

[210]   E. Cerpa, A. Krapp, R. Flores-Moreno, K. Donald, and G. Merino, "Influence of endohedral confinement on the electronic interaction between he atoms: A he2@c20h20 case study," *Chemistry – A European Journal*, vol. 15, no. 8, pp. 1985–1990, 2009.

[211]   T. Y. Nikolaienko and E. S. Kryachko, "Formation of dimers of light noble atoms under encapsulation within fullerene's voids," *Nanoscale Research Letters*, vol. 10, no. 1, 2015.

[212]   D. Paul, H. Dua, and U. Sarkar, "Confinement effects of a noble gas dimer inside a fullerene cage: Can it be used as an acceptor in a dssc?" *Frontiers in Chemistry*, vol. 8, p. 621, 2020.

[213]   A. Krapp and G. Frenking, "Is this a chemical bond? a theoretical study of ng2@c60 (ng=he, ne, ar, kr, xe)," *Chemistry – A European Journal*, vol. 13, no. 29, pp. 8256–8270, 2007.

[214]   S. Gómez and A. Restrepo, "Noble gas dimers confined inside c70," *Phys. Chem. Chem. Phys.*, vol. 21, pp. 15 815–15 822, 28 2019.

[215]   S. Jalife, J. Arcudia, S. Pan, and G. Merino, "Noble gas endohedral fullerenes," *Chem. Sci.*, vol. 11, pp. 6642–6652, 26 2020.

[216]   M. Khatua, S. Pan, and P. K. Chattaraj, "Confinement induced binding of noble gas atoms," *The Journal of Chemical Physics*, vol. 140, no. 16, p. 164 306, 2014.

[217]   S. Pan, M. Ghara, S. Kar, X. Zarate, G. Merino, and P. K. Chattaraj, "Noble gas encapsulated b40 cage," *Phys. Chem. Chem. Phys.*, vol. 20, pp. 1953–1963, 3 2018.

[218]   "Confinement induced binding in noble gas atoms within a bn-doped carbon nanotube," *Chemical Physics Letters*, vol. 621, pp. 29–34, 2015.

[219]   L. Brunet, J. Caillard, and P. André, "Thermodynamic calculation of n-component eutectic mixtures," *International Journal of Modern Physics C*, vol. 15, no. 05, pp. 675–687, 2004.

[220]   M. Martínez-Sánchez, R. Vargas, and J. Garza, "Shannon entropy for the hydrogen atom confined by four different potentials," *Quantum Reports*, vol. 1, no. 2, pp. 208–218, 2019.

[221]   H. Gholizadehkalkhoran, I. Ruokosenmäki, and T. Rantala, "Eigenstates and dynamics of hooke's atom: Exact results and path integral simulations," *Journal of Mathematical Physics*, vol. 59, no. 5, p. 052 104, 2018.

[222]   J. Katriel, H. Montgomery, A. Sarsa, and E. Buendía, "Hund's rule in open-shell states of two-electron systems: From free through confined and screened atoms, to quantum dots," *Nanosystems: Physics, Chemistry, Mathematics*, vol. 10, no. 1, pp. 31–41, 2019.

[223] M. Slamet and V. Sahni, "Kinetic effects in 2d and 3d quantum dots: Comparison between high and low electron correlation regimes," *Computational and Theoretical Chemistry*, vol. 1138, pp. 140–157, 2018.

[224] A. Odriazola, J. Solanpää, I. Kylänpää, A. Gonzalez, and E. Räsänen, "Universal scaling relations for the energies of many-electron hooke atoms," *Physical Review A*, vol. 95, no. 4, 2017.

[225] C. Downing, "Two-electron atom with a screened interaction," *Physical Review A*, vol. 95, no. 2, 2017.

[226] J. Ugalde and C. Sarasola, "Evaluation of screened nuclear attraction and electron repulsion molecular integrals over gaussian basis functions," *International Journal of Quantum Chemistry*, vol. 62, no. 3, pp. 273–278, 1997.

[227] A. Robles-Navarro, M. Rodriguez-Bautista, P. Fuentealba, and C. Cárdenas, "The change in the nature of bonding in the li2 dimer under confinement," *International Journal of Quantum Chemistry*, vol. n/a, no. n/a, e26644,

[228] I. Balakrishnan, N. Jawahar, S. Venkatachalam, and D. Debosmita, "A brief review on eutectic mixture and its role in pharmaceutical field," *International Journal of Research in Pharmaceutical Sciences*, vol. 11, pp. 3017–3023, Jul. 2020.

[229] A. Abbott, E. Ahmed, K. Prasad, I. Qader, and K. Ryder, "Liquid pharmaceuticals formulation by eutectic formation," *Fluid Phase Equilibria*, vol. 448, pp. 2–8, 2017, Deep Eutectic Solvents.

[230] C. Huang, X. Chen, C. Wei, H. Wang, and H. Gao, "Deep eutectic solvents as active pharmaceutical ingredient delivery systems in the treatment of metabolic related diseases," *Frontiers in Pharmacology*, vol. 12, 2021.

[231] Y. Chen and T. Mu, "Revisiting greenness of ionic liquids and deep eutectic solvents," *Green Chemical Engineering*, vol. 2, no. 2, pp. 174–186, 2021.

[232] L. P. Silva, M. A. R. Martins, J. H. F. Conceição, S. P. Pinho, and J. A. P. Coutinho, "Eutectic mixtures based on polyalcohols as sustainable solvents: Screening and characterization," *ACS Sustainable Chemistry & Engineering*, vol. 8, no. 40, pp. 15 317–15 326, 2020.

[233] X. Wen-Fang, "Two interacting electrons in a spherical gaussian confining potential quantum well," *Communications in Theoretical Physics*, vol. 42, no. 1, pp. 151–156, 2004.

[234] B. Boyacioglu and A. Chatterjee, "Heat capacity and entropy of a gaas quantum dot with gaussian confinement," *Journal of Applied Physics*, vol. 112, no. 8, p. 083 514, 2012.

[235] A. Boda, B. Boyacioglu, and A. Chatterjee, "Ground state properties of a two-electron system in a three-dimensional gaas quantum dot with gaussian confinement in a magnetic field," *Journal of Applied Physics*, vol. 114, no. 4, p. 044 311, 2013.

[236] H. Sharma, A. Boda, B. Boyacioglu, and A. Chatterjee, "Electronic and magnetic properties of a two-electron gaussian gaas quantum dot with spin-zeeman term: A study by numerical diagonalization," *Journal of Magnetism and Magnetic Materials*, vol. 469, pp. 171–177, 2019.

[237] V. Mughnetsyan, "Effect of donor impurity on aharonov–bohm oscillations in a double quantum ring with gaussian confinement," *Proceedings of the YSU, Physical and Mathematical Sciences*, vol. 51, pp. 205–212, 3 2018.

[238] Xu-Fang, W. Xin, Xiao-Xu, and L. Eerdunchaolu, "Asymmetric gaussian confinement potential and decoherence effect on polaron in quantum disk with electromagnetic field," *The European Physical Journal Plus*, vol. 135, p. 321, 2020.

[239] J. D. Castaño-Yepes and D. Amor-Quiroz, "Super-statistical description of thermo-magnetic properties of a system of 2d gaas quantum dots with gaussian confinement and rashba spin–orbit interaction," *Physica A: Statistical Mechanics and its Applications*, vol. 548, p. 123 871, 2020.

[240] K. Jahan, B. Boyacioglu, and A. Chatterjee, "Effect of confinement potential shape on the electronic, thermodynamic, magnetic and transport properties of a gaas quantum dot at finite temperature," *Scientific Reports*, vol. 9, 1 2019.

[241] N. Yahyah, M. Elsaid, and A. Shaer, "Heat capacity and entropy of gaussian spherical quantum dot in the presence of donor impurity," *Journal of Theoretical and Applied Physics*, vol. 13, 277–288 2019.

[242] M. Elsaid, M. Ali, and A. Shaer, "The magnetization and magnetic susceptibility of gaas gaussian quantum dot with donor impurityin a magnetic field," *Modern Physics Letters B*, vol. 1950422, 2019.

[243] W. Zhai, "A study of electric-field-induced second-harmonic generation in asymmetrical gaussian potential quantum wells," *Physica B: Condensed Matter*, vol. 454, pp. 50–55, 2014.

[244] Z.-H. Zhang, L. Zou, K.-X Guo, and J.-H. Yuan, "The nonlinear optical rectification in asymmetrical and symmetrical gaussian potential quantum wells with applied electric field," *Optics Communications*, vol. 359, pp. 316–321, Jan. 2016.

[245] H. Sari, E. Kasapoglu, S. Sakiroglu, I. Sökmen, and C. Duque, "Impurity-related optical response in a 2d and 3d quantum dot with gaussian confinement under intense laser field," *Philosophical Magazine*, vol. 100, pp. 619–641, 5 2019.

[246] H. Sari, F. Ungan, S. Sakiroglu, U. Yesilgul, E. Kasapoglu, and I. Sökmen, "Electron-related optical responses in gaussian potential quantum wells: Role of intense laser field," *Physica B: Condensed Matter*, vol. 545, pp. 250–254, 2018.

[247] Z.-H. Zhang, L. Zou, K.-X Guo, and J.-H. Yuan, "The nonlinear optical rectification in asymmetrical and symmetrical gaussian potential quantum wells with applied electric field," *Optics Communications*, vol. 359, pp. 316–321, Jan. 2016.

[248] L. A. A. Nikolopoulos and H. Bachau, "Theory of photoionization of two-electron quantum dots in the resonance region in thz and mid-ir fields," *Phys. Rev. A*, vol. 94, p. 053 409, 5 2016.

[249] J. D. Castaño-Yepes, D. Amor-Quiroz, C. Ramirez-Gutierrez, and E. Gómez, "Impact of a topological defect and rashba spin-orbit interaction on the thermo-magnetic and optical properties of a 2d semiconductor quantum dot with gaussian confinement," *Physica E: Low-dimensional Systems and Nanostructures*, vol. 109, pp. 59–66, 2019.

[250] L. E. Reichl and M. D. Porter, "Quasibound states in a triple gaussian potential," *Phys. Rev. E*, vol. 97, p. 042 206, 4 2018.

[251] R. Khordad and M. Servatkhah, "Study of entanglement entropy and exchange coupling in two-electron coupled quantum dots," *Optical and Quantum Electronics*, vol. 49, no. 6, 2017.

[252] A. Gharaati and R. Khordad, "A new confinement potential in spherical quantum dots: Modified gaussian potential," *Superlattices and Microstructures*, vol. 48, no. 3, pp. 276–287, 2010.

[253] S. Albeverio, S. Fassari, M. Gadella, L. Nieto, and F. Rinaldi, "The birman-schwinger operator for a parabolic quantum well in a zero-thickness layer in the presence of a two-dimensional attractive gaussian impurity," *Frontiers in Physics*, vol. 7, 2019.

[254] F. Iacob and M. Lute, "Exact solution to the schrödinger's equation with pseudo-gaussian potential," *Journal of Mathematical Physics*, vol. 56, no. 12, p. 121 501, 2015. eprint: https://doi.org/10.1063/1.4936309.

[255] S. Gómez and R. Romero, "Few-electron semiconductor quantum dots with gaussian confinement," *Open Physics*, vol. 7, Apr. 2008.

[256] K. D. Sen, H. E. Montgomery, B. Yu, and J. Katriel, "Excited states of the gaussian two-electron quantum dot," *The European Physical Journal D*, vol. 75, no. 6, 2021.

[257] S. Ali and A. Bodmer, "Phenomenological α-α potentials," *Nuclear Physics*, vol. 80, 99 1966.

[258] S. E. G. Stellin and U. Meißner, "Breaking and restoration of rotational symmetry in the low energy spectrum of light -conjugate nuclei on the lattice i: 8be and 12c," *Eur. Phys. J. A*, vol. 54, no. 232, 2018.

[259] O. Bayakhmetov, Z. Seksembayev, A. Azamatov, V. Kukulin, A. Pukhov, and S. Sakhiyev, "Static properties of the 9be nucleus in the ground and excited states in the cluster model," *Phys. Scr.*, vol. 94, no. 8, 2019.

[260] L. Phyu, H. Moriya, W. Horiuchi, K. Iida, K. Noda, and M. Yamashita, "Coulomb screening correction to the q value of the triple-alpha process in thermal plasmas," *Prog. Theor. Exp. Phys.*, vol. 093D01, 2020.

[261] W. J. Glover, R. E. Larsen, and B. J. Schwartz, "First principles multielectron mixed quantum/classical simulations in the condensed phase. i. an efficient fourier-grid method for solving the many-electron problem," *The Journal of Chemical Physics*, vol. 132, no. 14, p. 144 101, 2010.

[262] J. M. Elward, J. Hoffman, and A. Chakraborty, "Investigation of electron–hole correlation using explicitly correlated configuration interaction method," *Chemical Physics Letters*, vol. 535, pp. 182–186, 2012.

[263] J. M. Elward, B. Thallinger, and A. Chakraborty, "Calculation of electron-hole recombination probability using explicitly correlated hartree-fock method," *The Journal of Chemical Physics*, vol. 136, no. 12, p. 124 105, 2012.

[264] M. Piris, "Performance of the nof theory in the description of the four-electron harmonium atom in the singlet state," Dec. 2015.

[265] M. Rodríguez-Mayorga, E. Ramos-Cordoba, M. Via-Nadal, M. Piris, and E. Matito, "Comprehensive benchmarking of density matrix functional approximations," *Phys. Chem. Chem. Phys.*, vol. 19, pp. 24 029–24 041, 35 2017.

[266] J. Cioslowski, K. Strasburger, and E. Matito, "Benchmark calculations on the lowest-energy singlet, triplet, and quintet states of the four-electron harmonium atom," *The Journal of Chemical Physics*, vol. 141, no. 4, p. 044 128, 2014.

[267] *Proceedings of the Royal Society of London. Series A. Mathematical and Physical Sciences*, vol. 200, no. 1063, pp. 542–554, 1950.

[268] I. Shavitt, "The treatment of electron correlation. where do we go from here?" In *Advanced Theories and Computational Approaches to the Electronic Structure of Molecules*, ser. NATO ASI Series 133, C. E. D. (ed.), Ed., Springer Netherlands, 1984, pp. 185–196.

[269] E. Belasú and R. Carbó-Dorca, "The general gaussian product theorem," *Journal of Mathematical Chemistry*, vol. 49, pp. 1769–1784, 2011.

[270] J. R. Heath *et al.*, "Lanthanum complexes of spheroidal carbon shells," *Journal of the American Chemical Society*, vol. 107, no. 25, pp. 7779–7780, 1985.

[271] M. M. Olmstead, H. M. Lee, S. Stevenson, H. C. Dorn, and A. L. Balch, "Crystallographic characterization of isomer 2 of er2@c82 and comparison with isomer 1 of er2@c82," *Chem. Commun.*, pp. 2688–2689, 22 2002.

[272] A. A. Popov, S. Yang, and L. Dunsch, "Endohedral fullerenes," *Chemical Reviews*, vol. 113, no. 8, pp. 5989–6113, 2013.

[273] R. T. Harding *et al.*, "Spin resonance clock transition of the endohedral fullerene ^{15}N@C$_{60}$," *Phys. Rev. Lett.*, vol. 119, p. 140 801, 14 2017.

[274] A. W. Castleman and S. N. Khanna, "Clusters, superatoms, and building blocks of new materials," *The Journal of Physical Chemistry C*, vol. 113, no. 7, pp. 2664–2675, 2009.

[275] A. W. Castleman, "From elements to clusters: The periodic table revisited," *The Journal of Physical Chemistry Letters*, vol. 2, no. 9, pp. 1062–1069, 2011.

[276] P. Jena, "Beyond the periodic table of elements: The role of superatoms," *The Journal of Physical Chemistry Letters*, vol. 4, no. 9, pp. 1432–1442, 2013.

[277] P. Jena and Q. Sun, "Super atomic clusters: Design rules and potential for building blocks of materials," *Chemical Reviews*, vol. 118, no. 11, pp. 5755–5870, 2018.

[278] L. Wang, J. Zhao, Z. Zhou, S. B. Zhang, and Z. Chen, "First-principles study of molecular hydrogen dissociation on doped al12x (x = b, al, c, si, p, mg, and ca) clusters," *Journal of Computational Chemistry*, vol. 30, no. 15, pp. 2509–2514, 2009.

[279] H.-L. Wu, X.-B. Li, C.-H. Tung, and L.-Z. Wu, "Semiconductor quantum dots: An emerging candidate for co2 photoreduction," *Advanced Materials*, vol. 31, no. 36, p. 1 900 709, 2019.

[280] Z. Wang, T. Nguyen, L. Yeo, C. Tan, L. Gan, and A. Tok, "Periodic fto ios/cds nrs/cdse clusters with superior light scattering ability for improved photoelectrochemical performance," *Small*, vol. 16, no. 6, 2020.

[281] C. Palencia, K. Yu, and K. Boldt, "The future of colloidal semiconductor magic-size clusters," *ACS Nano*, vol. 14, no. 2, pp. 1227–1235, 2020.

[282] E. A. Weiss, "Designing the surfaces of semiconductor quantum dots for colloidal photocatalysis," *ACS Energy Letters*, vol. 2, no. 5, pp. 1005–1013, 2017.

[283] K. N. Lawrence, S. Dolai, Y.-H. Lin, A. Dass, and R. Sardar, "Enhancing the physicochemical and photophysical properties of small (¡2.0 nm) cdse nanoclusters for intracellular imaging applications," *RSC Adv.*, vol. 4, pp. 30 742–30 753, 58 2014.

[284] K. N. Lawrence, P. Dutta, M. Nagaraju, M. B. Teunis, B. B. Muhoberac, and R. Sardar, "Dual role of electron-accepting metal-carboxylate ligands: Reversible expansion of exciton delocalization and passivation of nonradiative trap-states in molecule-like cdse nanocrystals," *Journal of the American Chemical Society*, vol. 138, no. 39, pp. 12 813–12 825, 2016.

[285] M. R. Friedfeld, J. L. Stein, A. Ritchhart, and B. M. Cossairt, "Conversion reactions of atomically precise semiconductor clusters," *Accounts of Chemical Research*, vol. 51, no. 11, pp. 2803–2810, 2018.

[286] J. M. Matxain, L. A. Eriksson, E. Formoso, M. Piris, and J. M. Ugalde, "Endohedral (x@znisi)i=4-160,± nanoclusters, x = li, na, k, cl, br," *The Journal of Physical Chemistry C*, vol. 111, no. 9, pp. 3560–3565, 2007.

[287] E. Jimenez-Izal, J. M. Matxain, M. Piris, and J. M. Ugalde, "Structure and stability of the endohedrally doped (x@cdisi)i=4,9,12,15,16q=0,±1, x = na, k, cl, br, nanoclusters," *The Journal of Physical Chemistry C*, vol. 114, no. 6, pp. 2476–2483, 2010.

[288] ——, "Self-assembling endohedrally doped cds nanoclusters: New porous solid phases of cds," *Physical Chemistry Chemical Physics*, vol. 14, no. 27, p. 9676, 2012.

[289] E. Jimenez-Izal, J. Matxain, M. Piris, and J. Ugalde, "Second-row transition-metal doping of (znisi), i = 12, 16 nanoclusters: Structural and magnetic properties," *Computation*, vol. 1, no. 3, pp. 31–45, 2013.

[290] E. Jimenez-Izal, J. M. Azpiroz, R. Gupta, J. M. Matxain, and J. M. Ugalde, "Cds nanoclusters doped with divalent atoms," *Journal of Molecular Modeling*, vol. 20, no. 6, 2014.

[291] K. J. H. Giesbertz and R. van Leeuwen, "Natural occupation numbers: When do they vanish?" *J. Chem. Phys.*, vol. 139, no. 10, p. 104 109, 2013.

[292] S. Di Sabatino, J. A. Berger, L. Reining, and P. Romaniello, "Reduced density-matrix functional theory: Correlation and spectroscopy," *J. Chem. Phys.*, vol. 143, no. 2, p. 024 108, 2015.

[293] E. Matito, J. Cioslowski, and S. Vyboishchikov, "Properties of harmonium atoms from fci calculations: Calibration and benchmarks for the ground state of the two-electron species," *Phys. Chem. Chem. Phys.*, vol. 2, p. 6712, 2010.

[294] M. Rodríguez-Mayorga, E. Ramos-Cordoba, X. Lopez, M. Solà, J. M. Ugalde, and E. Matito, "The coulomb hole of the ne atom," *ChemistryOpen*, vol. 8, no. 4, pp. 411–417, 2019.